



FEDERAL UNIVERSITY OF SANTA CATARINA  
CENTER OF TECHNOLOGICAL  
GRADUATE PROGRAM IN CHEMICAL ENGINEERING

Jaqueline de Oliveira Brotto

**TORREFIED BIOMASS AS AN ALTERNATIVE FUEL IN ORE REDUCTION  
PROCESSES FOR MITIGATING CO<sub>2</sub> EMISSIONS**

Florianópolis  
2023

Jaqueline de Oliveira Brotto

**TORREFIED BIOMASS AS AN ALTERNATIVE FUEL IN ORE REDUCTION  
PROCESSES FOR MITIGATING CO<sub>2</sub> EMISSIONS**

Thesis presented to the Graduate Program in Chemical Engineering of the Federal University of Santa Catarina, as a requirement for obtaining the PhD degree in Chemical Engineering.

Advisor at UFSC: Prof<sup>a</sup>. Regina de Fatima Peralta Muniz Moreira, Dra.

Advisor at ICL: Prof. Paul Stephen Fennell, Dr.

Co-Advisor at UFSC: Prof. Humberto Jorge José, Dr.

Florianópolis

2023

### Work identification sheet

Brotto, Jaqueline de Oliveira

Torrefied biomass as an alternative fuel in ore reduction processes for mitigating CO<sub>2</sub> emissions/ Jaqueline de Oliveira Brotto; advisor at UFSC, Regina de Fatima Peralta Muniz Moreira, advisor at ICL, Paul Stephen Fennell, co-advisor at UFSC, Humberto Jorge José, 2023.

168 p.

Thesis (PhD) - Federal University of Santa Catarina, Technological Center, Graduate Program in Chemical Engineering, Florianópolis, 2023.

Includes references.

1. Chemical Engineering. 2. Solid Waste. 3. Wood Waste. 4. Thermal conversion. 5. Metallurgical industry. I. Moreira, Regina de Fátima Peralta Muniz. II. Fennell, Paul Stephen. III. José, Humberto Jorge. IV. Federal University of Santa Catarina. Graduate Program in Chemical Engineering. VI. Title.

Jaqueline de Oliveira Brotto

**TORREFIED BIOMASS AS AN ALTERNATIVE FUEL IN ORE REDUCTION  
PROCESSES FOR MITIGATING CO<sub>2</sub> EMISSIONS**

The presente work at the level of a doctoral thesis was evaluated and approved by an  
examining board composed of the following members:

Prof.<sup>a</sup> Elaine Virmond, Dra.

Federal University of Santa Catarina - UFSC

Prof.<sup>a</sup> Jaciane Lutz Ienczak, Dra.

Federal University of Santa Catarina - UFSC

Prof.<sup>a</sup> Silvia Layara Floriani Andersen, Dra.)

Federal University of Paraíba - UFPB

We certify that this is the **original version** of the final work that was judged suitable  
for a PhD thesis in Chemical Engineering.

---

Coordination of the Graduate Program

---

Prof.<sup>a</sup> Regina de Fátima Peralta Muniz Moreira, Dr.<sup>a</sup>  
Advisor at Federal University of Santa Catarina - UFSC

Florianópolis, 2023.

This thesis is dedicated to my  
parents, Ivete and José and  
sisters, Aline and Nicole.

## ACKNOWLEDGEMENTS

To God, for the life granted to me and for always guiding me during my earthly walk, giving me the opportunity to carry out this study.

To my parents Ivete Janice de Oliveira Brotto and José Antonio Brotto, for choosing to have children and giving me the opportunity to live earthly experiences. Thank you for the teachings, encouragement, inspiration and for loving me unconditionally.

To my sisters Aline de Oliveira Brotto and Nicole Cristine de Oliveira Brotto, for loving me unconditionally and for always being willing to have a friendly conversation, always encouraging me. You are inspiration to me.

To my niece and goddaughter, Lívia Brotto Kaibers, for every smile, every joke and every call “dadá” and “aunt Jaque”, moments that brought me a lot of joy and comfort in the most difficult and longing hours.

To my advisor, Dr. Regina de Fátima Peralta Muniz Moreira, for all the inspiration as a professional, as a person and as a woman, always present and available to talk, guide, advise, encourage and, above all, for believing in me. For the motivation to write projects and for providing part of my trip to Imperial College London to develop part of my research. Thank you so much for all the moments of growth and personal and professional development that you incorporated me.

To my advisor, Dr. Paul Stephen Fennell, for agreeing to advise me and for giving me the opportunity to develop part of my work at Imperial College London. For your availability, for the weekly group meetings, for guiding and discussing my work and for welcoming me so well into your research group. Your shared knowledge was essential for the development and growth of this work.

To my co-advisor, Dr. Humberto Jorge José, for his availability and opportunity to co-supervise me, his contribution was enriching for this work.

To my former bosses who became my great friends, Mauri Edgar Padilha de Lima and Kerling Fabiane Hornburg. For giving me the opportunity to work as a Chemical Engineer at CIGAMVALI, for believing in me and my work and for encouraging me to carry out this study by providing a change in working hours so that I could complete this postgraduate course.

To my friend Camilla Daniela Moura Nickel, my great encourager to attend this postgraduate course, who on the hardest days always reminds me of the best in me, supporting me and encouraging me to always move forward and believe in me.

To my friend Andréia De Rossi, for all the conversations, ideas and contributions to my work and to my life.

To my friends Carla Elionai de Barros Baez and Diúlia Stephani Baez de Góes for all the encouragement to always move forward, for all the advice and relaxed conversations, for the walks along the seaside washed down with chimarrão and for all the moments of joy that you shared. provided me.

To my friend Thaianne Andrade Cruz, who was by my side during most of the development of this study in the laboratory. Thank you for all your support, encouragement, exchange of personal and professional experiences, discussion of results, partnership and, above all, for always being available and willing to help.

To my friends Antonia Alana Lima Pacheco, Mariana Bianchini Silva and Fernanda Manaia Demarqui for all the conversations, exchange of experiences as researchers, tours, trips and especially for all the support and encouragement they gave me throughout my stay in London and which they give me to this day. You were essential at this time in my life. A friendship that started in London and that will last for life.

To my friend Selin Gueler for all the conversations, walks, lunches, coffees, shared knowledge and moments of relaxation. For welcoming me with joy and enthusiasm on my first day at Imperial College. For all availability and attention, always with a beautiful smile.

To my friend David Danaci for always being willing to help me and talk about my research. For patiently listening to me with each new idea to add to my study and for always discussing, encouraging and proposing new paths. For all the support during the development of my work at Imperial College London (ICL) and in the laboratory. For all the attention and relaxed conversations in the office. You have provided me with security and encouragement throughout my time at ICL.

To my colleagues at the Energy and Environment Laboratory (LEMA) who were always willing to help and teach me whenever I needed it.

To my colleagues in the Paul Fennell research group, who received me with great kindness and patience, always helping me, exchanging research ideas and relaxed conversations. Especially Haiyang Jiang, Liyan Tao and Tumisang Tsolope who shared the office with me and Michael High for always being available for a friendly conversation and concerned about my well-being.

To the Energy and Environment Laboratory (LEMA), where I carried out part of the laboratory tests for this work.

To the Research Laboratory of the Paul Fennell group, where I carried out the final part of my work.

To the secretary of the Graduate Program in Chemical Engineering, Edevilson Silva, for being patient, dear and responding promptly whenever requested.

To Susi Underwood for all the support, guidance and information provided so that I could study at Imperial College London.

To the Graduate Program in Chemical Engineering (PÓSEnq) at the Federal University of Santa Catarina (UFSC).

To the Graduate Program in Chemical Engineering at Imperial College London (ICL).



To the professors of the Graduate Program in Chemical Engineering (PÓSEnq), for complementing my knowledge, both personal and professional.

To UFSC and ICL for providing the development of this study.

To CAPES for the scholarship granted during part of my research in Brazil.

To CNPq for the scholarship granted to carry out part of my research in London.

To UKCCSRC and UKERC for the exchange of professional knowledge, networking, encouragement and support for the participation in Conferences, lectures and seminars.

To the professionals at Imperial College London, who were always available and provided me with security and support during my stay in London and at ICL. Special thanks to Jasiba Khurana-Chauhan from International Support Student (ISS) for all the conversations, information, tips and support offered.

Finally, thanks to everyone who in one way or another contributed to the completion of this work.

“Success is the sum of small efforts repeated daily.”

(Robert Collier).

## ABSTRACT

Aiming to reduce CO<sub>2</sub> emissions and propose the valorization of wood waste, this work aimed to produce solid fuel from the torrefaction of these biomasses to be applied as an alternative to metallurgical coke in the iron ore reduction process. In this context, four biomasses were initially selected for the study: *Eucalyptus* sawdust (SE), *Pine pellet* (PP), *Pine* chips (CV) and *Pine* bark (CC). All materials used are waste, except for *pellet*, which is already compacted and improved waste. For the proposed application, knowledge of the chemical and physical characteristics of the material is essential to evaluate its efficiency in the process. For this, were determined geometric characteristics, grindability and proximate analysis. The results of these analyzes showed that sawdust would not be a suitable material for the proposed application because it has a lower fixed carbon content compared to other biomasses. Subsequently, the elemental composition, calorific value, composition of lignocellulosic fractions, analysis of functional groups (FTIR) and characterization by nuclear magnetic resonance (*ss*-NMR) were determined. The effect of operational parameters on the torrefaction process was investigated using non-isothermal thermogravimetric tests from room temperature to 300 °C, using biomasses with different particle sizes (<106 μm and 106-300 μm), under inert or oxidizing atmosphere. After evaluating these parameters, the torrefaction tests were carried out in a fixed bed reactor, with temperatures of 250 and 290 °C, residence times of 30 and 60 min and inert atmosphere (N<sub>2</sub>). With the torrefied biomasses, non-isothermal tests were carried out in a thermogravimetric analyzer in order to evaluate the reactivity of these biomasses with CO<sub>2</sub>. Based on the results of the torrefied biomasses that showed the greatest reactivity with CO<sub>2</sub>, the optimal parameters of temperature and residence time for torrefaction were determined. Subsequently, the same characterizations mentioned above were carried out for the torrefied biomasses that showed greater reactivity. Furthermore, a methodology was proposed using the *ss*-NMR results to obtain kinetic torrefaction parameters. Analysis of the liquid and gaseous fractions generated during torrefaction were also carried out. Finally, tests were carried out to evaluate the reduction of hematite oxide (Fe<sub>2</sub>O<sub>3</sub>) from the torrefied biomass. The biomass characterization results showed that the selected samples have a low moisture and ash content, which is favorable for their use as fuel, and a high volatile matter content, which indicates that fuels made from this material are easily ignited even in relatively low temperatures. Furthermore, it was possible to assess that the chemical composition of PP and CV are very similar while CC had a higher lignin content in its composition. The results of reactivity with CO<sub>2</sub> showed that the best operational conditions for CC torrefaction were 250 °C and 60 min while PP and CV were 290 °C and 30 min, and the CC torrefaction biomass showed lower reactivity probably due to the high content of lignin. Here it is noted the importance of knowing the chemical composition of the material studied. The torrefaction generated a low amount of gases, even in the longest residence time and the presence of lignin in high concentration produced non-condensable gases rich in hydrogen and aliphatic ketones in high concentration in the condensable gases. First order kinetics results from *ss*-NMR showed low activation energies, in the range of 11.71-25.37 kJ mol<sup>-1</sup>. Finally, the reduction results with hematite showed that the torrefied biomasses have a greater reduction potential when compared to the as-received biomasses. The XPS results showed the presence of Fe and the oxides Fe<sub>2</sub>O<sub>3</sub>, Fe<sub>3</sub>O<sub>4</sub> and FeO and the conversion results indicated that the PP biomass has the greatest potential for reduction, followed by CV and CC. The values were 54.52, 51.28 and 50.34%, respectively.

**Keywords:** Solid waste. Wood waste. Thermal conversion. Iron ore reduction.

## RESUMO

Visando a redução das emissões de CO<sub>2</sub> e propor a valorização de resíduos de madeira, esse trabalho teve como objetivo produzir combustível sólido a partir da torrefação dessas biomassas para serem aplicados como uma alternativa ao coque metalúrgico no processo de redução do minério de ferro. Nesse contexto, inicialmente foram selecionadas quatro biomassas para o estudo: serragem de *eucalipto* (SE), *pellet* de *Pine* (PP), cavaco de *Pine* (CV) e casca de *Pine* (CC). Todos os materiais utilizados tratam-se de resíduos, exceto o *pellet*, que são resíduos já compactados e melhorados. Para a aplicação proposta, o conhecimento das características químicas e físicas das biomassas é essencial para avaliar a sua eficiência no processo. Para isso, foram determinadas as características geométricas, grindabilidade e análise imediata. Os resultados dessas análises mostraram que a serragem não seria um material adequado para a aplicação proposta por apresentar menor teor de carbono fixo comparado às outras biomassas. Posteriormente, foram determinados a composição elementar, o poder calorífico, a composição das frações lignocelulósicas, a análise de grupos funcionais (FTIR) e caracterização por ressonância magnética nuclear (*ss*-NMR). O efeito dos parâmetros operacionais sobre o processo de torrefação foi investigado utilizando ensaios termogravimétricos não-isotérmicos a partir da temperatura ambiente até 300 °C, utilizando biomassas com diferentes tamanhos de partícula (<106 µm e 106-300 µm), sob atmosfera inerte ou oxidante. Após avaliação desses parâmetros, os ensaios de torrefações foram realizados em reator de leito fixo, com temperaturas de 250 e 290 °C, tempos de residência de 30 e 60 min e atmosfera inerte. Com as biomassas torrefadas, foram realizados ensaios não-isotérmicos em analisador termogravimétrico visando avaliar a reatividade dessas biomassas com CO<sub>2</sub>. A partir dos resultados das biomassas torrefadas que apresentaram maior reatividade com CO<sub>2</sub>, foram determinados os parâmetros ótimos de temperatura e tempo de residência para a torrefação. Posteriormente, as mesmas caracterizações citadas anteriormente foram realizadas para as biomassas torrefadas que apresentaram maior reatividade. Ainda, foi proposta uma metodologia utilizando os resultados de *ss*-NMR para a obtenção de parâmetros cinéticos de torrefação. Análise das frações líquida e gasosa geradas durante a torrefação também foram realizadas. Por fim, foram feitos ensaios para avaliar a redução do óxido hematita (Fe<sub>2</sub>O<sub>3</sub>) a partir das biomassas torrefadas. Os resultados de caracterização das biomassas mostraram que as amostras selecionadas possuem um baixo teor de umidade e de cinzas, o que é favorável para a sua utilização como combustível e alto teor de matéria volátil o que indica que combustíveis desse material possuem facilidade de ignição mesmo em temperaturas relativamente baixas. Além disso, pôde-se avaliar que a composição química de PP e CV são muito semelhantes enquanto CC apresentou maior teor de lignina em sua composição. Os resultados de reatividade com CO<sub>2</sub> apontaram que as melhores condições operacionais de torrefação de CC foram de 250 °C e 60 min enquanto PP e CV foram de 290 °C e 30 min, sendo que a biomassa torrefada CC apresentou menor reatividade provavelmente devido ao alto teor de lignina. Aqui nota-se a importância de se conhecer a composição química do material estudado. A torrefação gerou uma baixa quantidade de gases, mesmo no maior tempo de residência e a presença de lignina em alta concentração produziu gases não condensáveis ricos em hidrogênio e cetonas alifáticas em alta concentração nos gases condensáveis. Os resultados de cinética de primeira ordem a partir de *ss*-NMR mostraram baixas energias de ativação, na faixa de 11,71-25,37 kJ mol<sup>-1</sup>. Por fim, os resultados de redução com hematita mostraram que as biomassas torrefadas têm maior potencial de redução quando comparadas às biomassas *as-received*. Os resultados de XPS mostraram a presença de Fe e dos óxidos Fe<sub>2</sub>O<sub>3</sub>, Fe<sub>3</sub>O<sub>4</sub> e FeO e os resultados de conversão apontaram que a biomassa PP tem maior potencial de redução, seguida de CV e CC. Os valores foram de 54.52, 51.28 e 50.34%, respectivamente.

**Palavras-chave:** Resíduo de madeira. Conversão térmica. Redução de minério de ferro.

## RESUMO EXPANDIDO

### INTRODUÇÃO

Um dos grandes problemas atuais é a alta geração de resíduos sólidos e a elevada emissão de gás dióxido de carbono (CO<sub>2</sub>), um dos gases causadores do efeito estufa. A Lei nº. 12.305/2010, que dispõe sobre a Política Nacional de Resíduos Sólidos, e diversos acordos e protocolos, como o Acordo de Paris na 21ª Conferência das Partes da Convenção-Quadro das Nações Unidas sobre Mudanças Climáticas em 2015, avançaram no estabelecimento de políticas para o controle das emissões de CO<sub>2</sub>, necessitando de desenvolvimento científico e tecnológico para diminuição e/ou reaproveitamento de resíduos sólidos e CO<sub>2</sub>.

Nesse contexto, as indústrias metalúrgicas se tornam destaque pois encontram-se no ranking das indústrias que mais emitem CO<sub>2</sub> principalmente devido ao uso de coque em sua produção. Por outro lado, estão as indústrias madeireira e de papel e celulose, as quais geram resíduos sólidos como lascas de madeira, serragem, maravalha e cascas de árvores provenientes do corte de árvores e da produção de madeira. Esses resíduos, também conhecidos como biomassas florestais, são matéria-prima que possuem grande abundância, renovabilidade, neutralidade de CO<sub>2</sub> e composição química com grande possibilidade de gerar produtos com maior valor agregado através de rotas de conversão.

Com isso, vislumbrou-se a utilização dessas biomassas em substituição ao coque metalúrgico visando assim a diminuição das emissões de CO<sub>2</sub> bem como a redução e utilização desses resíduos sólidos. Porém, o uso da biomassa como combustível sólido é atualmente limitado pelo seu alto teor de umidade, baixo poder calorífico, alto teor de oxigênio, natureza hidrofílica, baixa densidade energética e baixa eficiência de combustão. Assim, um pré-tratamento da biomassa através de processos termoquímicos é uma alternativa para superar as desvantagens e melhorar a produção de biocombustíveis sólidos de alta qualidade.

A torrefação é considerada um pré-tratamento promissor para biomassa, que é realizado em condições amenas para obter uma biomassa sólida torrefada. Esta técnica consiste em um processo de conversão térmica que normalmente é realizado em uma faixa de temperatura entre 200 e 300 °C. Após a torrefação, o material torrefado apresenta características de maior hidrofobicidade porque a maior parte de sua parte volátil e leve é extraída pelo aumento da temperatura. Além disso, o material torrefado pode ser transportado e armazenado com mais facilidade, pois diminui de tamanho, retarda a taxa de biodegradação e pode ser um tratamento inicial para produção de biocombustíveis e possíveis adsorventes.

Com isso esse trabalho propôs-se a estudar a utilização de biomassas florestais recebidas e torrefadas na aplicação em processos metalúrgicos em substituição ao coque. Para isso foram realizados estudos das propriedades das biomassas torrefadas e da eficiência do processo de torrefação bem como dos parâmetros operacionais e das características físico-químicas da biomassa bruta. Portanto, é essencial uma avaliação inicial das condições ótimas para torrefação de biomassa através de testes experimentais em escala laboratorial para então serem avaliadas no processo de redução de minério de ferro e posteriormente aplicação em escala industrial.

### OBJETIVOS

O objetivo geral deste trabalho foi investigar a cinética e o mecanismo de torrefação da biomassa lenhosa em combustível sólido com características adequadas para ser aplicado como fonte de energia e agente oxidante nos processos metalúrgicos. Adicionalmente foram

avaliadas características físicas e químicas das biomassas residuais (recebida e torrefada), a influência de parâmetros como taxa de aquecimento, temperatura, tempo de residência e tamanho de partícula no processo de torrefação de cada biomassa visando identificar as condições experimentais de torrefação adequadas para obtenção de combustível útil para aplicação em processos metalúrgicos. Por fim, foram analisados os produtos de torrefação não condensáveis e condensáveis e verificado as melhores condições experimentais para aplicação de biomassa torrefada na redução de minério de ferro.

## METODOLOGIA

A metodologia desenvolvida nesse estudo consistiu na avaliação de quatro biomassas lignocelulósicas, Pellet (PP) – gênero *Pinus*, Serragem (SE) – gênero *Eucalyptus*, Casca (CC) – gênero *Pinus* e Casca (CV) – gênero *Pinus*. Inicialmente, foi analisada apenas a biomassa PP, avaliando suas características físico-químicas por meio da análise imediata, da análise elementar, da espectroscopia no infravermelho com transformada de Fourier (FT-IR) e do poder calorífico superior (HHV). As amostras foram selecionadas aleatoriamente, trituradas em moinho de facas e separadas em diferentes tamanhos de partícula <106 µm e 106-300 µm.

Para avaliar os parâmetros de torrefação da biomassa PP foram realizados ensaios termogravimétricos com amostras com tamanho de partícula <106 µm e 106-300 µm. A torrefação foi realizada à temperatura de 350 °C, com taxa de aquecimento de 10 °C min<sup>-1</sup>, sob atmosfera inerte com aplicação de nitrogênio (N<sub>2</sub>) e atmosfera oxidante com ar sintético (Ar). Com os resultados desse ensaio foram escolhidos os parâmetros operacionais para torrefação utilizando analisador termogravimétrico. Os ensaios de torrefação ocorreram nas temperaturas de 270 °C e 290 °C em atmosfera inerte e 245 °C em atmosfera oxidante, utilizando tempos de residência de 15 e 60 minutos.

Foram realizados testes de reatividade não isotérmica utilizando um analisador termogravimétrico para analisar 40 mg de amostra a uma taxa de aquecimento de 10 °C min<sup>-1</sup> até atingir a temperatura de 900 °C. Por fim, foi realizada uma análise estatística com os resultados obtidos visando avaliar a influência e os melhores parâmetros de temperatura e tempo de residência no rendimento da biomassa torrefada.

Posteriormente, todas as amostras foram selecionadas aleatoriamente, trituradas em moinho de facas, separadas em tamanhos de partícula de 106-300 µm e caracterizadas por análise imediata. Com base nos resultados obtidos nessa etapa, a biomassa SE foi eliminada deste estudo, continuando apenas com as biomassas de PP, CC e CV.

A torrefação das biomassas PP, CC e CV foi feita em um reator tubular de leito fixo composto por um cilindro concêntrico de quartzo nas temperaturas de 250 °C e 290 °C, com tempos de residência de 30 min e 60 min e em atmosfera inerte. Esses parâmetros foram escolhidos de acordo com os resultados da análise termogravimétrica das três biomassas. Utilizou-se aproximadamente 1g de amostra recebida, ou seja, sem trituração. Em seguida, as biomassas torrefadas foram avaliadas qualitativamente em analisador termogravimétrico na presença de CO<sub>2</sub>. A reatividade ao CO<sub>2</sub> da biomassa torrefada foi determinada de forma não isotérmica até 900 °C com taxa de aquecimento de 10 °C min<sup>-1</sup> em atmosfera de CO<sub>2</sub> com vazão de 100 mL min<sup>-1</sup>.

Após a escolha dos parâmetros ótimos de torrefação, novas caracterizações das biomassas foram realizadas. Tanto a biomassa recebida quanto a torrefada foram caracterizadas por análise imediata, análise elementar, espectroscopia no infravermelho com transformada de Fourier (FT-IR), poder calorífico superior, poder calorífico superior (HHV), Ressonância Magnética Nuclear (*ss*-NMR) e composição de lignina, celulose e hemicelulose.

Com os resultados de *ss*-NMR das amostras torrefadas, um novo estudo foi proposto para o cálculo de parâmetros cinéticos como energia de ativação. Para isso, assumiu-se que a decomposição seguiu uma cinética de primeira ordem e que a conversão foi proporcional às áreas dos picos das curvas de *ss*-NMR. Além disso, após a torrefação do reator, os gases condensáveis foram caracterizados utilizando um espectrômetro de massa por cromatografia gasosa (GC-MS) e os gases não condensáveis foram continuamente detectados utilizando um analisador de gases.

Por fim, foram realizados os testes de redução do minério de ferro hematita utilizando biomassas recebidas e torrefadas. Inicialmente, as biomassas foram separadas em tamanho de partícula <106 µm e misturadas na proporção de 1:1 (50%/50%) com óxido de ferro hematita (Fe<sub>2</sub>O<sub>3</sub>). A redução do óxido de ferro (hematita) foi investigada experimentalmente por análise termogravimétrica (TGA) utilizando 15 mg de mistura, taxa de aquecimento de 10 °C min<sup>-1</sup> e vazão de 100 mL N<sub>2</sub> min<sup>-1</sup>.

Os experimentos foram feitos utilizando apenas as biomassas, apenas a hematita e as misturas. Os materiais foram aquecidos da temperatura ambiente até 105°C e mantidos por 10 minutos para remover a umidade. Em seguida, uma taxa de aquecimento constante de 10 °C min<sup>-1</sup> foi implementada até atingir 1000 °C. Os resultados da redução foram avaliados quanto à cor, por meio de fotos com microscópio, análise termodinâmica, espectroscopia de fotoelétrons de raios X (XPS), grau de redução (ΔW) e cálculo de conversão de redução de minério de ferro.

## RESULTADOS E DISCUSSÃO

Os primeiros resultados obtidos foram em relação à composição da biomassa PP. Em relação à composição química, pôde-se verificar que o conteúdo de materiais voláteis, cinzas, umidade e carbono fixo mostrou o potencial positivo da utilização da biomassa como combustível. Em relação ao tamanho de partícula (<106 µm e 106–300 µm), os resultados apontaram que houve menor perda de massa ao utilizar biomassa de tamanhos de partículas maiores (106–300 µm) em atmosfera inerte.

Quanto à análise térmica, essa apontou que a melhor temperatura de torrefação em atmosfera oxidante foi de 245 °C e em atmosfera inerte foi de 270 e 290 °C. Utilizando estas condições, foram realizados testes de torrefação com tempos de residência de 15 e 60 min e mostraram que temperaturas mais altas e tempos de residência mais longos diminuem o rendimento de massa.

Quanto à análise de reatividade com CO<sub>2</sub>, a biomassa PP torrefada a 290 °C, 60 min e em atmosfera inerte apresentou o resultado e reatividade mais satisfatórios. Em relação ao rendimento, os resultados mostraram que temperaturas mais altas e tempos de residência mais longos diminuem o rendimento de massa. De acordo com a análise estatística, constatou-se que é possível combinar temperaturas mais elevadas com tempos de residência mais baixos, ou vice-versa, para obter rendimentos de massa satisfatórios. Assim, considerando tanto o rendimento de massa quanto a reatividade com CO<sub>2</sub>, as melhores condições de torrefação para biomassa de PP são em atmosfera inerte, a 290 °C e 15 min.

Ao realizar os ensaios com todas as biomassas PP, CV, CC e SE verificou-se que apesar da biomassa SE apresentar baixo teor de cinzas (menos de 0,7%), o valor de carbono fixo de ~13% e a dificuldade de moagem, provavelmente devido ao seu alto teor de lignina e celulose, foram fatores determinantes para a não continuidade do processo. Os resultados de caracterização química das biomassas PP, CV e CC mostraram que são biomassas adequadas para a obtenção de combustíveis.

Os testes termogravimétricos das biomassas foram essenciais para a escolha inicial dos parâmetros operacionais para torrefação, sendo esses de 250 °C e 290 °C para temperatura e 30 e 60 minutos para tempo de residência em atmosfera inerte. Os resultados da avaliação da reatividade das biomassas torrefadas com CO<sub>2</sub> mostraram que o CC apresentou menor reatividade em relação à PP e CV, possivelmente devido ao maior teor de lignina. Os parâmetros ótimos de torrefação escolhidos nesta análise foram 250 °C e 60 minutos para CC e 290 °C e 30 minutos para PP e CV.

A caracterização química das biomassas torrefadas evidenciou diminuição no teor de materiais voláteis e aumento no teor de carbono fixo, mostrando assim melhoria nas características químicas para aplicação em processos metalúrgicos. Os resultados da caracterização lignocelulósica indicaram que as biomassas PP e CV apresentaram composições químicas muito semelhantes enquanto a biomassa CC foi a que apresentou maior quantidade de lignina em sua composição.

A nova metodologia proposta para obtenção de parâmetros cinéticos a partir dos resultados de *ss*-NMR apresentou baixos valores de energia de ativação de torrefação, em torno de 11,71-25,37 kJ mol<sup>-1</sup>. A fração líquida, composta por gases condensáveis gerados durante a torrefação, apresentou elevada concentração de cetonas alifáticas na composição com maior presença de lignina. Durante a torrefação foi gerada uma pequena quantidade de gás, mesmo no tempo de permanência mais longo. A presença de lignina em alta concentração (biomassa CC) produziu gases não condensáveis ricos em hidrogênio.

Os ensaios de redução de óxido de ferro hematita utilizando biomassas indicam que a redução ocorreu ao observar a coloração das amostras antes e após os ensaios termogravimétricos. A hematita possui uma coloração muito característica, vermelho intenso, a qual predominou mesmo após mistura com as biomassas. Após os testes de redução a coloração das amostras finais tornou-se mais escura, como preto e cinza escuro, indicando assim a ocorrência de redução.

Com as curvas TGA e DTG foi possível observar a perda de massa de cada amostra bem como os picos e as faixas de temperatura em que ocorreu cada redução. Comparando os resultados obtidos neste estudo com a literatura, acredita-se que a partir de 500 °C ocorreu a redução gradual de Fe<sub>2</sub>O<sub>3</sub>→Fe<sub>3</sub>O<sub>4</sub>→FeO→Fe, nas seguintes faixas de temperatura, respectivamente, 650-750 °C, 750-860 °C, 860-1000°C. Ainda nas curvas DTG, foi visualizado um pico em temperatura mais baixa, em torno de 350 °C. Embora este pico esteja relacionado à desvolatilização da biomassa, foi possível verificar pelos valores de ΔW e pela análise termodinâmica que a ocorrência de redução também é possível nesta temperatura.

Os resultados da caracterização XPS realizada nas misturas de hematita com biomassa torrefada após passar pelo processo de redução mostraram a presença de Fe e dos óxidos Fe<sub>2</sub>O<sub>3</sub>, Fe<sub>3</sub>O<sub>4</sub> e FeO. Os resultados da conversão de redução com hematita mostraram que as biomassas torrefadas apresentaram maior potencial de redução quando comparadas às biomassas recebidas. Apontaram também que a biomassa PP tem o maior potencial de redução, seguida por CV e CC. Os valores foram 54,52, 51,28 e 50,34%, respectivamente. Por fim, o uso de biomassa torrefada apresentou resultados satisfatórios na aplicação para redução de minério de ferro hematita.

## CONCLUSÃO

Com a realização deste estudo foi possível verificar que o conhecimento das características físicas, químicas e térmicas do material é essencial para avaliar adequadamente sua eficiência na aplicação proposta, assim como conhecer as condições experimentais ótimas de torrefação. Além disso, pôde-se verificar com esse estudo que os principais constituintes da



biomassa (celulose, hemiceluloses e lignina) são afetados de diversas maneiras pela torrefação, dependendo de sua reatividade. O alto teor de lignina presente na biomassa CC tornou a biomassa torrefada menos reativa, provavelmente devido ao papel protetor da celulose e lignina durante a torrefação.

Ainda, a torrefação gerou uma baixa quantidade de gases, mesmo no maior tempo de residência. A fração de gases condensáveis, não condensáveis e biomassa sólida torrefada é quase constante para toda a biomassa estudada neste trabalho. Os estudos de *ss*-NMR e sua aplicação na avaliação dos parâmetros cinéticos mostraram baixas energias de ativação para a decomposição dos componentes lignocelulósicos da biomassa.

Por fim, os resultados de redução de minério de ferro utilizando biomassa apontaram que as misturas que continham biomassa torrefada apresentaram maiores avanços quando misturadas com biomassas recebidas, mostrando assim a importância do processo de torrefação nesta aplicação. A maior conversão foi a mistura com PP torrefada seguida de CV torrefada e CC torrefada com valores de 54,52, 51,28 e 50,34%, apontando-se assim que o uso de biomassa torrefada para redução de minério de ferro é promissor.

**Palavras-chave:** Resíduo de madeira. Conversão térmica. *ss*-NMR. Reatividade com CO<sub>2</sub>. Redução de minério de ferro.

## LIST OF FIGURES

Figure 2.1 - Thermochemical conversions, operational parameters and products. ....	35
Figura 2.2 - Types and operating conditions of torrefaction. ....	38
Figure 2.3 - Changes in physical and chemical properties of forest residual biomass (lignocellulosic). ....	48
Figure 2.4 - Number of articles published since the first article published using the word “torrefaction”. ....	50
Figure 3.1 – General methodology on thesis. ....	60
Figure 4.1 - Schematic diagram of materials and methods. ....	65
Figure 4.2 – Images of PP biomass: (a) original; (b) 106-300 $\mu\text{m}$ ; and (c) 106 $\mu\text{m}$ . ....	68
Figure 4.3 - FTIR spectrum for PP biomass of 106 and 106-300 $\mu\text{m}$ . ....	70
Figure 4.4 – TGA and DTA torrefaction curves of PP biomass under different operational conditions: (a) particle size 106 $\mu\text{m}$ and under $\text{N}_2$ ; (b) particle size 106-300 $\mu\text{m}$ and under $\text{N}_2$ ; (c) particle size <106 $\mu\text{m}$ and under air; (d) particle size 106-300 $\mu\text{m}$ and under air. ....	72
Figure 4.5 - Torrefaction profiles under inert atmosphere ( $\text{N}_2$ ) and oxidizing atmosphere (synthetic air) at 270, 290 and 245 $^\circ\text{C}$ and residence times of 15 and 60 min. (a) TGA curves of mass (%) vs. time (min) and (b) DTA curves ( $\mu\text{V mg}^{-1}$ ) vs. time (min). ....	74
Figure 4.6 - Response curves (a) Pareto chart, (b) Predicted vs. observed values, (c) 2D response surface and (d) 3D response surface. ....	77
Figure 4.7 - $\text{CO}_2$ reactivity of torrefied PP biomass under different operating conditions. ....	78
Figure. S4.1 – Non-isothermal tests of biomass in inert and oxidizing atmosphere with particle sizes of <106 $\mu\text{m}$ and 106-300 $\mu\text{m}$ . ....	85
Figure S4.2 – Reactivity with $\text{CO}_2$ of torrefied biomass under different operating conditions in terms of mass (%) and temperature ( $^\circ\text{C}$ ). ....	85
Figure 5.1 - Diagram of the biomass torrefaction system. ....	91
Figure 5.2 - Side section of the fixed-bed tubular reactor. ....	91
Figure 5.3 - Reactivity evaluation of torrefied biomass with $\text{CO}_2$ . ....	96
Figure 6.1 - Thermal decomposition of biomasses CC (a), CV (b), and PP (c) under inert atmosphere. ....	108
Figure 6.2 - FTIR of in natura and torrefied biomass samples. ....	112
Figure 6.3 - NMR of CV and PP biomasses samples. ....	115

Figure 6.4 - Percentage of torrefied biomass, condensable and non-condensable gases and from torrefied biomasses. ....	119
Figure 6.5 - Condensable gases fraction (a) and evolution of non-condensable gases during the torrefaction of CC (250 °C, 60 minutes) (b); CV (290 °C, 30 minutes) (c); and PP (290 °C, 30 minutes) (d). ....	121
Figure S6.1 - Arrhenius plot and regression linear for CV and PP. ....	127
Figure 7.1 - Images of biomasses (as received and torrefied), hematite and mixture before reduction.....	141
Figure 7.2 - TGA and DTG reduction experiments .....	145
Figure 7.3 - (a) Direct reduction reactions (b) Boudouard and indirect reduction reactions. ....	149
Figure 7.4 – XPS characterization for mixtures using biomass torrefied and hematite. ....	154
Figure 7.5 – TGA theoretical, TGA experimental and $\Delta W$ .....	155
Figure S7.1 – Images of biomasses, hematite and mixture before and after reduction.....	162
Figure S7.2 – Preliminary tests a) and b) TGA and DTG of the as received biomass, hematite and mixtures of biomass and hematite using different particle sizes and 5 mg of sample c) e d) TGA and DTG of the as received biomass, hematite and mixtures of biomass and hematite varying nitrogen flow (10, 50 e 100 mL min <sup>-1</sup> ).....	163
Figure S7.3 – Images of mixture after reduction using 3 different flow rates. ....	164

## LIST OF TABLES

Table 2.1 - Lignocellulosic biomass and its chemical composition .....	44
Table 2.2 - Chemical, physical and thermal characteristics of metallurgical coke .....	51
Table 4.1 - Composition of PP biomass. ....	69
Table 4.2 - ANOVA of the regression model representing the mass yield of PP biomass after torrefaction at 270 and 290 °C and residence time of 15 and 60 min.....	75
Table 5.1 - Parameters proximate analysis.....	90
Table 5.2 - Physical characteristics of SE residual biomass.....	93
Table 5.3 - Chemical characteristics of biomasses in dry base. ....	94
Table 6.1 - Torrefied biomass yield and images of in natura and torrefied biomasses under different experimental conditions.....	109
Table 6.2 - Characteristics of in natura and torrefied biomasses.....	111
Table 6.3 - FTIR spectrum of raw wood. ....	113
Table 6.4 - Resonance assignment of <sup>13</sup> C CP-MAS spectrum of biomasses .....	116
Table 6.5 - Pseudo first order kinetic law considering different decays of the <i>ss</i> -NMR signals.....	118
Table S6.1 – Normalized area of different <i>ss</i> -NMR signals for biomasses after torrefaction under different operational conditions.....	128
Table 7.1 - Composition of biomasses. ....	137
Table 7.2 - Literature using Thermogravimetric analysis for ore reduction. ....	139
Table 7.3 - Temperatures occur reduction.....	147
Table 7.4. Range of increase of T (°C) in which reaction occurs according to $\Delta G$ .....	150
Table 7.5 - Samples after reduction process.....	152
Table 7.6 - Binding energies of iron oxides .....	154
Table 7.7 - Conversion related to iron ore reduction.....	157
Table S7.1 - Gibbs free energy values generated by Factsage software .....	165

## LIST OF DE ABBREVIATIONS AND ACRONYMS

ANOVA	Statistical analysis of variance
ASTM	American Society for Testing and Materials
CC	Biomass bark <i>Pine</i> genus
CCS	Carbon Capture and Storage
CCT	Biomass torrefied bark <i>Pine</i> genus
CCT106 $\mu$ m	Biomass torrefied bark <i>Pine</i> genus with particle size 106 $\mu$ m
CCT106 $\mu$ m+HM	Biomass torrefied bark <i>Pine</i> genus with particle size 106 $\mu$ m plus hematite
CCT25060	Biomass torrefied bark <i>Pine</i> genus at 250 °c and 60 minutes
CC106 $\mu$ m	Biomass as received bark <i>Pine</i> genus with particle size 106 $\mu$ m
CC106 $\mu$ m+HM	Biomass as received bark <i>Pine</i> genus with particle size 106 $\mu$ m plus hematite
CP-MAS	Cross-polarization and magic angle spinning
CV	Biomass chips <i>Pine</i> genus
CVT	Biomass torrefied chips <i>Pine</i> genus
CVT106 $\mu$ m	Biomass torrefied chips <i>Pine</i> genus with particle size 106 $\mu$ m
CVT106 $\mu$ m+HM	Biomass torrefied chips <i>Pine</i> genus with particle size 106 $\mu$ m plus hematite
CVT29030	Biomass torrefied chips <i>Pine</i> genus at 290 °c and 30 minutes
CV106 $\mu$ m	Biomass as received chips <i>Pine</i> genus with particle size 106 $\mu$ m
CV106 $\mu$ m+HM	Biomass as received chips <i>Pine</i> genus with particle size 106 $\mu$ m plus hematite
df	Degrees of freedom
DTG	Differential thermogravimetric analysis
F	F value estatistic
FT-IR	Fourier transform infrared spectroscopy
GC-MS	Gas chromatography mass spectrometry
HHV	Higher heating value
HI-ACT	Hydrogen integration for accelerated energy transitions
HM	Hematite
ICL	Imperial college london
ISS	Internation student suport
MAS	Magic angle spinning
MC	Maize cob
MS	Medium square
UKCCSRC	United kingdom carbon capture & storage research community
UKERC	United kingdom energy research centre
UV	Ultraviolet-visible spectrophotometer
p	p value estatistic
PCI	Pulverized charcoal injection
PH	Peanut hull

PP	Biomass pellet <i>Pine</i> genus
PPT	Biomass torrefied pellet <i>Pine</i> genus
PPT106µm	Biomass torrefied pellet <i>Pine</i> genus with particle size 106µm
PPT106-300µm	Biomass torrefied pellet <i>Pine</i> genus with particle size 106-300µm
PPT106µm+HM	Biomass torrefied pellet <i>Pine</i> genus with particle size 106µm plus hematite
PPT106-300µm+HM	Biomass torrefied pellet <i>Pine</i> genus with particle size 106-300µm plus hematite
PPT29030	Biomass torrefied pellet <i>Pine</i> genus at 290 °c and 30 minutes
PP106µm	Biomass as received pellet <i>Pine</i> genus with particle size 106µm
PPT106-300µm	Biomass as received pellet <i>Pine</i> genus with particle size 106-300µm
PP106-300µm+HM	Biomass as received chips <i>Pine</i> genus with particle size 106µm plus hematite
PS	Pine sawdust
RL	Rice lemma
SE	Biomass as received sawdust Eucalypto genus
SS	Sum of square
<i>ss</i> -NMR	Solid-State nuclear magnetic resonance
TGA	Thermogravimetric analysis
UFSC	Federal University of Santa Catarina
XPS	X-ray Photoelectron Excited Photoelectron Spectroscopy

## LIST OF SYMBOLS

Symbol	Description	Unit
A	Frequency factor or pre-exponential factor	min <sup>-1</sup>
CF	Fixed carbon contente	%
CZ	Ash contente	%
$\frac{dm}{dt}$	Change in mass loss (mg) at time t (min)	mg min <sup>-1</sup>
$\frac{d\alpha}{dt}$	Conversion rate as a function of time	min <sup>-1</sup>
HHV	Higher calorific value	MJ kg <sup>-1</sup>
Ea	Activation energy	J mol <sup>-1</sup>
k	Temperature-dependent kinetic constant	min <sup>-1</sup>
MV	Volatile material	%
$m_0$	Initial mass	mg
$m_{(t)}$	Mass of the sample as a function of time	mg
$m_{\text{final}}$	Mass after the torrefaction process	mg
$m_{\text{initial}}$	Mass before the torrefaction process	mg
$m_{\text{rotor}}$	Mass utilized in the ss NMR analysis	mg
$m_{2i}$	Initial mass in segment 2 of the immediate analysis	mg
$m_{3f}$	Final mass in segment 3 of the immediate analysis	mg
$m_{4f}$	Final mass in segment 4 of the immediate analysis	mg
$m_{6f}$	Final mass in segment 6 of the immediate analysis	mg
R	Universal gas constant	J K <sup>-1</sup> mol <sup>-1</sup>
r	Reaction rate	min <sup>-1</sup>
T	Temperature	K
t	Residence time of torrefaction	minute
$t_0$	Initial time of torrefaction	minute
$TGA_B$	TGA of the single biomass	%
$TGA_{\text{experimental}}$	Actual or experimental TGA	%
$TGA_H$	TGA of the single hematite	%
$TGA_{\text{theoretical}}$	TGA weigh changes of the single hematite ( $TGA_H$ ) and single biomass ( $TGA_B$ )	%
U	Moisture	%
$x_1$	Factor temperature	adimensional
$x_2$	Factor time	adimensional
$x_1x_2$	Interaction factor temperature and time	adimensional
Y	Solid yield	%
$y(x_1, x_2)$	Response variable (mass yield) at the level ( $x_1, x_2$ )	adimensional
$Y_B$	Mass fractions of biomass	adimensional
$Y_H$	Mass fractions of hematite	adimensional
X	Mass conversion	%

$\alpha$	Conversion	adimensional
$\Delta m$	Diference between $m_0$ and $m_{(t)}$	mg
$\Delta G_0$	Gibbs free energy	<b>kJ mol<sup>-1</sup></b>
$\Delta W$	Degree of reduction	%
$\beta_0$	Population value of the mean of all responses	adimensional
$\beta_1 x_1$	Population values of temperature	adimensional
$\beta_2 x_2$	Population values of residence time	adimensional
$\beta_{12} x_1 x_2$	Population values of interaction effect	adimensional



## SUMMARY

1	GENERAL INTRODUCTION .....	29
1.1	OBJECTIVES .....	31
<b>1.1.1</b>	<b>General objective .....</b>	<b>31</b>
<b>1.1.2</b>	<b>Specific objectives .....</b>	<b>31</b>
1.2	CONTENT OF THESIS .....	32
1.3	REFERENCES .....	33
2	LITERATURE REVIEW .....	35
2.1	BIOMASS THERMAL CONVERSION PROCESSES .....	35
2.2	TORREFACTION .....	37
<b>2.2.1</b>	<b>Definitions and fundamental aspects .....</b>	<b>37</b>
<i>2.2.1.1</i>	<i>Types of Torrefaction.....</i>	<i>38</i>
<i>2.2.1.2</i>	<i>Conventional or dry torrefaction.....</i>	<i>38</i>
<i>2.2.1.3</i>	<i>Wet torrefaction.....</i>	<i>39</i>
<i>2.2.1.4</i>	<i>Microwave torrefaction .....</i>	<i>40</i>
<b>2.2.2</b>	<b>Operational conditions used in the biomass torrefaction processes .....</b>	<b>42</b>
2.3	RESIDUAL BIOMASSES .....	43
<b>2.3.1</b>	<b>Characteristics .....</b>	<b>44</b>
<b>2.3.2</b>	<b>Residual biomass from wood .....</b>	<b>46</b>
2.4	APPLICATIONS OF TORREFIED BIOMASSES .....	48
<b>2.4.1</b>	<b>Applications of torrefied biomass in the metallurgical industry.....</b>	<b>50</b>
<i>2.4.1.1</i>	<i>Metallurgical industry.....</i>	<i>50</i>
<i>2.4.1.2</i>	<i>Applications of torrefied biomass.....</i>	<i>52</i>
2.5	REFERENCES .....	53
3	GENERAL METHODOLOGY .....	59

4	INVESTIGATION OF THE THERMAL BEHAVIOR OF <i>PINE</i> WOOD PELLETS DURING TORREFACTION FOR APPLICATION IN METALLURGICAL PROCESSES <sup>1</sup> .....	62
4.1	INTRODUCTION .....	63
4.2	MATERIALS AND METHODS .....	65
4.2.1	<b>Biomass selection and preparation</b> .....	<b>65</b>
4.2.2	<b>Characterization</b> .....	<b>65</b>
4.2.3	<b>Evaluation of the thermal decomposition of <i>Pine</i> pellet (PP)</b> .....	<b>66</b>
4.2.4	<b>Torrefaction runs</b> .....	<b>66</b>
4.2.5	<b>Statistical analysis</b> .....	<b>67</b>
4.2.6	<b>Reactivity evaluation of torrefied biomass with CO<sub>2</sub></b> .....	<b>67</b>
4.3	RESULTS AND DISCUSSION .....	68
4.3.1	<b>Biomass characterization</b> .....	<b>68</b>
4.3.2	<b>Evaluation of thermal decomposition</b> .....	<b>71</b>
4.3.3	<b>Torrefaction of biomass</b> .....	<b>73</b>
4.3.4	<b>Statistical analysis</b> .....	<b>75</b>
4.3.5	<b>Reactivity evaluation of torrefied biomass with CO<sub>2</sub></b> .....	<b>76</b>
4.4	CONCLUSIONS .....	80
4.5	REFERENCES .....	81
4.6	SUPPLEMENTARY MATERIAL .....	84
5	EVALUATION OF THE REACTIVITY OF LIGNOCELLULOSIC BIOMASSES TORREFIED WITH CO <sub>2</sub> FOR APPLICATION IN ORE REDUCTION PROCESSES .....	86
5.1	INTRODUCTION .....	87
5.2	MATERIALS AND METHODS .....	88
5.2.1	<b>Selection and preparation of biomasses</b> .....	<b>88</b>
5.2.2	<b>Characterization of biomasses</b> .....	<b>89</b>
5.2.2.1	<i>Physical characteristics</i> .....	89

5.2.2.2	<i>Chemical characteristics</i> .....	89
<b>5.2.3</b>	<b>Torrefaction tests in a fixed bed reactor</b> .....	<b>90</b>
<b>5.2.4</b>	<b>Reactivity evaluation of torrefied biomass with CO<sub>2</sub></b> .....	<b>92</b>
5.3	RESULTS AND DISCUSSION.....	92
<b>5.3.1</b>	<b>Characterization of biomasses</b> .....	<b>92</b>
5.3.1.1	<i>Physical characteristics</i> .....	92
5.3.1.2	<i>Chemical characteristics</i> .....	93
<b>5.3.2</b>	<b>Evaluation of reactivity of torrefied biomass obtained under different experimental conditions.</b> .....	<b>94</b>
5.4	CONCLUSIONS .....	97
5.5	REFERENCES .....	97
6	MECHANISTIC INSIGHTS AND KINETICS OF TORREFACTION OF PINE WOOD BIOMASSES USING SOLID-STATE NMR <sup>2</sup> .....	100
6.1	INTRODUCTION .....	101
6.2	MATERIALS AND METHODS .....	102
<b>6.2.1</b>	<b>Selection and preparation of biomasses</b> .....	<b>102</b>
<b>6.2.2</b>	<b>Evaluation of the thermal decomposition of biomass</b> .....	<b>103</b>
<b>6.2.3</b>	<b>Torrefaction experiments in a fixed bed reactor</b> .....	<b>103</b>
<b>6.2.4</b>	<b>Physico-chemical characterization</b> .....	<b>104</b>
<b>6.2.5</b>	<b>Characterization of condensable and non-condensable gases from the torrefaction process</b> .....	<b>105</b>
<b>6.2.6</b>	<b><i>ss</i>-NMR analysis and kinetics of torrefaction</b> .....	<b>106</b>
6.3	RESULTS AND DISCUSSION.....	107
<b>6.3.1</b>	<b>Evaluation of thermal decomposition of biomasses under inert atmosphere</b> .....	<b>107</b>
<b>6.3.2</b>	<b>Characterization of in nature and torrefied biomass</b> .....	<b>110</b>
<b>6.3.3</b>	<b>Evaluation of torrefaction mechanism and kinetics using <i>ss</i>-NMR analysis</b>	<b>114</b>

<b>6.3.4</b>	<b>Characterization of condensable and non-condensable gases products from torrefaction.....</b>	<b>119</b>
6.4	CONCLUSIONS .....	122
6.5	REFERENCES .....	123
6.6	SUPPLEMENTARY MATERIAL .....	126
7	ADVANCING LOW CARBON IRON AND STEEL PRODUCTION THROUGH BIOMASS TORREFACTION UTILIZATION.....	133
7.1	INTRODUCTION .....	134
7.2	MATERIALS AND METHODS .....	136
<b>7.2.1</b>	<b>Selection and preparation of materials.....</b>	<b>136</b>
<b>7.2.2</b>	<b>Preparation of the mixture of biomass with hematite.....</b>	<b>138</b>
<b>7.2.3</b>	<b>Evaluation of iron oxide reduction using thermogravimetric analysis.....</b>	<b>138</b>
<b>7.2.4</b>	<b>Evaluation after process iron reduction .....</b>	<b>139</b>
7.3	RESULTS AND DISCUSSION.....	140
<b>7.3.1</b>	<b>Color changes for biomass+hematite mixture after thermal treatment and reduction.....</b>	<b>140</b>
<b>7.3.2</b>	<b>Thermogravimetric analysis for iron reduction .....</b>	<b>142</b>
<b>7.3.3</b>	<b>Thermodynamic analysis of the reduction process using biomass.....</b>	<b>148</b>
<b>7.3.4</b>	<b>Characterization of materials after iron oxide reduction.....</b>	<b>151</b>
7.4	CONCLUSIONS .....	158
7.5	REFERENCES .....	159
7.6	SUPPLEMENTARY MATERIAL .....	162
8	FINAL REMARKS .....	166
9	SUGGESTION FOR FUTURE WORK.....	168

## 1 GENERAL INTRODUCTION

One of the major current problems is the high generation of solid waste and the high emission of carbon dioxide gas (CO<sub>2</sub>), one of the gases that cause the greenhouse effect, by the metallurgical industries due to the use of coke in their production. Law n°. 12.305/2010, which provides for the National Solid Waste Policy, and different agreements and protocols, such as the Paris Agreement at the 21st Conference of the Parties to the United Nations Framework Convention on Climate Change in 2015 have advanced in establishing policies for the control of CO<sub>2</sub> emissions, requiring scientific and technological development to decrease and / or reuse of solid waste and CO<sub>2</sub>.

Currently, one of the major concerns involving politics and the environment is the large generation of solid waste. If this residue is disposed of inappropriately, the damage to the environment and the beings that live in it is incalculable. Reducing solid waste emissions, reuse, recycling, composting and energy use are some operational solutions to minimize the environmental impacts caused by this waste.

The wood industry is a very strong sector in countries like Canada, United States, Germany, Brazil and Indonesia. In Brazil the great production is based on tropical forests. Operations such as administration, processing, chemical treatments and modeling are present in this industrial sector. After processing, various products can be obtained, such as furniture, boards for civil construction, cellulose for papermaking, among other wood derivatives. In addition to these products, a lot of waste is also generated during the process.

Wood chips, sawdust, shavings and tree bark are some of the residues supplied from tree cutting and wood production. Yun, Clift and Bi [1] state that only 47% (approximately) of the tree logs that arrive at the sawmills are converted into profitable wood. One of the reasons for this low percentage is due to imperfections in the cut trees, generating considerable waste and high waste generation [1]. In addition, forest biomass is a raw material that has great abundance, renewability, CO<sub>2</sub> neutrality and chemical composition with a great possibility of generating products with greater added value through conversion routes [2],[3],[4].

Biomass can be used as an alternative to reduce gaseous emissions caused by non-renewable fuels, such as coal and coke [5], [6]. Moreover, biomass from forest management presents a chemical composition with a great possibility of generating products (liquid, solid and non-condensable gases) with higher added value after conversion [2]. The composition of this class of biomass consists of 10-25% of lignin, 20-40% hemicellulose and 35-55% cellulose [7], [8], [9].

The use of biomass as solid fuel is currently limited by its high moisture content, low calorific value, high oxygen content, hydrophilic nature, low energy density, low combustion efficiency, a tenacious and fibrous structure and their heterogeneous composition makes the design and control of the conversion processes more complicated [8], [10], [11], [12], [13], [14]. Thus, a pretreatment of biomass through thermochemical processes is an alternative to overcome the drawbacks and improve the production of high-quality solid biofuels.

Torrefaction is considered a promising pretreatment for biomass, which is performed under mild conditions to obtain a torrefied solid biomass, a type of torrefied biomass [13]. This technique consists of a thermal conversion process that is normally carried out in a temperature range between 200 and 300 °C [8], [15]. After torrefaction, the torrefied material has characteristics of greater hydrophobicity because most of its volatile and light part is extracted by increasing the temperature. In addition, the torrefied material can be more easily transported and stored as it decreases in size, slows down the rate of biodegradation and can be an initial treatment for the production of biofuels and possible adsorbents.

For the steel industry, the total replacement of fossil fuels by renewable sources is a challenge [16]. Traditionally, this industry uses coke made from coal as a raw material in blast furnaces, and coke accounts for about 93% of the total greenhouse gas emissions from the steel industry, with an emission intensity of approximately 2 t/t steel [17], [18]. As a result, several efforts to reduce the energy and carbon intensity of iron and steel production have been made and include best practices to reduce coke consumption through the use of pulverized coal (PC), natural gas, oil, waste plastics [19], or agricultural residues [16].

Therefore, the use of products derived from biomass to replace other non-renewable fuels (such as coke) contributes to the reduction of CO<sub>2</sub> emissions. Torrefied biomass and biocoke were considered suitable for use in blast furnaces, in addition to charcoal. Mousa *et al.* [6] reported that, in the blast furnace, charcoal had the greatest potential for partial replacement of loaded coke and total replacement for pulverized coal injection (PCI).

The lower crushing force of this material, however, still represents the main challenges for loading it into large modern blast furnaces. In the case of the use of torrefied biomass, the study presented interesting results in the mitigation of CO<sub>2</sub> emissions with the use of fuels derived from biomass, replacing the use of fossil fuels, with the injection of torrefied/pyrolyzed biomass in the blast furnace [6]. However, knowledge about large modern blast furnaces is still lacking.

Furthermore, the properties of the torrefied biomasses and the efficiency of the torrefaction process strongly depend on the operational parameters and the characteristics of

the raw biomass [20]. Among the operational parameters are the reaction atmosphere, temperature and residence time, while the characteristics of the biomass include the physical-chemical parameters. Therefore, an initial evaluation of the optimal conditions for biomass torrefaction through experimental tests at laboratory scale for each biomass and of the conditions for a given industrial application is essential.

## 1.1 OBJECTIVES

### 1.1.1 General objective

The general objective of this work was to investigate the kinetics and mechanism of torrefaction of wood biomass to solid fuel with suitable characteristics to be applied as an energy source and oxidizing agent in the metallurgical processes.

### 1.1.2 Specific objectives

In order to achieve the proposed general objective, it was necessary to carry out the following steps:

- to evaluate the physical and chemical characteristics of the residual biomass (as received and torrefied);
- to evaluate the influence of parameters such as heating rate, temperature, residence time and particle size in the torrefaction process of each biomass;
- to determine the kinetic parameters and to evaluate their influence on the torrefaction process of each biomass;
- to verify the suitable experimental conditions for the torrefaction of each residual biomass to obtain useful fuel to be applied in metallurgical processes;
- to analyze the characteristics of the torrefied materials under different operating conditions;
- to analyze the non-condensable and condensable torrefaction products;
- to verify the best experimental conditions for the application of torrefied biomass in the reduction of iron ore.

## 1.2 CONTENT OF THESIS

This study was divided into 9 chapters, with chapters 4 to 7 containing introduction, material and methods, results and discussion, conclusions and references. These chapters were presented in paper format and the references were presented at the end of each one.

Chapter 1: provides a general introduction to the subject discussed in this thesis, the general and specific objectives and, a brief explanation of the component chapters of the thesis.

Chapter 2: presents a literature review about torrefaction, experimental parameters, biomass and its applications.

Chapter 3: provides a general presentation of the methodology applied in the study.

Chapter 4: describes the study carried out for the investigation of the thermal behavior of *Pine* wood pellets during torrefaction for application in metallurgical processes. In this chapter, the optimal experimental conditions for torrefaction of pine wood pellets were evaluated based on the best of the torrefied biomass reactivity with CO<sub>2</sub>. This chapter has been published in the Journal of Materials Research and Technology, 19 (2022) 3749-3759. <https://doi.org/10.1016/j.jmrt.2022.06.082>.

Chapter 5: presents the evaluation of the reactivity of lignocellulosic biomasses torrefied with CO<sub>2</sub> for application in ore reduction processes. In this stage, pellet, bark and chips biomass were evaluated in different experimental conditions of torrefaction and its reactivity with CO<sub>2</sub>.

Chapter 6: mechanistic insights and kinetics of torrefaction of pine wood biomasses were presented. In this chapter, a new methodology for obtaining kinetic parameters using solid-state NMR technique was proposed. Furthermore, this chapter simplifies the physical, chemical and thermal characterizations, before and after torrefaction, of all studied biomasses. This chapter has been published in Journal of Analytical and Applied Pyrolysis, 172 (2023) 106019. <https://doi.org/10.1016/j.jaap.2023.106019>

Chapter 7: presents the study carried out applying the selected biomasses (as received and torrefied) in the reduction of iron ore.

Chapter 8: show the general remarks of this study.

Chapter 9: presentes suggestions for future work.



## 1.3 REFERENCES

- [1] Yun, H., Clift, R. and Bi, X. Environmental and economic assessment of torrefied wood pellets from British Columbia. *Energy Conversion and Management*, 2020, 208, pp. 112513. <https://doi.org/10.1016/j.enconman.2020.112513>
- [2] Arteaga-Pérez, L.E., Segura, C., Espinoza, D., Radovic, L. R., Jiménez, R. Jiménez, Torrefaction of *Pine radiata* and *Eucalyptus globulus*: A combined experimental and modeling approach to process synthesis, *Energy Sustain Dev.*, 2015, 29 pp 13-23. <https://doi.org/10.1016/j.esd.2015.08.004>
- [3] Chen, D., Li, J., Zhang, T., Li, S., Wang, J., Niu, W., Liu, Y., Zheng, A., Zhao, Z. Advancing biomass pyrolysis by torrefaction pretreatment: Linking the productions of bio-oil and oxygenated chemicals to torrefaction severity, *Fuel*, 330, 2022, pp. 125514, <https://doi.org/10.1016/j.fuel.2022.125514>
- [4] Xu, J., Huang, M., Hu, Z., Zhang, W., Li, Y., Yang, Y., Zhou, Y., Zhou, S., Ma, Z. Prediction and modeling of the basic properties of biomass after torrefaction pretreatment, *J. Anal. Appl. Pyrolysis* 2021, 159, pp. 105287. <https://doi.org/10.1016/j.jaap.2021.105287>
- [5] Fick, G., Mirgaux, O., Neau, P., Patisson, F. Using Biomass for Pig Iron Production: A Technical, Environmental and Economical Assessment, *Waste Biomass Valorization*, 2014, 5, pp. 43-55. <https://doi.org/10.1007/s12649-013-9223-1>
- [6] Mousa, E., Wang, C., Riesbeck, J., Larsson, M. Biomass applications in iron and steel industry: An overview of challenges and opportunities. *Renewable and Sustainable Energy Reviews*, [s.l.], v. 65, p. 1247-1266, 2016. <https://doi.org/10.1016/j.rser.2016.07.061>
- [7] Cai, J., He, Y., Yu, X., Banks, S. W., Yang, Y., Zhang, X., Yu, Y., Liu, R., Bridgwater, A. V. Review of physicochemical properties and analytical characterization of lignocellulosic biomass. *Renewable and Sustainable Energy Reviews*, 2017, 76, pp. 309-322. <https://doi.org/10.1016/j.rser.2017.03.072>
- [8] Chai, M., Xie, L., Yu, X., Zhang, X., Yang, Y., Rahman, M.M., Blanco, P.H., Liu, R., Bridgwater, A.V., Cai, J. Poplar wood torrefaction: Kinetics, thermochemistry and implications, *Renew. Sust. Energ. Rev.*, 2021, 143, pp. 110962. <https://doi.org/10.1016/j.rser.2021.110962>
- [9] Wang, C., Yuan, X., Li, S., Zhu, X. Enrichment of phenolic products in walnut shell pyrolysis bio-oil by combining torrefaction pretreatment with fractional condensation, *Renew. Energy*, 2021, 169, pp. 1317-1329. <https://doi.org/10.1016/j.renene.2021.01.112>
- [10] Bennett, J. P. and Kwong, K. S. Failure mechanisms in high chrome oxide gasifier refractories, *Metallurgical and Materials Transactions A*, 2011, 42, pp. 888-904 <https://doi.org/10.1007/s11661-011-0635-x>
- [11] Namkung, H., Park, J-H., Lee, Y-J., Song, G-S., Choi, J.W., Park, S-J., Kim, S., Liu, J., Choi, Y-C. Performance evaluation of biomass pretreated by demineralization and torrefaction for ash deposition and PM emissions in the combustion experiments, *Fuel*, 2021, 292, pp. 120379. <https://doi.org/10.1016/j.fuel.2021.120379>

- [12] Yan, B., Jiao, L., Li, J., Zhu, X., Ahmed, S., Chen, G. Investigation on microwave torrefaction: Parametric influence, TG-MS-FTIR analysis, and gasification performance, *Energy*, 2021, 220, pp. 119794. <https://doi.org/10.1016/j.energy.2021.119794>
- [13] Ong, H.C., Yu, K.L., Chen, W.-H., Pillejera, M.K., Bi, X., Tran, K.-Q., Pétrissans, A., Pétrissans, M. Variation of lignocellulosic biomass structure from torrefaction: A critical review, *Renew. Sustain. Energy Rev.*, 2021, 152, 111698. <http://doi.org/10.1016/j.rser.2021.111698>
- [14] van der Stely, M. J. C., Gerhauser, H., Kiel, J. H. A., Ptasinski, K. J. Biomass upgrading by torrefaction for the production of biofuels: A review, *Biomass and Bioenergy*, 2011, 35, pp. 3748-3762. <https://doi.org/10.1016/j.biombioe.2011.06.023>
- [15] Chen, W-H., Lin, B-J., Lin, Y-Y., Chu, Y-S., Ubando, A.T., Show, P.L., Ong, H.C., Chang, J-S., Ho, S-H., Culaba, A.B., Pétrissans A., Pétrissans, M. Progress in biomass torrefaction: Principles, applications and challenges, *Prog. Energy Combust. Sci.*, 2021, 82, pp. 100887. <https://doi.org/10.1016/j.peccs.2020.100887>
- [16] Uwaoma, R.C., Stokes, W. G., Bunt, J.R., Strydom, C.A., Matjie, R.H. A metallurgical coke replacement derived from torrefied wood chips pre-treated by wet oxidation, *Bioresource Technology Reports*, 2022, 19, pp. 101141. <https://doi.org/10.1016/j.biteb.2022.101141>
- [17] Weldegiorgis, F. S. and Franks, D. M. Social dimensions of energy supply alternatives in steelmaking: comparison of biomass and coal production scenarios in Australia, *Journal of Cleaner Production*, 2014, 84, pp. 281-288. <https://doi.org/10.1016/j.jclepro.2013.09.056>
- [18] Zhao, P., and Dong, P.L. Carbon emission cannot be ignored in future of Chinese steel industry, *Iron Steel*, 2018, 53, pp. 1-7. <https://doi.org/10.13228/j.boyuan.issn0449-749x.20180081>
- [19] Nwachukwu, C. M., Wang, C. and Wetterlund, E. Exploring the role of forest biomass in abating fossil CO<sub>2</sub> emissions in the iron and steel industry – The case of Sweden, *Applied Energy*, 2021, 288, pp. 116558. <https://doi.org/10.1016/j.apenergy.2021.116558>
- [20] Maree, Z., Strydom, C. A. and Bunt, J. R. Chemical and physical characterization of spent coffee ground torrefied biomass treated by a wet oxidation method for the production of a coke substitute, *Waste Management*, 2020, 113, pp. 422-429. <https://doi.org/10.1016/j.wasman.2020.06.025>

## 2 LITERATURE REVIEW

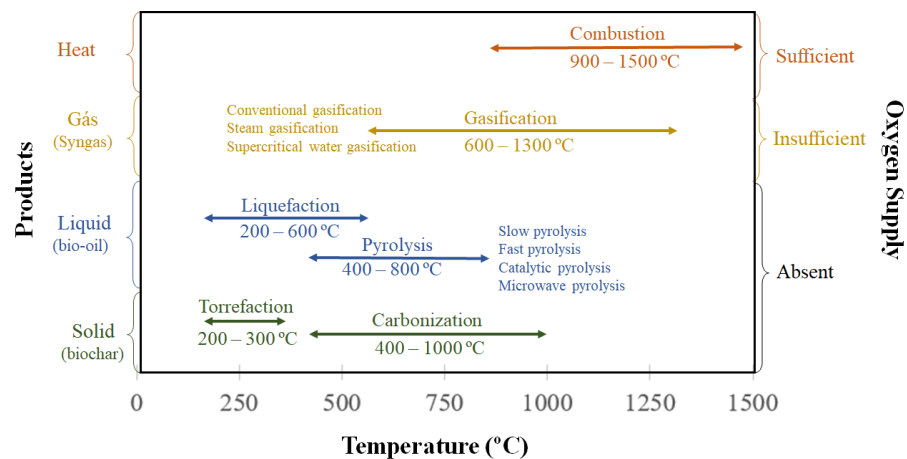
As previously mentioned, one of the major problems that Brazil and the world currently face is the high generation of solid waste and the difficulties for its environmentally correct disposal. Waste from the wood industries and the pulp and paper industries stands out here. As a result, alternatives such as reuse and recovery of these wastes have been addressed by researchers in recent years. Thus, in this topic, some technologies for thermal conversion of residual biomass used for the energy recovery of these materials were discussed, their advantages and disadvantages, and, finally, the choice of a better technology, as well as its operational parameters, to carry out this research.

### 2.1 BIOMASS THERMAL CONVERSION PROCESSES

Thermal conversion of biomass is the exposure of these materials to a relatively high temperature, which is capable of altering their chemical and physical composition. In the case of technologies that present cleaner treatments and energy recovery, thermochemical conversion is considered a promising alternative [1].

Combustion, pyrolysis, carbonization, gasification, torrefaction and liquefaction are examples of thermochemical conversions [2]. The differentiation of these is given by the different methods of operation such as oxygen supply and reaction temperature. Figure 2.1 illustrates the operating conditions cited for each thermochemical conversion using biomass as precursor, in addition to presenting the main products of each reaction.

Figure 2.1 - Thermochemical conversions, operational parameters and products.



Source: Adapted from Chen *et al.* [3].

Analyzing the Figure 2.1, it can be seen that carbonization, torrefaction, pyrolysis and liquefaction are carried out in conditions with the absence of oxygen, but they present different products. One reason is the exposure of materials to different temperatures. While liquefaction and torrefaction use lower temperatures (200-600 °C and 200-300 °C, respectively), carbonization and pyrolysis are operated at higher temperatures, reaching temperatures of up to 1000 °C. It can be said that torrefaction is a type of pyrolysis at low temperature and that carbonization is a type of slow pyrolysis at high temperatures.

Still on Figure 2.1, it can be noted that gasification occurs in an atmosphere with insufficient oxygen, while in combustion oxygen becomes essential for the process to occur. Regarding the use of temperature conditions, both are operated at high temperatures, reaching up to 1500 °C.

Regarding the products that can be obtained through these different methods, biofuels can be mentioned. Except combustion, all other technologies mentioned above can produce solid, liquid (alcohols, alkanes or bio-oil) and gaseous (methane or syngas) biofuels [2], [4]. Also, charcoal produced from biomass using these technologies can be applied in combustion as a solid fuel, in gasification as a raw material and in the metallurgical process as a reducing agent [3].

Although the aforementioned technologies have in common the production of biofuels, it is known that each product will have different physicochemical characteristics depending on its operating conditions (temperature, atmosphere and residence time) and also on the raw material used. However, a major disadvantage that unites pyrolysis, carbonization and gasification and combustion technologies is the use of high temperatures, which can lead to greater energy expenditure of equipment and, consequently, operating costs.

Furthermore, even if there are drying processes with dehydrators and paddle dryers, these equipment are insufficient to leave the sample with a low moisture content, making it impracticable to directly use thermochemical conversion processes such as combustion, gasification and pyrolysis. As a result, torrefaction has drawn the attention of researchers as this technology becomes an alternative as a thermal pre-treatment to reduce sample moisture [1].

In addition to using lower temperatures and producing a fuel similar to coal, during torrefaction, carbon dioxide capture can occur in the biomass growth stage, with this, negative carbon emissions can be obtained from the torrefied biomass. It is noteworthy that torrefaction also has its disadvantages such as low energy yield, however, it can be integrated with other thermal conversion processes or even iron manufacturing and make the process more efficient and economically viable compared to the use of a single process [3].

## 2.2 TORREFACTION

In this topic, the definition, types and operational parameters related to torrefaction will be discussed. Some studies published in recent years using this technology will also be shown.

### 2.2.1 Definitions and fundamental aspects

Torrefaction is a thermochemical process that uses temperatures between 200-300 °C in an inert atmosphere or low oxygen concentration for a certain residence time. This process consists of the decomposition of a certain raw material through thermal modification, which promotes the devolatilization of organic compounds. In addition, it removes water, improves the energy quality and the chemical and physical properties of the raw materials. This process increases the carbon content and the calorific value of the fuel per unit mass [5], [6], [7]. The product obtained from torrefaction is called torrefied material (torrefied biomass).

Higher energy density and calorific value, lower moisture and oxygen/carbon ratio are some of the characteristics that biomasses gain after undergoing the torrefaction process [8], [9], [10]. These are important factors when producing solid fuels to replace mineral coal [11]. Furthermore, due to its more compact and hydrophobic character, torrefied biomass reduces storage and transport costs [1], [9], [12].

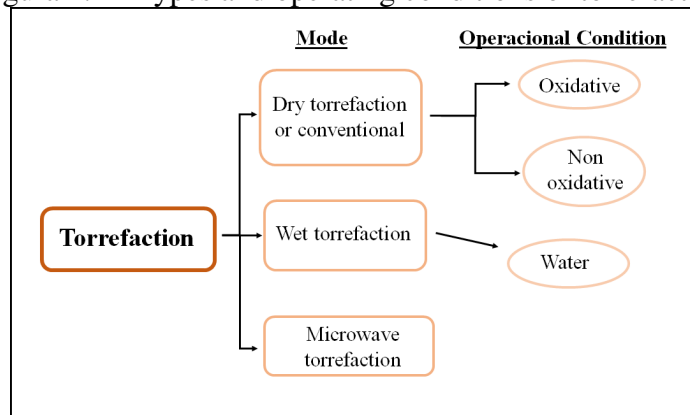
The torrefaction process increases the ash content of the biomass. This becomes a challenge as these ashes contain a higher content of alkali metals compared to coal, which can cause scale, slag and corrosion in steam generation systems. Another important aspect related to the presence of these metallic compounds is that they are the main factors in the emission of fine particles during combustion. However, an alternative to this challenge is to use biomass with low ash content.

During the thermal treatment, the fibrous structure of the original biomass is partially destroyed. This helps change its property from hygroscopic to hydrophobic and improve grinding. Furthermore, biomass is converted into a carbonaceous material similar to coal with excellent properties such as high energy density, compressible, crushable, and low H/C and O/C ratios [13], [14], [15].

### 2.2.1.1 Types of Torrefaction

Conventional or dry torrefaction, wet torrefaction and microwave torrefaction are some types of torrefaction. In this topic, characteristics of each of these types were exposed, as well as application studies. Figure 2.2 presents a summary of torrefaction types and some operating conditions.

Figura 2.2 - Types and operating conditions of torrefaction.



Source: Adapted from Chen *et al.* [3].

### 2.2.1.2 Conventional or dry torrefaction

Conventional or dry torrefaction usually takes place in electric ovens, in which heat is transferred via surface heat transfer [16]. Raw materials with lower moisture content are generally used in this type of torrefaction, after all, biomass with higher moisture content compromises the energy efficiency of the process [17]. A disadvantage of this type of torrefaction is the time it takes to heat up and, consequently, high energy consumption [18].

In dry torrefaction, the biomass is heated between 200 and 300 °C and oxidative and non-oxidative (inert) torrefaction can occur [19]. Oxidative torrefaction occurs in atmospheres containing oxygen, such as air, flue gas and other gases with different concentrations of oxygen, while non-oxidative torrefaction occurs in inert atmospheres, with nitrogen and argon being the gases most used to maintain the atmosphere free of oxygen [3], [20].

Due to the exothermic reactions that occur during thermal degradation, oxidative torrefaction has a higher reaction rate when compared to non-oxidative torrefaction [3]. However, there is a lower yield of solids and the temperature control is more difficult compared to non-oxidative torrefaction [3], [20].

Nakason *et al.* [9] studied cassava rhizome torrefaction in different sweep gases, N<sub>2</sub>, CO<sub>2</sub> and mixture (N<sub>2</sub> + CO<sub>2</sub>). Also, they varied the flow rates (50, 150 and 250 mL min<sup>-1</sup>) at temperatures of 200-300 °C for 30 min. The authors found that the sweep gas had less effect on the fuel properties of the torrefied product compared to the torrefaction temperature.

Based on this, the researchers claimed that torrefaction at 300 °C under 50 mL min<sup>-1</sup> of CO<sub>2</sub> was the best condition to produce torrefied biomass to replace lignite coal. Furthermore, the authors highlighted that torrefaction under a CO<sub>2</sub> atmosphere produced torrefied biomass with a minimum ash content. Furthermore, the use of residual CO<sub>2</sub> makes the process economically viable. Finally, Nakason *et al.* [9] verified that torrefaction mainly removed the oxygen and hydrogen contents of the studied biomass.

Aiming to verify the best atmosphere to be used in the pilot scale torrefaction of cedar wood, Mei *et al.* [8] used oxidative (flue gas) and non-oxidative (N<sub>2</sub>) atmospheres in a pilot scale rotary kiln was operated at different temperatures (200, 230, 260 and 290 °C). The authors verified that, the torrefied biomass showed an improvement in grinding and hydrophobicity. Furthermore, increasing the torrefaction temperature resulted in a decrease in milling energy consumption and an increase in the proportion of smaller particle sizes.

The oxidative atmosphere used in the research was synthesized by a mixture of 6% by volume of O<sub>2</sub>, 10% by volume of CO<sub>2</sub> and 84% by volume of N<sub>2</sub>. This atmosphere had a significant influence on the behavior of cedar wood during torrefaction and on the properties of the resulting solid products. Finally, Mei *et al.* [8] stated that the energy density as well its yield were optimized at a temperature of 260 °C in the presence of the oxidative atmosphere and that the torrefied samples presented combustion characteristics similar to those of lignite. This was a conclusion that Nakason *et al.* [9] also obtained when using residual CO<sub>2</sub> as atmosphere, even using different biomass (cassava rhizome).

### 2.2.1.3 Wet torrefaction

Wet torrefaction, also known as hydrothermal carbonization, unlike dry torrefaction, targets materials with higher moisture or liquid water contents. That is, the pre-thermal treatment of the material takes place in a hydrothermal medium or hot water, using temperatures between 180-260 °C. Therefore, in this type of torrefaction, there is no need for prior conventional thermal drying, thus reducing energy costs related to drying [21], [22].

Biomasses such as agricultural waste, sewage sludge and aquatic waste are used as raw materials for this technology due to their high moisture content [23]. Because it is a process

that takes place in water, wet torrefaction can use this medium to its advantage by facilitating desirable chemical reactions. Water can serve as an organic solvent due to its decreased polarity compared to non-hydrothermal media or even serve as an acid or base catalyst due to the increase in ionic products when subjected to high temperature and pressure [24].

The product of wet torrefaction can be called hydrochar (hydrochar) and it becomes more hydrophobic after the process, facilitating, if necessary, the subsequent drying process through mechanical or natural dehydration with less energy consumption [22]. There are studies that claim that wet torrefaction can improve the characteristics of biomass fuel under mild temperatures and short reaction times (5–240 min) [21].

An example of this is the study performed by Yu *et al.* [25], who used two microalgae biomasses to produce bioethanol. The raw materials were subjected to a dilute acid pretreatment using wet torrefaction to produce microalgae and torrefied biomass hydrolysates under operating conditions of 160-170 °C with residence times of 5-10 min. The hydrolysates were used for fermentation with the yeast *Saccharomyces cerevisiae* and the results for the production of bioethanol were considered reasonable.

Triyono *et al.* [26] used wet torrefaction as a pre-treatment for solid urban waste, aiming to increase the combustible properties of this waste. One of the major obstacles in using these residues as solid fuel is the high moisture content, irregular size and shape, and difficulty in classifying due to the mixture of plastic and organic residues.

In this context, the authors Triyono *et al.* [26] used mixed urban solid waste containing waste from the surface layer of the soil from forests and woods such as leaves, flowers, branches and animal waste (litter) (34.67%), food waste (23.33%), plant waste (14.33%), fruit waste (11.00%) and non-recycled plastic (colored plastic packaging - 16.67%).

The optimal condition found by the researchers was a temperature of 200 °C, a residence time of 30 min and a solid load of 1:2.5, ratio between the sample mass and the mass of water. The solid product obtained showed uniform physical characteristics, small particles, homogeneous particle size distribution and energy yield, comparison ratio between the energy content of the product and the energy content of the raw material in dry basis condition, of 89% [26].

#### 2.2.1.4 Microwave torrefaction

Microwave torrefaction is a thermochemical process that uses electromagnetic waves with frequencies of 0.3-300 GHz for heating, which are used to induce the interaction of the



heated material through dipole rotation and ionic conduction [18], [16]. Separation of negative and positive ions through the high-frequency magnetic field and breaking the electrical double layer structure on the surface of the biomass, changing the zeta potential and neutralizing the negative charge are some of the effects that microwave torrefaction can promote [27].

Microwave heating has characteristics such as high thermal efficiency, energy savings, selective heating and low energy loss during the heat transfer process [19], [27]. Furthermore, it can prevent unwanted side reactions and ensure product quality during the thermochemical process. In samples with high moisture, microwave torrefaction is recommended as it is a selective and rapid volumetric heating. Furthermore, moisture is an important feature for the initial heating of biomass as it serves as a microwave absorber [28].

Yan *et al.* [1] investigated the torrefaction of herb waste produced in the herbal medicine industry as a pre-treatment alternative to the gasification process. The researchers carried out conventional torrefaction tests and torrefaction using microwaves and concluded that the removal of water and the decomposition of hemicellulose and lignin present in the biomass were more efficient using microwave torrefaction. This efficiency is due to the hot spots present in microwaves and the activation of polar molecules. In addition, the scientists pointed out a significant improvement in the performance of steam gasification, which is an efficient hybrid system for the use of biomass residues with high moisture content.

One of the most widely used sewage treatments is the activated sludge process, however, the large amounts of sludge generated are considered a hazardous by-product, which requires adequate final disposal. For this, Zhang *et al.* [27] studied sludge dehydration through microwave torrefaction and the production of a solid biofuel. The researchers evaluated the effect of torrefaction oven power (480-800 W) and reaction time (5-25 min) and concluded that the greater the severity of the process (power and reaction time), the greater the degree of dehydration, but that in 10 min of operation, 80% of the sludge moisture is removed, which is quite reasonable.

In addition, they obtained a torrefied sludge whose calorific value is similar to that of mineral coal, which can be used in boilers or in co-firing with briquettes. Finally, the authors state that the highest total energy efficiency of the torrefaction process occurs with lower times and powers [27].

After presenting the existing types of torrefaction, there may still be the union of one or more types of torrefaction in a single study. For example, Yek *et al.* [28] who used enhanced microwave wet torrefaction incorporating microwave radiation and steam to produce a porous torrefied biomass from palm bark residue.

### 2.2.2 Operational conditions used in the biomass torrefaction processes

In the previous topic, the types of torrefaction were discussed and it was possible to see how the operational parameters are extremely important and directly impact on the product quality. Therefore, in addition to choosing the type of torrefaction to be used, parameters such as temperature, reaction time, atmosphere and particle size are also fundamental and directly influence the torrefaction process as well as its products. Still, due to the great variability and combination of these operational parameters, numerous torrefied biomasses can be obtained with very different characteristics and properties [29].

Temperature is an important operational parameter in biomass torrefaction processes. Patidar and Vashishtha [30] found in their study that the greater the severity in the torrefaction process ( $T \sim 300$  °C), the greater the thermal degradation of the biomass (residue from the mustard harvest). However, as the temperature is increased, the mass yield of the product tends to drop, after all, there is a greater release of inherent moisture, decomposition of hemicellulose and light aliphatic compounds due to its sensitivity to temperature.

Also, when low torrefaction temperatures are used, coal formation in the primary stage increases, as the dehydration and coal formation reactions occur in parallel [31]. In this context, it is extremely important to have a prior study of the characteristics of the biomass to be torrefied so that the best operating parameters for torrefaction can be obtained.

Regarding the atmosphere, oxidative or inert (non-oxidative), it can be seen from the previous topic that it is an extremely important factor, being a characteristic directly linked to the heat of reaction, carbon conversion, moisture content and carbon formation secondary [31]. Again, depending on the biomass used and the product to be obtained, certain types of torrefaction, as well as the atmosphere to be used in the process, are more recommended than others. For biomasses with higher moisture (75% by weight) wet or microwave torrefaction is recommended and when you want to obtain a product that replaces lignite coal is aimed, oxidative atmospheres are recommended [9], [20], [32].

The torrefaction reaction time also influences the results. There are studies that show that the torrefaction time has a direct connection with the carbon content of the product. By combining higher temperature and reaction time, it is possible to obtain higher fixed carbon and ash contents [33]. Times ranging from 15-60 min of operation are normally employed.

Another essential factor for the optimization of the process feed as well as for the thermal decomposition of the biomass is the particle size [31]. The larger the biomass particles,

the greater the resistance to conduction, that is, the lower the heat transfer, thus obtaining higher yields of solid coal during torrefaction [34].

Furthermore, it is also necessary to consider the processes that precede actual torrefaction, such as the collection, handling, storage and transport of biomass. After this stage, the material may require pre-treatments such as drying, grinding and sieving, aiming at homogeneity and efficiency in the torrefaction process. Feeding, conversion, separation and collection of intermediate products and collection of torrefied products should also be evaluated [2].

As previously mentioned, torrefaction promotes the removal of moisture and some basic constituents of the raw biomass. Therefore, it is necessary that the temperature to be used in the process be optimized according to the constituents of the biomass such as hemicellulose, cellulose and lignin [35]. Finally, selecting a biomass with specific characteristics is of paramount importance for optimal torrefaction efficiency and its applications.

## 2.3 RESIDUAL BIOMASSES

In this topic, the definition and general characteristics of biomass and some residual biomass from the timber industry and its potential for application in torrefaction were addressed. Emphasis were given to this residual biomass as it is within the scope of the thesis.

Industrial waste (e.g. sludge), non-industrial waste (e.g. food waste and municipal solid waste), agricultural waste (e.g. olive mill solid waste and rice husk) and forestry waste (e.g. willow) are some examples of residual biomass [33]. Biomass is a renewable energy source that can be converted into chemicals and fuels through biochemical and thermochemical processes [20].

As solid waste is highly susceptible to biological degradation, has a high moisture content and low energy density, produces an unpleasant odor and can cause soil and water pollution, processes that benefit and minimize these characteristics are extremely important, such as torrefaction [1], [35]. There are studies that promote co-torrefaction (or copyrolysis), in which two or more biomasses are mixed as raw material, such as sewage sludge and biowaste (including rice straw and leucaena) [16], food sludge and lignocellulosic waste [36], textile sludge and lignocellulosic waste [37], and optoelectronic waste sludge with mango seed and passion fruit peel [18].

There can be different types of biomass, such as lignocellulosic biomass, composed mainly of cellulose, hemicelluloses and lignin, and microalgal biomass, composed mainly of

carbohydrates, proteins and lipids [3]. Lignocellulosic biomasses become promising because they are renewable and abundant materials. Amongst the sectors which originate biomasses stand out agricultural, forestry and industry.

Still, due to their abundance and relatively low cost, agricultural and forest residues are the most promising for combustion, gasification and pyrolysis. Herbaceous crops, straw, sugarcane, corn, rice husks, sugarcane bagasse, corn cobs, sawdust and forest by-products such as wood chips and blocks are some examples of lignocellulosic biomass [2].

### 2.3.1 Characteristics

As previously mentioned, lignocellulosic biomass, as well as its residues, are materials that have lignin, hemicellulose and cellulose in their chemical composition [2], [38]. Lignin is a large, complex molecular structure that contains cross-linked phenolic polymers. Due to its structure, it is the most difficult chemical component to break down.

Hemicellulose (also called polyose) and cellulose are also polymers, whereas hemicellulose is composed of relatively small branched chains of sugars, cellulose is  $\beta$ -D-glucopyranose moieties linked through  $\beta$ -(1,4) glycosidic [2], [3]. Each lignocellulosic biomass has unique characteristics depending on the amount of these chemical components. Table 2.1 presents examples of biomasses and the percentages of their chemical composition.

Table 2.1 - Lignocellulosic biomass and its chemical composition

<b>Biomass</b>	<b>Cellulose (% w/w)</b>	<b>Hemicellulose (% w/w)</b>	<b>Lignin (% w/w)</b>
Hard wood (poplar)	50.8 - 53.3	26.2 - 28.7	15.5 - 16.3
Soft wood (pine)	45.0 - 50.0	25.0 - 35.0	25.0 - 35.0
Wheat straw	35.0 - 39.0	23.0 - 30.0	12.0 - 16.0
Corn cob	33.7 - 41.2	31.9 - 36.0	6.1 - 15.9
Corn	35.5 - 39.6	16.8 - 35.0	7.0 - 18.4
Rice straw	29.2 - 34.7	23.0 - 25.9	17.0 - 19.0
Rice husks	28.7 - 35.6	12.0 - 29.3	15.4 - 20.0
Sugar cane bagasse	25.0 - 45.0	28.0 - 32.0	15.0 - 25.0
Sorghum straw	32.0 - 35.0	24.0 - 27.0	15.0 - 21.0
Barley straw	36.0 - 43.0	24.0 - 33.0	6.3 - 9.8
Grasses	25.0 - 40.0	25.0 - 50.0	10.0 - 30.0

Source: Adapted from Cai *et al.* [2].

It is through the compositional analysis of the biomass that it is possible to evaluate the conversion yields and the economy of the process. For example, as the biodegradation of cellulose is greater than that of lignin, the overall conversion of biomass with higher cellulose content is greater than biomass with higher lignin content [2]. Lignin is decomposed around 400 °C while cellulose is decomposed at lower temperatures.

One of the major problems during the pyrolysis of lignocellulosic biomass is the formation of pyrolytic products from hemicellulose and cellulose, which include acids, furans and ketones. These compounds are responsible for the strong acidity and poor stability of the bio-oil. Thus, the torrefaction process as a pretreatment for pyrolysis will generate solids with low oxygen content, low acidity and strong stability [38]. In addition to these constituents, biomass also contains inorganic materials (also called ash) and organic materials (volatile material and fixed carbon), in different proportions depending on the nature of the biomass [3].

Moisture content, ash and alkaline metals are properties that indicate quality and knowing these characteristics is essential for the production of biofuel for energy purposes [39]. Biomasses with a high moisture content can increase operational energy costs because they require longer torrefaction time. Furthermore, the higher the moisture content of the sample, the lower the calorific value of the fuel [31].

Regarding the amount of ash in the biomass, this is a feature that has a direct impact on pyrolysis. Alkaline and alkaline earth metals (K, Ca, Na and Mg, for example) are the main components of ash. Studies state that these metals decrease the carbon yield of aromatic hydrocarbons [12].

Depending on the residual biomass to be used, some undesirable problems can be generated. Biomasses with high oxygen content (35%-45%) and ash content (1%-15%), for example, can generate a large number of unwanted oxygenated compounds during pyrolysis [12]. Rice straw, for example, is a biomass that has a relatively low total alkali content, which favors its decomposition and reaction to form charcoal. However, this biomass also has a high ash and silica content in its composition, characteristics that reduce its quality as a raw material [40].

Life cycle assessment and biomass availability are also extremely important for the choice of raw material. Verifying and analyzing the entire biomass production chain in order to investigate the environmental benefits of using certain raw materials for torrefaction and consequently the production of torrefied biomass is extremely important. Some residues can be used in the soil itself for the recycling of nutrients, characterizing competitive application.

Furthermore, the source of biomass has a significant impact on energy and environmental outcomes when considering a large-scale process. Thus, biomass with high regional availability should be preferably used, with characteristics close to and originating close to the processing site so that there are no costs with logistics and transport, in addition to possible deterioration of biomass during transport [4].

### **2.3.2 Residual biomass from wood**

Forest waste biomass is considered to be a renewable energy source with high carbon content and low impurity (such as ash and sulfur) content and is carbon neutral due to its absorption of CO<sub>2</sub> whilst growing [7], [41], [42]. These biomasses have low calorific value (12–25 MJ kg<sup>-1</sup>), low energy density, high moisture content and volatile matter, high oxygen content, low apparent density (approximately 150 kg m<sup>-3</sup>) and high heterogeneity, characteristics that are disadvantageous for use as received as solid fuel [43]. Regarding moisture, wood chips have a moisture content of 20-40% while processed pellets and briquettes have a relatively lower variation [31].

Dhaundiayal *et al.* [31] stated that the valorization of forest residues through thermal treatment can enhance its energy aspect and reduce costs with energy consumption when using these residues as fuel. The biomass of torrefied wood can be used as biofuel after undergoing a torrefaction process and has advantages such as less dependence on location and climate, easy storage, distribution and transportation [10].

Wood chips are biomass that are highly available worldwide. Wood pellets are also being used due to their uniform fuel properties and cheaper transportation costs compared to wood chips [43]. The bulk density of the pellet is greater than 600 kg m<sup>-3</sup>, while that of the chips is 220-250 kg m<sup>-3</sup> and, consequently, the energy density of the pellets is greater than that of the chips, being 3,12 MWh m<sup>-3</sup> and 0,6 MWh m<sup>-3</sup>, respectively [44].

The main sources of raw material for the manufacture of pellets are forestry, wood by-products and logs of low commercial value. The plant biomass is ground and compacted under high pressure, thus obtaining a granulated biofuel with high calorific value and good mechanical resistance. Because they are made from the reuse of by-products, the pellet production cost is usually low. Brazil showed a growth in pellet production from 57,000 tons in 2012 to 470,000 tons in 2017, exporting about 23% of its production, with Italy being the largest market for Brazil [44].

In 2019, the Associação Catarinense de Empresas Florestais (ACR) launched a study on the forestry base of the State of Santa Catarina, the “Statistical Yearbook of Forest Base for the State of Santa Catarina 2019 (base year 2018)”. The study showed that both from 2016 to 2017 and from 2017 to 2018 there was an increase in the growth of demand for wood. Furthermore, the survey states that the estimated wood stock in Santa Catarina is 240.5 million m<sup>3</sup>, of which 76% is represented by the genus *Pine* and 24% by *Eucalyptus*.

Brazil has about 1.6 million hectares planted with pine and wood industries that are not in the field of paper and cellulose production and reconstituted panels consume, annually, approximately 27.5 million m<sup>3</sup> of pine wood in logs. That is, considering the material that is not used by industries, it is estimated that around 1.6 million tons of pine pellets could be generated annually [44].

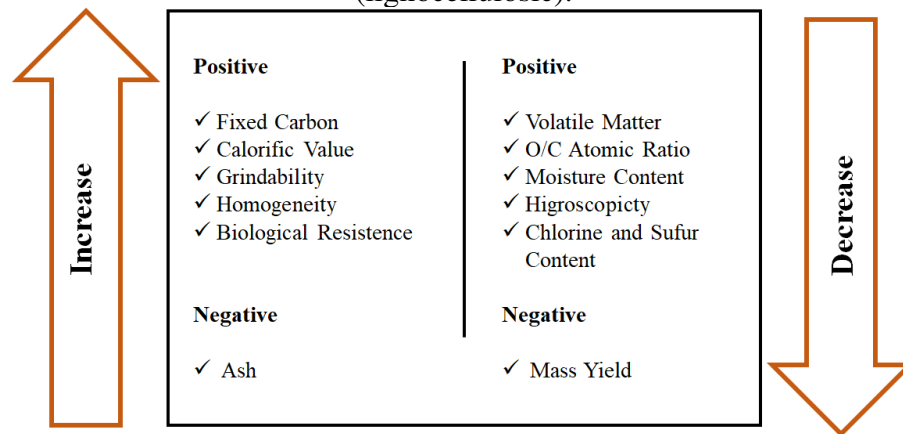
Figueiró *et al.* [45] studied the Brazilian potential for torrefaction of *Eucalyptus* wood chips for energy purposes. The researchers found increases in the energy quality of the biomass, a reduction in hygroscopicity and an increase in the fixed carbon content and in the calorific value of woody biomass, thus making it a favorable technique for energy purposes. Biomasses such as waste wood chips [43], waste wood-based panels [46], demolition and construction wood [47] are also reported in the literature by researchers that used torrefaction for the energy recovery of these raw materials.

The torrefaction of wood pellets also becomes an interesting process because it causes the volatilization of the hemicellulose and changes the properties of the biomass, making it hydrophobic, with a higher energy density (close to that of mineral coal, 20-23 GJ ton<sup>-1</sup>), lighter and more compact. These characteristics contribute to the reduction of costs related to transport, an important parameter since the competitiveness of pellets is sensitive to the cost of transport [44].

Torrefied wood pellets have characteristics close to those of mineral coal in the crushing/pulverizing process, which makes them an ideal substitute for co-combustion in thermoelectric plants, and can be mixed with coal in the production of electricity and in the gasification process in power plants. based on dry biomass in a fluidized bed. Thus, the use of this torrefied material could contribute to the reduction of the emission of fine particles and pollutants, such as carbon monoxide (CO), nitrogen oxides (NO<sub>x</sub>) and gaseous organic compounds (C<sub>x</sub>H<sub>y</sub>) when compared to the use of fossil fuels.

Finally, Figure 2.3 presents a summary of the changes in the physical and chemical properties of residual forest biomass (lignocellulosic) after being submitted to the torrefaction process.

Figure 2.3 - Changes in physical and chemical properties of forest residual biomass (lignocellulosic).



Source: Adapted from Figueiró *et al.* [45].

## 2.4 APPLICATIONS OF TORREFIED BIOMASSES

One of the most recurrent applications of torrefied biomass is in the development of biofuels. The great importance of this product lies in mitigating global warming and the greenhouse effect by reducing carbon dioxide emissions. Depending on which biomass is used to make the biofuel, this product can be classified into generations. Biomass from food crops generate first generation biofuels while inedible lignocellulosic biomass generates second generation biofuels. Third- and fourth-generation biofuels are produced from algal biomass (macroalgal and microalgal) and genetically modified algae and microbial systems, respectively [3].

Other applications of torrefied biomass are: manufacture of iron, adsorbent, biofertilizer, etc. [38]. In other words, there are numerous applications for torrefied biomass, but the choice of application must be made thoroughly in order to bring economic and environmental benefits. There may be cases where it will be more feasible to use biomass torrefied in the soil as fertilizer rather than biofuel, and vice versa.

Triyono *et al.* [26] studied the torrefaction of solid urban waste, however, they used wet torrefaction as a pre-treatment aimed at increasing the combustible properties of these wastes. The authors claim that this type of torrefaction is suitable for converting mixed urban solid waste (organic and plastic) into solid fuel with high energy density, partly renewable. Furthermore, the researchers suggest that this technique could also be used to produce material for other treatments, such as pyrolysis, to produce liquid fuel.



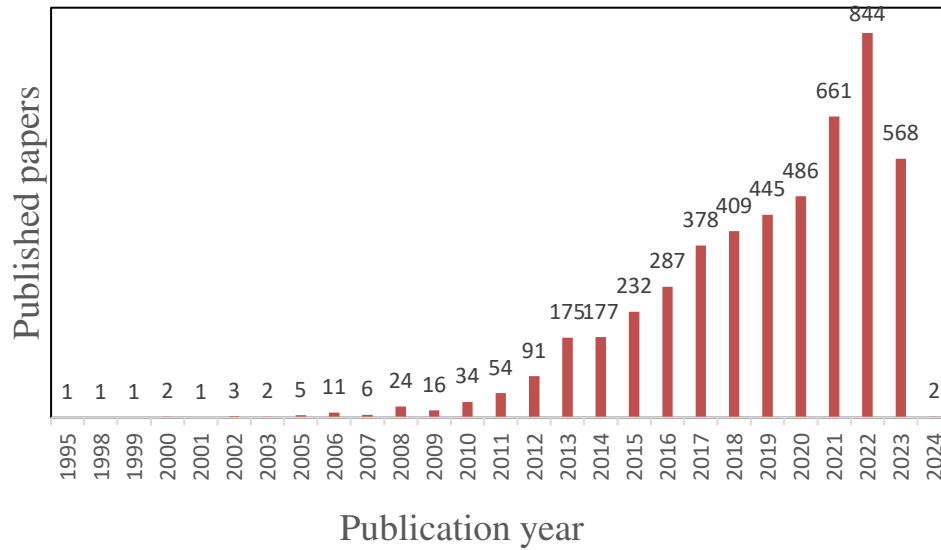
According to Chen *et al.* [3], in January 2020, a search was carried out using the keyword “torrefaction” based on the abstract, title and keywords on the website “sciencedirect.com”. In this research, more than 1,623 articles were suggested. Amongst the studies visualized in this research, torrefaction has been used for applications such as production of coffee beans, improvement of organoleptic properties of foods, wood treatment, besides others. In addition, torrefaction kinetics has also been studied by researchers to understand the thermal degradation behaviors of biomass [3].

In March 2021, a new search was performed using the keyword “torrefaction” based on the abstract, title and keywords on the website “sciencedirect.com”, but considering the last 5 years (2016-2021). The survey showed that 2,299 articles were published in that period, with 279 articles from 2021. In July 2023, 3413 articles were published between 2019-2023 with 568 articles from 2023 and 2 from 2024.

Analyzing the data, it is noted that torrefaction is a technology that has been attracting the attention of researchers over the last few years and that there has been a notable growth in the publication of new studies on this topic. Also, it should be noted that the survey was carried out in July, that is, until the end of the year, there are 5 more months to account for new publications in 2023. It is also observed that the number of articles published until July 2023 (568) was equivalent to 67% of the articles published in the last year (2022). In other words, torrefaction is a promising technology with high application potential.

Aiming at a greater approach, still in July 2023, another search was carried out using the keyword “torrefaction” based on the abstract, title and keywords on the website “sciencedirect.com”, however, considering all years since the first published article. The result of the research is shown in Figure 2.4, which again shows the growth of technology over the years, with the highest growth starting in 2017. The most significant growths were from 2012 to 2013 and 2016 to 2017, 2020 to 2021 and 2021 to 2022.

Figure 2.4 - Number of articles published since the first article published using the word “torrefaction”.



Source: The author, (2023)

## 2.4.1 Applications of torrefied biomass in the metallurgical industry

### 2.4.1.1 Metallurgical industry

The metallurgical industry is the industrial branch responsible for the foundry and production of non-ferrous metals, ferroalloys and pig iron, pipe manufacturing and steelworks. While the metallurgical industry operates in a broader field, producing various types of metals: aluminum, copper, titanium and iron, etc., the steel industry operates exclusively in the production of iron and steel, a kind of specialized metallurgical industry.

The manufacturing process of both industries (metallurgy and steel) basically follow the same principle, that is, the ore is melted at high temperatures to extract the desired metal. Iron, the raw material for steel, is one of the metals that most require high temperatures for its smelting and reduction, exceeding 1300 °C in blast furnaces, and in the classic route fossil coal is used, responsible for the most of the large CO<sub>2</sub> emissions.

According to Instituto Aço Brasil, in 2019, Brazil occupied the 9th position in the ranking of world production of crude steel with the production of 32.6 million tons of this product. Also, in 2019, Brazil produced 31.3 million tons of steel products, being the 12th World Exporter of Steel Products with 12.8 million tons exported directly. Brazil has an installed capacity of 51 million tons/year of crude steel, with 31 plants spread over 10 Brazilian states, most of which are located in the south and southeast regions.

The steel industry is currently facing enormous environmental pressure due to high CO<sub>2</sub> emissions. Amongst the various processes that occur in this industry are coking, pelletizing, sintering, blast furnace steelmaking and direct reduction, hot metal pre-treatment, steelmaking by converters and electric arc furnaces, besides others [48]. The control and management of emissions during these processes are essential for environmental protection. The blast furnace, for example, where the reduction process to produce metallic iron/pig iron occurs, contributes with approximately 70% of CO<sub>2</sub> emissions. This is because the main material used for reduction is coke/coking coal [7], [41].

One of the pig iron production routes uses iron ore fines, coke and anthracite fines. The materials are mixed, granulated and fired to form solid blocks of sintered iron ore. Then, in the blast furnace, the coke is burned and gasified generating a high-temperature, CO-rich gas, which reduces the sintered iron ores to produce pig iron (liquid iron saturated in C) and CO<sub>2</sub> [49]. The physical, chemical and thermal properties of metallurgical coke are very important as it is the only solid material in the high temperature zones of the blast furnace [50]. Table 2.2 presents some characteristics of metallurgical coke.

Table 2.2 - Chemical, physical and thermal characteristics of metallurgical coke

<b>Characteristic of metallurgical coke</b>	<b>Value</b>	<b>Unit</b>
Fixed carbon	86 - 89	%
Volatile materials	0.1 – 0.3	%
Ash	8 - 12	%
Moisture	1 - 6	%
Sulfur	0.45 – 0.90	%
Alkanes	< 0.3	%
Crush strength	100 - 130	kg cm <sup>-2</sup>
Particle size range	25 – 75	mm
Average specific heat (0 °C and 1000 °C)	1.50	kJ kg <sup>-1</sup> K <sup>-1</sup>
Calorific value	7200	kcal kg <sup>-1</sup>
Porosity	40 - 50	%
Reactivity (at 950 °C)	< 30	%
Resistance after reaction	> 60	%

Source: Adapted from Costa [51] and Cardona [52].

Finally, the reduction of iron oxides in a blast furnace can happen in a direct and/or indirect way according to reactions (2.1), (2.2), (2.3) and (2.4) [41], [53], [54].

Direct reduction:



Indirect reduction:



Char Gasification:



where a and b are the reaction rate ( $\text{mol min}^{-1}$ ) of each overall reaction [54].

Direct reduction occurs in presence of carbon (C) while indirect reductions occur in the presence of carbon monoxide (CO) gas, produced by char gasification or Boudouard reaction (Equation 2.4).

#### 2.4.1.2 Applications of torrefied biomass

The partial or complete replacement of fossil fuels used as a source of energy in the metallurgical industry by biomass has been studied and has shown promising results [44], [49], [55], [56]. One of the advantages of using torrefied biomass in the blast furnace is that it will react with the hot air blast producing heat from initially low temperature and reacts with  $CO_2$  to produce CO at lower temperatures and higher rates when compared to the conventional coke. This improves the reduction efficiency and saves energy in the blast furnace [54].

However, the addition of torrefied biomass to other coals with suitable physical properties is still a challenge [55]. One of the difficulties in adding any new material to the coal mix is the potential to interfere with graphitization, which negatively affects both the physical and chemical properties of the product. Biomasses with low mechanical strength, low calorific value, high sulfur and ash content, low porosity and heterogeneous physical and chemical characteristics are unfavorable for mixing with metallurgical coke [51].

Furthermore, the challenges for using biomass in the steel industry include the technical and economic aspects that require synergy between the steelmaking and bioenergy

sectors. Although the intensive work has been carried out separately, there is a lack of connection between the two vital sectors. The demand for biomass as a substitute for coke depends significantly on bioenergy markets.

Fick *et al.* [49] investigated different types of biomasses to replace 20% of the fossil fuel used in the production of iron. It was revealed that only biomass from wood and crop residues were able to meet the requirements of the study. However, due to its physical characteristics (size and/or mechanical strength) and low calorific value, it was recommended that the raw biomass should go through a pre-treatment, such as torrefaction, before being applied in the iron manufacturing process.

With that, Fick *et al.* [49] suggested pretreatment processes such as carbonization or torrefaction to produce solid coal with properties similar to fossil coal. Thus, the researchers found that carbonized biomass can be used as lumps loaded into the top of the blast furnace, as medium-sized fines in the sinter plant, and as powder sprayed through the blast furnace tuyeres, while torrefied biomass can be used like a pulverized powder injected through the tuyeres.

Proskurina *et al.* [57] studied the potential of using torrefied biomass in industrial applications and found that the fuel produced can replace coal in energy production and heat processing in a long-term perspective. The authors also stated that considerable investments are needed to establish integrated supply chains from sustainable raw material sources to end use, policy regulations and start the process of commoditization of torrefied biomass.

In this way, the torrefaction of residual biomass could be explored for use in metallurgical processes. As a promising technology for energy recovery from residual biomass, the torrefaction of biomass such as *Pine* and *Eucalyptus* residues could be used as a pre-treatment of biomass aiming at its complete and partial application in blast furnaces of metallurgical industries. The assessment of torrefaction conditions that lead to suitable properties for use in blast furnaces should therefore be investigated.

## 2.5 REFERENCES

- [1] Yan, B., Jiao, L., Li, J., Zhu, X., Ahmed, S., Chen, G. Investigation on microwave torrefaction: Parametric influence, TG-MS-FTIR analysis, and gasification performance, *Energy*, 2021, 220, pp. 119794. <https://doi.org/10.1016/j.energy.2021.119794>
- [2] Cai, J., He, Y., Yu, X., Banks, S. W., Yang, Y., Zhang, X., Yu, Y., Liu, R., Bridgwater, A. V. Review of physicochemical properties and analytical characterization of lignocellulosic biomass. *Renewable and Sustainable Energy Reviews*, 2017, 76, pp. 309-322. <https://doi.org/10.1016/j.rser.2017.03.072>

- [3] Chen, W-H., Lin, B-J., Lin, Y-Y., Chu, Y-S., Ubando, A.T., Show, P.L., Ong, H.C., Chang, J-S., Ho, S-H., Culaba, A.B., Pétrissans A., Pétrissans, M. Progress in biomass torrefaction: Principles, applications and challenges, *Prog. Energy Combust. Sci.*, 2021, 82, pp. 100887. <https://doi.org/10.1016/j.peccs.2020.100887>
- [4] Lee, M., Lin, Y., Chiueh, P., Den, W. Environmental and energy assessment of biomass residues to torrefied biomass as fuel: A brief review with recommendations for future bioenergy systems. *Journal of Cleaner Production*, 2020, 251, pp. 119714. <https://doi.org/10.1016/j.jclepro.2019.119714>
- [5] Director, L. B. and Sinelshchikov, V A. Numerical modeling of torrefaction reactor integrated in energy technological complex, *Energy*, 2019, 167, pp. 1194-1204. <https://doi.org/10.1016/j.energy.2018.11.044>
- [6] Silveira, E. A., Luz, S., Candelier, K., Macedo, L. A., Rousset, P. An assessment of biomass torrefaction severity indexes, *Fuel*, 2021, 288, pp. 119631. <https://doi.org/10.1016/j.fuel.2020.119631>
- [7] Zheng, K., Han, H., Hu, S., Ren, Q., Su, S., Wan, Y., Jiang, L., Xu, J., Li, H., Tong, Y., Xiang, J. Upgrading biomass waste to bio-coking coal by pressurized torrefaction: Synergistic effect between corncob and lignin, *Energy*, 2023, 267, pp. 126536. <https://doi.org/10.1016/j.energy.2022.126536>
- [8] Mei, Y., Liu, R., Yang, Q., Yang, H., Shao, J., Draper, C., Zhang, S., Chen, H. Torrefaction of cedarwood in a pilot scale rotary kiln and the influence of industrial flue gas, *Bioresour. Technol.*, 2015, 177, 355-360. <https://doi.org/10.1016/j.biortech.2014.10.113>
- [9] Nakason, K., Khemthong, P., Kraithong, W., Chukaew, P., Panyapinyopol, B., Kitkaew, D., Pavasant, P. Upgrading properties of torrefied biomass fuel derived from cassava rhizome via torrefaction: Effect of sweeping gas atmospheres and its economic feasibility, *Case Stud. Therm. Eng.*, 2021, 23, pp. 100823. <https://doi.org/10.1016/j.csite.2020.100823>
- [10] Yun, H., Clift, R. and e Bi, X. Environmental and economic assessment of torrefied wood pellets from British Columbia. *Energy Conversion and Management*, 2020, 208, pp. 112513. <https://doi.org/10.1016/j.enconman.2020.112513>
- [11] Javanmard, A., Patah, M. F. A., Zulhelmi, A., Daud, W. M. A. W. comprehensive overview of the continuous torrefaction method: Operational characteristics, applications, and challenges, *Journal of the Energy Institute*, 2023, 108, pp. 101199. <https://doi.org/10.1016/j.joei.2023.101199>
- [12] Cen, K., Zhuang, X., Gan, Z., Ma, Z., Li, M. Chen, D., Effect of the combined pretreatment of leaching and torrefaction on the production of bio-aromatics from rice straw via the shape selective catalytic fast pyrolysis, *Energy Rep.*, 2021, 7, pp. 732-739. <https://doi.org/10.1016/j.egy.2021.01.031>
- [13] Ivanovski, M., Goricanec, D., Kroppe, J., Urbancl, D. Torrefaction pretreatment of lignocellulosic biomass for sustainable solid biofuel production, *Energy*, 2022, 240, pp. 122483. <https://doi.org/10.1016/j.energy.2021.122483>

- [14] Ong, H.C., Yu, K.L., Chen, W.-H., Pillejera, M.K., Bi, X., Tran, K.-Q., Pétrissans, A., Pétrissans, M. Variation of lignocellulosic biomass structure from torrefaction: A critical review, *Renew. Sustain. Energy Rev.*, 2021, 152, 111698. <http://doi.org/10.1016/j.rser.2021.111698>
- [15] Zhang, Z., Duan, H., Zhang, Y., Guo, X., Yu, X., Zhang, X., Rahman, M.M., Cai, J. Investigation of kinetic compensation effect in lignocellulosic biomass torrefaction: Kinetic and thermodynamic analyses, *Energy*, 2020, 207, pp. 118290. <https://doi.org/10.1016/j.energy.2020.118290>
- [16] Huang, Y., Sung, H., Chiueh, P., Lo, S. Co-torrefaction of sewage sludge and leucaena by using microwave heating. *Energy*, 2016, 116, pp. 1-7. <https://doi.org/10.1016/j.energy.2016.09.102>
- [17] Ayub, Y., Zhou, J., Ren, J., He, C. An innovative integration of torrefaction, gasification, and solid oxide fuel cell for carbon-neutral utilization of biomass waste: Process development, economic, exergy, advanced exergy, and exergoeconomics analysis, *Energy Conversion and Management*, 2023, 292 pp 117426. <https://doi.org/10.1016/j.enconman.2023.117426>
- [18] Lin, Y. and Zheng, N. Biowaste-to-torrefied biomass through microwave-assisted wet co-torrefaction of blending mango seed and passion shell with optoelectronic sludge. *Energy*, 2021a, pp. 120213. <https://doi.org/10.1016/j.energy.2021.120213>
- [19] Yan, B., Jiao, L., Li, J., Zhu, X., Ahmed, S., Chen, G. Investigation on microwave torrefaction: Parametric influence, TG-MS-FTIR analysis, and gasification performance, *Energy*, 2021, 220, pp. 119794. <https://doi.org/10.1016/j.energy.2021.119794>
- [20] Mei, Y., Liu, R., Yang, Q., Yang, H., Shao, J., Draper, C., Zhang, S., Chen, H. Torrefaction of cedarwood in a pilot scale rotary kiln and the influence of industrial flue gas, *Bioresour. Technol.*, 2015, 177, 355-360. <https://doi.org/10.1016/j.biortech.2014.10.113>
- [21] He, C., Tang, C., Li, C., Yuan, J., Tran, K., Bach, Q., Qiu, R., Yang, Y. Wet torrefaction of biomass for high quality solid fuel production: A review. *Renewable and Sustainable Energy Reviews*, 91 (2018), pp. 259-271, <https://doi.org/10.1016/j.rser.2018.03.097>
- [22] Soh, M., Khaerudini, D. S., Chew, J. J., Sunarso, J. Wet torrefaction of empty fruit bunches (EFB) and oil palm trunks (OPT): Effects of process parameters on their physicochemical and structural properties, *South African Journal of Chemical Engineering*, 2021, 35, pp. 126-136, <https://doi.org/10.1016/j.sajce.2020.09.004>
- [23] Nguyen, Q., Nguyen, D. D., He, C., Bach, Q. Pretreatment of Korean pine (*Pine koraiensis*) via wet torrefaction in inert and oxidative atmospheres. *Fuel*, 2021, 291, pp. 119616. <https://doi.org/10.1016/j.fuel.2020.119616>
- [24] Bach, Q. and Skreiberg, O. Upgrading biomass fuels via wet torrefaction: a review and comparison with dry torrefaction. *Renewable and Sustainable Energy Reviews*, 2016, 54 pp 665-667. <https://doi.org/10.1016/j.rser.2015.10.014>
- [25] Yu, K. L., Chen, W., Sheen, H., Chang, J., Lin, C., Ong, H. C., Show, P. L., Ling, T.C. Bioethanol production from acid pretreated microalgal hydrolysate using microwave-assisted heating wet torrefaction. *Fuel*, 2020, 279, pp. 118435. <https://doi.org/10.1016/j.fuel.2020.118435>

- [26] Triyono, B., Prawisudha, P., Aziz, M., Mardiyati, Pasek, A.D., Yoshikawa, K. Utilization of mixed organic-plastic municipal solid waste as renewable solid fuel employing wet torrefaction, *Waste Management*, 95, 2019, pp. 1-9, <https://doi.org/10.1016/j.wasman.2019.05.055>
- [27] Zhang, C., Ho, S., Chen, W., Eng, C.F., Wang, C. Microwave wet torrefaction: Simultaneous implementation of sludge dewatering and solid biofuel production by microwave torrefaction. *Environmental Research*, 2021, 195, pp. 110775, <https://doi.org/10.1016/j.envres.2021.110775>
- [28] Yek, P.N.Y., Osman, M.S., Wong, C.C., Wong, C.S., Kong, S.H., Sie, T.S., Foong, S.Y., Lam, S.S., Liew, R.K. Microwave wet torrefaction: A catalytic process to convert waste palm shell into porous biochar, *Materials Science for Energy Technologies*, 2020, 3, pp. 742-747. <https://doi.org/10.1016/j.mset.2020.08.004>
- [29] Silveira, E. A., Luz, S., Candelier, K., Macedo, L. A., Rousset, P. An assessment of biomass torrefaction severity indexes, *Fuel*, 2021, 288, pp. 119631. <https://doi.org/10.1016/j.fuel.2020.119631>
- [30] Patidar, K. and Manish, V. Impact of torrefaction conditions on the physicochemical properties of mustard crop residue. *Materials today: Proceedings*, 2021, 44 (6), pp. 4072-4078. <https://doi.org/10.1016/j.matpr.2020.10.445>
- [31] Dhaundiayal, A., Singh, S.B., Atsu, D., Toth, L. Comprehensive analysis of pre-treated Austrian pine, *Fuel*, 2021, 287, pp. 119605. <https://doi.org/10.1016/j.fuel.2020.119605>
- [32] Olszewski, M. P., Nicola, S. A., Arauzo, P. J., Titirici, M., Kruse, A. Wet and dry? Influence of hydrothermal carbonization on the pyrolysis of spent grains. *Journal of Cleaner Production*, 2020, 260, pp. 121101. <https://doi.org/10.1016/j.jclepro.2020.121101>
- [33] Lin, Y. and Zheng, N. Torrefaction of fruit waste seed and shells for biofuel production with reduced CO<sub>2</sub> emission. *Energy*, 2021b, pp. 120226. <https://doi.org/10.1016/j.energy.2021.120226>
- [34] Trubetskaya, A., Grams, J., Leahy, J.J., Johnson, R., Gallagher, P., Monaghan, R.F.D., Kwapinska, M. The effect of particle size, temperature and residence time on the yields and reactivity of olive stones from torrefaction, *Renewable Energy*, 160, 2020, pp. 998-1011, <https://doi.org/10.1016/j.renene.2020.06.136>
- [35] Namkung, H., Park, J-H., Lee, Y-J., Song, G-S., Choi, J.W., Park, S-J., Kim, S., Liu, J., Choi, Y-C. Performance evaluation of biomass pretreated by demineralization and torrefaction for ash deposition and PM emissions in the combustion experiments, *Fuel*, 2021, 292, pp. 120379. <https://doi.org/10.1016/j.fuel.2021.120379>
- [36] Zheng, N., Lee, M., Li, Y., Samannan, B. Microwave-assisted wet co-torrefaction of food sludge and lignocellulose biowaste for torrefied biomass production and nutrient recovery, *Process Safety and Environmental Protection*, 2020, 144, pp. 273-283. <https://doi.org/10.1016/j.psep.2020.07.032>
- [37] Zheng, N., Lee, M. and Li, Y. Co-processing textile sludge and lignocellulose biowaste for biofuel production through microwave-assisted wet torrefaction, *Journal of Cleaner Production*, 2020, 268, pp. 122200. <https://doi.org/10.1016/j.jclepro.2020.122200>



- [38] Wang, C., Yuan, X., Li, S., Zhu, X. Enrichment of phenolic products in walnut shell pyrolysis bio-oil by combining torrefaction pretreatment with fractional condensation, *Renew. Energy*, 2021, 169, pp. 1317-1329. <https://doi.org/10.1016/j.renene.2021.01.112>
- [39] Kołodziej, B., Stachyra, M., Antonkiewicz, J., Bielińska, E., Wiśniewski, J. The effect of harvest frequency on yielding and quality of energy raw material of reed canary grass grown on municipal sewage sludge. *Biomass and Bioenergy*, 2016, 85, pp. 363-370. <https://doi.org/10.1016/j.biombioe.2015.12.025>
- [40] Liu, W, Jiang, H., and Yu, H. Development of Torrefied biomass-Based Functional Materials: Toward a Sustainable Platform Carbon Material. *Chemical Reviews*, 2015, 115, pp. 12251-12285 <https://doi.org/10.1021/acs.chemrev.5b00195>
- [41] Ubando, A. T., Chen, W., Ong, H. C. Iron oxide reduction by graphite and torrefied biomass analyzed by TG-FTIR for mitigating CO<sub>2</sub> emissions, *Energy*, 2019, 180, pp. 968-977. <https://doi.org/10.1016/j.energy.2019.05.149>
- [42] Ye, L., Peng, Z., Wang, L., Anzulevich, A., Bychkov, I., Tang, H., Rao, M., Zhang, Y., Li, G., Jiang, T. Preparation of core-shell iron ore-torrefied biomass composite pellets for microwave reduction, *Powder Technology*, 2018, 338, pp. 365-375. <https://doi.org/10.1016/j.powtec.2018.07.037>
- [43] Mokrzycki, J., Gazińska, M., Fedyna, M., Karcz, R., Lorenc-Grabowska, E., Rutkowski, P. Pyrolysis and torrefaction of waste wood chips and cone-like flowers derived from black alder (*Alnus glutinosa* L. Gaertn.) for sustainable solid fuel production. *Biomass and Bioenergy*, 2020, 143, pp. 105842. <https://doi.org/10.1016/j.biombioe.2020.105842>
- [43] Setkit, N., Li, X., Yao, H., Worasuwanarak, N. Torrefaction behavior of hot-pressed pellets prepared from leucaena wood, *Bioresour. Technol.*, 2021, 321, pp. 124502. <https://doi.org/10.1016/j.biortech.2020.124502>
- [44] Quéno, L.R.M., Souza, A.N., Costa, A.F., Valle, A.T., Joaquim, M.S. Aspectos técnicos da produção de pellets de madeira, *Cienc. Florest.*, 2019, 29(3), pp. 1478-1489. <https://doi.org/10.5902/1980509820606>
- [45] Figueiró, C. G., Vital, B. R., Carneiro, A. C. O., da Silva, C. M. S., Magalhães, M. A., Fialho, L. F. Energy valorization of woody biomass by torrefaction treatment: a brazilian experimental study. *Maderas: Ciencia y Tecnologia*, 21 (3) (2019), pp. 297-304, <http://dx.doi.org/10.4067/S0718-221X2019005000302>
- [46] Wang, N., Zhan, H., Zhuang, X., Xu, B., Yin, X., Wang, X., Wu, C. Torrefaction of waste wood-based panels: More understanding from the combination of upgrading and denitrogenation properties, *Fuel Processing Technology*, 2020, 206, pp. 106462. <https://doi.org/10.1016/j.fuproc.2020.106462>
- [47] Edo, M. Skoglund, N., Gao, Q., Persson, P., Jansson, S. G. Fate of metals and emissions of organic pollutants from torrefaction of waste wood, MSW, and RDF. *Waste Management*, 2017, 68, pp. 646-652. <https://doi.org/10.1016/j.wasman.2017.06.017>

- [48] Wang, H., Zhang, C., Qie, J., Zhou, J., Liu, Y., Li, X., Shanguan, F. Development trends of environmental protection technologies for Chinese steel industry, *Journal of Iron and Steel Research, International*, 2017a, 24, pp. 235-242. [https://doi.org/10.1016/S1006-706X\(17\)30035-3](https://doi.org/10.1016/S1006-706X(17)30035-3)
- [49] Fick, G., Mirgoux, O., Neau, P., Patisson, F. Using Biomass for Pig Iron Production: A Technical, Environmental and Economical Assessment, *Waste Biomass Valorization*, 2014, 5, pp. 43-55. <https://doi.org/10.1007/s12649-013-9223-1>
- [50] Cheng, H., Liang, Y., Guo, R., Sun, Z., Wang, Q., Xie, Q., Wang, J. J., Zhang, T., Li, S., Wang, J. Effects of solution loss degree, reaction temperature, and high temperature heating on the thermal properties of metallurgical cokes., *Fuel*, 283, 2021, pp. 118936, <https://doi.org/10.1016/j.fuel.2020.118936>
- [51] Costa, D. S. Thermal balance as a control parameter of the coking process. 2018. 85 f. Monograph (Metallurgical Engineering), Federal University of Ceará, 2018. Available at: <[http://www.repositorio.ufc.br/bitstream/riufc/33357/3/2018\\_tcc\\_dscosta.pdf](http://www.repositorio.ufc.br/bitstream/riufc/33357/3/2018_tcc_dscosta.pdf)>
- [52] Cardona, L. M. V. Effect of the main manufacturing process variables on the properties of briquettes made from fossil coal and charcoal mixtures for steelmaking. 2017. 184 f. Thesis (Doctorate in Science), University of São Paulo, São Paulo, 2017. Available at: <<https://teses.usp.br/teses/disponiveis/3/3133/tde-23052018-082753/publico/LinaMariaVaronCardonaOrig17.pdf>>
- [53] Sheshukov, O., Mikheenkov, M., Vedmid, L., Nekrasov, I., Egiazaryan, D., Mechanism of Ion-Diffusion Solid-Phase Reduction of Iron Oxides of Technogenic Origin in the Presence of the Liquid Phase and without it, *Metals*, 2020, 10(12), pp. 1564. <https://doi.org/10.3390/met10121564>
- [54] Hu, Q., Yao, D., Xie, Y., Zhu, Y., Yang, H., Chem, Y., Chen, H. Study on intrinsic reaction behavior and kinetics during reduction of iron ore pellets by utilization of torrefied biomass, *Energy Conversion and Management*, 2018, 158, pp. 1-8. <https://doi.org/10.1016/j.enconman.2017.12.037>
- [55] Mousa, E., Wang, C., Riesbeck, J., Larsson, M. Biomass applications in iron and steel industry: An overview of challenges and opportunities. *Renewable and Sustainable Energy Reviews*, [s.l.], v. 65, p. 1247-1266, 2016. <https://doi.org/10.1016/j.rser.2016.07.061>
- [56] Wang, C., Mellin, P., Lövgren, J., Nilsson L., Yang, W., Salman, H., Hultgren, A., Larsson, M. Biomass as blast furnace injectant – Considering availability, pretreatment and deployment in the Swedish steel industry, *Energy Convers. Manag.*, 2015, 102, pp. 217-226. <https://doi.org/10.1016/j.enconman.2015.04.013>
- [57] Proskurina, S., Heinimö, J., Schipfer, F., Vakkilainen, E. Biomass for industrial applications: The role of torrefaction. *Renewable Energy*, 2017, 111, pp. 265-274. <https://doi.org/10.1016/j.renene.2017.04.015>

### 3 GENERAL METHODOLOGY

The general methodology applied in this thesis was described in Figure 3.1 and each chapter contains its detailed methodology. In this thesis, four lignocellulosic biomasses were studied, Pellet (PP) – *Pine genus*, Sawdust (SE) – *Eucalyptus genus*, Bark (CC) - *Pine genus* and Chips (CV) - *Pine genus*. The first biomass studied was PP, which makes up Chapter 4. The samples were randomly selected, crushed in a knife mill and separated into different particle size <106  $\mu\text{m}$  and 106-300  $\mu\text{m}$ . Later were characterized by proximate analysis, ultimate analysis, Fourier-transform infrared spectroscopy (FT-IR), Higher Calorific Value (HHV).

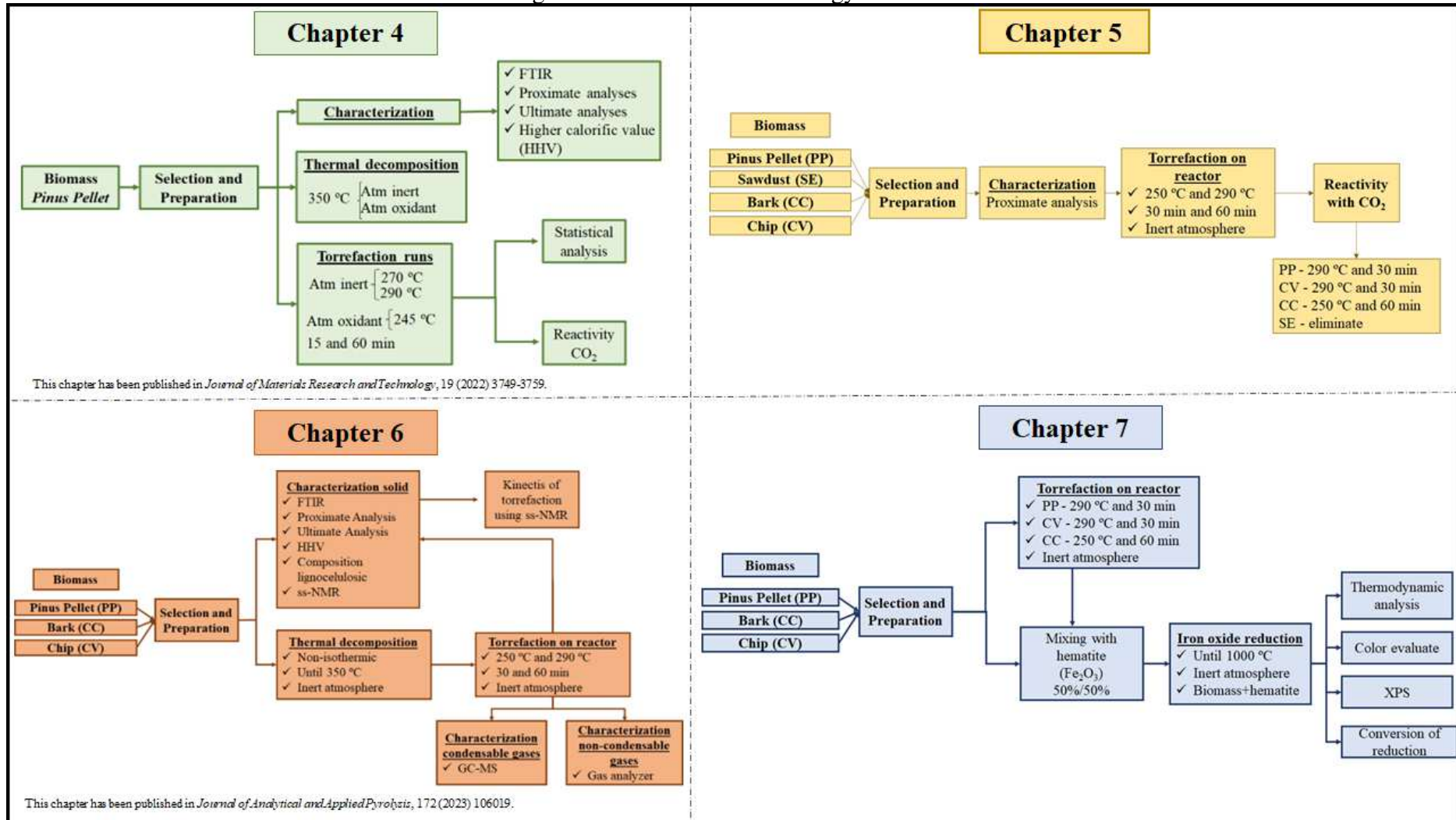
To evaluate the torrefaction parameters, a thermogravimetric tests was carried out with samples with particle sizes of 106  $\mu\text{m}$  and 106-300  $\mu\text{m}$ . The torrefaction was conducted at a temperature of 350  $^{\circ}\text{C}$ , at heating rate of 10  $^{\circ}\text{C min}^{-1}$ , under inert atmosphere applying nitrogen ( $\text{N}_2$ ) and oxidizing atmosphere using synthetic air (Air). With the results of this test, the operational parameters for torrefaction using thermogravimetric analyzer were chosen. The torrefaction tests occurred at temperatures of 270  $^{\circ}\text{C}$  and 290  $^{\circ}\text{C}$  in an inert atmosphere and 245  $^{\circ}\text{C}$  in an oxidizing atmosphere, using residence times of 15 and 60 minutes.

Finally, the torrefaction results were evaluated by statistical analysis and the torrefied biomasses were qualitatively studied according to their reactivity with  $\text{CO}_2$ . For non-isothermal reactivity tests, a thermogravimetric analyzer was used to analyze, 40 mg of sample at a heating rate of 10  $^{\circ}\text{C min}^{-1}$  until reaching a temperature of 900  $^{\circ}\text{C}$ .

In chapter 5, three new biomasses were inserted, SE, CC and CV, in addition to PP biomass. These biomasses were selected, crushed and separated into particle size of 106-300  $\mu\text{m}$ . The characterization was carried out for proximate analysis and, based on the results of such analysis, the SE biomass was eliminated from this study.

Thus, the PP, CC and CV biomasses were torrefied in a fixed bed tubular reactor composed of a concentric quartz cylinder at temperatures of 250  $^{\circ}\text{C}$  and 290  $^{\circ}\text{C}$ , with residence times of 30 min and 60 min and in an inert atmosphere. Then, the torrefied biomasses were qualitatively evaluated in a thermogravimetric analyzer in the presence of  $\text{CO}_2$ . The  $\text{CO}_2$  reactivity of the torrefied biomass was determined non-isothermally until 900  $^{\circ}\text{C}$  with a heating rate of 10  $^{\circ}\text{C min}^{-1}$  in an atmosphere of  $\text{CO}_2$  with a flow rate of 100  $\text{mL min}^{-1}$ . The optimum torrefaction results that showed the highest reactivity were obtained for samples torrefied at 290  $^{\circ}\text{C}$  and for 30 min for PP and CV biomasses and at 250  $^{\circ}\text{C}$  and for 60 min for CC biomass.

Figure 3.1 – General methodology on thesis.



Source: The author, (2023)

After choosing the optimal torrefaction parameters, new characterizations of the biomasses were carried out, composing chapter 6. Both the as received and the torrefied biomasses were characterized by proximate analysis, ultimate analysis, Fourier-transform infrared spectroscopy (FT-IR), Higher Calorific Value (HHV), Nuclear Magnetic Resonance (ss-NMR) and composition of lignin, cellulose and hemicellulose.

With the ss-NMR results of the torrefied samples, a new study was proposed for the calculation of kinetic parameters such as activation energy. For this, it was assumed that the decomposition followed first-order kinetics and that the conversion was proportional to the peak areas. Also, after reactor torrefaction, the condensable gases were characterized using a gas chromatography mass spectrometer (GC-MS) and the non-condensable gases were continuously detected using a gas analyzer.

Finally, in chapter 7, the hematite iron ore reduction tests were performed using as received and torrefied biomasses. Initially, the biomasses were separated into particle size  $<106 \mu\text{m}$  and mixed in a 1:1 ratio (50%/50%) with hematite iron oxide ( $\text{Fe}_2\text{O}_3$ ). The reduction of iron oxide (hematite) was experimentally investigated by TGA analysis using 15 mg of mixture, heating rate of  $10 \text{ }^\circ\text{C min}^{-1}$  and flow rate of  $100 \text{ mL N}_2 \text{ min}^{-1}$ .

The experiments were made using only the biomasses, only the hematite, and the mixtures. The materials were heated from room temperature to  $105 \text{ }^\circ\text{C}$  and held for 10 minutes to remove moisture. Then, a constant heating rate of  $10 \text{ }^\circ\text{C min}^{-1}$  was implemented until  $1000 \text{ }^\circ\text{C}$  was reached. The reduction results were evaluated according to color, via photos using a microscope, thermodynamic analysis, X-ray photoelectron spectroscopy-XPS and iron ore reduction conversion calculation. It is emphasized that each methodology used in this work is detailed in each corresponding chapter.

#### 4 INVESTIGATION OF THE THERMAL BEHAVIOR OF *PINE* WOOD PELLETS DURING TORREFACTION FOR APPLICATION IN METALLURGICAL PROCESSES<sup>1</sup>

##### ABSTRACT

The aim of this study is to investigate the thermal behavior of *Pine* wood pellets during torrefaction under different operational conditions, as well as to evaluate the potential application of the torrefied product in metallurgical processes. Torrefaction tests were carried out in an oxidizing atmosphere (245 °C) and in an inert atmosphere (270 and 290 °C) at residence times of 15 and 60 min. The results of torrefaction in inert atmosphere were also statistically evaluated. To evaluate the potential application of torrefied biomass in metallurgical processes, reactivity tests with CO<sub>2</sub> were performed in the temperature range of 200–1000 °C. The results showed that high torrefaction temperature and residence time decreased the mass yield. Statistical analysis showed the possibility of combining high temperatures with low residence times, or vice versa, to obtain satisfactory mass yields. The experimental results showed the highest reactivity for the torrefied biomass obtained in an inert atmosphere, at 290 °C and 60 min. However, considering the mass yield and reactivity with CO<sub>2</sub>, the best torrefaction conditions for biomass with potential application in metallurgical processes were in an inert atmosphere, at 290 °C and a residence time of 15 min.

**Keywords:** biomass; torrefaction; thermogravimetry, wood waste; thermal conversion

---

<sup>1</sup>This chapter has been published in *Journal of Materials Research and Technology*, 19 (2022) 3749-3759. <https://doi.org/10.1016/j.jmrt.2022.06.082>

## 4.1 INTRODUCTION

In last decades, biomass has attracted much interest as a promising energy source due to its renewability, abundance and carbon dioxide (CO<sub>2</sub>) neutrality [1]. Biomass can be used as an alternative to reduce gaseous emissions caused by non-renewable fuels, such as coal and coke [2],[3]. Moreover, biomass from forest management presents a chemical composition with a great possibility of generating products (liquid, solid and non-condensable gases) with higher added value after conversion [4]. The composition of this class of biomass consists of 10–25% of lignin, 20–40% hemicellulose and 35–55% cellulose [5], [6], [7].

The use of biomass as solid fuel is currently limited by its high moisture content, low calorific value and high oxygen content, which lead to low conversion efficiency as well as a high cost of biomass collection, storage and transportation [6],[8], [9], [10]. Thus, a pretreatment of biomass through thermochemical processes is an alternative to overcome the drawbacks and improve the production of high-quality solid biofuels.

Torrefaction is considered a promising pretreatment for biomass, which is performed under mild conditions mainly to obtain torrefied solid biomass, a type of biochar [11]. This technique consists of a thermal conversion process that is normally carried out in a temperature range between 200 and 300 °C [6], [12]. Higher energy density and calorific value, lower moisture and oxygen/carbon ratio are some of the characteristics that biomasses gain after undergoing the torrefaction process [13], [14], [15]. Furthermore, due to its more compact and hydrophobic character, torrefied biomass reduces storage and transport costs [9], [14], [16].

The partial or complete replacement of fossil fuels used as a source of energy in the metallurgical industry by biomass has been studied and has shown promising results [2], [3], [17], [18]. Fick *et al.* [2] investigated different types of biomasses to replace 20% of the fossil fuel used in the production of pig iron. It was revealed that only biomass from wood and crop residues were able to meet the requirements of the study. However, due to its physical characteristics (size and/or mechanical strength) and low calorific value, it was recommended that the raw biomass should go through a pre-treatment, such as torrefaction, before being applied in the iron manufacturing process.

Mousa *et al.* [3] studied the use of charcoal in the blast furnace and found that this biomass had a higher potential for partial replacement of loaded coke and full replacement for pulverized coal injection (PCI). However, the lower crushing force of this material till represents the main challenges for its loading in modern large blast furnaces. In the case of using torrefied biomass, the mathematical modelling showed interesting results in mitigating

CO<sub>2</sub> emissions with the use of biofuels instead of fossil fuels, with the injection of torrefied/pyrolyzed biomass in the blast furnace.

Wang *et al.* [17] carried out a study on the use of pelletized, torrefied and pyrolyzed biomass in blast furnaces instead of pulverized coal (PC) of fossil sources. Wood pellets were, in general, produced by grinding and compacting at high pressure to be used as granulated biofuel and present higher calorific value, good mechanical resistance, higher bulk density (600 kg m<sup>-3</sup>), higher energy density (3.12 MWh m<sup>-3</sup>), uniform properties and cheaper production and transport costs [18], [19]. Through mathematical modelling, Wang *et al.* [17] found that charcoal from pyrolysis can fully replace PC, while torrefied material and pelletized wood can replace 22.8% and 20.0% (w/w), respectively. The authors also cite benefits such as higher blast furnace gas generation, resulting in lower fuel consumption in an integrated plant, less limestone requirement, lower slag generation rate and lower energy consumption, since enrichment of oxygen reduces the total volume of gas.

Quéno *et al.* [18] verified in their study that the torrefied wood pellets presented characteristics similar to coal in the crushing/pulverization process, which makes it an ideal substitute in the co-combustion process in thermoelectric plants. The product can also be mixed with coal in the production of electricity and in the gasification process in plants with dry biomass-based fluidized bed feed. Thus, the researchers claim that the use of torrefied wood pellets could contribute to reduce the emission of fine particles and gaseous pollutants, such as carbon monoxide (CO), nitrogen oxides (NO<sub>x</sub>) and gaseous organic compounds (C<sub>x</sub>H<sub>y</sub>), compared with the use of fossil fuels.

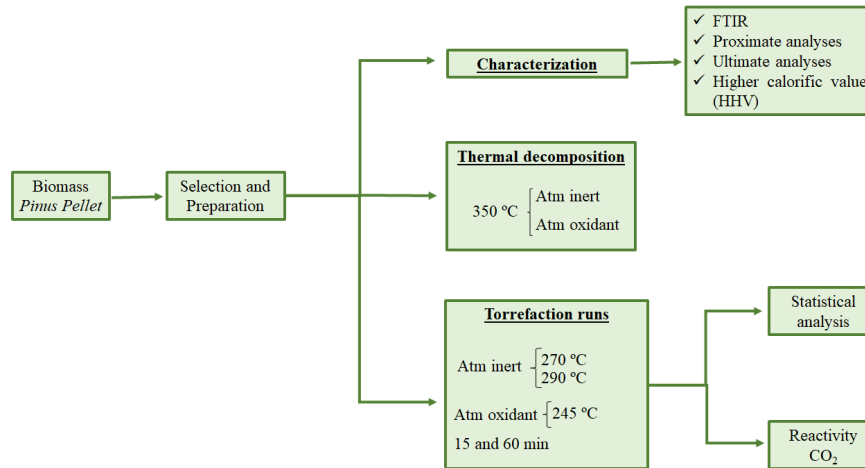
In this context, given the importance of biomass pre-treatment by torrefaction, a detailed study of the effect of operating conditions on the process is necessary to obtain parameters that ensure better chemical and thermal characteristics of the product, as well as a higher yield for application in metallurgical processes. Thus, the main objective of this study was to evaluate the thermal behavior of the wood pellet biomass of the *Pine genus* during torrefaction process, using different parameters, such as atmosphere (inert and oxidizing), temperature (245, 270 and 290 °C) and residence time (15 and 60 min) and evaluate the reactivity of biomass torrefied with CO<sub>2</sub>.



## 4.2 MATERIALS AND METHODS

Figure 4.1 shows a schematic diagram for this section.

Figure 4.1 - Schematic diagram of materials and methods.



Source: Brotto *et al.*, (2022).

### 4.2.1 Biomass selection and preparation

Initially, the selection of pelletized biomass (*Pine Genus*) (5 mm in diameter and 16 mm in length), supplied by the Brazilian company placed in Paraná State (Brazil) was made through random sampling to ensure the homogeneity and reliability of the results obtained. After selection, the dried biomass was ground in an IKA A 11 knife mill (Staufen, Germany), sieved and separated into different particle sizes: smaller than  $<106 \mu\text{m}$  (mesh Tyler 150) and between 106 and  $300 \mu\text{m}$  (mesh Tyler 48). Samples were placed in sealed vials until testing.

### 4.2.2 Characterization

FT-IR analysis was performed using a Spectrum 100 spectrophotometer (PerkinElmer, USA) by scanning between  $4000$  and  $400 \text{ cm}^{-1}$ . For this procedure, the samples were dried and pressed with potassium bromide powder (KBr) at a ratio of 1:100 according to ASTM D2702-05 [20].

Proximate analyses (moisture, ash, volatile matter and fixed carbon) were performed according to the standard ASTM E-1131-08 [21], using a DTG-60 thermogravimetric analyzer (Shimadzu, Japan), using 40 mg of sample, heating rate  $90 \text{ °C min}^{-1}$ , and a gas flow rate of

100 mL min<sup>-1</sup> [22]. Ultimate analyses were performed using a 2400 Series II CHNS/O analyzer (PerkinElmer, USA) according ASTM D5373-08 [23] to determine the content of carbon, hydrogen and nitrogen. The oxygen content was determined from the difference among carbon, hydrogen, nitrogen, ash and moisture. Proximate and ultimate analysis were performed in duplicate.

The higher calorific value (HHV) was determined by the correlation described by Eq. (4.1), where HHV is the higher calorific value in MJ kg<sup>-1</sup>. The validity of this correlation was established for fuels with a wide range of elemental composition, that is, C – 0.00-92.25%, H – 0.43-25.15%, O – 0.00-50.00%, N – 0.00-5.60%, S – 0.00- 94.08% and ash content – 0.00 – 71.4%. The mean absolute error of the correlation is 1.45% [24].

$$HHV = 0.3491C + 1.1783H + 0.1005S - 0.1034O - 0.00151N - 0.0211A \quad (4.1)$$

where, C, H, O, N, S and A represent the contents of carbon, hydrogen, oxygen, nitrogen, sulfur and ash of material, respectively, expressed in percentages (w/w) on a dry basis.

#### 4.2.3 Evaluation of the thermal decomposition of *Pine pellet* (PP)

The thermal behavior of biomass with different particle sizes (<106 μm and 106-300 μm) and in different atmospheres (inert-pure N<sub>2</sub> and oxidant-synthetic air) was studied through non-isothermal tests. Thermogravimetric analyses (TGA) and differential thermal analysis (DTA) were carried out in a DTG-60 thermogravimetric analyzer (Shimadzu, Japan) using 40 mg of sample and a heating rate of 10 °C min<sup>-1</sup> until reaching 300 °C (maximum temperature for torrefaction).

#### 4.2.4 Torrefaction runs

Isothermal torrefaction was also performed in a DTG-60 thermogravimetric analyzer (Shimadzu, Japan) with 40 mg of sample (106-300 μm granulometry), and a gas flow of 100 mL<sub>N<sub>2</sub></sub> min<sup>-1</sup> under atmospheric pressure. The sample was heated in an inert atmosphere at 10 °C min<sup>-1</sup> until torrefaction temperature. Then, for the inert atmosphere torrefaction process, pure nitrogen was used at temperatures of 270 and 290 °C and with residence times of 15 and 60 min. For torrefaction in an oxidizing atmosphere, the gas was switched from N<sub>2</sub> to synthetic air, once the desired temperature was reached (245 °C), and the same residence times were used (15

and 60 min). The use of temperatures in torrefaction runs was determined by the results of thermal decomposition. All tests were performed in duplicate. Eq. (4.2) was used to obtain the solid yield ( $Y$ ) of torrefied biomass [25].

$$Y = \frac{m_{final}}{m_{initial}} \times 100\% \quad (4.2)$$

Where  $m_{final}$  is the mass after the torrefaction process (mg) and  $m_{initial}$  is the mass before the torrefaction process (mg).

#### 4.2.5 Statistical analysis

The statistical analysis of the torrefaction process in inert atmosphere was performed by the evaluation of two experimental parameters, temperature ( $x_1$ ) and residence time ( $x_2$ ), as well as their interaction, on the mass yield of torrefied samples. For this purpose, a  $2^2$  factorial design was performed with a significance interval of 95%. The coded levels -1 and +1 corresponded to temperatures of 270 and 290 °C and residence times of 15 and 60 min, respectively. Results were analyzed using Statistica 9.1 software (StatSoft Inc., USA).

The statistical model used to describe the responses of the factorial design was formulated in terms of the effects per unit variation of the factor and can be represented by the Eq. (4.3).

$$y(x_1, x_2) = \beta_0 + \beta_1 x_1 + \beta_2 x_2 + \beta_{12} x_1 x_2 \quad (4.3)$$

where  $y(x_1, x_2)$  is the response variable (mass yield) at the level  $(x_1, x_2)$ ,  $\beta_0$  is the population value of the mean of all responses,  $\beta_1$ ,  $\beta_2$  and  $\beta_{12}$  are the population values of the experimental parameters (temperature and residence time) and the interaction effect.

#### 4.2.6 Reactivity evaluation of torrefied biomass with CO<sub>2</sub>

The CO<sub>2</sub> reactivity of the torrefied biomass was determined non-isothermally by thermogravimetric analysis. In a typical experiment, the sample was heated from 300 °C to 1000 °C with a heating rate of 10 °C min<sup>-1</sup> in an atmosphere of CO<sub>2</sub> with a flow rate of 100 mL<sub>N2</sub> min<sup>-1</sup>.

The loss of mass that occurs during gasification with CO<sub>2</sub> injection is due to the consumption of carbon present in the torrefied biomass and follows the Boudouard reaction expressed by Eq. (4.4).



Reactivity, which represents the consumption of reagent as a function of reaction time, was determined by Eq. (4.5) [26].

$$r = -\frac{1}{m_0} \left( \frac{dm}{dt} \right) \quad (4.5)$$

where  $r$  is the reaction rate ( $\text{min}^{-1}$ ),  $m_0$  is the mass initial ash free (mg),  $\frac{dm}{dt}$  is the change in mass loss (mg) at time  $t$  (min).

### 4.3 RESULTS AND DISCUSSION

#### 4.3.1 Biomass characterization

The visual characteristics of the *Pine* pellet (PP) biomass *in natura* are shown in Figure 4.2, highlighting its irregular cylindrical shape. According to Cai *et al.* [5], the shape and size of biomass particles affect the quality of mixing and fluidization, the surface area for heat and mass transfer, and the flow behavior of biomass particles. Thus, different shapes and sizes of biomass lead to different conversion efficiencies.

Figure 4.2 – Images of PP biomass: (a) original; (b) 106-300  $\mu\text{m}$ ; and (c) 106  $\mu\text{m}$ .



Source: Brotto *et al.*, (2022).

Samples were ground and particle sized before to thermal treatments to achieve uniform composition and particle sizes. The biomass composition was presented in Table 4.1 and shows that PP biomass contains low moisture content (around 2%), high volatile matter content (83-85%), low ash content (less than 0.7%) and fixed carbon ranging between 14 and 16.08%. All values were obtained on a dry basis. Still, the values of C, H, N and O were expressed in molar terms.

The low moisture content favors the thermochemical processes due to the lower energy demand in the preliminary drying process to remove the moisture present. In addition, it minimizes the effects of biological degradation during storage [27]. The high content of volatile matter contained in the biomass contributes to the development of a more porous structure in the char, increasing the reactivity and conversion efficiency of these materials. Furthermore, biofuels from raw materials with a high content of volatile matter are easier to ignite even at relatively low temperatures, compared to fossil fuels [22].

The low ash content (< 10% on a dry basis) favors thermochemical processes due to the lower probability of accumulation and fouling in reactors. Silica, aluminum, iron, calcium, magnesium, titanium, sodium, and potassium oxides are some of the components that may be present in the ash [5,22]. Fixed carbon is defined as the solid fuel residue that remains after volatile matter is released [5].

Table 4.1 - Composition of PP biomass.

		Particle size ( $\mu\text{m}$ )	
		<106	106-300
Proximate analysis (%)	Moisture	$2.83 \pm 0.10$	$2.06 \pm 0.09$
	Volatile matter	$84.92 \pm 1.52$	$83.28 \pm 1.63$
	Ash content	$0.49 \pm 0.06$	$0.63 \pm 0.08$
	Fix carbon	$14.60 \pm 0.36$	$16.08 \pm 0.43$
Ultimate analysis (%)	C		$48.45 \pm 0.30$
	H		$6.68 \pm 0.02$
	N		$0.12 \pm 0.01$
	O		$42.06 \pm 0.30$
	O/C		0.65
	H/C		1.65

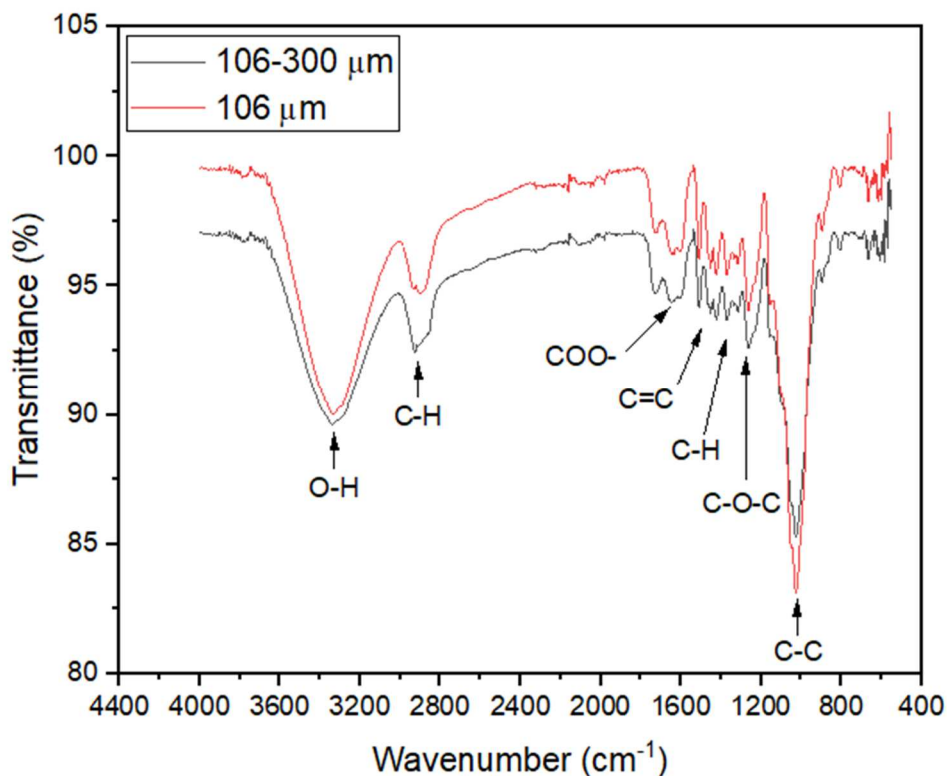
Source: Brotto *et al.*, (2022).

The higher amount of fixed carbon present in the biomass, the higher the calorific value of this material, releasing more energy during the thermal conversion process. The higher calorific value (HHV) for the sample with 106-300  $\mu\text{m}$  was  $20.42 \text{ MJ kg}^{-1}$ . According to Keipi *et al.* [28], the HHV for woody biomass was about  $20 \text{ MJ kg}^{-1}$  based on dry mass. In the study performed by da Silva *et al.* [26], HHV values of  $19.05 \pm 0.27$ ,  $18.29 \pm 0.10$  and  $18.42 \pm 0.23 \text{ MJ kg}^{-1}$  were obtained from *Pine elliottii*, *Eucalyptus dunnii* and *Eucalyptus benthamii*,

respectively. As expected, biomass is mostly composed of carbon and oxygen, followed by lower concentrations of hydrogen and nitrogen. The high value of HHV can be associated to the ultimate composition (hydrogen and carbon) combined with the low moisture and ash content [24], [29].

The FT-IR spectra of PP biomass are shown in Figure 4.3. Samples of different particle sizes (<106  $\mu\text{m}$  and 106-300  $\mu\text{m}$ ) were analyzed and both followed the same behavior. The absorption band at 3329 and 1645  $\text{cm}^{-1}$  are assigned to hydroxyl groups vibration stretching and bending as present in water, respectively [25], [30]. Bands at 2935 and 2898  $\text{cm}^{-1}$  are associated with symmetrical stretch in aliphatic methyl and methylene groups ( $\text{CH}_3$  and  $\text{CH}_2$ ), which are typical for hemicellulose and cellulose containing materials. Also, bands at 1375  $\text{cm}^{-1}$  (C-H deformation) and 1155  $\text{cm}^{-1}$  (C-O-C stretching) are associated with groups present in cellulose and hemicellulose. Peaks at 1733 and 1260  $\text{cm}^{-1}$  are related to carboxylic group (C=O) and C-O stretching of hemicellulose [30], [31].

Figure 4.3 - FTIR spectrum for PP biomass of 106 and 106-300  $\mu\text{m}$ .



Source: Brotto *et al.*, (2022).

The peaks around 1604, 1512 and 1451  $\text{cm}^{-1}$  correspond to C=C stretching vibrations, and C=C stretching vibration and C-H deformation in aromatic ring of lignin, respectively.

Absorption bands at 1421 and 1320  $\text{cm}^{-1}$  are characteristic of  $\text{CH}_2$  vibrations and at 895  $\text{cm}^{-1}$  correspond to C-OH stretching vibrations of cellulose [31], [32]. The most prominent bands at 1000-1110  $\text{cm}^{-1}$  can be assigned to C-OH band vibration in cellulose and hemicellulose (1093  $\text{cm}^{-1}$ ), C-O and C-C stretching in cellulose and hemicellulose (1052  $\text{cm}^{-1}$ ), aromatic C-H in plane deformation of guaiacyl unit, and C-O stretching in cellulose, hemicellulose and lignin (1027  $\text{cm}^{-1}$ ), respectively [30], [31].

#### 4.3.2 Evaluation of thermal decomposition

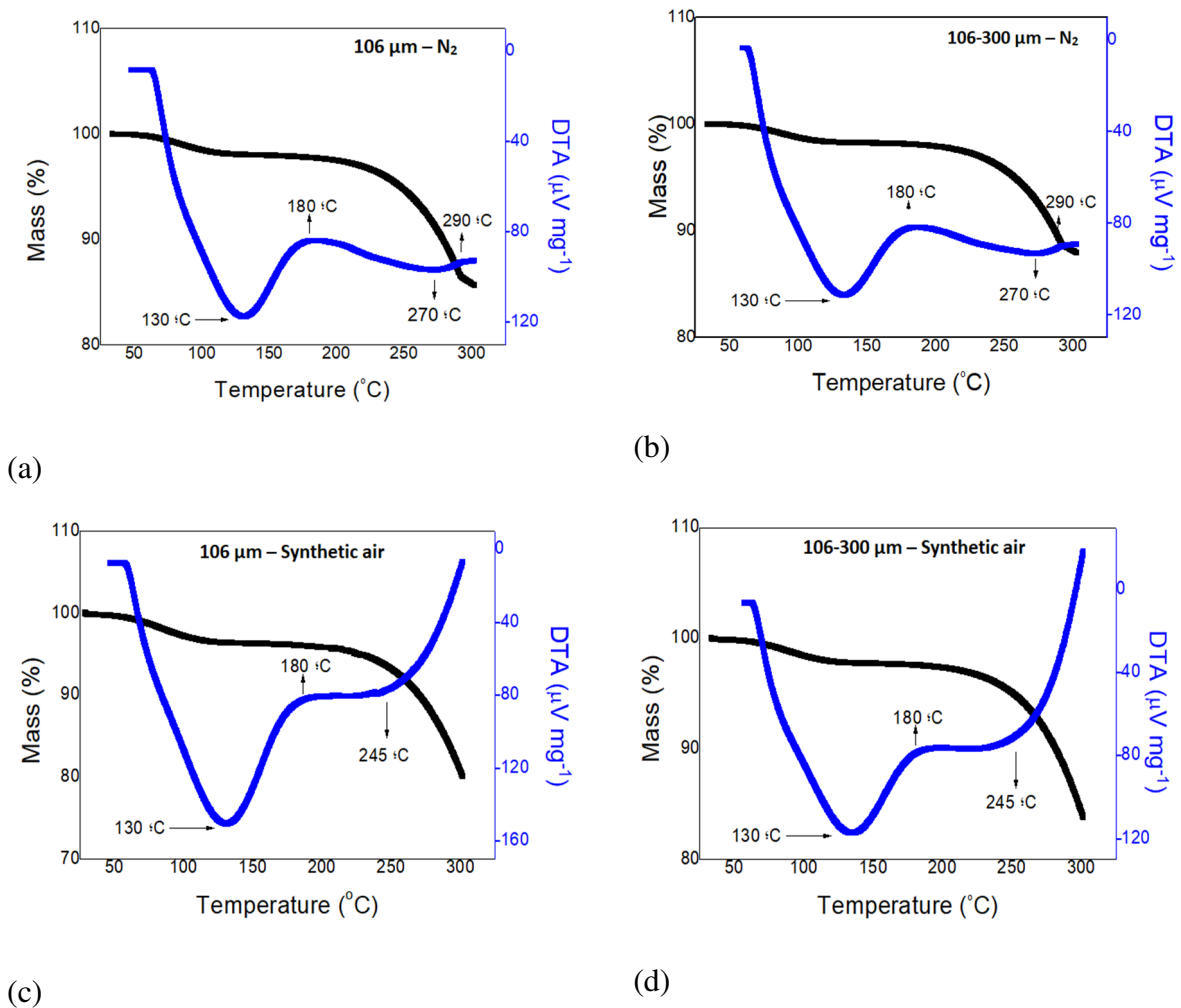
The evaluation of the thermal behavior of the biomass with different granulometries (<106 and 106-300  $\mu\text{m}$ ) was conducted non-isothermally in an inert atmosphere ( $\text{N}_2$ ) and in an oxidizing atmosphere (synthetic air) (Figure S1 – Supplementary material). In general, at temperatures between 25 and 100  $^\circ\text{C}$ , drying of the biomass occurs causing mass loss due to the free-water or moisture release. Between 100 and 200  $^\circ\text{C}$ , the mass loss is subtle than in other temperature ranges, being considered almost a “chemical freeze” [12]. Finally, between 200 and 300  $^\circ\text{C}$ , the loss of mass occurs due to chemical degradation characteristic of the torrefaction process. In this stage, devolatilization processes occur with the release of part of the volatile matter.

According to Figure S4.1 (Supplementary material), the condition that presented the highest loss of mass was in an oxidizing atmosphere for samples with a smaller particle size (106  $\mu\text{m}$ ), where a 19.30% of mass loss was observed. The condition that suffered the smallest loss of mass was in an inert atmosphere with particles of particle size between 106 and 300  $\mu\text{m}$ , with 11.91% of mass loss. The other two conditions showed 14.21 and 15.67% of mass loss in an inert atmosphere with particles of 106  $\mu\text{m}$  and in an oxidizing atmosphere with particles of 106-300  $\mu\text{m}$ , respectively, as expected [14]. Moreover, it is noted that the curves that use inert gas present an inflection around 290  $^\circ\text{C}$ , indicating a stabilization trend in mass loss, unlike the samples submitted to pre-treatment in an oxidizing atmosphere in which the increase in temperature favors mass loss by oxidation.

To identify the optimal temperatures for the torrefaction process, the TGA and DTA analysis were performed (Figure 4.4). In the DTA curves, an endothermic peak was identified for all samples at approximately 130  $^\circ\text{C}$ , showing a loss of mass caused by biomass dehydration and partial decomposition of hemicellulose [29]. This first peak was followed by the start of an endothermic transition (Figure 4.4 (a) and b) or a plateau (Figure 4.4 (c) and d) at the temperature of 180  $^\circ\text{C}$ . Moreover, there is an increase in the biomass decomposition

characterized by the mass loss of the cellulosic component and the partial decomposition of lignin, identified by an endothermic peak at 270 °C for samples in inert atmosphere and by an exothermic peak at 245 °C for samples in oxidizing atmosphere [29,32]. Note that, in this case, the particle size did not affect the decomposition temperature, as expected.

Figure 4.4 – TGA and DTA torrefaction curves of PP biomass under different operational conditions: (a) particle size 106  $\mu\text{m}$  and under  $\text{N}_2$ ; (b) particle size 106-300  $\mu\text{m}$  and under  $\text{N}_2$ ; (c) particle size <106  $\mu\text{m}$  and under air; (d) particle size 106-300  $\mu\text{m}$  and under air.



Source: Brotto *et al.*, (2022).

In the case of samples in oxidizing atmosphere, an exothermic behavior was observed at temperatures above 245 °C due to the combustion of volatile components, in which oxidation of the released gases may have occurred, which would increase the surface temperature causing an increase in DTA [32]. The different behavior of the DTA curves for samples in inert atmosphere and oxidative atmosphere, observed at 290 °C, may be due to oxidative torrefaction



being a complex process that combines oxidation, carbonization and devolatilization, in which torrefaction and oxidation occur in parallel but are not related to each other [33].

### 4.3.3 Torrefaction of biomass

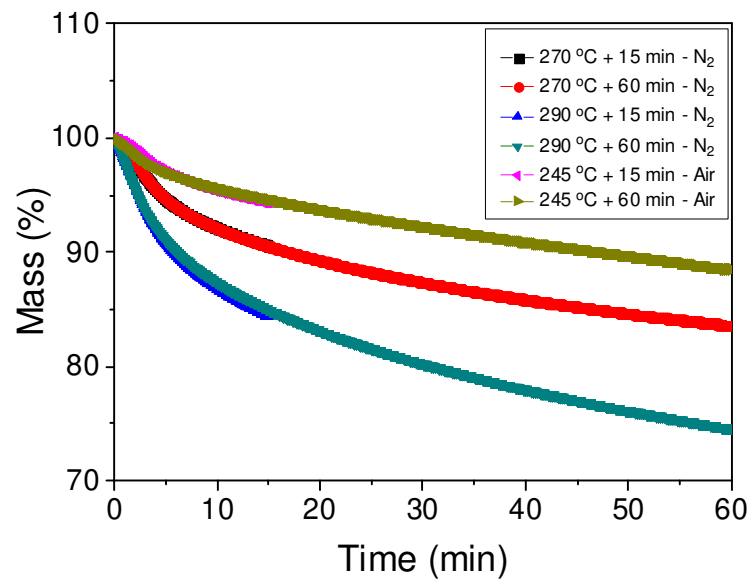
The isothermal torrefaction experiments were carried out at temperatures of 270 and 290 °C for samples in an inert atmosphere, and 245 °C for samples in an oxidizing atmosphere. Furthermore, all samples (106-300 µm granulometry) remained at constant temperature for 15 or 60 min. Figure 4.5 shows the TGA and DTA curves for the isothermal torrefaction tests of the samples. From Figure 4.5(a) it is possible to observe that the curves follow the same behavior trend. The overlapping of the curves of 245, 270 and 290 °C, being differentiated only by the residence times (15 and 60 min).

It can be seen that the longer the residence time, the greater the loss of mass, which is due to the decomposition of the chemical components of the sample, such as cellulose, hemicellulose and lignin. This decomposition can be better visualized in Figure 4.5(b) by the left and right shoulders of the DTA curves, which represent the degradation of hemicellulose and cellulose. In addition, the long tail represents lignin degradation [34]. Thus, as the results obtained in Figure 4.5(b) indicate, longer residence times are required for better lignin degradation.

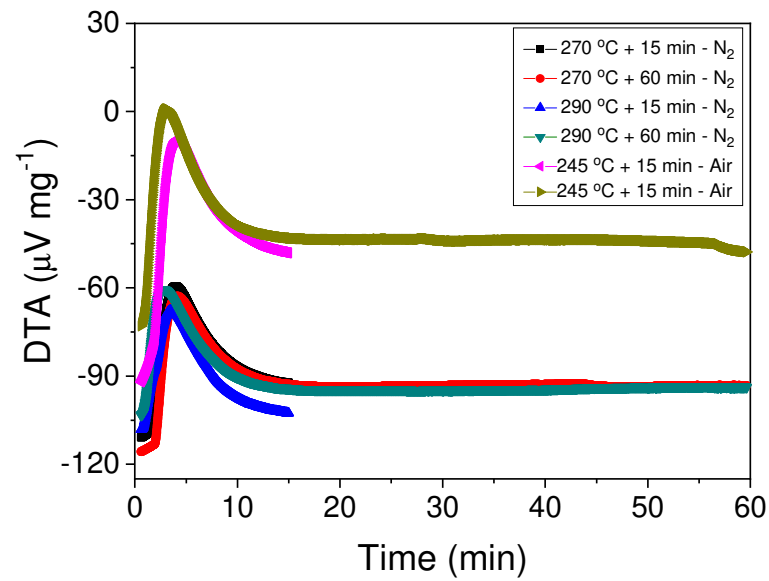
The biomass yields after torrefaction in an inert atmosphere, at a temperature of 270 °C and residence times of 15 and 60 min were, respectively, 90.59% and 83.58%. At a temperature of 290 °C and residence times of 15 and 60 min were, respectively, 84.37% and 74.49%. For torrefaction in an oxidizing atmosphere, at 245 °C and residence times of 15 and 60 min, the mass yields were, respectively, 94.31% and 88.50%.

For inert atmosphere, it is noted that the results obtained for mass yield using 270 °C and 60 min and 290 °C and 15 min were very similar (83.58% and 84.37%). Although higher temperatures and residence times generally tend to decrease mass yield, it is possible to combine higher temperatures with lower residence times, or vice versa, to obtain satisfactory mass yields. In this sense, statistical analysis is very important to verify the influence and significance of these parameters in torrefaction.

Figure 4.5 - Torrefaction profiles under inert atmosphere ( $N_2$ ) and oxidizing atmosphere (synthetic air) at 270, 290 and 245 °C and residence times of 15 and 60 min. (a) TGA curves of mass (%) vs. time (min) and (b) DTA curves ( $\mu V mg^{-1}$ ) vs. time (min).



(a)



(b)

Source: Brotto *et al.*, (2022).

#### 4.3.4 Statistical analysis

To statistically evaluate two important operational parameters in inert atmosphere torrefaction, temperature and residence time, as well as their significance in the process, the response surface methodology based on a  $2^2$  factorial design was performed. Table 4.2 (ANOVA) describes the meaning of the terms that influence the system to be optimized, in this case, the mass yield after torrefaction.

Table 4.2 - ANOVA of the regression model representing the mass yield of PP biomass after torrefaction at 270 and 290 °C and residence time of 15 and 60 min.

Factor	df	SS	MS	Effect	F	p
Temperature; $x_1$	1	117.35	117.35	-7.66	284.92	$7.2 \cdot 10^{-5}$
Time; $x_2$	1	142.30	142.30	-8.43	345.49	$4.9 \cdot 10^{-5}$
Interaction; $x_1x_2$	1	4.09	4.09	-1.43	9.93	$3.34 \cdot 10^{-2}$
Error	4	1.65	0.41	0.44		
Total SS	7	265.38				

df: degrees of freedom; SS: sum of squares; MS: medium square.

Source: Brotto *et al.*, (2022).

From Table 4.2, it is noted that all the  $p$  values are lesser than  $5 \cdot 10^{-3}$ , within the established range of significance. This means that both the temperature and residence time factors and their interaction are statistically significant. Thus, all the parameters compose the statistical model described by Equation (4.6).

$$y(x_1, x_2) = 83.25 - 7.66x_1 - 8.43x_2 - 1.43x_1x_2 \quad (4.6)$$

Regarding Equation (4.6),  $83.25 \pm 0.22$  represents the effect of intercept factor. Terms referring to temperature, residence time and the interaction between the two parameters are negative. This means that these parameters are inversely proportional to the mass yield, that is, to obtain a higher mass yield after the torrefaction process, it is necessary to use lower temperatures and/or reduce the residence time. The opposite is also true, higher temperatures and longer residence times resulted in lower mass yields.

Also, to assess the goodness of fit-of the statistical model, the F values obtained in Table 4.2 can be compared with the theoretical F value, using the Fisher-Snedecor test. Since

the value of  $F_{(3,4)0.95}$  is equal to 6.59, it is noted that the  $F$  values of the analyzed factors as well as their interaction are greater than the  $F$  tabulated at the 5% probability level. This means that the model has a good fit to the results.

Figure 4.6 presents the graphs obtained after the statistical analysis, where Figure 4.6 (a) is the Pareto chart, which illustrates the magnitude and influence, positive or negative, of the effects. It is observed that the vertical line present in the Pareto chart corresponds to the  $p$  value of  $5 \cdot 10^{-3}$ . Values that exceed this vertical line are considered statistically significant [35]. This confirms that the factors temperature and residence time, as well as their interaction, are significant. Also, because it has a larger horizontal bar, temperature is the most important factor when considering mass yield as a response in torrefaction, followed by residence time and the interaction of these two parameters.

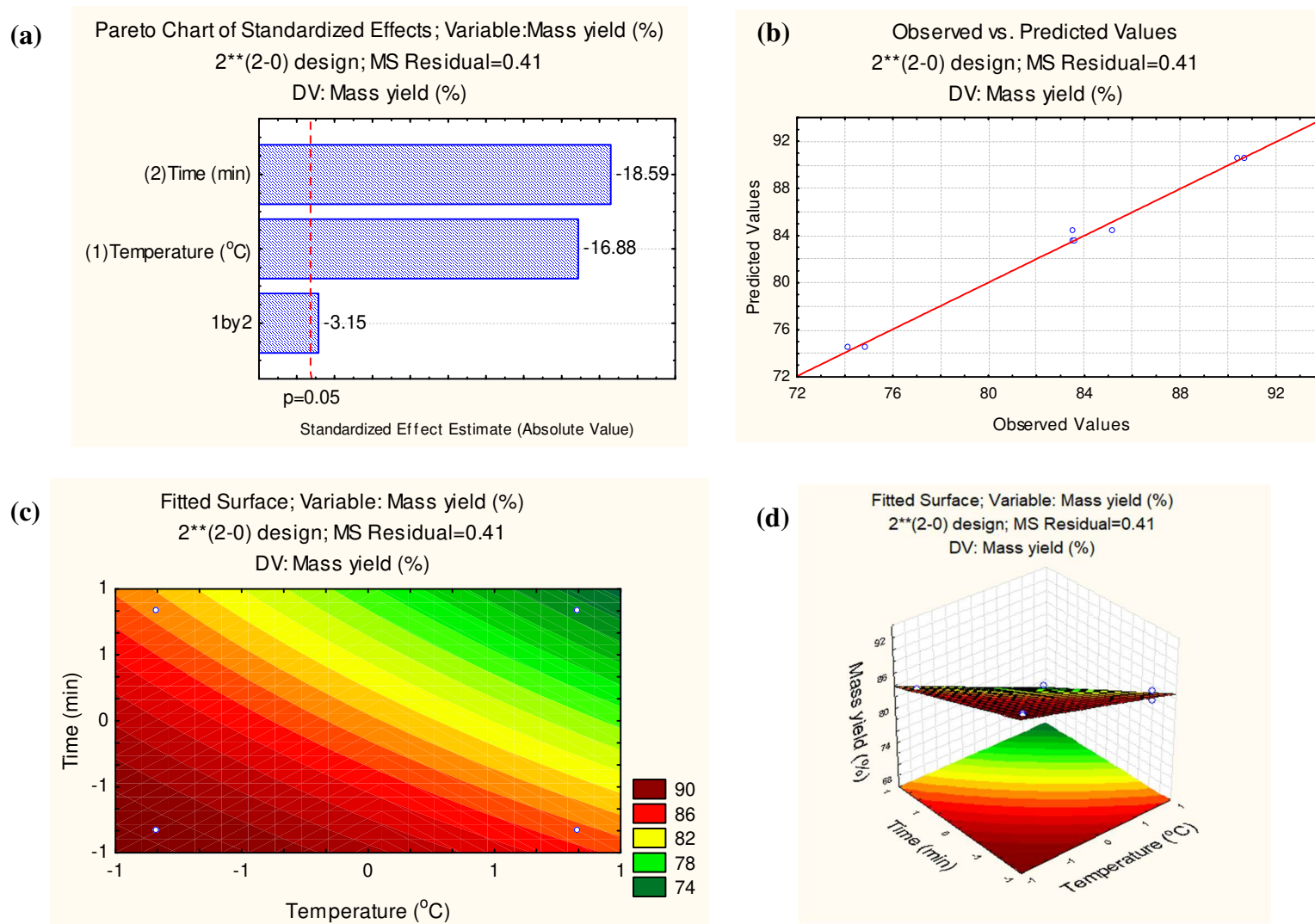
Figure 4.6 (b) shows the relationship between the predicted and observed values, demonstrating that the linear fit of Equation (4.6) is satisfactory, with an  $R^2$  of 0.99. Figure 4.6 (c) and (d) show the response surfaces obtained in 2D and 3D, respectively, indicating that to obtain higher values of mass yield it is necessary to use lower temperatures and residence times, confirming the evidence brought by the other statistical parameters.

The temperature and residence time parameters that represent the negative levels in this study are 270 °C and 15 min. From the statistical analysis, equal or lower values of these parameters will result in higher mass yields. Furthermore, as the interaction parameter is also negative, it is possible to combine positive and negative levels to obtain a higher mass yield. Thus, in terms of mass yield, it is better to use shorter residence times for higher temperatures and longer residence times for lower temperatures.

#### 4.3.5 Reactivity evaluation of torrefied biomass with CO<sub>2</sub>

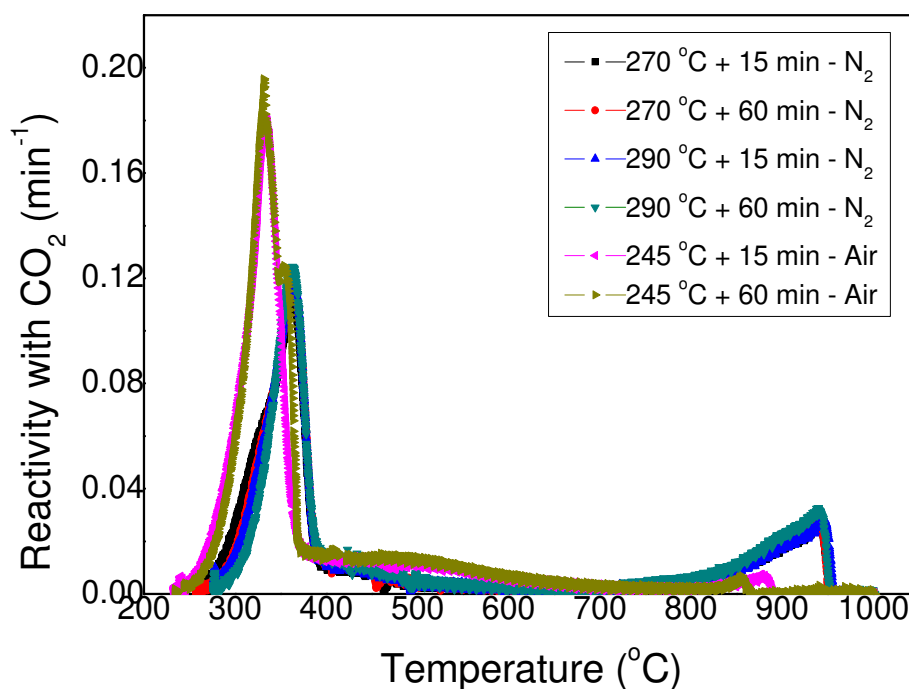
To evaluate the best operational conditions for PP biomass torrefaction aiming its application in metallurgical processes, the reactivity of torrefied biomass with CO<sub>2</sub> was evaluated, as shown in Figure S4.2 (Supplementary material) and Figure 4.7. In general, the non-isothermal gasification process can be divided into two main steps (Figure S4.2 - Supplementary material). The first stage, which occurs within 300-650 °C for samples torrefied in N<sub>2</sub> and 300-800 °C for samples torrefied in synthetic air, is responsible for mass loss due to devolatilization. The second stage, within 650-950 °C for torrefied biomass in an inert atmosphere and 800-900 °C for torrefied biomass in an oxidizing atmosphere, is responsible for the gasification reaction, Equation (4.4).

Figure 4.6 - Response curves (a) Pareto chart, (b) Predicted vs. observed values, (c) 2D response surface and (d) 3D response surface.



Source: Brotto *et al.*, (2022).

Figure 4.7 - CO<sub>2</sub> reactivity of torrefied PP biomass under different operating conditions.



Source: Brotto *et al.*, (2022).

Figure S4.2 (Supplementary material) shows that, up to a temperature around 400 °C, the behavior of the curves is similar, regardless of the atmosphere, temperature and residence time. However, when exceeding 400 °C, a small inclination can be seen in the curves corresponding to torrefaction in an inert atmosphere, while in torrefaction in an oxidizing atmosphere the curves continue to decline until the biomass is completely degraded at around 850 °C.

A behavior close to linearity is observed between temperatures of 400 and 800 °C, with an abrupt curve at 850 °C and, close to 950 °C, the biomass is totally degraded, as shown in Figure S2 (Supplementary material) for torrefaction in an inert atmosphere. It is also noted that torrefaction at a lower temperature (270 °C) promoted a greater loss of mass compared to a temperature of 290 °C. That is, biomass torrefied at 290 °C could react for a longer time because it has a greater amount of mass. Furthermore, the longer the torrefaction residence time (60 min) the better the reactivity with CO<sub>2</sub>.

Analyzing Figure 4.7, a similar behavior over time is observed for all samples torrefied under different conditions. There is a large initial peak assigned to the devolatilization process that involves thermal degradation reactions of residual hemicellulose (200-320 °C), in addition to cellulose (320-420 °C) and lignin (220-500 °C) [36], [37]. These peaks are significantly

higher for the samples torrefied at 245 °C and in an oxidizing atmosphere, since these were the samples that had the lowest mass loss during torrefaction, only 5.69% (15 min) and 11.50% (60 min), while samples torrefied at 270 °C and inert atmosphere have 9.41% (15 min) and 16.42% (60 min) of mass loss and those torrefaction at 290 °C during 15 and 60 min have 15.63% and 25.51% of mass loss, respectively. Confirming the effect of torrefaction temperature on the thermal decomposition of biomass with elimination of volatile materials. That is, increasing the torrefaction temperature results in a decrease in mass yield.

During torrefaction with synthetic air, in addition to devolatilization, another important mechanism that occurs is oxidation, thus, the composition of the solid torrefied in different atmospheres is likely to be different [38], [39]. Additionally, a shoulder is observed in the second half of the devolatilization peaks at about 350 to 450 °C (Fig. 4.7), associated with the thermal decomposition of lignin [36], [40]. These shoulders are more pronounced in samples torrefied at a lower temperature (245 °C), indicating the presence of a higher lignin content in the composition of these pretreated biomasses.

The second peak present in all curves between 830 and 950 °C, Figure 4.7, is related to the reactivity of the torrefied biomasses with CO<sub>2</sub>. The more intense peak was torrefied biomass at 290°C and 60 min (N<sub>2</sub>), with a reactivity of 0.034 min<sup>-1</sup>, which is comparable with others combustibles used in metallurgical processes [41].

Under the conditions of 290°C and 15 min (N<sub>2</sub>), 270°C and 15 min (N<sub>2</sub>) and 270°C and 60 min (N<sub>2</sub>), the peaks were superimposed, showing reactivity values close to 0.026 min<sup>-1</sup>. Finally, the most satisfactory result was obtained for the biomass torrefied at 290°C and 60 min (N<sub>2</sub>), that produced the greater release of volatiles during torrefaction. It has been reported that the release of volatiles during the thermal treatment of biomass increase the consequently, the number of reactive sites available for reactions [42]. On the other hand, the lowest reactivity peaks were observed for samples torrefied in synthetic air, ~ 0.0070 min<sup>-1</sup>, because oxidation reactions occur in this atmosphere and can also consume part of the carbon present in the sample [38].

Kieush *et al.* [42] studied the influence of wood pellets on the reactivity of coke with CO<sub>2</sub>. The authors added 5% by mass of biomass pellets to the coke, thus obtaining biocoke. By comparing the results of coke and biocoke reactivity tests with CO<sub>2</sub>, the authors found that biocoke samples react and terminate earlier compared to coke. This is explained by the preferential consumption of charcoal particles in the Boudouard reaction (Equation 4.4), which takes place in the shaft region of the blast furnace, where the carbonaceous material is gasified to form carbon monoxide [43,44]. In the blast furnace, in order to have high production with

low fuel consumption, it is necessary that the ascending gases are used to the maximum, that is, when they leave the blast furnace with the highest CO<sub>2</sub> content and the lowest possible temperature.

Thus, considering only the reactivity with CO<sub>2</sub>, the PP biomass torrefied at 290 °C for 60 min and in an inert atmosphere showed the best results. However, these conditions do not promote the best mass yield. Comparing the mass yield of the process that took place at 270 °C for 60 min and 290 °C for 15 min, it is noted that the reactivity of the latter was better. According to this, to achieve a better mass yield with good reactivity with CO<sub>2</sub>, the best torrefaction condition for PP biomass in an inert atmosphere should be considered, at 290 °C for 15 min.

Moreover, another alternative to obtain satisfactory results considering mass yield and reactivity with CO<sub>2</sub> would be the mixture of biomasses torrefied at 290 °C, with residence times of 15 and 60 min and in an inert atmosphere. The combination of biomass torrefied at 290 °C and shorter residence times can achieve higher mass yields and, at longer residence times, better reactivity with CO<sub>2</sub>. Furthermore, mixing torrefied biomass in the metallurgical industry can affect coke reactivity, decrease in the gasification temperature in blast furnaces, decreasing the amount of coke needed to produce one ton of hot metal and minimizing total consumption of carbon. In this way, CO<sub>2</sub> emissions would also be reduced [3], [41], [44].

#### 4.4 CONCLUSIONS

From this study, the importance of investigating and analyzing the influence of experimental parameters in torrefaction for its potential application in metallurgical processes was verified. The first parameter analyzed was the particle size (<106 μm and 106–300 μm), in which there was less loss of mass when using biomass of larger particle sizes (106–300 μm) in an inert atmosphere.

Regarding the thermal analysis, it pointed out that the best torrefaction temperature in an oxidizing atmosphere was 245 °C and in an inert atmosphere it was 270 and 290 °C. Using these conditions, torrefaction tests were carried out with residence times of 15 and 60 min and showed that higher temperatures and longer residence times decrease mass yield. However, according to the statistical analysis, it could be seen that it is possible to combine higher temperatures with lower residence times, or vice versa, to obtain satisfactory mass yields.

Finally, regarding the analysis of reactivity with CO<sub>2</sub>, the biomass PP torrefied at 290 °C, 60 min and in an inert atmosphere presented the most satisfactory result and reactivity



equal to  $0.034 \text{ min}^{-1}$ , which is comparable with others combustibles used in metallurgical processes. Additionally, considering both the mass yield and the reactivity with  $\text{CO}_2$ , the best torrefaction conditions for PP biomass are in an inert atmosphere, at  $290 \text{ }^\circ\text{C}$  and 15 min.

#### 4.5 REFERENCES

- [1] J. Xu, M. Huang, Z. Hu, W. Zhang, Y. Li, Y. Yang, *et al.* Prediction and modeling of the basic properties of biomass after torrefaction pretreatment J Anal Appl Pyrolysis, 159 (2021), Article 105287, 10.1016/j.jaap.2021.105287
- [2] G. Fick, O. Mirgaux, P. Neau, F. Patisson Using biomass for pig iron production: a technical Environmental and Economical Assessment, Waste Biomass Valorization, 5 (2014), pp. 43-55, 10.1007/s12649-013-9223-1
- [3] E. Mousa, C. Wang, J. Riesbeck, M. Larsson Biomass applications in iron and steel industry: an overview of challenges and opportunities Renew Sustain Energy Rev, 65 (2016), pp. 1247-1266, 10.1016/j.rser.2016.07.061
- [4] L.E. Arteaga-Pérez, C. Segura, D. Espinoza, L.R. Radovic, R. Jiménez Torrefaction of *Pine radiata* and *Eucalyptus globulus*: a combined experimental and modeling approach to process synthesis Energy Sustain Dev, 29 (2015), pp. 13-23, 10.1016/j.esd.2015.08.004
- [5] J. Cai, Y. He, X. Yu, S.W. Banks, Y. Yang, X. Zhang, *et al.* Review of physicochemical properties and analytical characterization of lignocellulosic biomass Renew Sustain Energy Rev, 76 (2017), pp. 309-322, 10.1016/j.rser.2017.03.072
- [6] M. Chai, L. Xie, X. Yu, X. Zhang, Y. Yang, M.M. Rahman, *et al.* Poplar wood torrefaction: kinetics, thermochemistry and implications Renew Sustain Energy Rev, 143 (2021), Article 110962, 10.1016/j.rser.2021.110962
- [7] C. Wang, X. Yuan, S. Li, X. Zhu Enrichment of phenolic products in walnut shell pyrolysis bio-oil by combining torrefaction pretreatment with fractional condensation Renew Energy, 169 (2021), pp. 1317-1329, 10.1016/j.renene.2021.01.112
- [8] H. Namkung, J.-H. Park, Y.-J. Lee, G.-S. Song, J.W. Choi, S.-J. Park, *et al.* Performance evaluation of biomass pretreated by demineralization and torrefaction for ash deposition and PM emissions in the combustion experiments Fuel, 292 (2021), Article 120379, 10.1016/j.fuel.2021.120379
- [9] B. Yan, L. Jiao, J. Li, X. Zhu, S. Ahmed, G. Chen Investigation on microwave torrefaction: parametric influence, TG-MS-FTIR analysis, and gasification performance Energy, 220 (2021), Article 119794, 10.1016/j.energy.2021.119794
- [10] J.P. Bennett, K.S. Kwong Failure mechanisms in high chrome oxide gasifier refractories Metall Mater Trans, 42 (2011), pp. 888-904, 10.1007/s11661-011-0635-x
- [11] H. Ong, K. Yu, W. Chen, M. Pillejera, X. Bi, K. Tran, *et al.* Variation of lignocellulosic biomass structure from torrefaction: a critical review Renew Sustain Energy Rev, 152 (2021), Article 111698, 10.1016/j.rser.2021.111698

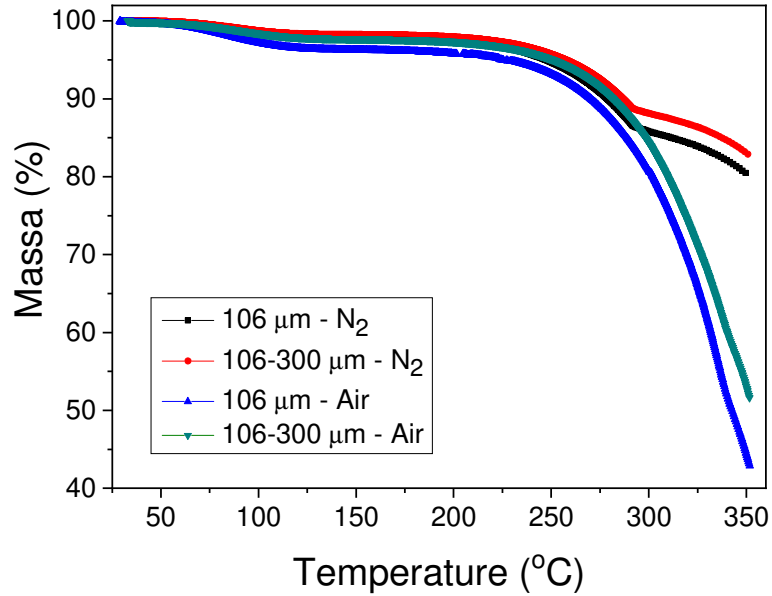
- [12] W.-H. Chen, B.-J. Lin, Y.-Y. Lin, Y.-S. Chu, A.T. Ubando, P.L. Show, *et al.* Progress in biomass torrefaction: principles, applications and challenges  
Prog Energy Combust Sci, 82 (2021), Article 100887, 10.1016/j.peccs.2020.100887
- [13] Y. Mei, R. Liu, Q. Yang, H. Yang, J. Shao, C. Draper, *et al.* Torrefaction of cedarwood in a pilot scale rotary kiln and the influence of industrial flue gas  
Bioresour Technol, 177 (2015), pp. 355-360, 10.1016/j.biortech.2014.10.113
- [14] K. Nakason, P. Khemthong, W. Kraithong, P. Chukaew, B. Panyapinyopol, D. Kitkaew, *et al.* Upgrading properties of biochar fuel derived from cassava rhizome via torrefaction: effect of sweeping gas atmospheres and its economic feasibility  
Case Stud Therm Eng, 23 (2021), Article 100823, 10.1016/j.csite.2020.100823
- [15] H. Yun, R. Clift, X. Bi Environmental and economic assessment of torrefied wood pellets from British Columbia Energy Convers Manag, 208 (2020),  
Article 112513, 10.1016/j.enconman.2020.112513
- [16] K. Cen, X. Zhuang, Z. Gan, Z. Ma, M. Li, D. Chen Effect of the combined pretreatment of leaching and torrefaction on the production of bio-aromatics from rice straw *via* the shape selective catalytic fast pyrolysis  
Energy Rep, 7 (2021), pp. 732-739, 10.1016/j.egyr.2021.01.031
- [17] C. Wang, P. Mellin, J. Lövgren, L. Nilsson, W. Yang, H. Salman, *et al.* Biomass as blast furnace injectant – considering availability, pretreatment and deployment in the Swedish steel industry Energy Convers Manag, 102 (2015), pp. 217-226, 10.1016/j.enconman.2015.04.013
- [18] L.R.M. Quéno, A.N. Souza, A.F. Costa, A.T. Valle, M.S. Joaquim Aspectos técnicos da produção de pellets de madeira Ciência Florest, 29 (3) (2019), pp. 1478-1489, 10.5902/1980509820606
- [19] N. Setkit, X. Li, H. Yao, N. Worasuwanarak Torrefaction behavior of hot-pressed pellets prepared from leucaena wood Bioresour Technol, 321 (2021),  
Article 124502, 10.1016/j.biortech.2020.124502
- [20] ASTM D2702-05: standard practice for rubber chemicals — determination of infrared absorption characteristics Annu. B. ASTM Stand. (2016), p. 4, 10.1520/D2702-05R16
- [21] ASTM E1131-08: standard test method for compositional analysis by thermogravimetry ASTM International, West Conshohocken (2014), pp. 1-6, 10.1520/E1131
- [22] T.R. Pacioni, D. Soares, M.D. Domenico, M.F. Rosa, R.F.P.M. Moreira, H.J. José Bio-syngas production from agro-industrial biomass residues by steam gasification  
Waste Manag, 58 (2016), pp. 221-229, 10.1016/j.wasman.2016.08.021
- [23] ASTM D5373-08 Standard test methods for instrumental determination of carbon, hydrogen, and nitrogen in laboratory samples of coal and coke  
Annu. B. ASTM Stand, ASTM International, West Conshohocken (2016), p. 4, 10.1520/D5373-16
- [24] S.A. Channiwala, P.P. Parikh A unified correlation for estimating HHV of solid, liquid and gaseous fuels Fuel, 81 (2002), pp. 1051-1063, 10.1016/S0016-2361(01)00131-4

- [25] R.K. Singh, A. Sarkar, J.P. Chakraborty Effect of torrefaction on the physicochemical properties of eucalyptus derived biofuels: estimation of kinetic parameters and optimizing torrefaction using response surface methodology (RSM) *Energy*, 198 (2020), Article 117369, 10.1016/j.energy.2020.117369
- [26] J.G. Pohlmann, E. Osório, A. CF Vilela, M.A. Diez, A.G. Borrego Pulverized combustion under conventional (O<sub>2</sub>/N<sub>2</sub>) and oxy-fuel (O<sub>2</sub>/CO<sub>2</sub>) conditions of biomasses treated at different temperatures *Fuel Process Technol*, 155 (2017), pp. 174-182, 10.1016/j.fuproc.2016.05.025
- [27] A. Dhaundiayal, S.B. Singh, D. Atsu, L. Toth Comprehensive analysis of pre-treated Austrian pine Fuel, 287 (2021), Article 119605, 10.1016/j.fuel.2020.119605
- [28] T. Keipi, H. Tolvanen, L. Kokko, R. Raiko The effect of torrefaction on the chlorine content and heating value of eight woody biomass samples *Biomass Bioenergy*, 66 (2014), pp. 232-239, 10.1016/j.biombioe.2014.02.015
- [29] J.C.G. Silva, J.L.F. Alves, W.V.A. Galdino, S.L.F. Andersen, R.F. Sena Pyrolysis kinetic evaluation by single-step for waste wood from reforestation *Waste Manag*, 72 (2018), pp. 265-273, 10.1016/j.wasman.2017.11.034
- [30] G. Toscano, V. Maceratesi, P. Stipa, E. Laudadio, S. Sabbatini FTIR spectroscopy for determination of the raw materials used in wood pellet production *Fuel* (2022), Article 123017, 10.1016/j.fuel.2021.123017
- [31] R. Moreira, C.V.T. Mendes, M.B.F. Banaco, M.G.V.S. Carvalho, A. Portugal New insights in the fractionation of *Pine* pinaster wood: sequential autohydrolysis, soda ethanol organosolv and acidic precipitation *Ind Crop Prod*, 152 (2020), Article 112499, 10.1016/j.indcrop.2020.112499
- [32] D. Simóm, N. Quaranta, S. Gass Ceramic bricks containing Ni ions from contaminated biomass used as an adsorbent *Sustain. Environ Res*, 30 (2020), p. 26, 10.1186/s42834-020-00067-3
- [33] T.O. Olugbade, O.T. Ojo Biomass torrefaction for the production of high-grade solid biofuels: a review *Bioenerg Res*, 13 (2020), pp. 999-1015, 10.1007/s12155-020-10138-3
- [34] T.R.K.C. Doddapaneni, J. Konttinen, T.I. Hukka, A. Moilanen Influence of torrefaction pretreatment on the pyrolysis of Eucalyptus clone: a study on kinetics, reaction mechanism and heat flow *Ind Crop Prod*, 92 (2016), pp. 244-254, 10.1016/j.indcrop.2016.08.013
- [35] A. Rubio-Clemente, J. Gutiérrez, H. Henao, A.M. Melo, J.F. Pérez, E. Chica Adsorption capacity of the biochar obtained from *Pine patula* wood micro-gasification for the treatment of polluted water containing malachite green dye *J King Saud Univ Eng Sci* (2021), 10.1016/j.jksues.2021.07.006
- [36] K.-Q. Tran, H.-H. Bui, A. Luengnaruemitchai, L. Wang, Ø. Skreiberg Isothermal and non-isothermal kinetic study on CO<sub>2</sub> gasification of torrefied forest residues *Biomass Bioenergy*, 91 (2016), pp. 175-185, 10.1016/j.biombioe.2016.05.024
- [37] A. Sarvaramini, F. Larachi Integrated biomass torrefaction – chemical looping combustion as a method to recover torrefaction volatiles energy *Fuel*, 116 (2014), pp. 158-167, 10.1016/j.fuel.2013.07.119

- [38] W.-H. Chen, K.-M. Lu, S.-H. Liu, C.-M. Tsai, W.-J. Lee, T.-C. Lin  
Biomass torrefaction characteristics in inert and oxidative atmospheres at various superficial velocities *Bioresour Technol*, 146 (2013), pp. 152-160, 10.1016/j.biortech.2013.07.064
- [39] H.C. Ong, K.L. Yu, W.-H. Chen, M.K. Pillejera, X. Bi, K.-Q. Tran, *et al.*  
Variation of lignocellulosic biomass structure from torrefaction: a critical review  
*Renew Sustain Energy Rev*, 152 (2021), Article 111698, 10.1016/j.rser.2021.111698
- [40] Q. He, Q. Guo, L. Ding, J. Wei, G. Yu CO<sub>2</sub> gasification of char from raw and torrefied biomass: reactivity, kinetics and mechanism analysis *Bioresour Technol*, 293 (2019), Article 122087, 10.1016/j.biortech.2019.122087
- [41] L. Florentino-Madiedo, E. Díaz-Faes, C. Barriocanal Reactivity of biomass containing briquettes for metallurgical coke production *Fuel Process Technol*, 193 (2019), pp. 212-220, 10.1016/j.fuproc.2019.05.017
- [42] J.G. Pohlmann, A.G. Borrego, E. Osório, M.A. Diez, A. CF Vilela Combustion of eucalyptus charcoals and coal of similar volatile yields aiming at blast furnace injection in a CO<sub>2</sub> mitigation environment *J Clean Prod*, 129 (2016), pp. 1-11, 10.1016/j.jclepro.2016.04.138
- [43] L. Kieush, J. Schenk, A. Pfeiffer, A. Koveria, G. Rantitsch, H. Hopfinger Investigation on the influence of wood pellets on the reactivity of coke with CO<sub>2</sub> and its microstructure Properties *Fuel*, 309 (2022), Article 122151, 10.1016/j.fuel.2021.122151
- [44] G. Rantitsch, A. Bhattacharyya, A. Günbati, M. Schultn, J. Schenk, I. Letofsky-Papst, *et al.*  
Microstructural evolution of metallurgical coke: evidence from Raman spectroscopy  
*Int J Coal Geol*, 227 (2020), Article 103546, 10.1016/j.coal.2020.103546

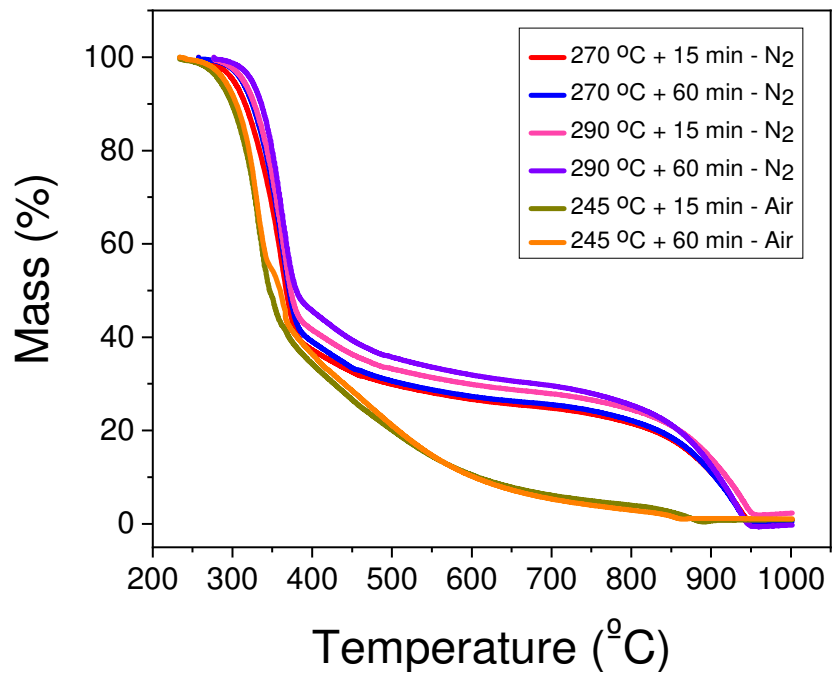
#### 4.6 SUPPLEMENTARY MATERIAL

Figure. S4.1 – Non-isothermal tests of biomass in inert and oxidizing atmosphere with particle sizes of  $<106 \mu\text{m}$  and  $106\text{-}300 \mu\text{m}$ .



Source: Brotto *et al.*, 2022.

Figure S4.2 – Reactivity with  $\text{CO}_2$  of torrefied biomass under different operating conditions in terms of mass (%) and temperature ( $^\circ\text{C}$ ).



Source: Brotto *et al.*, 2022.

## 5 EVALUATION OF THE REACTIVITY OF LIGNOCELLULOSIC BIOMASSES TORREFIED WITH CO<sub>2</sub> FOR APPLICATION IN ORE REDUCTION PROCESSES

### ABSTRACT

This study aimed to evaluate the reactivity of lignocellulosic biomasses torrefied with CO<sub>2</sub> aiming at the partial and/or total replacement of metallurgical coke for the mitigation of CO<sub>2</sub> emissions. For this, 4 biomasses were initially studied: *Eucalyptus* sawdust (SE), *Pine* pellets (PP), *Pine* chips (CV) and *Pine* bark (CC). Knowledge of the chemical and physical characteristics of biomass is essential to assess its efficiency in the process. For this, the physical characteristics were determined: particle size, color, geometry and grindability and the chemical characteristics of volatile material content, ash and fixed carbon by means of proximate analyses. Subsequently, for torrefaction of these biomasses, a fixed-bed reactor was used, operating at the temperatures of 250 °C and 290 °C and residence time of 30 min and 60 min, in an inert atmosphere (N<sub>2</sub>). After the torrefaction process, the biomasses were submitted to non-isothermal thermogravimetric tests up to 900 °C, in a CO<sub>2</sub> atmosphere, aiming at evaluating the reactivity of the torrefied biomasses. The characterization results carried out on a dry basis showed that all biomasses have low ash content (<1%), volatile material between 86.15-65.79% and fixed carbon between 13.85-33.30%. Because it presented the lowest percentage of fixed carbon in its composition (13.85%) compared to the other biomasses, it was decided to end the studies with the SE biomass, continuing only with the PP, CV and CC biomasses. The results of reactivity with CO<sub>2</sub> showed that the operational conditions that ended up in torrefied product with greater reactivity were 290 °C and 30 min for the PP and CV biomasses and 250 °C and 60 min for the CC biomass.

**Keywords:** biomass; torrefaction; wood waste; CO<sub>2</sub> reactivity.

## 5.1 INTRODUCTION

One of the world's biggest problems today is the high level of CO<sub>2</sub> emissions, around 70% of which are linked to the production of iron and steel. One of the reasons for this high percentage generated by the steel industry is the use of coke in blast furnaces [1]. Azadi *et al.* [2] reports that the industrial blast furnace annually produces around 4 million tonnes of liquid iron and a total of more than 7 million tonnes of CO<sub>2</sub> emissions per year. Mineral coal is one of the world's main sources of energy and seeking alternatives to reduce CO<sub>2</sub> emissions and achieve carbon neutrality is a challenge that industries and researchers are currently facing [3].

A renewable source material that has potential for application as a biofuel and other products from the biorefinery concept is biomass. Zhang *et al.* [4] cited that biomass is a widely used energy source in the world, accounting for around 14% of the world's annual energy consumption. Furthermore, biomass is a carbon-neutral energy source and can be converted into solid, liquid and gaseous forms of renewable biofuels [4]. Biomass can also be used to produce heat directly in burners [5].

Dashti *et al.* [5] claimed that coal-fired power stations are interested in partially replacing coal with biomass, without any changes to the equipment, in order to reduce fossil fuel consumption and, consequently, CO<sub>2</sub> emissions. Pohlmann *et al.* [6] cited that the combination of biomass combustion as a partial substitute for coal in industrial processes together with CO<sub>2</sub> capture technologies can lead to negative emissions, reducing CO<sub>2</sub> emissions from power plants and steel mills.

However, when using lignocellulosic biomass as a source for the production of clean energy, it is necessary to improve some characteristics such as decrease the volatile matter and increase the percentage of fixed carbon. In addition, properties such as low grinding capacity, low energy density, high moisture content, irregular shape and size, biological instability and hydrophilicity are unfavorable for application as a fuel [7]. In this context, torrefaction becomes a promising pretreatment technique to improve these characteristics of lignocellulosic biomass [7], [8].

Torrefaction is a thermal process in which the biomass is subjected to temperatures of 200-300 °C, in an inert or oxidizing atmosphere and for a certain residence time, which can vary from 15-120 min [8]. Thus, after passing through the torrefaction process, the biomass will have its physical and chemical properties altered, such as a reduction in the volatile matter

content and an increase in the percentage of fixed carbon, in addition to improving the other characteristics mentioned above, such as an increase in energy density.

The blast furnace is a multiphase countercurrent reactor which is charged by solid carbon-based materials such as coke and iron-containing material. This material is subjected to hot air and, after a sequence of chemical and physical interactions, metal is produced as the main product and top gas and slag as by-products [2]. Iron ore can also be reduced to sponge iron or solid reduced iron by means of direct reduction processes using pure H<sub>2</sub> as the reducing gas [9]. When using lignocellulosic biomass in blast furnaces, direct generation of CO and CO<sub>2</sub> can occur from carboxyl, carbonyl groups and aliphatic hydrocarbons [4].

The coal gasification process can be processed in air, steam or CO<sub>2</sub>, but in a CO<sub>2</sub> atmosphere it is the most prevalent in metal production processes [10], [11]. To measure the CO<sub>2</sub> reactivity of the carbon reducer for metal production, a 100% CO<sub>2</sub> atmosphere is used at 1100 °C [10]. With this, the material rich in carbon (metallurgical coke or biomass) will react with the CO<sub>2</sub> and form the CO reducing gas, which will assist in the reduction of iron oxide to metallic iron in the metal production process. Therefore, evaluating the reactivity with CO<sub>2</sub> of the torrefied biomass is extremely important for its substitution to metallurgical coke, after all, the greater this reactivity, the greater the formation of CO and the greater the reduction content of iron oxide.

In this context, the aim of this study was to evaluate the CO<sub>2</sub> reactivity potential of torrefied biomass. Four lignocellulosic biomasses were studied: sawdust (SE) from the *Eucalyptus* genus, pellet (PP), bark (CC) and chip (CV), all from the *Pine* genus. The physical and chemical characteristics of these biomasses were analysed and then the materials were torrefied in a fixed-bed reactor. Finally, the reactivity of the torrefied biomass with the CO<sub>2</sub> atmosphere was measured using non-isothermal thermal analysis.

## 5.2 MATERIALS AND METHODS

### 5.2.1 Selection and preparation of biomasses

To carry out the tests proposed in this research, the following biomasses were used: Sawdust (SE), Pellet (PP), Bark (CC) and Chips (CV). The first biomass of the *Eucalyptus* genus was provided by Stark Engenharia and the others of the *Pine* genus, with PP supplied by Albrecht Equipamentos Industriais S.A. while CC and CV were provided by Paper and Pulp Industry Irani - SC.



The biomasses were selected through random sampling in order to guarantee homogeneity and reliability in the obtained results. After the selection, the dried biomass was ground in an IKA A 11 knife mill (Staufen, Germany) and separated into particle size 106-300  $\mu\text{m}$ . The samples were placed in sealed bottles until the moment of the tests. Before each experiment, the samples were dried at a temperature of 105  $^{\circ}\text{C}$ , using a moisture analyzer (Moisture Analyzer, model MX-50, A&D Company, Japan).

## 5.2.2 Characterization of biomasses

To determine the operating conditions of the system, it is extremely important to know the characteristics and physical-chemical properties of the biomasses.

### 5.2.2.1 *Physical characteristics*

The physical characteristics of each biomass were determined. Among the existing characteristics, it was decided to evaluate the samples according to particle size, geometry, color and, grinding capacity. Particle size was determined using sieves of particle sizes 106-300  $\mu\text{m}$ . The geometry of the samples was determined by means of comparison with existing geometric solids. The grinding capacity was evaluated during the crushing of the biomass. These characteristics were analyzed before the torrefaction tests.

### 5.2.2.2 *Chemical characteristics*

Proximate analyses (moisture, ash, volatile matter and fixed carbon) were performed according to the standard ASTM E-1131-08 [12], using a DTG-60 thermogravimetric analyzer (Shimadzu, Japan), using 40 mg of sample, heating rate 90  $^{\circ}\text{C min}^{-1}$ , and a gas flow rate of 100  $\text{mL min}^{-1}$  [13].

The programming in a thermogravimetric analyzer was carried out in 6 segments, with the step of purging the reaction chamber of the thermogravimetric analyzer and later, the stabilization of the sample and removal of residual moisture (segments 2 and 3, respectively). Then the volatile matter was released, the temperature was adjusted and the fixed carbon was burned (segments 4, 5 and 6, respectively) [13]. Table 5.1 shows all the parameters used in each step described above.

Table 5.1 - Parameters proximate analysis

Segment	Heating rate (°C min <sup>-1</sup> )	Temperature (°C)	Time (min)	Carrier gas
1	10	35	60	N <sub>2</sub>
2	50	50	5	N <sub>2</sub>
3	50	110	5	N <sub>2</sub>
4	90	950	15	N <sub>2</sub>
5	-90	800	0	N <sub>2</sub>
6	0,1	800	Up to constant	Synthetic air

Source: Pacioni [13].

To obtain the values of moisture (U), volatile matter (MV), ash (CZ) and fixed carbon (CF), all in %, Equations (5.1), (5.2), (5.3) and (5.4) were used, respectively.

$$U = \frac{m_{2i} - m_{3f}}{m_{2i}} \cdot 100\% \quad (5.1)$$

$$MV = \frac{m_{3f} - m_{4f}}{m_{3f}} \cdot 100\% \quad (5.2)$$

$$CZ = \frac{m_{6f}}{m_{2i}} \cdot 100\% \quad (5.3)$$

$$CF = 100\% - MV - CZ \quad (5.4)$$

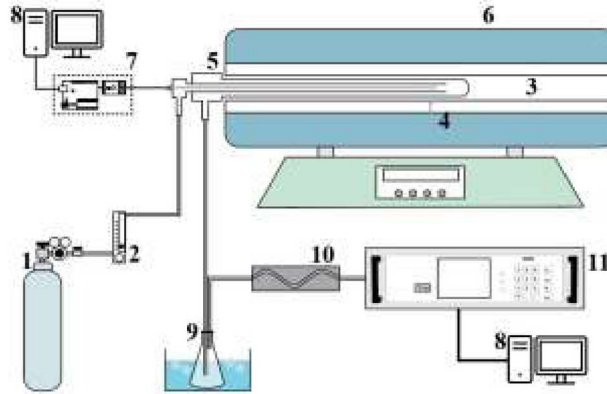
where  $m_{2i}$  is the initial mass in segment 2,  $m_{3f}$  is the final mass in segment 3 (which is equal to the initial mass in segment 4),  $m_{4f}$  is the final mass in segment 4,  $m_{6f}$  is the final mass in segment 6. Used mg as a unit for all the masses mentioned.

### 5.2.3 Torrefaction tests in a fixed bed reactor

Torrefaction tests were carried out using a fixed bed tubular reactor composed of a concentric quartz cylinder (the inner cylinder had an external diameter of 17.0 mm and was 1.35 mm thick, the external cylinder had an external diameter of 23.0 mm and was 2.60 mm

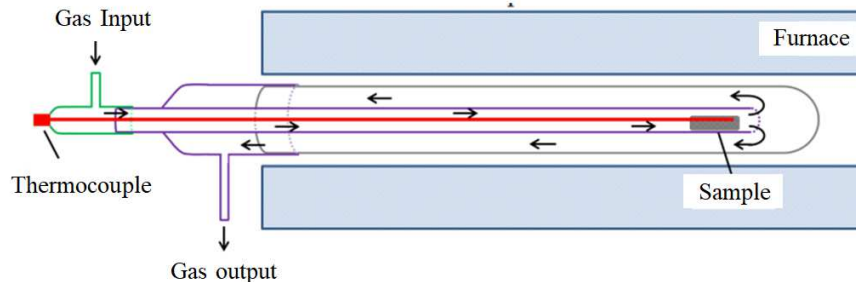
thick) an electric furnace. Figure 5.1 shows the system used for torrefaction, while Figure 5.2 shows a side view of the tubular reactor.

Figure 5.1 - Diagram of the biomass torrefaction system.



(Caption: 1: nitrogen or synthetic air cylinder; 2: rotameter; 3: electric oven; 4: electric furnace thermocouple; 5: fixed-bed tubular reactor; 6: sample thermocouple; 7: microcontroller system; 8: computers to monitor gas composition and temperature data; 9: condenser system; 10: gas analyzer). Source: adapted from da Silva *et al.*, [14].

Figure 5.2 - Side section of the fixed-bed tubular reactor.



Source: Adapted from Pacioni [13].

For the torrefaction tests, about 1 g of biomass as received was used. After introducing the biomass into the reactor, a purge was performed under a nitrogen gas flow (99.996%) of  $410 \text{ mL N}_2 \text{ min}^{-1}$  for 15 min at room temperature, thus ensuring an inert atmosphere. Then, the heat source from the electric oven heated up the sample and its temperature was measured by a K-type thermocouple.

The temperature and residence time were determined from thermogravimetric tests previously carried out. The system was then raised to the reaction temperature at  $250 \text{ }^\circ\text{C}$  and  $290 \text{ }^\circ\text{C}$  and held at residence times of 30 minutes and 60 minutes. The nomenclature used *XXYYYYZZ* corresponds respectively to: *XX* is the biomass used, *YYY* is the temperature, and

ZZ is the residence time. For example, PP29030 corresponds to the biomass *Pine Pellet* at a temperature of 290 °C and residence time of 30 minutes.

At the end of the determined reaction time, the reactor was removed from the furnace and cooled to room temperature when maintaining the flow of inert nitrogen gas (410 mL min<sup>-1</sup>) inside the reactor. After cooling, the obtained product was removed, weighed and stored in a desiccator for further analyses.

## 5.2.4 Reactivity evaluation of torrefied biomass with CO<sub>2</sub>

The CO<sub>2</sub> reactivity of the torrefied biomass was determined non-isothermally by thermogravimetric analysis. In a typical experiment, the sample was heated from 300 °C to 1000 °C with a heating rate of 10 °C min<sup>-1</sup> in an atmosphere of CO<sub>2</sub> with a flow rate of 100 mL min<sup>-1</sup>.

The loss of mass that occurs during gasification with CO<sub>2</sub> injection is due to the consumption of the carbon present in the torrefied biomass and follows the Boudouard reaction expressed by Eq. (5.5).



Reactivity, which represents the consumption of reagent as a function of reaction time, was determined by Eq. (5.6) [6].

$$r = -\frac{1}{m_0} \left( \frac{dm}{dt} \right) \quad (5.6)$$

where  $r$  is the reaction rate (min<sup>-1</sup>),  $m_0$  is the initial mass in an ash free basis (mg),  $\frac{dm}{dt}$  is the rate of mass loss (mg) at  $t$  (min) is the reaction time.

## 5.3 RESULTS AND DISCUSSION





### 5.3.1 Characterization of biomasses

#### 5.3.1.1 Physical characteristics

Initially, the physical characteristics of the biomass were determined, i.e. particle size, colour, geometry and grinding capacity. With regard to particle size, after the biomass had gone

through the grinding process, it was separated using a 106-300  $\mu\text{m}$  sieve. With regard to colour and geometry, Table 5.2 shows these physical aspects of the biomass. It can be seen that the colours of the PP, SE and CV biomass are very close to each other, a light yellow colour, while the CC biomass has a darker brown colour.

Table 5.2 - Physical characteristics of SE residual biomass.

<b>Biomass as received</b>			
<b><i>Pine Pellet (PP)</i></b>	<b><i>Sawdust (SE)</i></b>	<b><i>Bark (CC)</i></b>	<b><i>Chip (CV)</i></b>
			

Source: The author (2023).

Still analysing the images in Table 5.2, it can be seen that the PP biomass has a more uniform geometry, similar to an irregular cylindrical shape, while the CC and CV biomasses are closer to irregular rectangles. On the other hand, SE biomass does not have a specific geometry, but is made up of numerous "fibers" of different sizes. According to Cai *et al.* [15], the shape and size of the biomass feedstock particles affect mixing and fluidisation, the surface area for heat and mass transfer and the flow behaviour of the biomass particles, i.e. different shapes and sizes may have different conversion efficiencies.

With regard to milling capacity, it was realised that the PP biomass milled faster than the other biomasses, with less energy and time spent. The increasing order of grinding difficulty was  $\text{PP} < \text{CV} < \text{CC} < \text{SE}$ . Cai *et al.* [15] state that the lignocellulosic components of biomass, mainly cellulose and lignin, are very fibrous and difficult to grind. As a result, it is possible that SE biomass has a higher percentage of cellulose and lignin in its composition due to the difficulty of grinding. In addition, SE biomass is very close to "fibers", which also makes it difficult to grind.

### 5.3.1.2 Chemical characteristics

There are various analytical methods for assessing the energy potential of solid fuels, with proximate analyses being the primary method for assessing parameters such as volatile material, ash and fixed carbon [16]. The results of proximate analysis, in a dry basis, are presented in Table 5.3. Analyzing the values in Table 5.3, it can be seen that the SE biomass

had the highest volatile matter content (~86%) compared to the other biomasses. Then there is the PP biomass with 83.28%, the CV biomass with 78.16% and, finally, the CC biomass with 65.79%. Biomasses with a higher content of volatile material can generate greater amounts of condensable gases during torrefaction [13].

Table 5.3 - Chemical characteristics of biomasses in dry base.

<b>Biomass</b>	<b>Volatile materials (%)</b>	<b>Ash (%)</b>	<b>Fixed carbon (%)</b>
PP	83.28	0.63	16.08
SE	86.15	0.35	13.85
CC	65.79	0.92	33.30
CV	78.16	0.84	21.00

Source: The author (2023).

Table 5.3 also shows that all the biomass had an ash content below 1%. The ash content represents the amount of mineral matter contained in the sample which remains from complete burning. This is a parameter that is directly linked to the potential risk of slagging and fouling problems in boilers during biomass combustion or gasification. Silica, aluminium, iron, calcium, magnesium, titanium, sodium oxide and potassium are some of the components that can be contained in ash [13], [15]. In the case of the biomasses studied in this work, all had low ash content, showing their potential for application in thermal processes such as torrefaction.

The solid combustible residue that remains after volatile matter is expelled is fixed carbon [15]. This parameter indicates that the greater the amount present in the biomass, the greater the calorific value of this material, releasing more energy during the thermal conversion process. Since this is an important parameter for application in metallurgical processes and as the results of the proximate analysis showed that the SE biomass has a lower fixed carbon content compared to the other biomasses, it was decided not to continue with the studies of this biomass. In addition, as already reported, SE biomass is more difficult to grind compared to other biomasses, probably due to the higher percentage of cellulose and lignin in its composition.

### **5.3.2 Evaluation of reactivity of torrefied biomass obtained under different experimental conditions.**

At this stage of the study, the CC, CV and PP biomasses torrefied at two temperatures, 250 °C and 290 °C and two residence times, 30 and 60 min, were analyzed. The reactivity of

the torrefied biomass with CO<sub>2</sub> depends on its chemical and physical properties, such as pore volume, surface area, ash yield and crystalline structure [17], and it is a key factor to allow it to replace metallurgical coke. Initially, analyzing the thermogravimetric profiles obtained for the three biomasses, in terms of mass loss (Figure 5.3), it is noted that, for the CC biomass, the greatest mass loss in CO<sub>2</sub> atmosphere occurred at a temperature of 250 °C and residence time of 60 min.

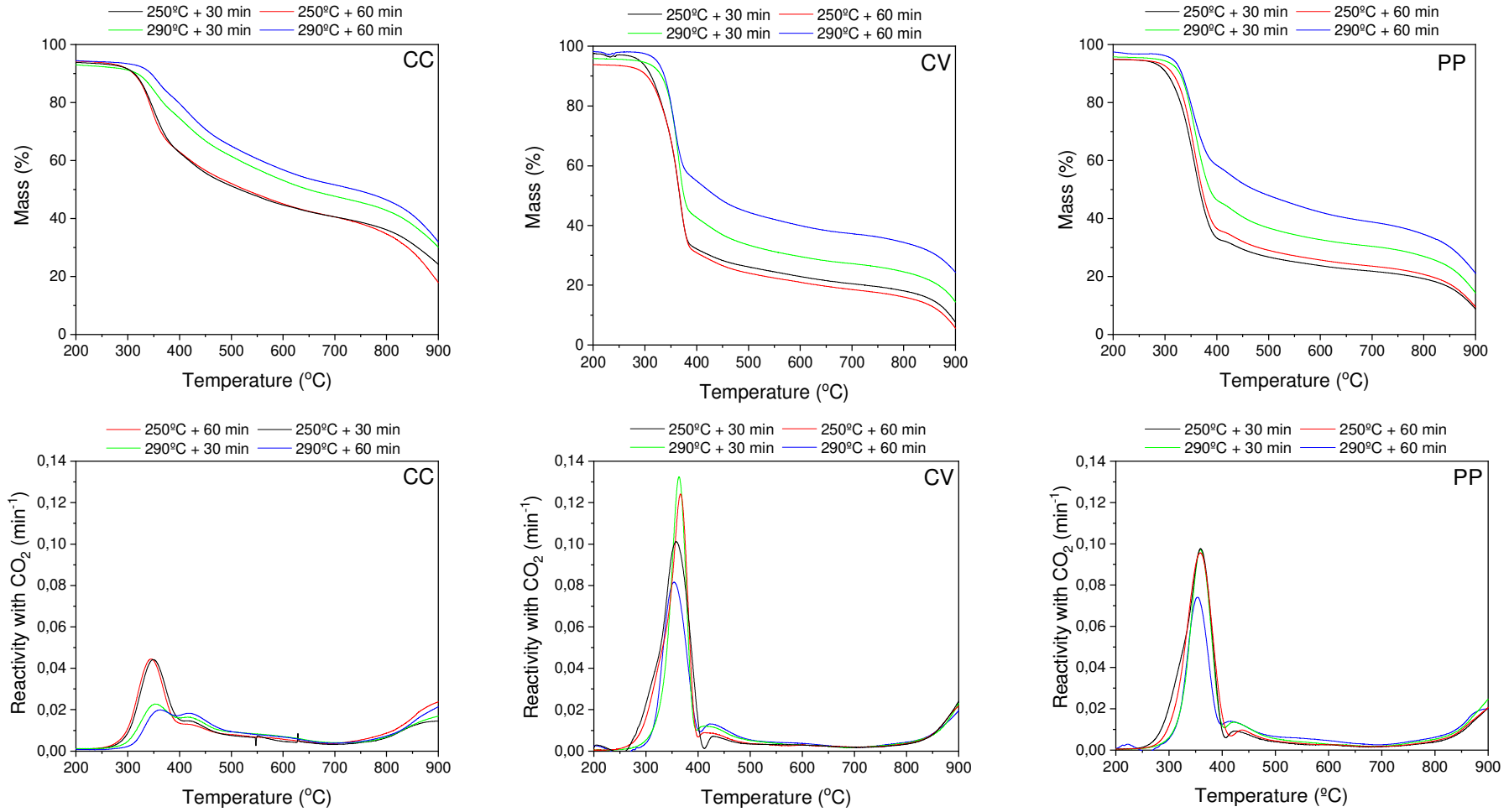
The greater mass loss was observed from 750 °C onwards, above this temperature the mass loss curves at 250 °C and 30 min and 250 °C and 60 min were no longer superimposed. At 290 °C and residence times of 30 and 60 min, this overlap did not occur, and it was clearly visible that the greatest mass loss at this temperature occurs at a residence time of 30 min, with the lowest mass loss at 290 °C and 60 min.

The curves that depict mass of the CV and PP biomasses behaved very similarly, with the only difference in the curves at the temperature of 250 °C. For CV biomass, the greatest mass loss occurred at a temperature of 250 °C and a residence time of 60 min, while for PP biomass this occurs at a temperature of 250 °C and 30 min.

Observing the curves obtained for non-isothermal gasification in terms of reactivity, this process can be divided into two main stages. For CC biomass, the first stage occurred between 280 – 700 °C, while for CV and PP biomass, the peak started at 250 °C and decayed at 500 °C. The second stage was situated between 750 °C and 900 °C, and was present in all curves. In the literature, researchers suggest that the non-isothermal gasification can be divided into two main stages, the first stage being responsible for mass loss due to devolatilization and the second stage responsible for coal gasification. In the devolatilization process, the thermal behavior for hemicellulose, cellulose and lignin are different, with thermal degradation occurring in the temperature ranges of 200-320 °C for hemicellulose, 320-420 °C for cellulose and 220-500 °C for lignin [18], [19], [20].

Observing Figure 5.3, it is noted that for CC biomass, the peaks were less intense than for CV and PP biomass. Furthermore, for CC biomass, the highest peaks were at the temperature of 250 °C, while at 290 °C the peaks were smaller. For the CV and PP biomasses, it was noted that the peak intensity is much higher than that of the CC biomass. This variation is probably related to the chemical composition of each biomass, more likely the volatiles, presented in Table 5.3. In addition, for the PP biomass, the peaks overlapped, except for the temperature peak of 290 °C and 60 min, which was slightly lower than the others.

Figure 5.3 - Reactivity evaluation of torrefied biomass with CO<sub>2</sub>.



Source: The author (2023).



In the literature, researchers studied the non-isothermal reactivity of torrefied biomass composed of German lignite (GL) and olive pomace (OB) with CO<sub>2</sub> and found two stages with reactivity peaks, the first between 400 and 550 °C and the second between 600 and 700°C. They verified through the graph of reactivity as a function of temperature that the torrefied biomass with the highest reactivity with CO<sub>2</sub> was the one with 40% OB/GL, which presented the highest peak in both phases [6].

One of the objectives of this research is to use the torrefied biomass in metallurgical processes as a total or partial substitute for coke aiming at the reduction of greenhouse effect gas emission. Thus, by using a compound with higher reactivity, coke degradation can be reduced since there will be a reaction of CO<sub>2</sub> with the torrefied biomass.

In this context, considering the highest peaks of the two mentioned stages presented in Figure 5.3, the operational conditions to obtain high reactivity of CV-torrefied biomass and PP-torrefied biomass in CO<sub>2</sub> atmosphere were the same (290 °C and 30 min), while CC-torrefied biomass required lower temperature and longer residence time (250 °C and 60 min), probably due to differences in lignin, hemicellulose, and cellulose contents, which was addressed in future studies.

#### 5.4 CONCLUSIONS

With this study, it was possible to evaluate the potential application of different torrefied biomasses in metallurgical processes through the reactivity with CO<sub>2</sub>. It could also be noticed the importance of knowing the chemical and physical characteristics of the biomasses. After all, even with low ash content (less than 0.7%), the fixed carbon value of ~13% of the SE biomass and the difficulty in milling, probably due to its high lignin and cellulose contents, were determining factors for not continuing the torrefaction study for this biomass. Finally, the results of reactivity with CO<sub>2</sub> showed that the torrefied biomasses that presented greater reactivity were treated in the operational conditions of torrefaction of 290 °C and 30 minutes for the PP and CV biomasses and 250 °C and 60 minutes for the CC biomass.

#### 5.5 REFERENCES

- [1] S. Kumar, Z. Xiong, J. Held, P. Bruggeman, U. R. Kortshagen Rapid carbon-free iron ore reduction using an atmospheric pressure hydrogen microwave plasma  
Chemical Engineering Journal, 472 (2023), pp. 145025, <https://doi.org/10.1016/j.cej.2023.145025>

- [2] P. Azadi, H. Elwan, R. Klock, S. Engell. Improved operation of a large-scale blast furnace using a hybrid dynamic model based optimizing control scheme. *Journal of Process Control*, 129 (2023), pp. 103032, <https://doi.org/10.1016/j.jprocont.2023.103032>
- [3] J. Chen, Z. Lu, J. Jian, Z. Bao, J. Cai, S. Yao. Effect of torrefaction on yield, reactivity and physicochemical properties of pyrolyzed char from three major biomass constituents *Journal of Analytical and Applied Pyrolysis*, 173 (2023), pp. 106104, <https://doi.org/10.1016/j.jaap.2023.106104>
- [4] S. Zhang, S. Yu, O. Li, B. A. Mohamed, Y. Zhang, H. Zhou. Insight into the relationship between CO<sub>2</sub> gasification characteristics and char structure of biomass. *Biomass and Bioenergy*, 163 (2022), pp. 106537, <https://doi.org/10.1016/j.biombioe.2022.106537>
- [5] A. Dashti, A. S. Noushabadi, M. Raji, A. Razmi, S. Ceylan, A. H. Mohammadi. Estimation of biomass higher heating value (HHV) based on the proximate analysis: Smart modeling and correlation. *Fuel*, 257 (2019), pp. 115931, <https://doi.org/10.1016/j.fuel.2019.115931>
- [6] J.G. Pohlmann, E. Osório, A. CF Vilela, M.A. Diez, A.G. Borrego Pulverized combustion under conventional (O<sub>2</sub>/N<sub>2</sub>) and oxy-fuel (O<sub>2</sub>/CO<sub>2</sub>) conditions of biomasses treated at different temperatures *Fuel Process Technol*, 155 (2017), pp. 174-182, [10.1016/j.fuproc.2016.05.025](https://doi.org/10.1016/j.fuproc.2016.05.025)
- [7] K. Głód, J. A. Lasek, K. Supernok, P. Pawłowski, R. Fryza, J. Zuwała. Torrefaction as a way to increase the waste energy potential. *Energy*, 285 (2023), pp. 128606, <https://doi.org/10.1016/j.energy.2023.128606>
- [8] M. Jagadale, S. Gangil, M. Jadhav. Enhancing fuel characteristics of jute sticks (*Corchorus Sp.*) using fixed bed torrefaction process. *Renewable Energy*, 215 (2023), pp. 118992, <https://doi.org/10.1016/j.renene.2023.118992>
- [9] Z. Du, Y. Ge, F. Liu, C. Fan, F. Pan. Effect of different modification methods on fluidized bed hydrogen reduction of cohesive iron ore fines. *Powder Technology*, 400 (2022), pp. 117226, <https://doi.org/10.1016/j.powtec.2022.117226>
- [10] L. Wang, Ø. Skreiberg, N. Smith-Hanssen, S. Jayakumari, S. Rørvik, G. Jahrsengene, S. Turn. Investigation of gasification reactivity and properties of biocarbon at high temperature in a mixture of CO/CO<sub>2</sub>. *Fuel*, 346, (2023), pp. 128233, <https://doi.org/10.1016/j.fuel.2023.128233>
- [11] R. Lee, J. M. Sohn. A study on the effect of the CO<sub>2</sub>/steam mixtures and the addition of natural minerals on the reactivity of Adaro coal gasification. *International Journal of Hydrogen Energy*, 47, (2022), pp. 31852-31863, <https://doi.org/10.1016/j.ijhydene.2022.04.280>
- [12] ASTM E1131-08: standard test method for compositional analysis by thermogravimetry ASTM International, West Conshohocken (2014), pp. 1-6, [10.1520/E1131](https://doi.org/10.1520/E1131)
- [13] Pacioni, Tatiana Ramos. Obtaining synthesis gas through the gasification of agro-industrial residues with steam. 2017. 183 f. Thesis (PhD in Chemical Engineering), Federal University of Santa Catarina, Florianópolis, 2017. Available at: <https://repositorio.ufsc.br/xmlui/handle/123456789/176803>
- [14] da Silva, J.C.G., Leque, J., Pereira, C., Andersen, S.L.F., Moreira, R. F. P. M., José, H. J. Torrefaction of ponkan peel waste in tubular fixed-bed reactor: In-depth bioenergetic evaluation

of torrefaction products. *Energy*, 2020, 210, pp. 118569.  
<https://doi.org/10.1016/j.energy.2020.118569>

[15] Cai, J., He, Y., Yu, X., Banks, S. W., Yang, Y., Zhang, X., Yu, Y., Liu, R., Bridgwater, A. V. Review of physicochemical properties and analytical characterization of lignocellulosic biomass. *Renewable and Sustainable Energy Reviews*, 2017, 76, pp. 309-322.  
<https://doi.org/10.1016/j.rser.2017.03.072>

[16] S. Park, S. J. Kim, K. C. Oh, L. Cho, Y. K. Jeon, C. Lee, D. Kim. Thermogravimetric analysis-based proximate analysis of agro-byproducts and prediction of calorific value. *Energy Reports*, 8 (2022), pp. 12038-12044, <https://doi.org/10.1016/j.egy.2022.09.040>

[17] Zhang, C., Ho, S., Chen, W., Xie, Y., Liu, Z., Chang, J. Torrefaction performance and energy usage of biomass wastes and their correlations with torrefaction severity index, *Applied Energy*, 2018, 220, pp. 598-604. <https://doi.org/10.1016/j.apenergy.2018.03.129>

[18] J. O. Brotto, J. S. Salla, J. C. G. da Silva, E. Rodríguez-Castellón, H. J. José, S. M. Amorim, R. F. P. M. Moreira. Investigation of the thermal behavior of *Pine* wood pellets during torrefaction for application in metallurgical processes, *Journal of Materials Research and Technology*, 2022, 19, pp. 3749-3759. <https://doi.org/10.1016/j.jmrt.2022.06.082>

[19] Sarvaramini, A. and Larachi, F. Integrated biomass torrefaction – Chemical looping combustion as a method to recover torrefaction volatiles energy, *Fuel.*, 2014, 116, pp. 158–167. <http://doi.org/10.1016/j.fuel.2013.07.119>

[20] Tran, K.-Q., Bui, H.-H., Luengnaruemitchai, A., Wang, L., Skreiberg, Ø. Isothermal and non-isothermal kinetic study on CO<sub>2</sub> gasification of torrefied forest residues, *Biomass and Bioenergy.*, 2016, 91, pp. 175–185. <http://doi.org/10.1016/j.biombioe.2016.05.024>

## 6 MECHANISTIC INSIGHTS AND KINETICS OF TORREFACTION OF PINE WOOD BIOMASSES USING SOLID-STATE NMR<sup>2</sup>

### ABSTRACT

The purpose of this study is to investigate the potential use of torrefied biomass of the genus *Pine*, in the form of wood bark (CC), chips (CV) and wood pellets (PP), as substitutes for metallurgical coke to reduce the high CO<sub>2</sub> emissions from the use of metallurgical coke in blast furnaces. Thermogravimetric analysis were used to optimize the torrefaction temperature (250 °C or 290 °C), residence time (30 or 60 min) under inert atmosphere. All of the torrefied biomasses were analyzed to determine physical and chemical characteristics (proximate analyses, ultimate analyses, higher calorific value (HHV), Fourier transform infrared spectroscopy (FTIR) and *ss*-NMR. The composition of condensable and non-condensable gases formed during torrefaction process were also measured. The results showed that the two most promising biomasses were CV and PP torrefied at a temperature of 290 °C at a residence time of 30 min. The kinetics of torrefaction was analyzed by solid state *ss*-NMR characterization of the torrefied biomass at different time reactions and temperature (250–290 °C) under inert atmosphere, and followed a pseudo-first order kinetic model. The kinetics of evolution of *ss*-NMR signals related to C-1 of cellulose; C-4 of cellulose in ordered cellulose; C-4 of cellulose in disordered/amorphous cellulose; C-6 of cellulose, and carbon atoms of methoxyl groups in lignins, at different temperatures were used to estimate the activation energy, and values in the range 11–25 kJ mol<sup>-1</sup> were obtained.

**Keywords:** biomass; torrefaction; wood waste; thermal conversion; *ss*-NMR.

---

<sup>2</sup>This chapter has been published in *Journal of Analytical and Applied Pyrolysis*, 172 (2023) 106019. <https://doi.org/10.1016/j.jaap.2023.106019>

## 6.1 INTRODUCTION

Climate change is the main driving force for new technologies and low-emission energy sources, thus, studies are being conducted of renewable energy and alternative fuel sources. For the steel industry, the total replacement of fossil fuels by renewable sources is a challenge [1]. Traditionally, this industry uses coke made from coal as a raw material in blast furnaces, and coke accounts for about 93% of all greenhouse gas emissions from the steel industry, with an emission intensity of approximately 2 t/t steel [2], [3]. As a result, several efforts to reduce the energy and carbon intensity on iron and steel production have been made and include best practices to reduce coke consumption through the use of pulverized coal (PC), natural gas, oil, waste plastics [4], or agricultural residues [1]. As a renewable energy source, biomass has advantages such as low cost, and low carbon emissions, and is a component in great abundance [5].

Nevertheless, biomasses have high oxygen content, low calorific value, a hydrophilic nature, high moisture content, low energy density, low combustion efficiency, a tenacious and fibrous structure, and their heterogeneous composition makes the design and control of the processes more complicated [6], [7].

Torrefaction is a thermal treatment useful for improving the properties of lignocellulosic biomass [8]. This process, also known as soft pyrolysis, is a thermal treatment in which biomass is subjected to temperatures between 200 and 300 °C at given residence times, generally using an inert atmosphere. During the thermal treatment, water and light volatiles containing most of the oxygen from the biomass are removed and the fibrous structure of the original biomass is partially destroyed. This helps change its property from hygroscopic to hydrophobic and improve grinding. Furthermore, biomass is converted into a carbonaceous material similar to coal with excellent properties such as high energy density, compressible, crushable, and low H/C and O/C ratios [7], [9], [10].

The complete replacement of injected fossil fuels with charcoal in the steel industry can reduce CO<sub>2</sub> emissions in loco by 28.1% (torrefied material and wood pellets can reduce CO<sub>2</sub> emissions a maximum of 6.4% and 5.7%, respectively) or 17.3% of industry-wide emissions [11]. Thus, the use of wood-based biomass as a raw material in the production of bio-reducers can pave the way to achieving national renewable energy targets [12]. In addition, biochar derived from the depolymerization of torrefied biomass will produce less slag due to lower ash yield when compared to metallurgical coke, and therefore is expected to have economic advantages [1]. The production of high-quality biomass-derived fuels depends on

various chemical and physical requirements set by the metallurgical industry, so their characterization is extremely important [13].

Most of kinetic studies about biomass torrefaction have used thermogravimetric measurements (TGA). However, the mass loss is not directly correlated with chemical evolution of functional groups during torrefaction, and the mass loss cannot be the only criterion to characterize torrefaction severity [14]. Moreover, the chemical evolution of the solid during torrefaction should depend on the xylan content in hemicellulose, lignin content, and cellulose crystallinity [14]. Recently, da Silva *et al.* [15] have described the torrefaction kinetics according to a two-step mechanism, where the complete decomposition of the solid occurs through two consecutive reactions. In the first reaction, the raw biomass would be decomposed to form a solid intermediate and volatile compounds. The solid intermediate would be decomposed in the consecutive reactions to produce others volatiles compounds and torrefied biomass. Nevertheless, the identification of the intermediate compounds was reported.

Solid-state  $^{13}\text{C}$  NMR spectroscopy has been considered a very useful analytical tool for determining the composition of wood and its chemical derivatives components. Furthermore, solid-state  $^{13}\text{C}$  NMR spectroscopy using the technique of cross polarization and sample rotation at a magic angle (CP-MAS) was successfully used for quantitative composition of wood [16]. Thus, this study evaluates the physical, chemical, and thermal characteristics of biomasses torrefied produced by thermal treatment of different biomasses derived from the *Pine Genus*, which are found in great abundance in Brazil. The kinetics of torrefaction process at different temperatures was studied using  $^{13}\text{C}$  NMR spectroscopy, and *as-received* and torrefied samples were completely characterized.

## 6.2 MATERIALS AND METHODS

### 6.2.1 Selection and preparation of biomasses

In this study, three different biomasses were selected, wood bark (CC) and chips (CV) of *Pine Genus*, both supplied by a Brazilian paper company located in Santa Catarina state, and the pelletized biomass of *Pine Genus* (PP), supplied by the company located in Paraná State, (Brazil).

The biomasses were selected through random sampling to ensure the homogeneity and reliability of the results. After selection, the biomasses were dried in an oven at a temperature of 100 °C for about 2 h and placed in sealed vials until testing. For characterization of

biomasses *in natura*, samples were ground in an IKA A 11 knife mill (Staufen, Germany) and separated into particle sizes between 106 and 300  $\mu\text{m}$  (mesh Tyler 48). Samples were placed in sealed vials until testing.

### 6.2.2 Evaluation of the thermal decomposition of biomass

The thermal behavior of the three biomasses were studied in non-isothermal tests using an inert atmosphere (pure  $\text{N}_2$ ). About 40 mg of sample were weighed and placed in a thermogravimetric analyzer (DTG-60 thermogravimetric analyzer, Shimadzu, Japan) until reaching 300  $^\circ\text{C}$  (maximum temperature for torrefaction) under a heating rate of 10  $^\circ\text{C min}^{-1}$ . Thermogravimetric analyses (TGA) and differential thermal analyses (DTA) were obtained.

### 6.2.3 Torrefaction experiments in a fixed bed reactor

The torrefaction tests were conducted using a fixed bed tubular reactor composed of concentric quartz cylinders (the inner cylinder had an external diameter of 17.0 mm and was 1.35 mm thick, the external cylinder had an external diameter of 23.0 mm and was 2.60 mm thick). Before the tests, the biomass was dried in an oven at 100  $^\circ\text{C}$  for 4 h. Approximately 1 g of dried biomass was used to carry out the tests, measured on a model MX-50 scale (A&D Weighing, San Jose, United States). After introducing the biomass into the reactor, a purge was performed under a nitrogen ( $\text{N}_2$ ) gas flow (99.996%) of 410  $\text{mLmin}^{-1}$  for 15 min at room temperature, thus ensuring an inert atmosphere inside the reactor. Then, the reactor was placed in an electric oven MOD DI-600RP DIST (São Paulo, Brazil) whose internal temperature, that is the sample temperature, was measured by a type K thermocouple.

The torrefaction tests conducted under experimental conditions selected from previous tests (temperatures: 250 and 290  $^\circ\text{C}$ ; residence time: 30 and 60 min). These experimental conditions usually are reported to describe mild and severe torrefaction [17]. Torrefied biomasses were identified as XXYZ (where XX = biomass nomenclature, Y = temperature ( $^\circ\text{C}$ ); and Z = residence time (min)). For example, CC29060, PP25030, and CV25060. The experiments were performed in duplicate.

During the test, the volatiles that were released passed through a condenser under a bath of liquid nitrogen and then through a gas analyzer (SICK Maihak S710/MULTORTHERMOR, Germany). At the end of the determined reaction time, the reactor was removed

from the oven and cooled to room temperature, maintaining the flow of inert nitrogen gas (410 mL min<sup>-1</sup>) inside the reactor.

After cooling, the solid product obtained was removed, weighed, and stored in a desiccator for further physico-chemical characterization. Equation (6.1) was used to obtain the solid yield (Y) while Equation (6.2) was used to obtain the conversion (X) [18].

$$Y = \frac{m_{final}}{m_{initial}} \times 100\% \quad (6.1)$$

$$X = \frac{m_{initial} - m_{final}}{m_{initial}} \times 100\% \quad (6.2)$$

where  $m_{final}$  is the mass after the torrefaction process (mg) and  $m_{initial}$  is the mass before the torrefaction process (mg).

#### 6.2.4 Physico-chemical characterization

For the characterization of the biomasses before and after the torrefaction process, the following analyses were performed: proximate analysis, ultimate analyses, higher calorific value (HHV), Fourier transform infrared spectroscopy (FTIR), composition (lignin, cellulose, and hemicellulose), and *solid-state* Nuclear Magnetic Resonance (*ss*-NMR).

For the proximate analyses, a DTG-60 thermogravimetric analyzer (Shimadzu, Japan) was used, in which 40 mg of sample were weighed at a heating rate of 10 °C min<sup>-1</sup> and a gas flow rate of 100 mL min<sup>-1</sup> to the standard ASTM E-1131-08 [19]. For the ultimate analyses, a 2400 Series II CHNS/O analyzer (Perkin Elmer, USA) was used. The samples were encapsulated in tin crucibles with combustion at 925 °C and reduction at 640 °C according to ASTM D5373-08 [20].

The higher calorific value (HHV) of the biomass were calculated according to Eq. (6.3) [21]. The mean Absolute error of the correlation is 1.45% and the elemental composition is C – 0.00-92.25%, H – 0.43-25.15%, O – 0.00-50.00%, N – 0.00-5.60%, S – 0.00- 94.08% and ash content – 0.00 – 71.4%.

$$HHV = 0.3491C + 1.1783H + 0.1005S - 0.1034O - 0.00151N - 0.0211A \quad (6.3)$$



where, C, H, O, N, S and A represent the contents of carbon, hydrogen, oxygen, nitrogen, sulfur and ash of material, respectively. All element values were used as mass percentage values on a dry basis.

The FTIR analysis were performed in an Alpha spectrophotometer (Bruker, USA) and Mentor management software. For this procedure, the samples were dried and pressed with potassium bromide powder (KBr) at a ratio of 1:100 according to ASTM D2702–05 [22] and scanned between 4000 and 400  $\text{cm}^{-1}$ .

Chemical characterization of the lignocellulosic biomass (cellulose, hemicellulose, lignin, extractives, ashes) was determined according to [23]. This procedure is based on a two-stage sulfuric acid hydrolysis to fractionate biomass for gravimetric and instrumental analyses. Particle sizes smaller than 0.5 mm were subjected to organic solvent extraction (using ethanol and cyclohexane) and aqueous extraction in a Soxhlet system to determine the gravimetric extractive content. The biomass devoid of extractives were subjected two-stage sulfuric acid hydrolysis process.

The initial step of hydrolysis involved treating the biomass with 72% (w/w) sulfuric acid for 2 h at room temperature. Subsequently, a second-stage of hydrolysis was carried out using 3% (w/w) acid under reflux conditions for 4 h. The resulting suspension was filtered, and the filtrate underwent chromatographic analysis to determine the concentrations of glucose, xylose, arabinose, galactose, and acetic acid. Measurement of soluble lignin in the filtrate was performed by scanning the sample using a UV spectrophotometer in the range 190–400 nm. The absorbance at wavelengths of 280 nm and 215 nm was utilized to calculate the percentage of soluble lignin. Gravimetric determination of insoluble lignin involved measuring the solid residue remaining after hydrolysis, with subtracting the ash content.

### **6.2.5 Characterization of condensable and non-condensable gases from the torrefaction process**

After removing the torrefied biomass from the reactor, the liquid fraction contained in the condenser was removed using about 2 mL of dichloromethane (Sigma Aldrich, Darmstadt, Germany). This liquid was stored in amber flasks at -22 °C for later identification of the composition using gas chromatography (GCMS-QP2010 Plus Shimadzu). In addition, a gas analyzer (SICK|Maihak S710/MULTORTHERMOR) was used to capture  $\text{CO}_2$ , CO,  $\text{CH}_4$  and  $\text{H}_2$  during the process.

### 6.2.6 *ss*-NMR analysis and kinetics of torrefaction

The *ss*-NMR measurements were acquired with a spectrometer equipped with a 14.1 T narrow bore magnet operating at Larmor frequencies of 600.09 MHz and 150.91 MHz for  $^1\text{H}$  and  $^{13}\text{C}$ , respectively. Powdered samples were packed into 4.0 mm  $\text{ZrO}_2$  rotors and rotated at room temperature at magic angle spinning (MAS) rates of 10 kHz. For the standard  $^{13}\text{C}$  CP-MAS (cross-polarization and magic angle spinning) experiments, each 5 s pulse delay was followed by a proton preparation pulse of duration of 3.8  $\mu\text{s}$ , 2 ms of contact time, and 45 ms of acquisition time. Glycine was used as an external reference for the  $^{13}\text{C}$  spectra and to set the Hartmann-Hahn matching condition in the CP experiments in  $^{13}\text{C}$  spectra. The SPINAL64 sequence was used for heteronuclear decoupling during acquisition. Transients were averaged over 10k transients for CP experiments.

The *ss*-NMR results have been done in a 4-mm rotor (~50-70 mg) in the present work. Particularly, the results in a 3.2-mm rotor (~30-50 mg) were in concordance with those done in a 4-mm probe demonstrating the reproducibility of the *ss*-NMR results. However, longer acquisition times were needed for the experiments performed in a 3.2-mm rotor in comparison with a 4-mm rotor in order to get a better signal to noise ratio for the different *ss*-NMR signals in the  $^{13}\text{C}$  CP-MAS experiments. In addition, *ss*-NMR experiments were previously reported for torrefaction transformation in wood [24]. Furthermore, the precision of this technique was previously proved by Kostryukov *et al.* [17].

The kinetics of torrefaction was analyzed from the *ss*-NMR results of the samples torrefied at temperature in the range 250 - 290  $^\circ\text{C}$  at different residence time and temperatures. The kinetic study of the thermal decomposition process assumes that the decomposition follows first-order kinetics, that is, the reaction rate of a sample can be obtained by Equation (6.4).

$$\frac{d\alpha}{dt} = k(1 - \alpha) \quad (6.4)$$

where  $\alpha$  is the conversion,  $\frac{d\alpha}{dt}$  is the conversion rate as a function of time in  $\text{min}^{-1}$ , and  $k$  is the temperature-dependent kinetic constant. By integrating of Equation (6.4) yields Equation (6.5).

$$\ln \alpha = k(t - t_0) \quad (6.5)$$

where  $t$  is the residence time throughout the torrefaction and  $t_0$  is the initial time. It was assumed that the conversion  $\alpha$  is proportional to the normalized area of each peak obtained from the *ss*-NMR analysis (Equation 6.6) [24]. Quantitative data from the CP-MAS experiments were obtained by application of a correction factor taking into account the dynamics of the  $^{13}\text{C}$  magnetisation build-up during the proton-to-carbon cross polarisation step [24].

$$\text{Normalized area} = \frac{\text{peak area} (1-\Delta m)}{m_{rotor}} \quad (6.6)$$

where  $\Delta m = m_0 - m_{(t)}$ ,  $m_0$  is the initial mass,  $m_{(t)}$  is the mass of the sample as a function of time, and  $m_{rotor}$  is the mass utilized in the *ss*-NMR analysis.

The kinetic constant  $k$  depends on the temperature according to the Arrhenius Equation (Equation 6.7).

$$k = A e^{\frac{-Ea}{RT}} \quad (6.7)$$

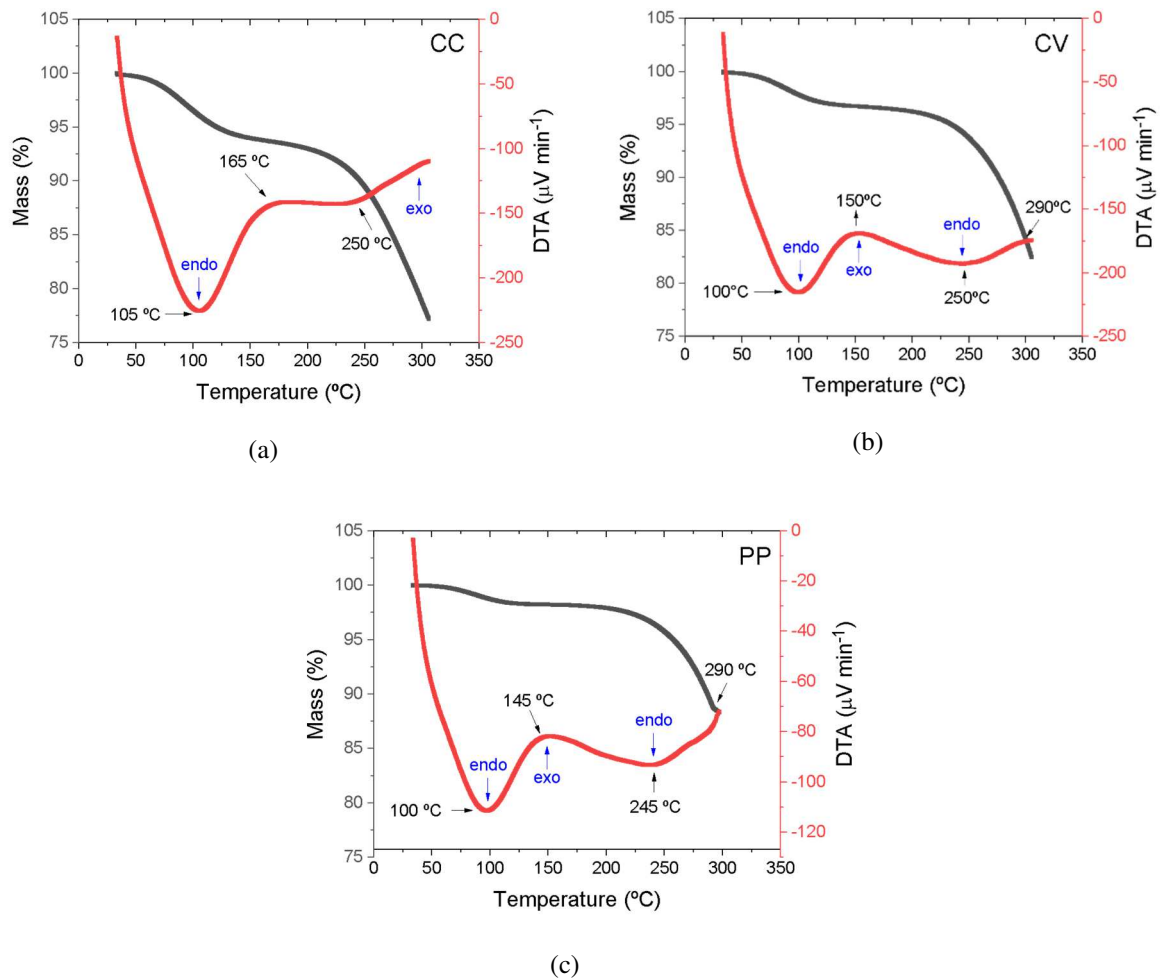
where  $Ea$  is the activation energy ( $\text{kJ mol}^{-1}$ ),  $A$  is the frequency factor or pre-exponential factor ( $\text{min}^{-1}$ ),  $R$  is the universal gas constant ( $8.314 \text{ J K}^{-1} \text{ mol}^{-1}$ ) and  $T$  is the temperature (K).

## 6.3 RESULTS AND DISCUSSION

### 6.3.1 Evaluation of thermal decomposition of biomasses under inert atmosphere

The TGA curves for CC, CV and PP under nitrogen atmosphere are shown in Figure 6.1. An endothermic of weight loss peak close to  $100 \text{ }^\circ\text{C}$  is present for all samples, due to the moisture release [25], [26]. The exothermic weight loss peak is observed in the temperature range of  $145 \text{ }^\circ\text{C} - 165 \text{ }^\circ\text{C}$  is related to the partial thermal decomposition of hemicellulose [27] in CC, CV and PP. Finally, at temperatures higher than  $245 \text{ }^\circ\text{C}$ , the weight loss peak is ascribed to the cellulose and lignin decomposition [26], [27]. Thus, according to the peaks identified in Figure 6.1, the temperatures selected to perform the thermal decomposition processes are  $250$  and  $290 \text{ }^\circ\text{C}$ , that are considered moderate and severe torrefaction processes, respectively [27].
















Figure 6.1 - Thermal decomposition of biomasses CC (a), CV (b), and PP (c) under inert atmosphere.



Source: Brotto *et al.*, (2023).

A biomass darkening is observed (Table 6.1) as the temperature and residence time increases, due to the intra and intermolecular rearrangement of the biomass components, which results in greater crosslinking and thermal stability. Depolymerization also occurs, which consists of breakage of the bonds between the monomer units of the polymers. After each break, stabilization reactions occur at the two new ends of the chain, that is, depolymerization results in a decrease in the degree of polymerization of the chains until the molecules produced become volatile [27]. Images also indicate that all biomasses maintained their original shape, but decreased in size (Table 6.1), which was expected due to the breakdown of component bonds, as well as the elimination of volatile materials. The torrefied biomass yield decreased as the temperature and residence time increased, as expected (Table 6.1).

Table 6.1 - Torrefied biomass yield and images of in natura and torrefied biomasses under different experimental conditions.

Biomass	Images <i>in natura</i>	T (°C)	Images after torrefaction for different reaction times		Torrefied biomass yield, % (w/w)	
			30 minutes	60 minutes	30 minutes	60 minutes
CC		250			72.46±2.98	70.52±1.94
		290			63.01±1.91	63.42±0.52
CV		250			78.69±2.34	77.01±2.48
		290			63.59±0.58	54.71±3.71
PP		250			81.05±0.85	77.48±4.35
		290			60.68±4.02	54.22±4.26

Source: Brotto *et al.*, (2023).

The characteristics of the CC, CV and PP *in natura* and after torrefaction processes are shown in Table 6.1, highlighting its irregular cylindrical shape and sizes, which can affect the torrefaction process [28]. It is also observed that CC is darker than CV and PP, probably due to the high presence of lignin, as it will be discussed.

### 6.3.2 Characterization of in nature and torrefied biomass

Table 6.2 presents the results of approximate analysis, ultimate analysis, HHV and the lignocellulosic chemical components for in nature and torrefied biomass obtained under the experimental conditions. It can be observed that in nature CV and PP biomasses are similar in composition, while CC in nature presents high lignin content. After torrefaction, all samples presented increase on carbon content and decrease on oxygen content, as expected.

Analyzing Table 6.2, it can be observed that there was a decrease in the percentage of hemicellulose and cellulose and an increase in the lignin content. As hemicellulose and cellulose are degraded during torrefaction, the relative lignin content increases despite its partial degradation. Thus, lignin becomes the main component of the sample. When a fraction of hemicellulose, cellulose and/or lignin is removed, consequently, in percentage, an increase in the remaining fractions is verified.

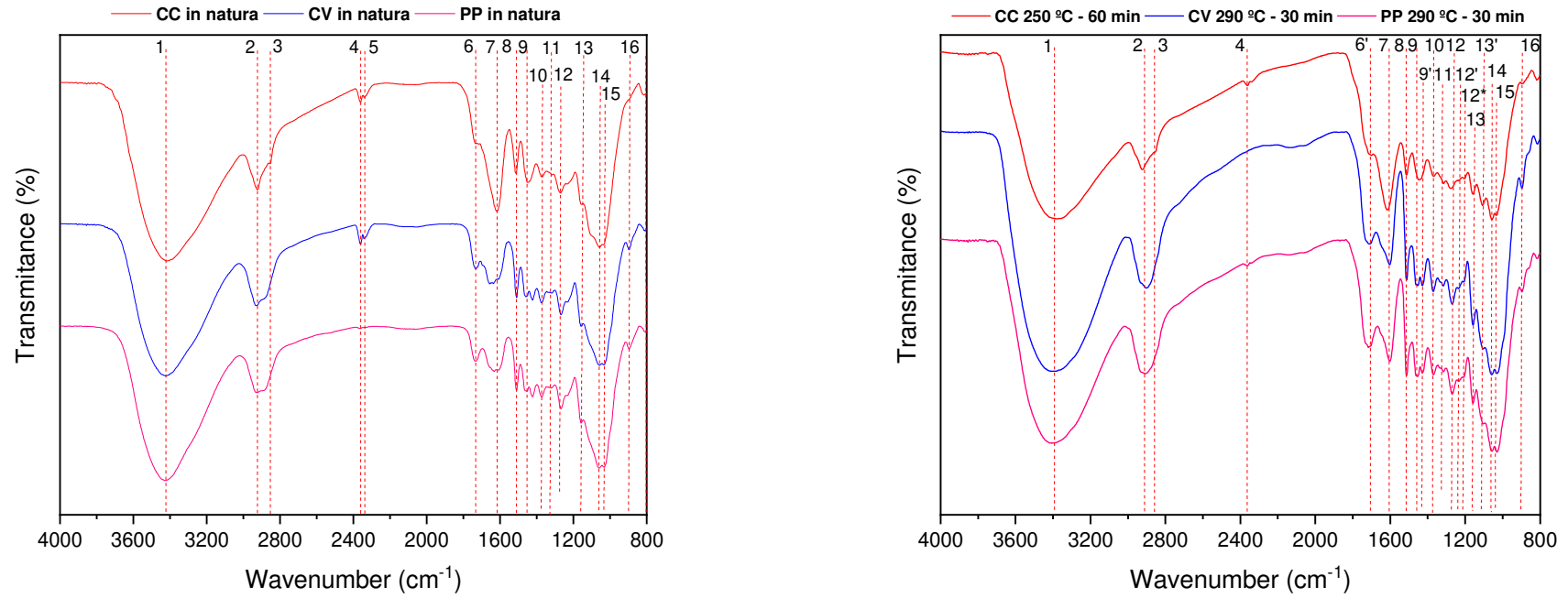
Figure 6.2 presents the curves referring to the FTIR analysis for the *in natura* and torrefied biomasses, while Table 6.3 presents all the spectral band assignments of the main peaks observed in the FTIR spectra of the biomasses. When comparing the peaks of the raw material and the torrefied material, the disappearance of peaks 5 (C–O bond) and 6 (C = O carbonyls in ester groups and acetyl groups in xylan) and the appearance of peaks 6' (C=O stretching, carboxylic acid), 9' (C–H asymmetric deformation in methoxyl, aromatic skeletal vibrations, lignin), 12' (C = O, C–H, C–O–C, C–O deformation or stretching), 12\* (CH<sub>2</sub> and O–H), and 13' (C–O–C stretching in cellulose and hemicellulose) are noted. Peak 6, at 1730 cm<sup>-1</sup>, is related to the characteristic CO stretching vibrations in ketone, carbonyl and unconjugated aliphatic xylan groups commonly found in hemicellulose [29], [30]. The absence of peak 6 in torrefied biomasses indicates that hemicellulose was decomposed during the torrefaction.

Table 6.2 - Characteristics of in natura and torrefied biomasses

		Biomasses <i>in natura</i>			Torrefied biomass		
		CC	CV	PP	CC25060	CV29030	PP29030
Proximate analysis (%), (w/w)	Volatile matter	65.79	78.16	83.28	52.31	66.45	60.88
	Ash content	0.92	0.84	0.63	1.81	0.64	0.68
	Fixed carbon	33.30	21.00	16.08	45.88	32.91	38.43
Ultimate analysis (%) (w/w)	C	46.66	46.00	46.41	55.64	53.56	55.56
	H	6.18	6.71	6.49	5.36	5.49	5.82
	N	0.34	0.24	0.08	0.49	0.11	0.16
	O	46.82	47.05	42.06	38.51	40.84	38.46
Molar ratio	O/C	0.75	0.76	0.68	0.52	0.57	0.52
	H/C	1.59	1.75	1.69	1.16	1.23	1.26
HHV (MJ kg <sup>-1</sup> )		19.41	19.08	19.49	21.72	20.94	22.26
Chemical components of lignocellulosic (%)	Cellulose	14.38 ± 0.27	41.77 ± 1.30	38.98 ± 0.92	9.75 ± 1.18	39.06 ± 1.24	30.11 ± 0.10
	Hemicellulose	5.75 ± 0.17	16.22 ± 0.74	15.43 ± 0.35	0.00 ± 0.00	2.53 ± 0.10	0.00 ± 0.00
	Lignin	59.53 ± 1.75	37.12 ± 0.15	35.28 ± 0.20	84.36 ± 1.33	55.55 ± 0.45	65.31 ± 0.85
	Extractives	15.93 ± 0.07	3.33 ± 0.85	6.41 ± 0.16	0.00 ± 0.00	0.00 ± 0.00	0.00 ± 0.00
	Ashes	1.54 ± 0.15	0.35 ± 0.02	0.47 ± 0.01	1.84 ± 0.14	0.27 ± 0.06	0.81 ± 0.14
	Total	97.13 ± 1.40	98.78 ± 1.55	96.57 ± 1.25	95.95 ± 0.17	97.41 ± 1.63	96.23 ± 0.73

Source: Brotto *et al.*, (2023).

Figure 6.2 - FTIR of in natura and torrefied biomass samples



Source: Brotto *et al.*, (2023).



Table 6.3 - FTIR spectrum of raw wood.

Number	Frequency ( $\text{min}^{-1}$ )	Assignment
1	3322	O–H stretching vibration from water, cellulose, hemicellulose and lignin [31]
2	2919	C–H vibrations of polysaccharides (glucomannans and arabinogalactan) and lignin [32]
3	2858	C–H vibrations of polysaccharides (glucomannans and arabinogalactan) and lignin [32]
4	2364	C–O bond [33]
5	2343	C–O bond [33]
6	1730	C = O carbonyls in ester groups and acetyl groups in xylan [31]
6'	1709	C=O stretching, carboxylic acid [34]
7	1610	C = O stretching conjugated to the aromatic ring, and in carboxylic groups in lignin, carboxylic acid, ester compounds [31]
8	1510	C = C stretching of the aromatic ring, C = O bond vibrations in extractive compounds [31]
9	1455	CH <sub>2</sub> stretching, HCH, OCH bending vibrations(in-plane), CH deformation [29]
9'	1425	C–H asymmetric deformation in methoxyl, aromatic skeletal vibrations, lignin [31]
10	1360	C–H deformation in cellulose and hemicelluloses [31]
11	1315	CH <sub>2</sub> wagging in crystalline cellulose [31]
12	1265	C–O vibration in guaiacyl rings [31]
12'	1240	C = O, C–H, C–O–C, C–O deformation or stretching [35]
12*	1211	CH <sub>2</sub> and O–H [36]
13	1155	C–O–C asymmetric stretching in cellulose and hemicellulose [31]
13'	1105	C–O–C stretching in cellulose and hemicellulose [31]
14	1055	C–O stretching of secondary alcohols [31]
15	1025	C–O stretching in primary alcohols in cellulose [32]
16	900	CH deformation of beta-glycosidic linkages in cellulose [31]

Source: Brotto *et al.*, (2023).

Finally, the lignin composition differs by the type of wood, soft or hard. For softwood, lignin is a polymer composed mainly of guaiacyl units, with a small amount of p-hydroxyphenyl and syringyl units, while in hardwood it is composed of syringyl and guaiacyl units, with a small number of p-hydroxyphenyl units. Bands with intensity of 1594, 1326 and 1234  $\text{cm}^{-1}$  are easily detected in hardwood spectra and refer to the syringyl units, while the band at 1265  $\text{cm}^{-1}$  is more evident in softwood and represents the guaiacyl unit [29], [31]. Thus, and with the results obtained from FTIR, it is possible to verify that the biomasses come from softwood.

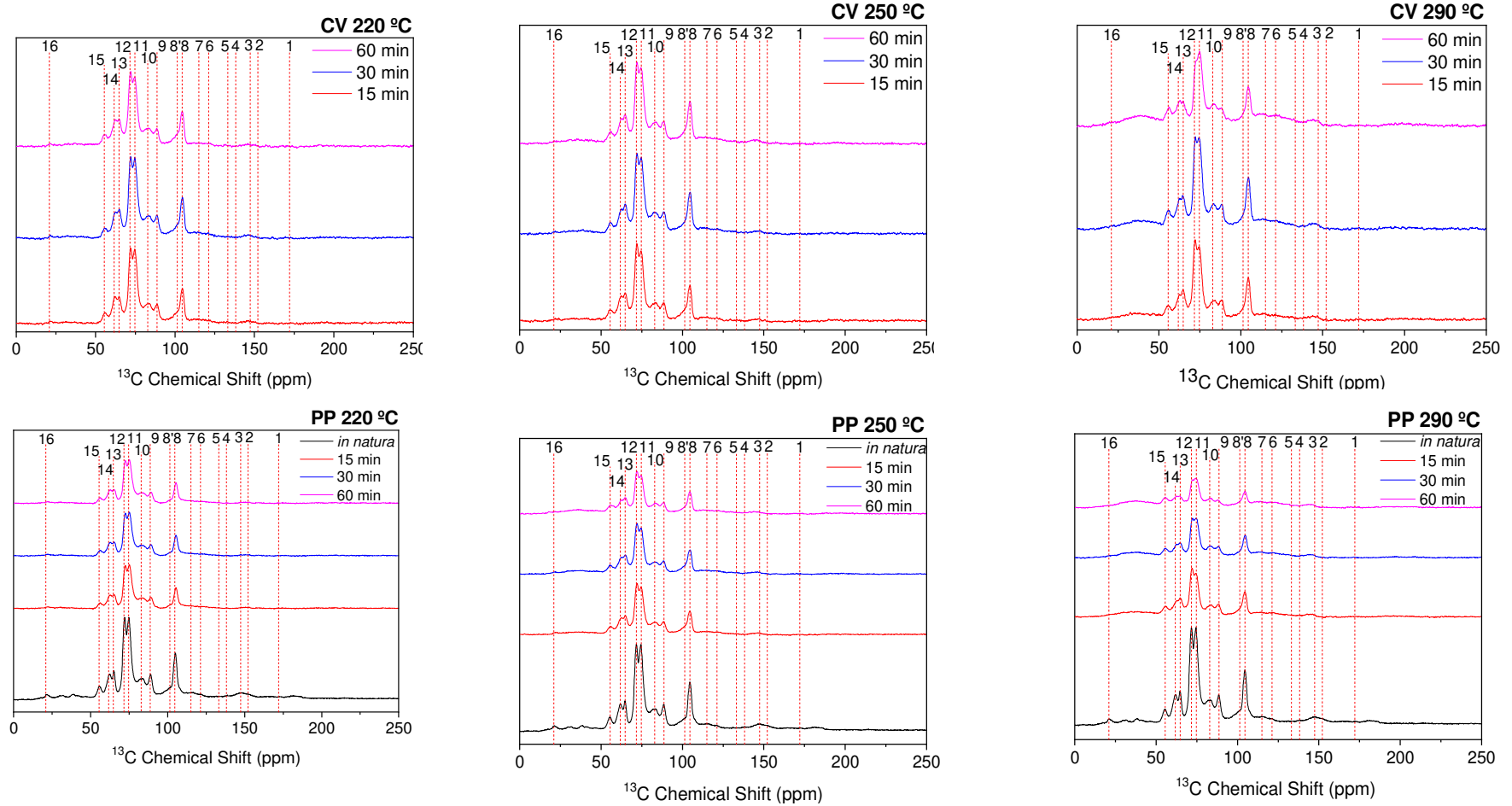
### 6.3.3 Evaluation of torrefaction mechanism and kinetics using *ss*-NMR analysis

Mechanistic insights about the torrefaction process were explored by using *ss*-NMR analysis of the *in natura* and torrefied biomasses. For this approach, the biomasses CV and PP were torrefied under different temperatures (220 °C, 250 °C and 290 °C) for different reaction times (0, 15, 30 and 60 minutes), and the NMR spectra for the solid torrefied samples are shown in Figure 6.3.

The  $^{13}\text{C}$  resonance signals 1 and 16 refer to the carbonyl and methyl carbon compounds of acetyl groups in hemicelluloses, while 8' represents C-1 of hemicellulose (Table 6.4). For cellulose, carbon atoms are characterized by peaks 8, 9, 10 and 13, which are equivalent respectively to C-1 of cellulose, C-4 of cellulose in ordered cellulose, C-4 of cellulose in disordered/amorphous cellulose, and C-6 of cellulose. Also, the sum of the amounts of carbon from peaks 9 and 10 is equivalent to the total amount of C-4 in cellulose. Finally, for lignin, C-3 and C-5 of syringyls in etherified structures are represented by peak 2 and in non-etherified by peak 3.  $^{13}\text{C}$  resonance 3 also contains a contribution of C-3 and C-4 from guaiacyls in etherified and non-etherified structures and peak 15 represents carbon atoms from methoxyl groups [24].

Figure 6.3 shows that the  $^{13}\text{C}$  resonance signals for all samples generated through CV or PP torrefaction at various temperature and reaction time settings are comparable, albeit varying in intensities. It is noted that the signals presented by the *in natura* biomass are similar to those of the torrefied PP biomasses. However, it is observed the presence of two more very subtle  $^{13}\text{C}$  resonance signals in the *in natura* PP biomass, namely, peaks 16 and 3, referring to hemicelluloses ( $\text{CH}_3\text{-CO}_2\text{-}$ ) and lignin (S-3(ne), S-5(ne), G-3(ne, e), G4(ne, e)).

Figure 6.3 - NMR of CV and PP biomasses samples.



Source: Brotto *et al.*, (2023).

Table 6.4 - Resonance assignment of  $^{13}\text{C}$  CP-MAS spectrum of biomasses

Resonance number	Chemical shift (ppm)	Assignment
1	172	Hemicelluloses: $\text{-COO-R}$ , $\text{CH}_3\text{-COO-}$
2	152.6	Lignin: S-3(e), S-5(e)
3	148-147	Lignins: S-3(ne), S-5(ne), G-3(ne, e), G4(ne, e)
4	138-138.5	Lignins: S-1(e), S-4(e), G-1(e)
5	134-133	Lignins: S-1(ne), S-4(ne), G-1(ne)
6	121	Lignins; G-6
7	114-106	Lignins; G-5, G-6, S-2, S-6
8	104.8	Cellulose: C-1
8'	104-101	Hemicelluloses: C-1
9	88.7	Carbohydrates: C-4 cellulose (ordered)
10	83.8	Lignins: C $\beta$ Carbohydrates: C-4 cellulose (disordered)
11	74.8	Lignins: C $\alpha$ Carbohydrates: C-2, -3, -5
12	72.2	Carbohydrates: C-2, -3, -5
13	64.7	Carbohydrates: C-6 cellulose (ordered)
14	61.6	Lignins: C $\gamma$ Carbohydrates: C-6 cellulose (disordered)
15	55.7	Lignins: O $\underline{\text{C}}\text{H}_3$
16	21	Hemicelluloses: $\underline{\text{C}}\text{H}_3\text{-COO-}$

Legend: S: carbon in syringyls (aromatic unit with two methoxyl groups), G: carbon in guaiacyls (aromatic unit with only methoxyl), ne: in non-ethererified arylglycerol  $\beta$ -aryl ethers, e: in etherified arylglycerol  $\beta$ -aryl ethers [24].

Source: Brotto *et al.*, (2023).

The non-appearance of these signals in the torrefied samples is probably due to the fact that these bonds were broken during the torrefaction treatment. Furthermore, the non-appearance of peaks 1, 8' and 16, referring to hemicellulose, in the torrefied biomass is consistent with the results obtained from the composition of hemicellulose.

To obtain mechanistic insights about the transformation of polymers (deacetylation of hemicelluloses, demethoxylation of lignin, changes in the cellulose

structure was studied considering the  $^{13}\text{C}$  chemical shifts ( $\delta^{13}\text{C}$ ) at 104.8, 88.7, 83.8, 64.7, and 55.7 ppm [24] (Table S6.1 – Supplementary material).

The kinetics of evolution of *ss*-NMR signals ascribed to C-1 of cellulose; C-4 of cellulose in ordered cellulose; C-4 of cellulose in disordered/amorphous cellulose; C-6 of cellulose, and carbon atoms of methoxyl groups in lignins were used to estimate the activation energy of each decomposition reaction during torrefaction. It was considered that each reaction obeys a pseudo-first order reaction and the activation energies were evaluated according to the Arrhenius Equation (Figure S6.1 - Supplementary material).

Table 6.5 show parameters kinetics obtained using *ss*-NMR. According this table,  $k_{NMR}$  values increased with the temperature, and the kinetics evolution of signal 15 (lignin:  $\text{OCH}_3$ ) is the slowest for both CV and PP. In fact, lignin is reported to undergo softening at  $T > 200^\circ\text{C}$  [24], while bulk lignin polymers can remain quite stable. Furthermore, it is worth mentioning that the decomposition of cellulose occurs between 300 and  $390^\circ\text{C}$  [27] and that the maximum torrefaction temperature used in this study was  $290^\circ\text{C}$ , that is, the total decomposition of cellulose probably did not occur [24].

The torrefaction activation energies ranged from  $11.85 \pm 1.47$  to  $25.37 \pm 1.31$   $\text{kJ mol}^{-1}$  and  $11.71 \pm 0.35$  to  $18.24 \pm 2.88$   $\text{kJ mol}^{-1}$ , for CV and PP, respectively (Table 6.5). The temperature ranges used to evaluate the activation energy ( $220$ ,  $250$ , and  $290^\circ\text{C}$ ) were chosen to encompass light, moderate, and severe torrefaction, respectively. A close examination of the curves within this temperature range reveals a satisfactory fit. These values are in the same magnitude order than those reported by da Silva *et al.* [15] using thermogravimetric measurements. In general, the activation energy calculated from thermogravimetric experiments varies mostly between the values of  $11$   $\text{kJ mol}^{-1}$  to  $151$   $\text{kJ mol}^{-1}$ , considering one or multi-step mechanisms [37].

More recently, some authors reported different approaches to describe complex reactions for torrefaction and pyrolysis of biomass. In those studies, the biomass pseudo-components would react independently and different activation energy values were obtained for the thermal decomposition of hemicellulose, cellulose and lignin using thermogravimetric studies [38].

Table 6.5 - Pseudo first order kinetic law considering different decays of the *ss*-NMR signals.

<sup>13</sup> C Chemical shift (ppm)	Chips (CV)				Pine Pellet (PP)		
	T (°C)	$k_{NMR}$ (min <sup>-1</sup> )	Activation energy (kJ mol <sup>-1</sup> )	R <sup>2</sup> (%)	$k_{NMR}$ (min <sup>-1</sup> )	Activation energy (kJ mol <sup>-1</sup> )	R <sup>2</sup> (%)
104.8	220	$0.0130 \pm 6.46 \cdot 10^{-3}$			$0.0179 \pm 6.60 \cdot 10^{-3}$		
	250	$0.0167 \pm 1.18 \cdot 10^{-3}$	$17.18 \pm 0.37$	99.95	$0.0208 \pm 4.50 \cdot 10^{-4}$	$15.21 \pm 2.32$	97.72
	290	$0.0219 \pm 9.62 \cdot 10^{-3}$			$0.0283 \pm 8.90 \cdot 10^{-3}$		
88.7	220	$0.0149 \pm 4.26 \cdot 10^{-3}$			$0.0175 \pm 5.6 \cdot 10^{-3}$		
	250	$0.0168 \pm 1.00 \cdot 10^{-3}$	$11.85 \pm 1.47$	98.46	$0.0209 \pm 1.60 \cdot 10^{-4}$	$18.24 \pm 2.88$	97.57
	290	$0.0213 \pm 5.89 \cdot 10^{-3}$			$0.0303 \pm 7.00 \cdot 10^{-3}$		
83.8	220	$0.0150 \pm 7.46 \cdot 10^{-3}$			$0.0185 \pm 5.30 \cdot 10^{-3}$		
	250	$0.0182 \pm 1.23 \cdot 10^{-3}$	$11.98 \pm 0.95$	99.36	$0.0219 \pm 7.50 \cdot 10^{-4}$	$11.71 \pm 0.35$	99.91
	290	$0.0216 \pm 1.12 \cdot 10^{-3}$			$0.0264 \pm 8.4 \cdot 10^{-3}$		
64.7	220	$0.0111 \pm 3.85 \cdot 10^{-3}$			$0.0162 \pm 4.70 \cdot 10^{-3}$		
	250	$0.0214 \pm 1.46 \cdot 10^{-3}$	$25.37 \pm 1.31$	99.73	$0.0175 \pm 6.66 \cdot 10^{-3}$	$13.56 \pm 4.17$	91.34
	290	$0.0240 \pm 1.35 \cdot 10^{-3}$			$0.0243 \pm 4.47 \cdot 10^{-3}$		
55.7	220	$0.0109 \pm 1.37 \cdot 10^{-3}$			$0.0102 \pm 4.70 \cdot 10^{-3}$		
	250	$0.0141 \pm 1.98 \cdot 10^{-3}$	$16.31 \pm 1.09$	99.56	$0.0133 \pm 3.24 \cdot 10^{-3}$	$14.32 \pm 1.13$	97.24
	290	$0.0179 \pm 1.42 \cdot 10^{-3}$			$0.0158 \pm 5.55 \cdot 10^{-3}$		

Source: Brotto *et al.*, (2023).

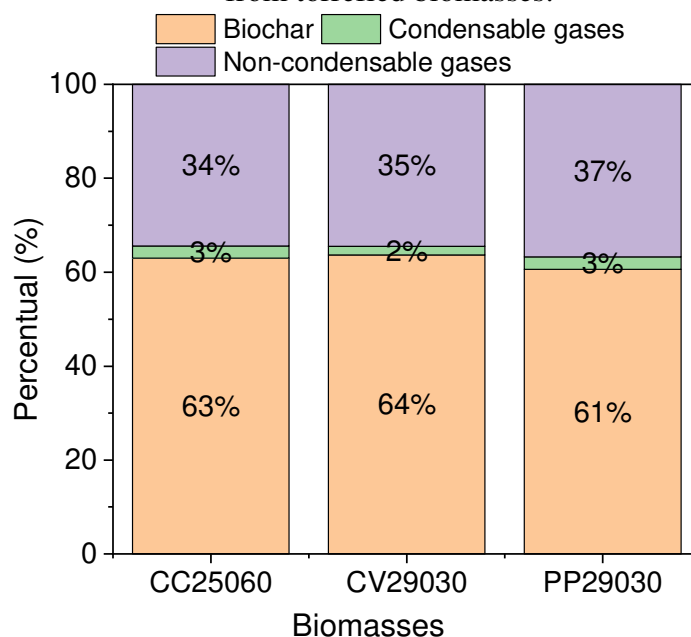
The results showed that the activation energy for the thermal decomposition of four hemicellulose pseudo-components varied between 30.09 and 144.16 kJ mol<sup>-1</sup> for heating rates of 1-5 °C min<sup>-1</sup>, and 47.51-194.35 kJ mol<sup>-1</sup> for heating rates of 20-40 °C min<sup>-1</sup>. Regarding the lignin pseudo-components, the activation energy ranged from 20.97 to 636.53 kJ mol<sup>-1</sup> for the heating rate of 1 °C min<sup>-1</sup>, and from 51.66 to 672.97 kJ mol<sup>-1</sup> for heating rates of 5, 20 and 40 °C min<sup>-1</sup> [3]. The authors assume that the low activation energy indicates the demethoxylation reaction of guaiacol.

Nevertheless, the kinetics of evolution of *ss*-NMR signals can give access to the molecular transformations occurring within the cellulose, hemicellulose and lignin [24], and no assumption for the pseud-components is required

### 6.3.4 Characterization of condensable and non-condensable gases products from torrefaction

Figure 6.4 shows that the percentage of the solid (torrefied biomass), liquid (condensable gases) and non-condensable gases fractions obtained during torrefaction of CC (at 250°C for 60 minutes), CV (at 290°C for 60 minutes), and PP (at 290°C for 60 minutes) is quite similar, and all biomasses are promisor to produce torrefied biomass.

Figure 6.4 - Percentage of torrefied biomass, condensable and non-condensable gases and from torrefied biomasses.



Source: Brotto *et al.*, (2023).

The composition of each fraction (gaseous and liquid products) formed during the torrefaction process to produce CC25060, CV29030 and PP29030 were analyzed (Figure 6.5). Aromatic esthers, aldehyde, aliphatic and aromatic alcohols, aliphatic ketones and aromatic heterocyclic compounds were found in different proportions, depending on the biomass source, being aliphatic ketones the main component in the condensable gases produced by torrefaction.

The highest percentage obtained in all torrefied biomass was aliphatic ketones, and CC25060 presented the highest percentage, 65.73%. Heterocyclic aromatic compounds appeared as the second most present component in the CV29030 biomass, with 17.36% and also in the CC25060 biomass, with 6.23%. The lowest amount in the CC25060 biomass was that of aromatic esters, a compounds that also appeared in the PP29030 biomass. In the CV29030 and PP29030 biomasses, aliphatic alcohols and aromatic alcohols also appeared, which shows that the condensable liquid of sample CC25060 does not have any alcohol formed.

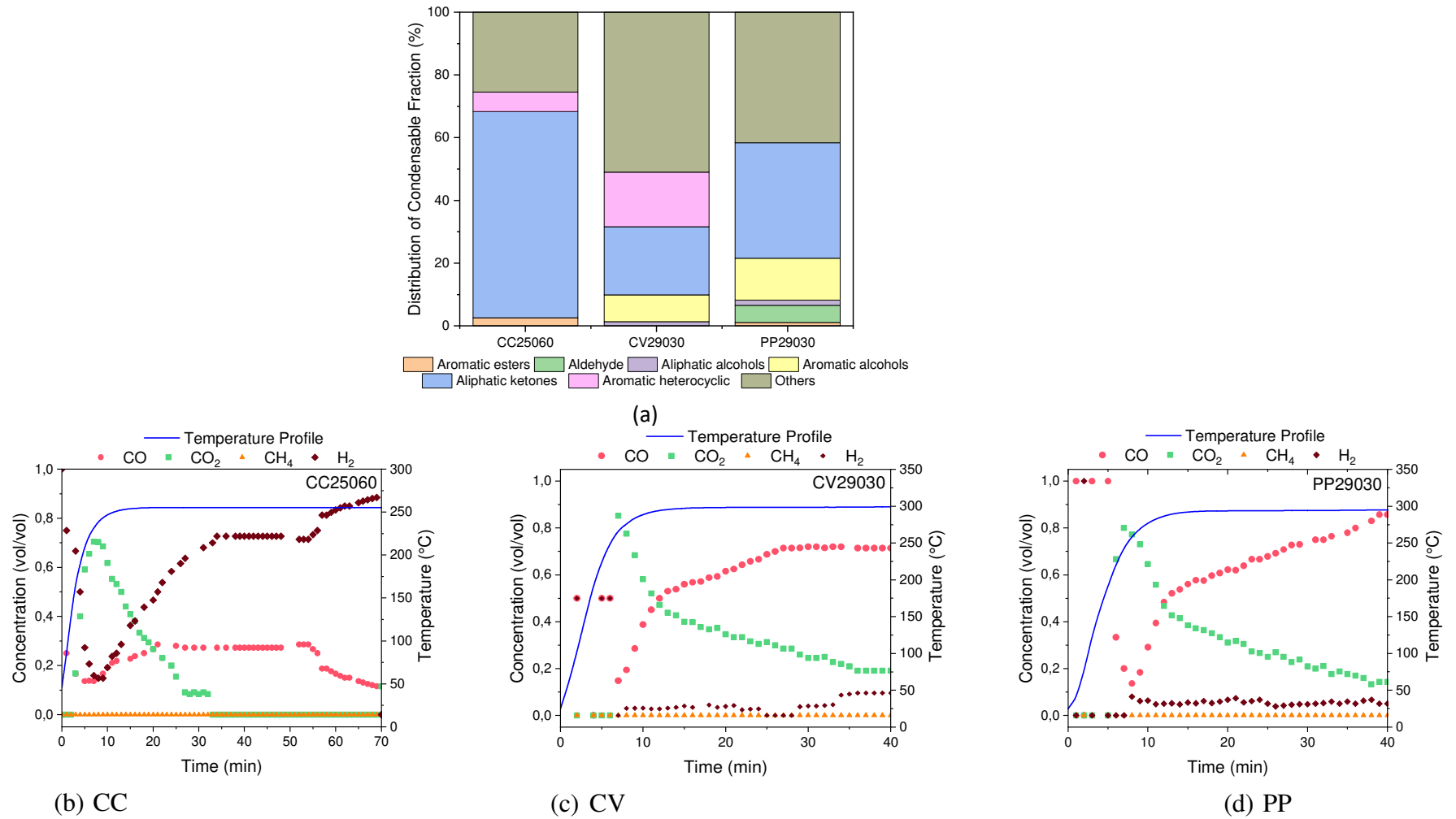
As in the previous analyses, a similarity between the condensable gases (Figure 6.5a) and non-condensable gases (Figure 6.5b-d) produced from CV and PP at the same experimental conditions (290°C, 30 minutes) is noted, while CC produced mainly aliphatic ketones (condensable gases) and H<sub>2</sub> (non-condensable gases) possibly due to its higher lignin content (Table 6.2).

The main component released during all torrefaction conditions was CO<sub>2</sub>, which had a high release at the beginning of torrefaction because it is the point at which the gases begin to be released from the breaking of the chemical bonds of lignocellulose [39]. The high release of CO<sub>2</sub> is associated with decarboxylation reactions of polysaccharides in hemicellulose, such as the cleavage of acetyl groups in xylan [40].

Analyzing the CC25060 biomass curve, it is noted that initially there is a higher concentration of H<sub>2</sub>, a little CO while CO<sub>2</sub> and CH<sub>4</sub> are equal to zero. As the temperature increases until it reaches 250 °C, there is a decrease in the emission of H<sub>2</sub> and CO and an increase in the emission of CO<sub>2</sub>. The maximum and minimum peaks of CO<sub>2</sub> and H<sub>2</sub>, respectively, occur when the temperature is close to 250 °C. After that, there is a decrease in CO<sub>2</sub>, which stabilizes after about 25 min.



Figure 6.5 - Condensable gases fraction (a) and evolution of non-condensable gases during the torrefaction of CC (250 °C, 60 minutes) (b); CV (290 °C, 30 minutes) (c); and PP (290 °C, 30 minutes) (d).



Source: Brotto *et al.*, (2023).

For the CV29030 and PP29030 biomasses, the gases products follow the same tendency in terms of gas composition. As the increase in CO occurs, the decrease in CO<sub>2</sub> occurs, and for the CV29030 biomass after 35 minutes of reaction, the values of CO and CO<sub>2</sub> emission become constant. For the PP29030 biomass, this behavior is not observed, as CO continues to increase and CO<sub>2</sub> continues to decrease. There is no emission of CH<sub>4</sub> during torrefaction.

It is known that the torrefaction is a global deoxygenation reaction, with oxygen in the biomass being released mainly in the form of H<sub>2</sub>O and oxygen-containing compounds (carboxylic acids, alcohols, furans, and phenols) in the liquid products, and CO<sub>2</sub>/CO in the gas products [40]. The breaking of C-C and C-O bonds mainly involves decarboxylation (the release of CO<sub>2</sub>) and decarbonylation (the release of CO) [40]. In the torrefaction reactions dehydration, demethoxylation (the release of methanol) and dehydrogenation (the emission of H<sub>2</sub>) also occur. Considering the analysis of the condensable and non-condensable gases fractions during torrefaction, it can be said that the most promising torrefied biomass is CV29030 followed by PP29030 and, finally, CC25060.

#### 6.4 CONCLUSIONS

The results of this study indicate that the main constituents of biomass (cellulose, hemicelluloses, and lignin) are affected in several ways by torrefaction, depending on their reactivity. The high lignin content present in CC produced torrefied biomass less reactive probably due to the protecting role towards cellulose during torrefaction.

Torrefaction generated a low amount of gases, even at the longest residence time. The fraction of condensable, non-condensable gases and solid torrefied biomass is almost constant for all biomass studied in this work. The presence of lignin in high concentration produced non-condensable gases rich in hydrogen and aliphatic ketones in high concentration in the condensable gases.

Studies of *ss*-NMR and their application in evaluation of the kinetic parameters showed low activation energies for the decomposition of lignocellulosic components of the biomass. The kinetic biomass torrefaction was studied using *ss*NMR for the first time, and the activation energy to decompose each biomass component is in the range 11.71-25.37 kJ mol<sup>-1</sup>.

## 6.5 REFERENCES

- [1] R.C. Uwaoma, W.G. Stokes, J.R. Bunt, C.A. Strydom, R.H. Matjie  
A metallurgical coke replacement derived from torrefied wood chips pre-treated by wet oxidation *Bioresour. Technol. Rep.*, 19 (2022), Article 101141, 10.1016/j.biteb.2022.101141
- [2] F.S. Weldegiorgis, D.M. Franks Social dimensions of energy supply alternatives in steelmaking: comparison of biomass and coal production scenarios in Australia *J. Clean. Prod.*, 84 (2014), pp. 281-288, 10.1016/j.jclepro.2013.09.056
- [3] P. Zhao, P.L. Dong Carbon emission cannot be ignored in future of Chinese steel industry *Iron Steel*, 53 (2018), pp. 1-7, 10.13228/j.boyuan.issn0449-749x.20180081
- [4] C.M. Nwachukwu, C. Wang, E. Wetterlund Exploring the role of forest biomass in abating fossil CO<sub>2</sub> emissions in the iron and steel industry – The case of Sweden *Appl. Energy*, 288 (2021), Article 116558, 10.1016/j.apenergy.2021.116558
- [5] B. Yi, M. Chen, Y. Gao, C. Cao, Q. Wei, Z. Zhang, L. Li Investigation on the co-combustion characteristics of multiple biomass and coal under O<sub>2</sub>/CO<sub>2</sub> condition and the interaction between different biomass *J. Environ. Manag.*, 325 (2023), Article 116498, 10.1016/j.jenvman.2022.116498
- [6] M.J.C. van der Stely, H. Gerhauser, J.H.A. Kiel, K.J. Ptasiński Biomass upgrading by torrefaction for the production of biofuels: a review *Biomass-Bioenergy*, 35 (2011), pp. 3748-3762, 10.1016/j.biombioe.2011.06.023
- [7] H.C. Ong, K.L. Yu, W. Chen, M.K. Pillejera, X. Bi, K. Tran, A. Pétrissans, M. Pétrissans Variation of lignocellulosic biomass structure from torrefaction: a critical review *Renew. Sustain. Energy Rev.*, 152 (2021), Article 111698, 10.1016/j.rser.2021.111698
- [8] L.B. Director, V.A. Sinelshchikov Numerical modeling of torrefaction reactor integrated in energy technological complex *Energy*, 167 (2019), pp. 1194-1204, 10.1016/j.energy.2018.11.044
- [9] M. Ivanovski, D. Goricanec, J. Krope, D. Urbancl Torrefaction pretreatment of lignocellulosic biomass for sustainable solid biofuel production *Energy*, 240 (2022), Article 122483, 10.1016/j.energy.2021.122483
- [10] Z. Zhang, H. Duan, Y. Zhang, X. Guo, X. Yu, X. Zhang, M.M. Rahman, J. Cai Investigation of kinetic compensation effect in lignocellulosic biomass torrefaction: Kinetic and thermodynamic analyses *Energy*, 207 (2020), Article 118290, 10.1016/j.energy.2020.118290
- [11] C. Wang, P. Mellin, J. Lövgren, L. Nilsson, W. Yang, H. Salman, A. Hultgren, M. Larsson Biomass as blast furnace injectant – Considering availability, pretreatment and deployment in the Swedish steel industry *Energy Convers. Manag.*, 102 (2015), pp. 217-226, 10.1016/j.enconman.2015.04.013
- [12] H. Suopajarvi, E. Pongrácz, T. Fabritius The potential of using biomass-based reducing agents in the blast furnace: a review of thermochemical conversion technologies and

assessments related to Sustainability. *Renew. Sustain. Energy Rev.*, 25 (2013), pp. 511-528, 10.1016/j.rser.2013.05.005

[13] Z. Maree, C.A. Strydom, J.R. Bunt. Chemical and physical characterization of spent coffee ground biochar treated by a wet oxidation method for the production of a coke substitute *Waste Manag.*, 113 (2020), pp. 422-429, 10.1016/j.wasman.2020.06.025

[14] E. Rodriguez-Alonso, C. Dupont, L. Heux, Denilson Da Silva Perez, Jean-Michel Commandre, Christophe Gourdon Study of solid chemical evolution in torrefaction of different biomasses through solid-state  $^{13}\text{C}$  cross-polarization/magic angle spinning NMR (nuclear magnetic resonance) and TGA (thermogravimetric analysis) *Energy*, 97 (2016), pp. 381-390, 10.1016/j.energy.2015.12.120

[15] J.C.G. da Silva, J.L.F. Alves, G.D. Mumbach, S.L.F. Andersen, R.F.P.M. Moreira, H.J. José Torrefaction of low-value agro-industrial wastes using macro-TGA with GC-TCD/FID analysis: physicochemical characterization, kinetic investigation, and evolution of non-condensable gases *J. Anal. Appl. Pyrolysis*, 166 (2022), Article 105607, 10.1016/j.jaap.2022.105607

[16] S.G. Kostryukov, P.S. Petrov, V.S. Tezikova, Y.Y. Masterova, T.J. Idris, N.S. Kostryukov. Determination of wood composition using solid-state  $^{13}\text{C}$  NMR spectroscopy *Cellul. Chem. Technol.*, 55 (5–6) (2021), pp. 461-468, 10.35812/CelluloseChemTechnol.2021.55.42

[17] C. Zhang, S. Ho, W. Chen, Y. Xie, Z. Liu, J. Chang. Torrefaction performance and energy usage of biomass wastes and their correlations with torrefaction severity index *Appl. Energy*, 220 (2018), pp. 598-604, 10.1016/j.apenergy.2018.03.129

[18] R.K. Singh, A. Sarkar, J.P. Chakraborty Effect of torrefaction on the physicochemical properties of eucalyptus derived biofuels: estimation of kinetic parameters and optimizing torrefaction using response surface methodology (RSM) *Energy*, 198 (2020), Article 117369, 10.1016/j.energy.2020.117369

[19] ASTM, 2014. E1131–08: Standard Test Method for Compositional Analysis by Thermogravimetry. ASTM International, West Conshohocken, pp. 1–6. <https://doi.org/10.1520/E1131>.

[20] ASTM, D5373–08 Standard test methods for instrumental determination of carbon, hydrogen, and nitrogen in laboratory samples of coal and coke *Annu. B. ASTM Stand*, ASTM International, West Conshohocken, 2016, p. 4, <https://doi.org/10.1520/D5373-16>.

[21] S.A. Channiwala, P.P. Parikh A unified correlation for estimating HHV of solid, liquid and gaseous fuels *Fuel*, 81 (2002), pp. 1051-1063, 10.1016/S0016-2361(01)00131-4

[22] ASTM. D2702–05: Standard Practice for Rubber Chemicals — Determination of Infrared Absorption Characteristics. *Annu. B. ASTM Stand.*, 2016, pp. 4. <https://doi.org/10.1520/D2702-05R16>.

[23] J.B. Sluiter, H. Chum, A.C. Gomes, R.P.A. Tavares, V. Azevedo, M.T.B. Pimenta, S.C. Rabelo, K. Marabezi, A.A.S. Curvelo, A.R. Alves, W.T. Garcia, W. Carvalho, P.J. Esteves, S.

Mendonça, P.A. Oliveira, J.A.A. Ribeiro, T.D. Mendes, M.P. Vicentin, C.L. Duarte, M.N. Mori. Evaluation of Brazilian sugarcane bagasse characterization: An interlaboratory comparison study. *J. AOAC Int.*, 99 (3) (2016), pp. 579-585, 10.5740/jaoacint.15-0063

[24] T. Melkior, S. Jacob, G. Gerbaud, S. Hediger, L.L. Pape, L. Bonnefois, M. Bardet NMR analysis of the transformation of wood constituents by torrefaction *Fuel*, 92 (2012), pp. 271-280, 10.1016/j.fuel.2011.06.042

[25] R. Barzegar, A. Yozgatligil, H. Olgun, A.T. Atimtay TGA and kinetic study of different torrefaction conditions of wood biomass under air and oxy-fuel combustion atmospheres *J. Energy Inst.*, 93 (2020), pp. 889-898, 10.1016/j.joei.2019.08.001

[26] J.O. Brotto, J.S. Salla, J.C.G. daSilva, E. Rodríguez-zastellón, H.J. José, S.M. Amorim, R.F.P.M. Moreira. Investigation of the thermal behavior of *Pine* wood pellets during torrefaction for application in metallurgical processes. *J. Mater. Res. Technol.*, 19 (2022), pp. 3749-3759, 10.1016/j.jmrt.2022.06.082

[27] F. Collard, J. Blin. A review on pyrolysis of biomass constituents: mechanisms and composition of the products obtained from the conversion of cellulose, hemicelluloses and lignina. *Renew. Sustain. Energy Rev.*, 38 (2014), pp. 594-608, 10.1016/j.rser.2014.06.013

[28] J. Cai, Y. He, X. Yu, S.W. Banks, Y. Yang, X. Zhang, Y. Yu, R. Liu, A.V. Bridgwater Review of physicochemical properties and analytical characterization of lignocellulosic biomass. *Renew. Sustain. Energy Rev.*, 76 (2017), pp. 309-322, 10.1016/j.rser.2017.03.072

[29] V. Sharma, J. Yadav, R. Kumar, D. Tesarova, A. Ekielski, P.K. Mishra On the rapid and non-destructive approach for wood identification using ATR-FTIR spectroscopy and chemometric methods *Vib. Spectrosc.*, 110 (2020), Article 103097, 10.1016/j.vibspec.2020.103097

[30] M. Traoré, J. Kaal, A.M. Cortizas. Variation of wood color and chemical composition in the stem cross-section of oak (*Quercus* spp.) trees, with special attention to the sapwood-heartwood transition zone *Spectrochim. Acta Part A: Mol. Biomol. Spectrosc.*, 285 (2023), Article 121893, 10.1016/j.saa.2022.121893

[31] G. Toscano, V. Maceratesi, E. Leoni, P. Stipa, E. Laudadio, S. Sabbatini FTIR spectroscopy for determination of the raw materials used in wood pellet production *Fuel*, 313 (2022), Article 123017, 10.1016/j.fuel.2021.123017

[32] M. Traoré, J. Kaal, A.M. Cortizas Differentiation between pine woods according to species and growing location using FTIR-ATR. *Wood Sci. Technol.*, 52 (2018), pp. 487-504, 10.1007/s00226-017-0967-9

[33] D.C. Lingegowda, J.K. Kumar, A.G.D. Prasad, M. Zarei, S. Gopal. Ftir spectroscopic studies on cleome gynandra – comparative analysis of functional group before and after extraction, *Romanian J. Biophys.* (2013), pp. 137-143  
<<https://www.researchgate.net/publication/255486350>>

- [34] H. Sun, X. Chen, D. Chen, M. Dong. Influences of surface coatings and components of FePt nanoparticles on the suppression of glioma cell proliferation. *Int. J. Nanomed.* (2012), pp. 295-307, 10.2147/IJN.S32678
- [35] R. Herrera, E. Hermoso, J. Labidi, J.I. Fernandez-Golfin. Non-destructive determination of core-transition-outer wood of *Pine nigra* combining FTIR spectroscopy and prediction models. *Microchem. J.*, 179 (2022), Article 107532, 10.1016/j.microc.2022.107532
- [36] V. Emmanuel, B. Odile, R. Céline. FTIR spectroscopy of woods: a new approach to study the weathering of the carving face of a sculpture. *Spectrochim. Acta Part A: Mol. Biomol. Spectrosc.*, 136 (2015), pp. 1255-1259, 10.1016/j.saa.2014.10.011
- [37] S.K. Thengane, K.S. Kung, A. Gomez-Barea, A.F. Ghoniem. Advances in biomass torrefaction: Parameters, models, reactors, applications, deployment, and market. *Prog. Energy Combust. Sci.*, 93 (2022), Article 101040, 10.1016/j.peccs.2022.101040
- [38](a) A. Sori-Verdugho, W. Cano-Pleite, A. Panahi, A.F. Ghoniem. Kinetics mechanism of inert and oxidative torrefaction of biomass. *Energy Convers. Manag.*, 267 (2022), Article 115892, 10.1016/j.enconman.2022.115892  
(b) J.C.G. da Silva, J. Leque, C. Pereira, S.L.F. Andersen, R.F.P.M. Moreira, H.J. José. Torrefaction of ponkan peel waste in tubular fixed-bed reactor: In-depth bioenergetic evaluation of torrefaction products. *Energy*, 210 (2020), Article 118569, 10.1016/j.energy.2020.118569
- [39](a) W.-H.-Hsin Chen, C.F. Eng, Y.-Y. Lin, Q.-V. Bach. Independent parallel pyrolysis kinetics of cellulose, hemicelluloses and lignin at various heating rates analyzed by evolutionary computation. *Energy Convers. Manag.*, 221 (2020), Article 113165, 10.1016/j.enconman.2020.113165  
(b) X. Zhou, W. Li, R. Mabon, L.J. Broadbelt. A critical review on hemicellulose pyrolysis. *Energy Technol.*, 5 (2017), pp. 52-113179, 10.1002/ente.201600327
- [40] D. Chen, J. Li, T. Zhang, S. Li, J. Wang, W. Niu, Y. Liu, A. Zheng, Z. Zhao. Advancing biomass pyrolysis by torrefaction pretreatment: linking the productions of bio-oil and oxygenated chemicals to torrefaction severity. *Fuel*, 330 (2022), Article 125514, 10.1016/j.fuel.2022.125514

## 6.6 SUPPLEMENTARY MATERIAL

Figure S6.1 - Arrhenius plot and regression linear for CV and PP.

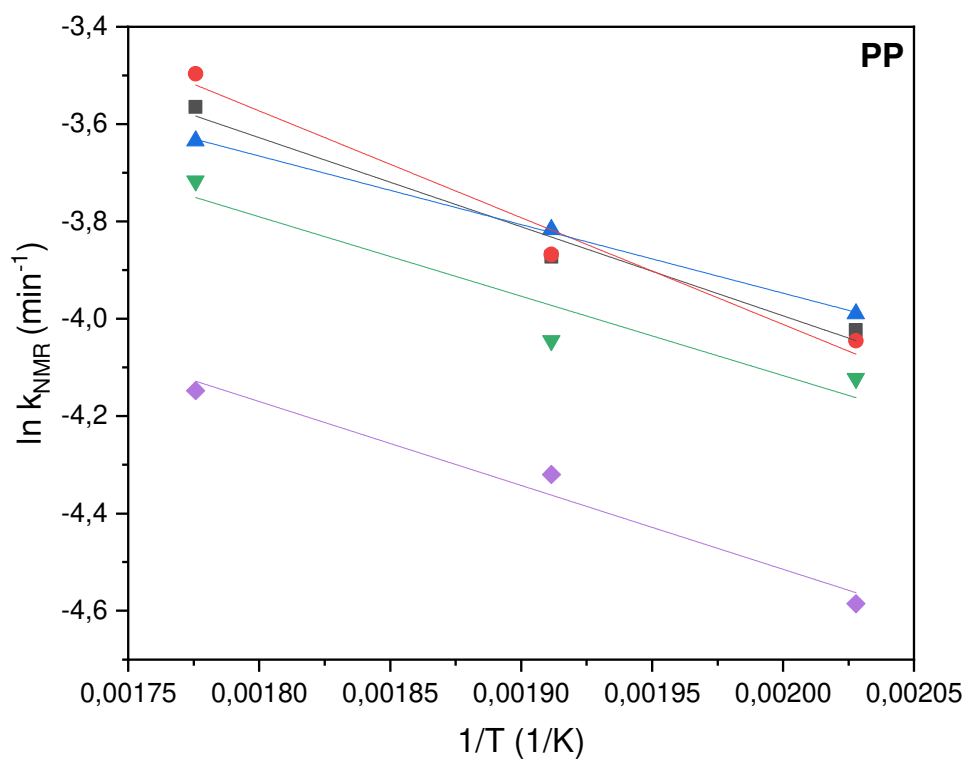
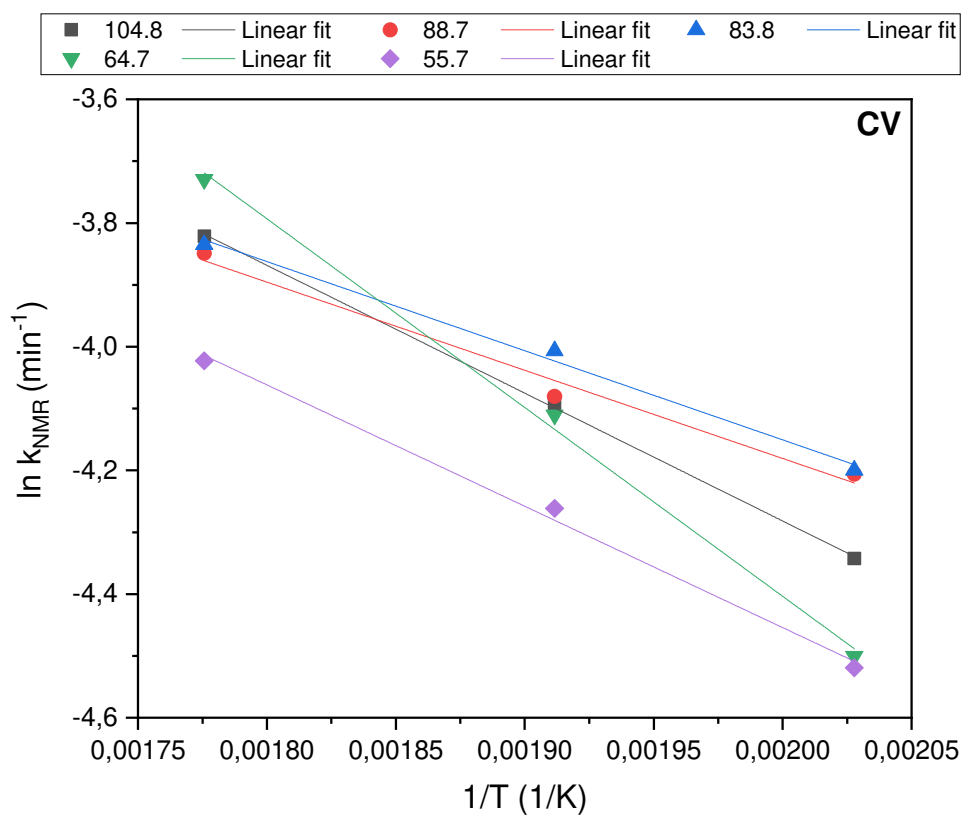
Source: Brotto *et al.*, 2023.

Table S6.1 – Normalized area of different *ss*-NMR signals for biomass after torrefaction under different operational conditions.

Assignment	<sup>13</sup> C Chemical shift (ppm)	T (°C)	Chips (CV)				<i>Pine Genus</i> (PP)				
			Time (min)	Peak area	Δm	m <sub>rotor</sub> (mg)	Normalized area	Peak area	Δm	m <sub>rotor</sub> (mg)	Normalized area
C-1 of cellulose and hemicelluloses	104.8	220	0	0.00	0.00	50.00	0.00	39207.10	0.00	50.00	784.14
			15	12459.75	0.15	23.39	450.57	20166.40	0.10	47.58	382.96
			30	14189.98	0.18	41.56	280.24	20166.40	0.11	62.35	286.70
			60	11826.84	0.20	39.79	237.16	20235.70	0.24	63.39	243.41
		250	0	0.00	0.00	50.00	0.00	39639.90	0.00	50.00	792.80
			15	11385.9	0.22	15.39	580.16	22414.80	0.14	63.39	302.74
			30	15247.93	0.23	43.46	270.25	23005.30	0.20	42.57	434.72
			60	15796.15	0.25	48.10	247.15	19205.00	0.26	62.79	227.57
		290	0	0.00	0.00	50.00	0.00	39639.90	0.00	50.00	792.80
			15	16465.64	0.34	23.79	457.35	19537.90	0.27	43.29	330.99
			30	18948.75	0.37	55.11	217.22	16716.20	0.36	62.30	170.43
			60	15404.00	0.48	50.99	157.35	13335.40	0.43	56.64	134.75
C-4 of cellulose in ordered	88.7	220	0	0.00	0.00	50.00	0.00	17818.38	0.00	50.00	356.37
			15	7062.69	0.15	23.39	255.40	9984.00	0.10	47.58	189.59
			30	8601.92	0.18	41.56	169.88	9899.53	0.11	62.35	140.74
		60	6286.05	0.20	39.79	126.05	9588.72	0.24	63.39	115.34	
		250	0	0.00	0.00	50.00	0.00	17818.38	0.00	50.00	356.37
			15	5775.4	0.22	15.39	294.28	10830.26	0.14	63.39	146.28



			30	8202.58	0.23	43.46	145.38	9995.51	0.20	42.57	188.88
			60	8039.83	0.25	48.10	125.79	8587.71	0.26	62.79	101.76
			0	0.00	0.00	50.00	0.00	17818.38	0.00	50.00	356.37
		290	15	6229.15	0.34	23.79	173.02	9169.43	0.27	43.29	155.34
			30	8493.47	0.37	55.11	97.37	8241.54	0.36	62.30	84.03
			60	6161.39	0.48	50.99	62.94	5360.43	0.43	56.64	54.16
			0	0.00	0.00	50.00	0.00	25242.72	0.00	50.00	504.85
		220	15	12675.19	0.15	23.39	458.36	14535.91	0.10	47.58	276.03
			30	13414.08	0.18	41.56	264.92	13736.91	0.11	62.35	195.29
			60	10900.07	0.20	39.79	218.58	12946.82	0.24	63.39	155.73
			0	0.00	0.00	50.00	0.00	25242.72	0.00	50.00	504.85
		250	15	9552.46	0.22	15.39	486.74	14905.33	0.14	63.39	201.31
			30	12217.67	0.23	43.46	216.55	14381.23	0.20	42.57	271.75
			60	12293.46	0.25	48.10	192.35	11413.84	0.26	62.79	135.25
			0	0.00	0.00	50.00	0.00	25242.72	0.00	50.00	504.85
		290	15	10501.44	0.34	23.79	291.69	12182.32	0.27	43.29	206.38
			30	11318.63	0.37	55.11	129.75	11943.66	0.36	62.30	121.77
			60	9809.32	0.48	50.99	100.20	9298.47	0.43	56.64	93.96
			0	0.00	0.00	50.00	0.00	14918.55	0.00	50.00	298.37
		220	15	7367.61	0.15	23.39	266.43	9265.23	0.10	47.58	175.94
			30	9668.77	0.18	41.56	190.95	9061.87	0.11	62.35	128.83
			60	7804.50	0.20	39.79	156.50	8864.67	0.24	63.39	106.63
			0	0.00	0.00	50.00	0.00	14918.55	0.00	50.00	298.37
		250	15	7079.57	0.22	15.39	360.73	14672.85	0.14	63.39	198.17
			30	10197.18	0.23	43.46	180.73	13167.44	0.20	42.57	248.82
			0	0.00	0.00	50.00	0.00	14918.55	0.00	50.00	298.37

C-4 of cellulose in  
disordered/amorphous  
cellulose

83.8

C-6 of cellulose

64.7

			60	10069.75	0.25	48.10	157.56	8779.45	0.26	62.79	104.27
			0	0.00	0.00	50.00	0.00	14918.55	0.00	50.00	298.37
		290	15	8959.54	0.34	23.79	248.86	11673.71	0.27	43.29	197.77
			30	8436.12	0.37	55.11	96.71	9995.85	0.36	62.30	101.91
			60	7346.49	0.48	50.99	75.05	7009.14	0.43	56.64	70.82
			0	0.00	0.00	50.00	0.00	0.00	0.00	50.00	0.00
		220	15	0.00	0.15	23.39	0.00	0.00	0.10	47.58	0.00
			30	0.00	0.18	41.56	0.00	0.00	0.11	62.35	0.00
			60	0.00	0.20	39.79	0.00	0.00	0.24	63.39	0.00
			0	0.00	0.00	50.00	0.00	0.00	0.00	50.00	0.00
Carbonyl carbons of acetyl groups in hemicelluloses	172	250	15	0.00	0.22	15.39	0.00	0.00	0.14	63.39	0.00
			30	0.00	0.23	43.46	0.00	0.00	0.20	42.57	0.00
			60	0.00	0.25	48.10	0.00	0.00	0.26	62.79	0.00
			0	0.00	0.00	50.00	0.00	0.00	0.00	50.00	0.00
		290	15	0.00	0.34	23.79	0.00	0.00	0.27	43.29	0.00
			30	0.00	0.37	55.11	0.00	0.00	0.36	62.30	0.00
			60	0.00	0.48	50.99	0.00	0.00	0.43	56.64	0.00
			0	0.00	0.00	50.00	0.00	675.85	0.00	50.00	13.52
		220	15	0.00	0.15	23.39	0.00	0.00	0.10	47.58	0.00
			30	0.00	0.18	41.56	0.00	0.00	0.11	62.35	0.00
			60	0.00	0.20	39.79	0.00	0.00	0.24	63.39	0.00
			0	0.00	0.00	50.00	0.00	675.85	0.00	50.00	13.52
Methyl carbons of acetyl groups in hemicelluloses	21	250	15	0.00	0.22	15.39	0.00	0.00	0.14	63.39	0.00
			30	0.00	0.23	43.46	0.00	0.00	0.20	42.57	0.00
			60	0.00	0.25	48.10	0.00	0.00	0.26	62.79	0.00

			0	0.00	0.00	50.00	0.00	675.85	0.00	50.00	13.52
		290	15	0.00	0.34	23.79	0.00	0.00	0.27	43.29	0.00
			30	0.00	0.37	55.11	0.00	0.00	0.36	62.30	0.00
			60	0.00	0.48	50.99	0.00	0.00	0.43	56.64	0.00
			0	0.00	0.00	50.00	0.00	0.00	0.00	50.00	0.00
		220	15	0.00	0.15	23.39	0.00	0.00	0.10	47.58	0.00
			30	0.00	0.18	41.56	0.00	0.00	0.11	62.35	0.00
			60	0.00	0.20	39.79	0.00	0.00	0.24	63.39	0.00
			0	0.00	0.00	50.00	0.00	0.00	0.00	50.00	0.00
Syringyls in etherified	156.2	250	15	0.00	0.22	15.39	0.00	0.00	0.14	63.39	0.00
			30	0.00	0.23	43.46	0.00	0.00	0.20	42.57	0.00
			60	0.00	0.25	48.10	0.00	0.00	0.26	62.79	0.00
			0	0.00	0.00	50.00	0.00	0.00	0.00	50.00	0.00
		290	15	0.00	0.34	23.79	0.00	0.00	0.27	43.29	0.00
			30	0.00	0.37	55.11	0.00	0.00	0.36	62.30	0.00
			60	0.00	0.48	50.99	0.00	0.00	0.43	56.64	0.00
			0	0.00	0.00	50.00	0.00	4418.53	0.00	50.00	88.37
		220	15	0.00	0.15	23.39	0.00	0.00	0.10	47.58	0.00
			30	0.00	0.18	41.56	0.00	0.00	0.11	62.35	0.00
			60	0.00	0.20	39.79	0.00	0.00	0.24	63.39	0.00
			0	0.00	0.00	50.00	0.00	4418.53	0.00	50.00	88.37
Syringyls in non-etherified structures	147-148	250	15	0.00	0.22	15.39	0.00	0.00	0.14	63.39	0.00
			30	0.00	0.23	43.46	0.00	0.00	0.20	42.57	0.00
			60	0.00	0.25	48.10	0.00	0.00	0.26	62.79	0.00
		290	0	0.00	0.00	50.00	0.00	4418.53	0.00	50.00	88.37

			15	0.00	0.34	23.79	0.00	0.00	0.27	43.29	0.00
			30	0.00	0.37	55.11	0.00	0.00	0.36	62.30	0.00
			60	0.00	0.48	50.99	0.00	0.00	0.43	56.64	0.00
			0	0.00	0.00	50.00	0.00	7901.4	0.00	50.00	158.03
		220	15	3917.06	0.15	23.39	141.65	4132.59	0.10	47.58	85.70
			30	3503.64	0.18	41.56	69.19	3621.52	0.11	62.35	66.72
			60	4327.59	0.20	39.79	86.78	3393.44	0.24	63.39	56.50
			0	0.00	0.00	50.00	0.00	7901.4	0.00	50.00	158.03
Carbon atoms of methoxyl groups	55.7	250	15	3630.52	0.22	15.39	184.99	7978.48	0.14	63.39	96.91
			30	3582.10	0.23	43.46	63.49	6647.22	0.20	42.57	110.87
			60	5288.87	0.25	48.10	82.75	6014.28	0.26	62.79	61.30
			0	0.00	0.00	50.00	0.00	7901.4	0.00	50.00	158.03
		290	15	5803.09	0.34	23.79	161.19	9320.89	0.27	43.29	157.91
			30	7346.57	0.37	55.11	84.22	8955.29	0.36	62.3	91.30
			60	6903.99	0.48	50.99	70.53	9160.74	0.43	56.64	92.56

Fonte: Brotto *et al.*, 2023.

## 7 ADVANCING LOW CARBON IRON AND STEEL PRODUCTION THROUGH BIOMASS TORREFACTION UTILIZATION

### ABSTRACT

This study aimed to investigate the potential use of as-received and torrefied biomass of the genus *Pine*, wood bark (CC), chips (CV) and pelletized wood (PP), as a substitute for metallurgical coke, to reduce the high generation of CO<sub>2</sub> derived from its use in blast furnaces. Initially, CO<sub>2</sub> reactivity tests were performed using biomasses torrefied under different experimental conditions, aiming to determine the method to produce samples that exhibited the best reactivity. In this context, the temperature conditions of 290 °C and residence time of 30 min exhibited the highest reactivity for the CV and PP biomasses, while for the CC biomass this occurred at 250 °C and residence time of 60 min was most reactive. Subsequently, the ore reduction tests were performed in a TGA using a mixture in the proportion of 1:1 of hematite (Fe<sub>2</sub>O<sub>3</sub>) with biomasses both as-received and torrefied. The tests were performed in inert atmosphere (N<sub>2</sub>) with a flow rate of 100 mL N<sub>2</sub> min<sup>-1</sup> and heating rate of 10 °C min<sup>-1</sup> until a temperature of 900 °C. Tests were performed with the pure samples in comparison with the mixtures. The reduction results were evaluated by comparing the theoretical and experimental reduction curves, DTG curves and XPS characterization. In addition, a microscope was used to visualize the coloration of the mixtures before and after reduction. The results showed that the use of torrefied biomass provided a greater reduction when compared to fresh biomass. Although all torrefied biomasses have presented reduction, the PP torrefied biomass stood out presenting a reduction percentage of 54% according to the conversion. Moreover, the DTG peaks were better visualized in the mixture with PP, followed by CC and then CV.

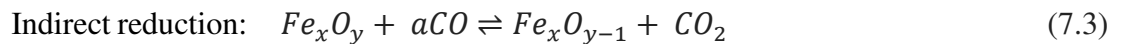
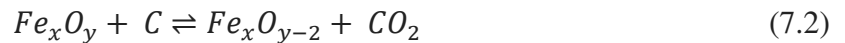
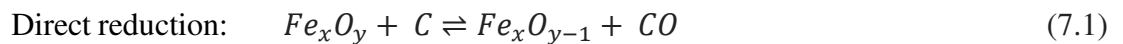
**Keywords:** biomass; torrefaction; wood waste; thermal conversion; ore reduction.

## 7.1 INTRODUCTION

One of the major current problems is the high generation of solid waste and the high emission of carbon dioxide (CO<sub>2</sub>), one of the greenhouse gases. Law n°. 12.305/2010, which provides for the National Solid Waste Policy, and several agreements and protocols, have advanced in the establishment of CO<sub>2</sub> emission control policies, requiring scientific and technological development for the reduction and/or reuse of solid waste and CO<sub>2</sub>. Khanna *et al.* [1] report that the iron and steel sector uses almost 70% of the consumed energy produced from coal-fired power plants, being this the sector responsible for ~ 5% to 7% of global CO<sub>2</sub> emissions.

The control and management of emissions during these processes are essential for environmental protection [2]. The blast furnace, for example, where the reduction process to produce metallic iron / pig iron occurs, contributes approximately 70% of CO<sub>2</sub> emissions. This is because the main material used for reduction is coke/coking coal [3], [4].

During iron oxide reduction, the internal energy of the ore changes continuously and is influenced by external (temperature) and internal (steam pressure, reducing agent composition, degree of phase contact, etc.) parameters. It is a heterogeneous process, as it involves liquid, solid and gaseous substances [5]. The reduction of iron oxides can happen in a direct and/or indirect way according to reactions (7.1), (7.2), (7.3) and (7.4) [5], [6]. Direct reduction consists of the reaction of iron oxides such as hematite (Fe<sub>2</sub>O<sub>3</sub>), magnetite (Fe<sub>3</sub>O<sub>4</sub>) and wustite (FeO) in the presence of carbon (C) while indirect reductions occur in the presence of carbon monoxide (CO) gas. In indirect reduction, the Boudouard reaction, which occurs between carbon (C) and carbon dioxide (CO<sub>2</sub>) produces CO which will be used for the indirect reduction of iron oxides.



where a and b are the reaction rate (mol min<sup>-1</sup>) of each overall reaction (Hu *et al.*, 2018).

For the reduction of iron oxide to occur, carbon-rich materials such as charcoal, coal and coke and metals such as silicon, aluminum and magnesium can be used as reducing agents [3], [7]. Thus, using biomass (renewable energy source) as a reducing agent in the reduction of

iron oxide to metallic iron in total and/or partial replacement of metallurgical coke or coal (fossil fuels) is one of the ways to reduce CO<sub>2</sub> emissions by the blast furnace.

Forest waste biomass is considered a renewable energy source with high carbon content and low impurity (such as ash and sulfur) content and is carbon neutral due to its absorption of CO<sub>2</sub> whilst growing [3], [4], [8]. However, because it has high volatile and oxygen contents, low fixed carbon, and energy density, using biomass directly as a replacement for coking coal may not be as advantageous, and a pre-treatment (such as torrefaction) is frequently required.

Torrefaction is a thermochemical process that uses temperatures between 200-300 °C in an inert atmosphere for a certain residence time. This process is interesting because it reduces the fixed oxygen content and increases the carbon content and calorific value of the fuel per unit mass [4]. After the biomass goes through the torrefaction process, the resulting solid is called biochar. One of the advantages of using biochar in the blast furnace is that it will react with the hot air blast producing heat from initially low temperature and react with CO<sub>2</sub> to produce CO at lower temperatures and higher rates when compared to the conventional coke. This improves the reduction efficiency and saves energy in the blast furnace [6].

Some studies have shown that the use of biomass and coke blends in the metallurgical industry can result in lowering the gasification temperature in blast furnaces, thus decreasing the carbon and, consequently, CO<sub>2</sub> consumption. However, adding biomass to other coals to produce biochar with suitable physical properties is still a challenge [9].

Lu *et al.* [10] and Surup [11] reported that the addition of biochar with coke can have negative impacts considering coke strength after reaction (CSR), coke reactivity index (CRI) and fluidity. Jha *et al.* [12] reported that they were successful in replacing coke for iron sintering with 10% sawdust, 30% charcoal and 30% of a combination of sawdust and charcoal. However, the study failed in production when they tried complete replacement of coke with biomass.

Thus, this study aims to evaluate the reduction of hematite iron oxide (Fe<sub>2</sub>O<sub>3</sub>) using as-received and torrefied biomass, genus *Pine*, typical Brazilian biomass. The effect of the hematite iron ore: biomass ratio, particle size and drag gas flow on iron oxide reduction was investigated. This enables evaluation of the best biomasses or derivatives for total and/or partial replacement of metallurgical coke.

## 7.2 MATERIALS AND METHODS

### 7.2.1 Selection and preparation of materials

In this study, three different biomasses were selected, wood bark (CC) and chips (CV) of *Pine* Genus, both supplied by the Brazilian Paper Industry located in Santa Catarina State, (Brazil), and pelletized wood of *Pine* Genus (PP), supplied by the Brazilian company placed in Paraná State, (Brazil).

For the torrefaction of the biomasses, approximately 1 g of each biomass (as-received) was thermally treated in a fixed bed tubular reactor. The reactor was a concentric quartz cylinders (the inner cylinder had an external diameter of 17.0 mm and was 1.35 mm thick, the external cylinder had an external diameter of 23.0 mm and was 2.60 mm thick). An inert nitrogen gas ( $410 \text{ mL N}_2 \text{ min}^{-1}$ ) was initially purged through the system at room temperature.

The system was then raised to the reaction temperature at 250 or 290 °C and held at a residence time of 30 or 60 minutes. To identify the samples used in this study, they were designated the as-received biomass as XXYY (XX = biomass nomenclature and YY = particle size, for example, PP106 $\mu\text{m}$ ). Torrefied biomasses were designated as XXTTY (XX = biomass nomenclature, T=torrefied and YY = particle size), for example, PPT106 $\mu\text{m}$ .

Table 7.1 shows the composition of each biomass before and after the most beneficial torrefaction process (250 °C and 60 minutes for CC biomass; 290 °C and 30 minutes for PP and CV biomass, all in an inert atmosphere) [13]. According to Ye *et al.* [8], one of the requirements of the reduction process is the high content of fixed carbon and low ash content, so both the as-received biomass and torrefied biomass meet this requirement.

Hematite ( $\text{Fe}_2\text{O}_3$ , Inoxia Ltda Company) was used as an iron ore model compound. The oxide used has red coloration and particle size of 95% <170 mesh ( $\sim 53\mu\text{m}$ ), 50% <8.5  $\mu\text{m}$ . It has impurities of 7%  $\text{SiO}_2$  and 3% of  $\text{Al}_2\text{O}_3$ .



Table 7.1 - Composition of biomasses.

		Biomasses <i>in natura</i>			Torrefied biomass		
		CC	CV	PP	CC25060	CV29030	PP29030
Proximate analysis (%)	Volatile matter	65.79	78.16	83.28	52.31	66.45	60.88
	Ash content	0.92	0.84	0.63	1.81	0.64	0.68
	Fix carbon	33.30	21.00	16.08	45.88	32.91	38.43
Ultimate analysis (%)	C	46.66	46.00	46.41	55.64	53.56	55.56
	H	6.18	6.71	6.49	5.36	5.49	5.82
	N	0.34	0.24	0.08	0.49	0.11	0.16
	O	46.82	47.05	42.06	38.51	40.84	38.46
Molar ratio	O/C	0.75	0.76	0.68	0.52	0.57	0.52
	H/C	1.59	1.75	1.69	1.16	1.23	1.26
HHV (MJ kg <sup>-1</sup> )		19.41	19.08	19.49	21.72	20.94	22.26
Chemical components of lignocellulosic (%)	Cellulose	14.38 ± 0.27	41.77 ± 1.30	38.98 ± 0.92	9.75 ± 1.18	39.06 ± 1.24	30.11 ± 0.10
	Hemicellulose	5.75 ± 0.17	16.22 ± 0.74	15.43 ± 0.35	0.00 ± 0.00	2.53 ± 0.10	0.00 ± 0.00
	Lignin	59.53 ± 1.75	37.12 ± 0.15	35.28 ± 0.20	84.36 ± 1.33	55.55 ± 0.45	65.31 ± 0.85
	Extractives	15.93 ± 0.07	3.33 ± 0.85	6.41 ± 0.16	0.00 ± 0.00	0.00 ± 0.00	0.00 ± 0.00
	Ashes	1.54 ± 0.15	0.35 ± 0.02	0.47 ± 0.01	1.84 ± 0.14	0.27 ± 0.06	0.81 ± 0.14
	Total	97.13 ± 1.40	98.78 ± 1.55	96.57 ± 1.25	95.95 ± 0.17	97.41 ± 1.63	96.23 ± 0.73

Source: Brotto *et al.*, (2023).

### 7.2.2 Preparation of the mixture of biomass with hematite

The mixing of the biomass samples with hematite was conducted manually at a 1:1 mass ratio and for a time of approximately 5 min. These conditions were chosen according to the studies of Ubando *et al.* [3], Kasai, Mae and Saito [14] and Wang *et al.* [15]. The biomass samples (as-received) were milled using an IKA A 11 knife mill (Staufen, Germany), and subsequently separated into particle sizes of smaller than  $<106\ \mu\text{m}$  (mesh Tyler 150) and  $106\text{--}300\ \mu\text{m}$  (mesh Tyler 48). The biomass samples that underwent the torrefaction process were ground using a mortar and pestle and then separated into the same particle sizes as the as-received samples.

The nomenclature for mixtures with as-received biomass is XXYY+HM (XX = biomass nomenclature, YY = particle size and HM=hematite) for example, PP106 $\mu\text{m}$ +HM and for biomass torrefied is XXTYY+HM (XX = biomass nomenclature, T=torrefied, YY = particle size and HM = hematite), for example, PPT106 $\mu\text{m}$ +HM.

### 7.2.3 Evaluation of iron oxide reduction using thermogravimetric analysis

The reduction of iron oxide (hematite) was experimentally investigated by TGA analysis (TA Instruments, Q500). Initially, tests were performed using the two particle sizes of the PP biomass  $<106\ \mu\text{m}$  (mesh Tyler 150) and  $106\text{--}300\ \mu\text{m}$  (mesh Tyler 48)) to verify which particle size would provide greater reduction of hematite. Thermogravimetric studies were accomplished using pure biomass, pure hematite, and the mixtures biomass+hematite, under a  $\text{N}_2$  flow rate of  $100\ \text{mL min}^{-1}$  and mass of 5 mg of each mixture. The materials were heated from room temperature to  $105\ ^\circ\text{C}$  and held for 10 minutes to remove moisture. Then, a constant heating rate of  $10\ ^\circ\text{C min}^{-1}$  was adjusted until  $1000\ ^\circ\text{C}$  was reached. The mass loss was monitored and recorded. The differential thermogravimetric (DTG) curves were also determined for all samples.

The shape and size of biomass particles affect the surface area for heat and mass transfer. Thus, different shapes and sizes of biomass lead to different conversion efficiencies [16]. After the first results were obtained, it was decided to use only the mixture using biomass with lower particle size ( $<106\ \mu\text{m}$ ) due to mass transfer limitations exhibited. In addition, it was decided to increase the amount of sample analyzed to 15 mg to allow for more intimate contact between the biomass and the iron ore.

The second evaluation carried out was in relation to the nitrogen flow rate to be used. Table 7.2 presents some flow rates used in the literature using biomass and thermogravimetric analyses for ore reduction. The reduction behavior was evaluated using a flow rate of 10, 50 and 100 mL N<sub>2</sub> min<sup>-1</sup> and the results indicated that 100 mL N<sub>2</sub> min<sup>-1</sup> was optimal.

Table 7.2 - Literature using Thermogravimetric analysis for ore reduction.

<b>Biomass for reduction</b>	<b>Flow rate (mL N<sub>2</sub> min<sup>-1</sup>)</b>	<b>Reference</b>
Rice lemma (RL), Peanut hull (PH), Maize cob (MC) and <b>pine sawdust (PS)</b>	<b>100</b>	[2]
Forest residue biomass (pellet wood)	<b>200</b>	[3]
Woody-chars	<b>200</b>	[17]
Pine sawdust	<b>60</b>	[18]
Bamboo powder	<b>20</b>	[19]

Source: The author, (2023).

Finally, after the preliminary tests using PP biomass, the best conditions chosen to operate the TGA reduction tests were mass of 15 mg, particle size biomass (<106 μm), heating rate of 10 °C min<sup>-1</sup> and 100 mL N<sub>2</sub> min<sup>-1</sup>. The experiments were made using only the biomasses, only the hematite, and the mixtures. The materials were heated from room temperature to 105 °C and held for 10 minutes to remove moisture. Then, a constant heating rate of 10 °C min<sup>-1</sup> was implemented until 1000 °C was reached. The mass loss was monitored and recorded. Along with the TGA results, the DTG curves were also determined for all samples.

#### 7.2.4 Evaluation after process iron reduction

In order to evaluate the oxidation state of the iron after reduction, the X-ray Photoelectron Excited Photoelectron Spectroscopy - XPS technique was used (APSL) K-Alpha (RSM LG.11). In addition, images were captured using a Seben Microscope (Magnification 2x) using Webcam Companion and Arcsoft Webcam Companion software.

The degree of reduction ( $\Delta W$ ) was verified by the difference between the theoretical and experimental TGA curves (Eq 7.5) [20].

$$\Delta W = TGA_{theoretical} - TGA_{experimental} \quad (7.5)$$

$$TGA_{theoretical} = Y_H \cdot TGA_H + Y_B \cdot TGA_B \quad (7.6)$$

Where  $\Delta W$  is the degree of reduction (% by weigh);  $TGA_H$  and  $TGA_B$  are the weight loss (% by weight) of single hematite and biomass, respectively; and  $Y$  are the mass fractions of hematite ( $Y_H$ ) and biomass ( $Y_B$ ).  $TGA_{experimental}$  is the weight loss (% by weight) of the corresponding mixture of hematite and biomass.

When  $\Delta W > 0$ , a reduction process takes place, while  $\Delta W = 0$  indicates absence of reaction between the iron oxide and the torrefied biomass. Equation (7.7) was used to obtain the conversion of reduction ( $X$ ).

$$X = \frac{m_{initial} - m_{final}}{m_{initial}} \times 100\% \quad (7.7)$$

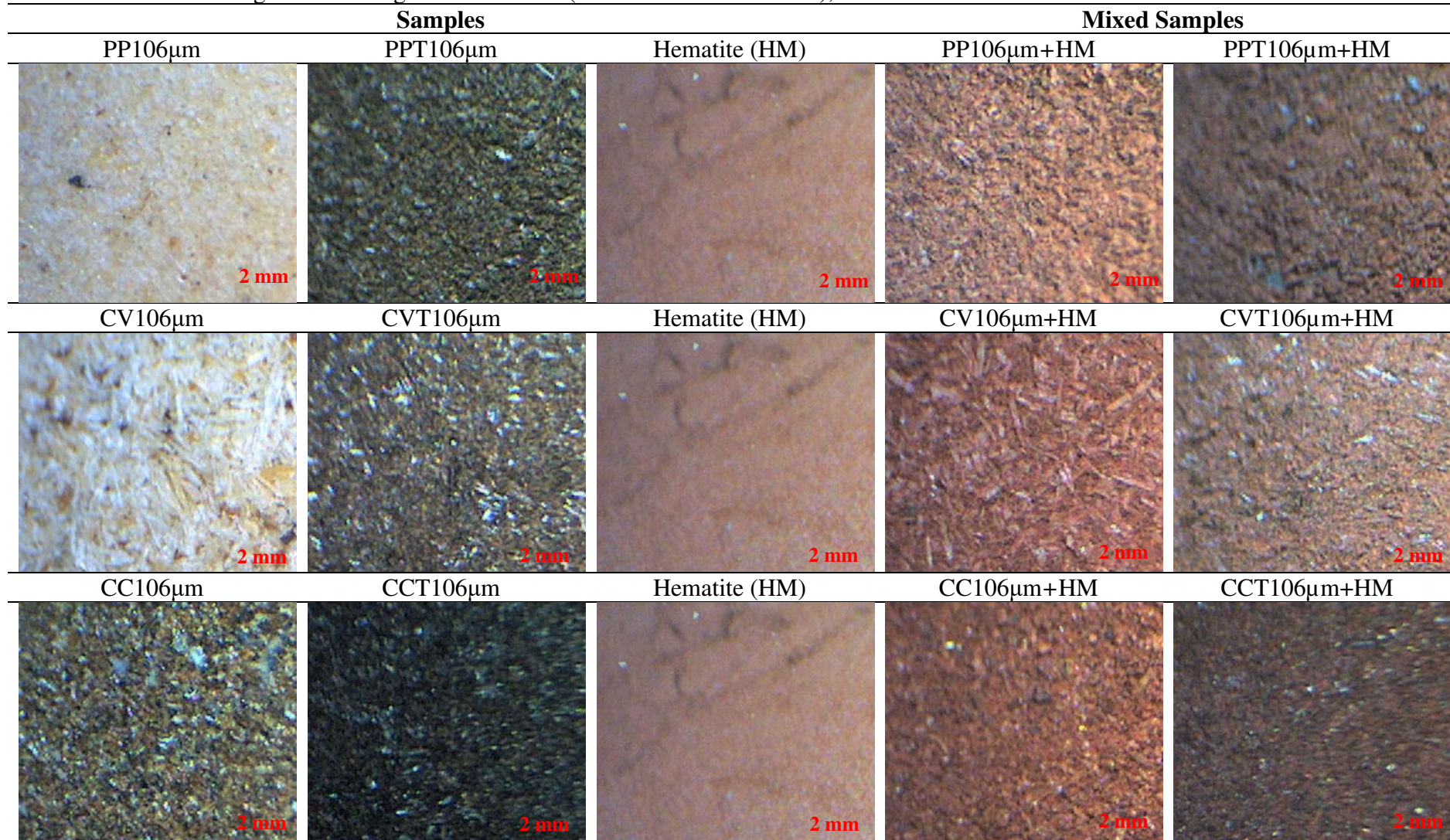
where  $m_{final}$  is the mass after the reduction process (mg) and  $m_{initial}$  is the mass before the reduction process (mg).

## 7.3 RESULTS AND DISCUSSION

### 7.3.1 Color changes for biomass+hematite mixture after thermal treatment and reduction

Figure 7.1 shows the PP, CV and CC biomass images (before and after torrefaction), hematite and the mixture biomass+hematite (50%/50%) (before and after torrefaction with hematite). Analyzing the images, the predominance of the red coloration of the iron oxide after mixing with the biomasses is noted. Moreover, the coloration of the pine biomasses PP and CV are similar, close to a light yellow, while the coloration of the biomass CC presents a darker coloration. After torrefaction, all biomasses presented a darker coloration, however, when mixed with hematite the reddish colour predominated.

Figure 7.1 - Images of biomasses (as received and torrefied), hematite and mixture before reduction.



Source: The author, (2023).

The first tests performed aiming at iron reduction were using the PP biomass as-received and using two particle size distributions (<106  $\mu\text{m}$  and 106-300  $\mu\text{m}$ ). The visual characteristics of the as-received biomass, hematite and mixtures before and after the reduction process are shown in Supplementary material, Figure S7.1. Again, it can be observed that while the hematite presents a very reddish coloration, the biomass PP presents a lighter coloration, close to yellow. Observing the mixture of biomass with hematite before reduction, it is noted that the predominant color is red due to the presence of hematite.

After the reduction of the hematite on mixture, it is noted that the reddish coloration changes to dark brown, indicating reduction of hematite. However, it is noted that the test with the biomass of lower particle size distribution presented darker coloration than the one with higher particle size distribution, which may indicate further reduction.

In addition, small transparent/white patches can be seen in the images after reduction in Supplementary material, Figure S7.1. These fillets are from the quartz wool (coarse, 9-30 micron) used to protect the sample holder from the sample. Also, due to the small amount of sample used in the test (5 mg), it is noted that the amount after reduction is even smaller, making the analysis difficult. Thus, the subsequent tests used 15 mg. It should be noted that in all tests a 1:1 ratio was used for mixtures of hematite with biomass.

### 7.3.2 Thermogravimetric analysis for iron reduction

The TGA and DTG curves of the as-received biomass, hematite and mixtures of biomass and hematite are shown in Supplementary material, Figure S7.2, (a) and (b), respectively and images on Figure S7.3. It can be observed that the particle size of the biomass affected the mass loss, since particle size <106  $\mu\text{m}$  presented a greater loss of mass than 106-300  $\mu\text{m}$  particles. In the DTG curve, the same behavior of the two particle size distributions is observed, however, when using the biomass with lower particle size distribution it is possible to verify an increase in the peak area since it is more intense. With this, the subsequent analyses were performed using particle size of <106  $\mu\text{m}$ .

No external diffusion resistance was observed during the thermal treatment under nitrogen gas flow rate in the ranges 10-100 mL  $\text{N}_2 \text{ min}^{-1}$ , as shown in Figure S7.2. The TGA and DTA curves can be seen in the Supplementary material, Figure S7.2, (c) and (d), respectively and images on Figure S7.3, and similar TGA and DTG curves are obtained. These results agree with Wang *et al.* [2] in the study of reduction of iron oxide using four types of pyrolyzed biomass, rice lemma (RL), peanut shell (PH), corn cob (MC) and pine sawdust (PS).

The authors carried out preliminary tests varying the gas flow and verified that the compounds would suffer reduction in gas flow greater than 80 mL N<sub>2</sub> min<sup>-1</sup>.

Therefore, a nitrogen gas flow rate of 100 mL N<sub>2</sub> min<sup>-1</sup> was adopted in the further tests to guarantee that the mass transfer restrictions were eliminated. Thus, the tests using as-received and torrefied biomasses (PP, CV and CC) were performed using 15 mg, particle size of <106 μm, nitrogen gas flow rate of 100 mL N<sub>2</sub> min<sup>-1</sup> and heating rate of 10 °C min<sup>-1</sup> until reaching the temperature of 1000 °C (Figure 7.2). The curves of as-received biomass and hematite are used as a basis for comparison with the mixtures.

Firstly, it is observed from Figure 7.2 (TGA curves) that the hematite mass loss is very small compared to that of any of the biomasses or mixtures. Moreover, the DTG curve of hematite shows only one peak around 700 °C. This peak may be related to the impurities present in hematite (77% SiO<sub>2</sub> and 3% of Al<sub>2</sub>O<sub>3</sub>). From Figure 7.2, it is also possible to observe that the behavior of the TGA and DTG curves of the PP and CV biomasses, up to ~750 °C, is similar, probably due proximity to the chemical composition of the two biomasses (Table 7.1).

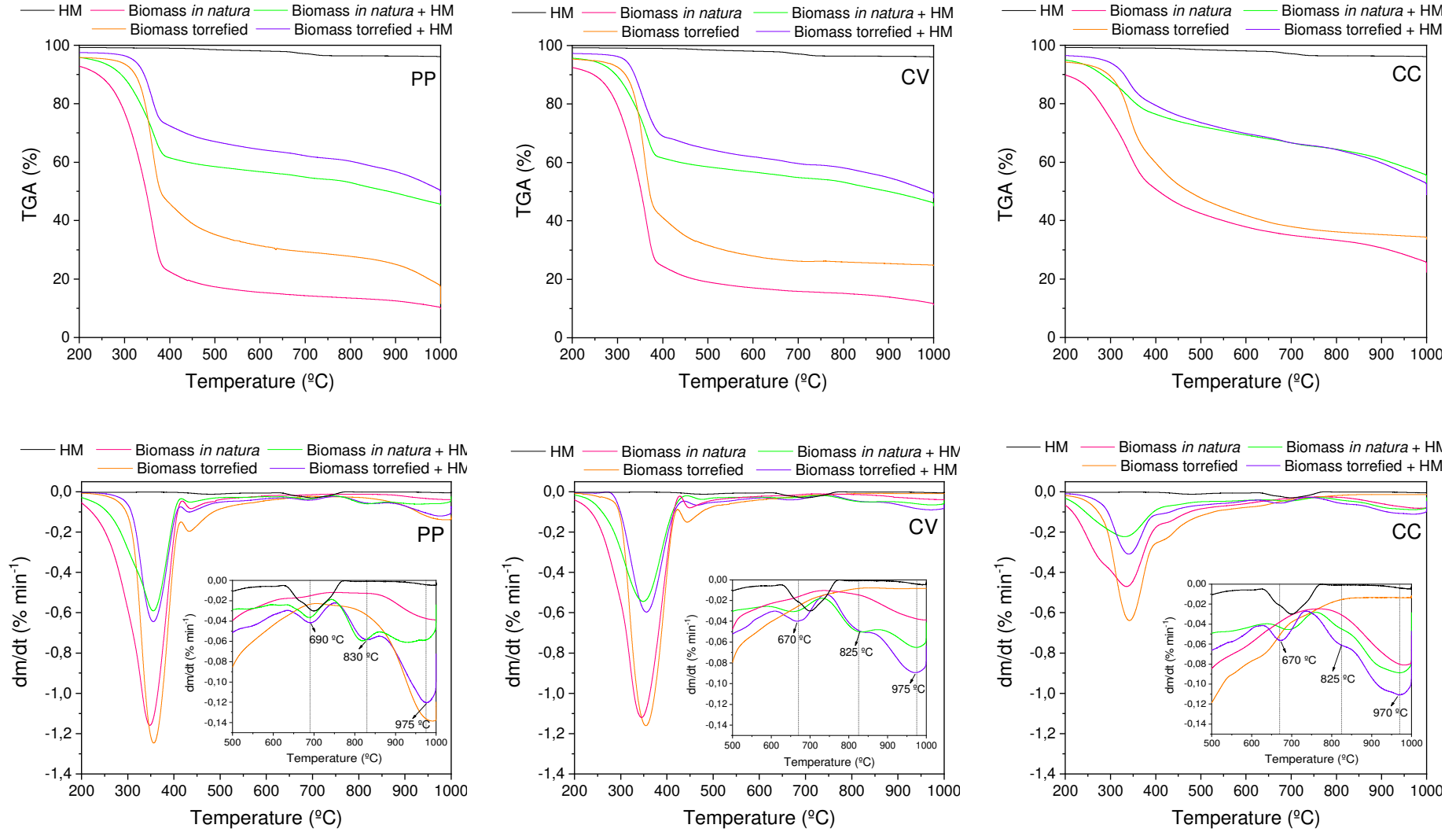
Regarding the mass loss of the biomasses (TGA curves – Figure 7.2), clearly, in the three biomasses, the highest mass loss is related to the corresponding as-received biomass. This is already expected, after all, with the increase of temperature the volatile material present in the samples is driven off to a further extent thus generating a greater loss of mass. In the torrefied biomass, however, the mass loss is not so accentuated compared to as-received biomass, since hemicellulose, cellulose and lignin were partially degraded by the previous torrefaction. Regarding the as-received biomasses, the mass loss decreases in the order PP ~ CV > CC as expected, since CC biomass has a higher lignin content than PP and CV (Table 7.1).

Figure 3 shows that the greatest mass loss of biomass occurs at ~350 °C, probably due to the greater degradation of lignocellulosic components. Lignin, one of the components present in biomass, has a variety of chemical functions that differ in thermal stability, and its decomposition can occur between 200 to 800 °C, being higher at temperatures between 360 and 400 °C. In addition, in this temperature range occurs the decomposition of hemicellulose (200 - 300°C) and cellulose (300 and 390°C) [21], [22], [23].





Figure 7.2 - TGA and DTG reduction experiments



Source: The author, (2023).

For the PP and CV biomasses, from 400 °C the mass loss is apparently constant compared to the CC biomass. Again, this is related to the chemical composition of the samples (Table 7.1), after all, the CC biomass, which has higher lignin content, continues to show a degradation behavior due to the greater amount of this component.

Researchers also report in their study of pyrolysis of lignocellulosic biomass, the slow decomposition of lignin above 430 °C [22]. In addition, the initial weight loss of the samples observed in the TGA results, and the peak identified from the DTG curve agree with the results of [3] and [24] which is mainly attributed to the biomass devolatilization. The greater the amount of volatile material released during the process, the greater the porosity and pore structure of the biomass [25].

As expected, the mixtures of hematite with as-received biomass showed a higher mass loss compared to the mixtures with torrefied biomass. An exception is the curve of biomass CC, in which the mixture of hematite with torrefied biomass showed a greater loss of mass from 800 °C when compared with the mixture with the biomass as-received. This may have occurred due to the occurrence of reduction reactions or breaking of other chemical bonds present in the mixture.

Analyzing the DTG curves it is possible to verify the temperatures at the beginning and end of the reaction. The sharp peaks show the succession of reactions that occur that often cannot be visualized only with the TGA curves, besides pointing out the maximum speed of reaction and its corresponding temperature. Furthermore, the peaks in the DTG curve represent the occurrence of endothermic reaction, indicative of the reduction process [3], [26].

It can be noticed that the peaks DTG containing the mixture with torrefied biomass are more pronounced compared to those of fresh biomass, suggesting a greater occurrence of chemical reactions. Moreover, it is possible to observe 4 main peaks. The first peak is the largest and is related to biomass devolatilization. It is noticed an arm in this peak when the mixture was used in the TGA tests. This may be an indication that a first reduction may be occurring due to the CO gas released during devolatilization.

The other 3 peaks that appear in the DTA curves are at the temperatures of 670-690, 825-830 and 970-975 °C. These peaks represent the temperature at which the maximum speed of the reaction occurs. It is also noted that the mixtures containing fresh biomass present small peaks in the same temperature range. Table 7.3 presents some studies that used biomass as a reducing agent and the temperatures that the oxide change was observed. Using Table 7.3 as a reference, it can be observed that the peak temperatures visualized in this study follow the

gradual reduction  $\text{Fe}_2\text{O}_3 \rightarrow \text{Fe}_3\text{O}_4 \rightarrow \text{FeO} \rightarrow \text{Fe}$ . Also, the temperature ranges of the phase changes in this work are present in Table 7.3.

Table 7.3 - Temperatures occur reduction.

	Hematite → Magnetite	Magnetite → Wustita	Wustita → Iron	Reference
	$\text{Fe}_2\text{O}_3 \rightarrow \text{Fe}_3\text{O}_4$	$\text{Fe}_3\text{O}_4 \rightarrow \text{FeO}$	$\text{FeO} \rightarrow \text{Fe}$	
	370°C	830 °C	1011-1038 °C	[3]
	640 - 745 °C	745 - 925 °C	925 - 1100 °C	[15]
Peak	365 - 555°C	595 - 799 °C	799 - 1200°C	[17]
	564 °C	650 - 731 °C	850 - 1200 °C	[24]
	310 - 430 °C 650 - 750 °C	750 - 860 °C	860 - 1000 °C	This research

Source: The author, (2023).

Comparing the DTG peaks of the mixture of the three torrefied biomasses with hematite, it is noted that the intensity of the first two peaks is similar in the three mixtures. However, in the last peak, which is probably related to the reduction of iron, the peak of the mixture containing the torrefied biomass PP is more intense, which may indicate a greater reduction.

El-Tawil *et al.* [17] cite in their work the reduction of  $\text{Fe}_2\text{O}_3$  using thermally treated woody biomass. They used 4 temperatures for heat treatment (300, 350, 400 and 450 °C) in an inert atmosphere and then performed the mixture with  $\text{Fe}_2\text{O}_3$ , obtaining C/O molar ratios of 0.39, 0.60, 0.87 and 1.00, respectively. The authors state that the reduction occurred gradually ( $\text{Fe}_2\text{O}_3 \rightarrow \text{Fe}_3\text{O}_4 \rightarrow \text{FeO} \rightarrow \text{Fe}$ ) and confirmed the presence of iron using XRD analysis. As the C/O molar ratio increased, the predominance of metallic iron increased. The authors state that the reduction occurred due to gases developed from the thermal decomposition of volatile material.

Ubando *et al.* [3] studied the reduction of iron oxide by graphite and torrefied forest residue biomass using thermogravimetric analysis (TGA) coupled to Fourier transform infrared spectrometer (FTIR) to analyze the evolved gases during the reduction processes. The authors found that the reduction of iron ore by graphite occurs at higher temperatures (> 950 °C), while the reduction of iron oxide using torrefied biomass is more significant for low to medium

temperatures with an initial temperature of 300 °C. It represents an important energy consumption economy beside a greener process in relation to CO<sub>2</sub> emissions.

The results obtained by Ubando *et al.* [3] showed that direct reduction of iron oxides by carbon occurs in graphite and torrefied biomass and the release of CO<sub>2</sub> instead of CO. A gradual reduction procedure is observed that is triggered by the evolved gases released from the devolatilization of torrefied biomass at 370 °C. At this temperature, there is a peak present in the DTG curve for the torrefied biomass and the mixtures (biomass and hematite), which occurs the degradation of mass and release of volatiles along with other aromatic compounds due to the higher volatile matter content (68.44% by weight) and lower fixed carbon content (25.65% by weight).

With this, the authors proposed that the reduction that occurs at low temperatures can be governed by means of the direct reduction reactions because the release of CO compared to CO<sub>2</sub> is substantially lower, suggesting that the reduction is mainly due to the carbon from the torrefied biomass. In addition, Ubando *et al.* [3] suggest that the presence of oxygen in the aromatic compounds, alcohol and phenols in the torrefied biomass aided their devolatilization in this temperature range allowing the initial reduction to occur at this low temperature.

Furthermore, Chen *et al.* [27] suggests that the transformation from one iron oxide phase to another can occur simultaneously in each temperature range, i.e., it is possible to have the simultaneous change from hematite to magnetite and from magnetite to wustite at the same temperature. As well as magnetite into wustite and wustite into metallic iron in the same temperature range.

The direct solid-solid reduction is much slower compared to the indirect gas-solid reduction reaction and the coal gasification reaction [6]. Sheshukov *et al.* [5] reported the difficulty of explaining the high reduction rate of iron oxides under conditions of practically no diffusion of reactants in the solid phase using the provisions of the classical atomic-molecular theory of reduction, since at temperatures above 700 °C and 800 °C reduction reactions are thermodynamically possible. Then, an thermodynamic study to evaluate the Gibbs free energy for each reaction in different temperatures could be useful to understand the mechanism for hematite reduction.

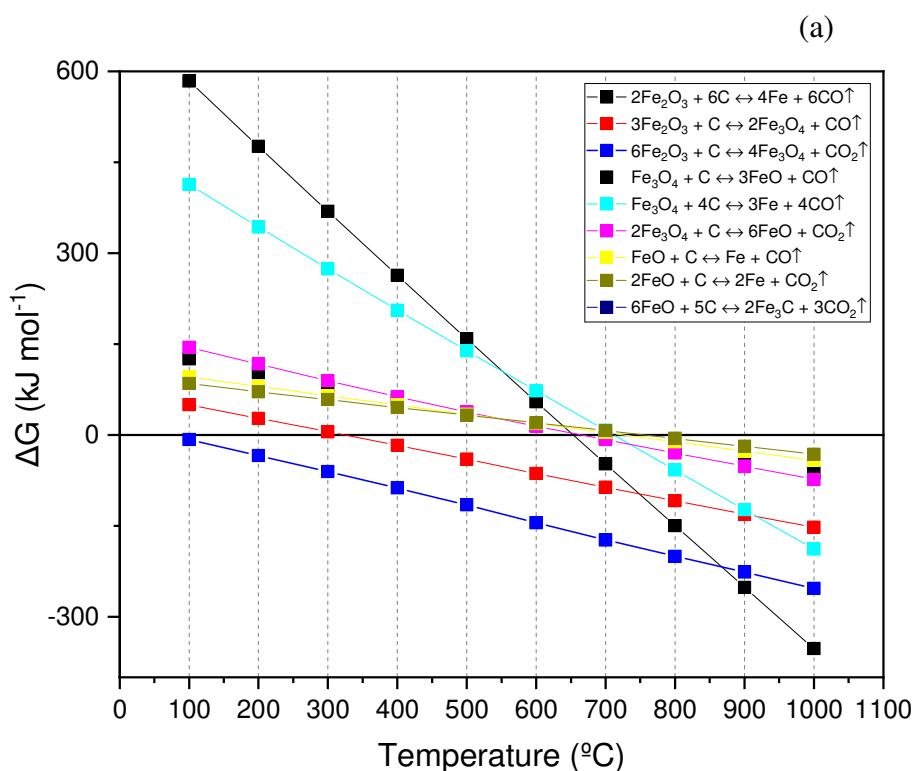
### **7.3.3 Thermodynamic analysis of the reduction process using biomass**

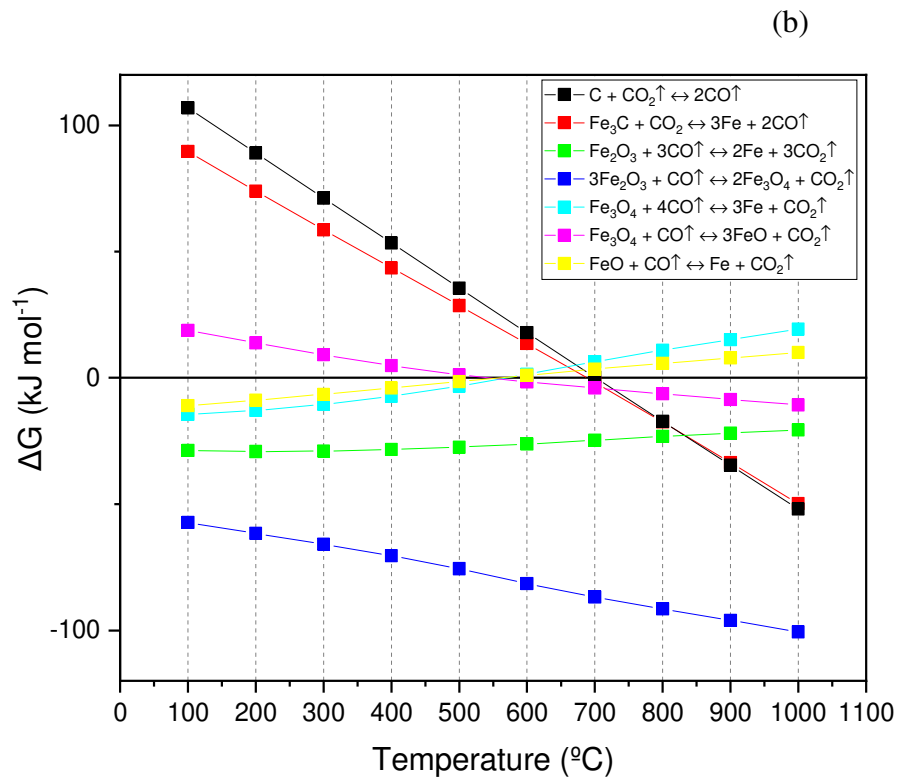
In this topic, thermodynamic calculations were performed to determine the temperature range in which the reduction reactions of iron oxides can occur through the solid and gaseous

phases. The possible reduction reactions in the solid phase, that is, the direct reactions and the possible gas-solid reactions, indirect reactions, are presented in Figure 7.3 and Table 7.4. To determine the temperature range in which each reduction reaction occurs, the Gibbs free energy ( $\Delta G$ ) was used. Thermodynamically, reactions that present  $\Delta G < 0$  are possible to occur. To obtain the values of  $\Delta G$  for each temperature in each reaction it was used the software FactSage© 8.0 (FACT - Facility for the Analysis of Chemical Thermodynamics). All the obtained values are present in Table S7.1 of the supplementary material.

Moreover, with the values obtained a graph (Figure 7.3) of  $\Delta G$  was plotted as a function of temperature for each reaction in order to define the temperature range that the reactions can occur thermodynamically. The graph was divided into direct reactions and indirect reactions and Boudouard reactions. Furthermore, with the results of the graph it was possible to determine the temperature range for each reaction, as shown in Table 7.4.

Figure 7.3 - (a) Direct reduction reactions (b) Boudouard and indirect reduction reactions.





Source: The author, (2023).

Table 7.4. Range of increase of T (°C) in which reaction occurs according to  $\Delta G$

Reaction	Range T (°C)
$Fe_2O_3 + 3CO \rightleftharpoons 2Fe + 3CO_2^c$	100 – 1000
$3Fe_2O_3 + CO \rightleftharpoons 2Fe_3O_4 + CO_2^c$	100 – 1000
$6Fe_2O_3 + C \rightleftharpoons 4Fe_3O_4 + CO_2^a$	100 – 1000
$6FeO + 5C \rightleftharpoons 2Fe_3C + 3CO_2^a$	100 – 1000
$FeO + CO \rightleftharpoons Fe + CO_2^c$	100 - 560
$Fe_3O_4 + 4CO \rightleftharpoons 3Fe + 4CO_2^c$	100 – 570
$3Fe_2O_3 + C \rightleftharpoons 2Fe_3O_4 + CO^a$	320 – 1000
$Fe_3O_4 + CO \rightleftharpoons 3FeO + CO_2^c$	540 – 1000
$2Fe_3O_4 + C \rightleftharpoons 6FeO + CO_2^a$	660 – 1000
$2Fe_2O_3 + 6C \rightleftharpoons 4Fe + 6CO^a$	680 – 1000
$Fe_3O_4 + C \rightleftharpoons 3FeO + CO^a$	680 – 1000
$C + CO_2 \rightleftharpoons 2CO^b$	690 – 1000
$Fe_3C + CO_2 \rightleftharpoons 3Fe + 2CO^c$	701 – 1000
$Fe_3O_4 + 4C \rightleftharpoons 3FeO + 4CO^a$	710 – 1000
$FeO + C \rightleftharpoons Fe + CO^a$	725 – 1000
$2FeO + C \rightleftharpoons 2Fe + CO_2^a$	755 – 1000

<sup>a</sup> Direct reduction reactions, <sup>b</sup> Boudouard reaction and <sup>c</sup> Indirect reduction reactions.

Source: The author, (2023).

According to Table 7.4, it can be noted that the reduction process can occur at temperatures in the range 100-1000 °C both directly and indirectly. The indirect reduction at low temperatures could happen due to the devolatilization process, after all, one of the gases generated during this process is CO. However, this does not occur by the Boudouard reaction, since this reaction is only thermodynamically possible at temperatures above 690 °C.

The standard Gibbs free energy of iron ore reduced by solid carbon decreased with temperature, indicating that higher temperatures favored the occurrence of indirect reactions. That is, at higher temperatures occurs the transfer of oxygen atoms in the iron ore to carbon promoting the generation of CO. The process of each reaction varies according to the dosage of iron ore, that is, depending on the amount used, the supply of oxygen atoms will be excessive or insufficient [18].

El-Tawil *et al.* [17] argued that the reduction of iron oxide increases when biomass is used as a reductant because it contains a considerable amount of volatile materials. Moreover, they suggest that light gases of CO, H<sub>2</sub>, CO<sub>2</sub>, CH<sub>4</sub> and C<sub>2</sub>H<sub>6</sub> are developed in the range of 350 - 600 °C. Finally, above 600 °C, the authors cite that the hydrocarbon complex consisting of large carbon and hydrogen chains are released and the released volatile is dissociated at higher temperatures to generate highly reducing gases such as CO and H<sub>2</sub> [17].

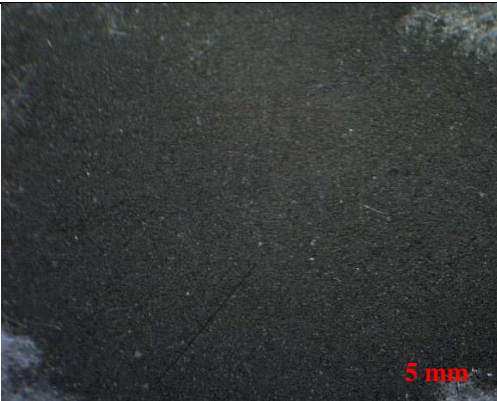
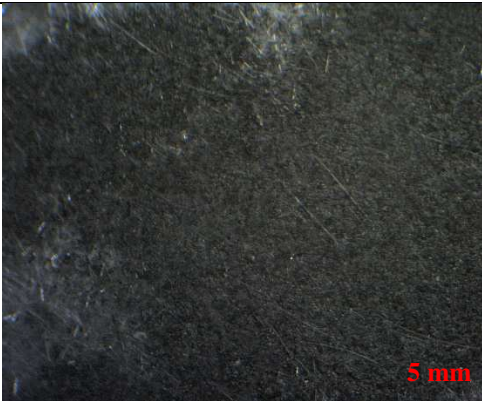
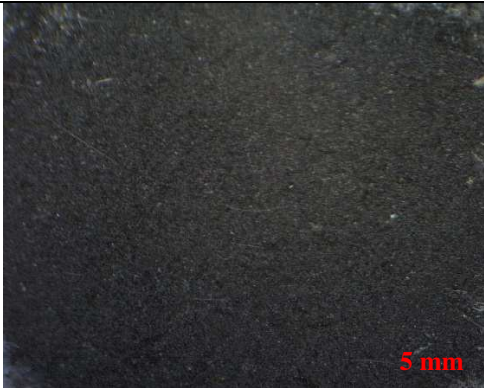
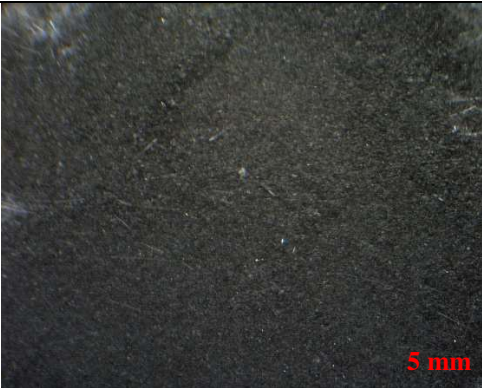
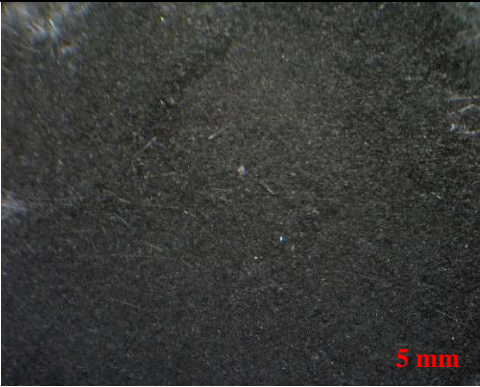
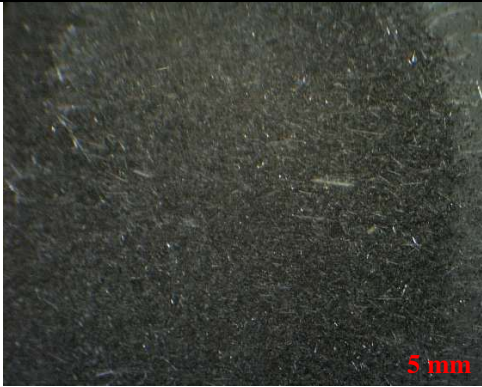
Another study was done using coal produced by sawdust pyrolysis as a reducing agent in the iron oxide reduction process. They argued that solid carbon was hardly gasified at low temperature ( $\leq 400$  °C), and the partial pressure of CO approached 100% when the temperature reached 980 °C. At temperatures above 980 °C the atmosphere of pure CO can be formed by the conversion of solid carbon. Although CO is released quickly, it is also carried out of the reaction system by the carrier gas (N<sub>2</sub>) during the experiment. On the other hand, the conversion efficiencies of pine sawdust and iron ore were related not only to temperature but also to the dosage of iron ore [18].

### **7.3.4 Characterization of materials after iron oxide reduction**

The characterization of the iron-reduced materials using as-received and torrefied biomass were investigated using microscope images and X-ray excited photoelectron spectroscopy - XPS. Table 7.5 presents the images taken after the reduction tests. Firstly, it is noted that all samples present dark coloration, which indicates that the reduction occurred, since, the mixtures of biomass with hematite, both as-received and torrefied, presented a reddish

coloration (Figure 7.1). In addition, small white/transparent fragments are seen in the images. This is due to the quartz wool used to protect the sample holder from TGA. Subtly, a darker coloration is visualized in the torrefied PP mixture with hematite, which may suggest a higher presence of iron, i.e. a higher reduction compared to the other biomasses.

Table 7.5 - Samples after reduction process

<i>As received</i>	<b>Torrefied</b>
<b>PP106<math>\mu</math>m+HM</b>	<b>PPT106<math>\mu</math>m+HM</b>
	
<b>CV106<math>\mu</math>m+HM</b>	<b>CVT106<math>\mu</math>m+HM</b>
	
<b>CC106<math>\mu</math>m+HM</b>	<b>CCT106<math>\mu</math>m+HM</b>
	

Source: The author, (2023).



The XPS characterization was carried out to verify oxidation of each mixture performed after the iron oxide thermal reduction. As the samples with mixtures containing torrefied biomass showed more than one range of reduction temperature (as was the case of PPT106 $\mu$ m+HM and CCT106 $\mu$ m+HM), lower temperature at the beginning of the reduction and higher peaks in the DTG curves, only these samples, or that is, all mixtures containing torrefied biomass were analyzed using this characterization. The XPS results are shown in Figure 7.4 and Table 7.6 show values of binding energies of iron oxide.

Analyzing the curves in Figure 7.4, it can be seen that all of them show the same behavior obtained by Biesenger *et al.* [28], McIntyre & Zetaruk [29] and Wirecka *et al.* [30] in their studies seeking to verify the presence of iron oxides using the XPS technique. This technique is considered challenging due to the complexity of its 2p spectra resulting from peak asymmetries, complex multiples and overlapping energy curves [28].

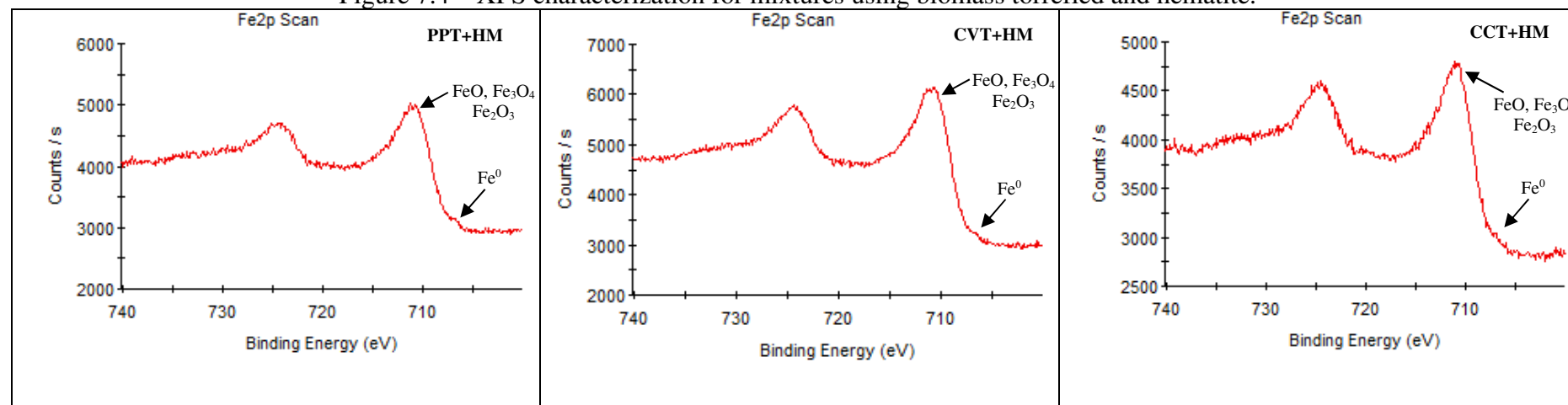
These superimposed energy curves are visualized in all 2p spectra of Figure 7.4, thus making it difficult to differentiate the curve of each oxide present. In this context, using the values contained in Table 7.6, it was possible to verify the presence of metallic iron and all oxides (FeO, Fe<sub>3</sub>O<sub>4</sub>,  $\alpha$ Fe<sub>2</sub>O<sub>3</sub> e  $\gamma$ Fe<sub>2</sub>O<sub>3</sub>) in the three mixtures using torrefied biomass and hematite.

It is also noted in Figure 7.4 that the peak corresponding to the binding energy of metallic iron is more visible in the mixture using PPT biomass, suggesting that this mixture provided greater reduction compared to the other biomasses. For mixtures with CVT biomass, the metallic Fe peak was lower compared to the mixture with PPT biomass, and for mixtures with CCT, this peak is very subtle. Thus, it can be stated that the reduction process of hematite iron oxide occurred using the three torrefied biomasses.

El-Tawil *et al.* [17] also studied the reduction of hematite iron ore (Fe<sub>2</sub>O<sub>3</sub>) from heat-treated biomass. By XRD analysis, the authors verified the presence of Fe<sub>3</sub>O<sub>4</sub>, FeO and metallic iron oxides in the mixture that used biomass with lower temperature heat treatment (300°C) and FeO and metallic iron in the mixture with biomass treated at 350°C. For the other two temperatures, only the presence of metallic iron was verified, thus proving the increase in the efficiency of the thermally treated biomass in the reduction of hematite [17].

Figure 7.5 presents the theoretical and experimental TGA curves, as well as the variation of the degree of reduction ( $\Delta W$ ) values during the temperature variation. Initially, observing the theoretical and experimental of the three biomasses it is noted that an overlapping behavior at the beginning of the tests, and from a certain temperature the curves separate.

Figure 7.4 – XPS characterization for mixtures using biomass torrefied and hematite.



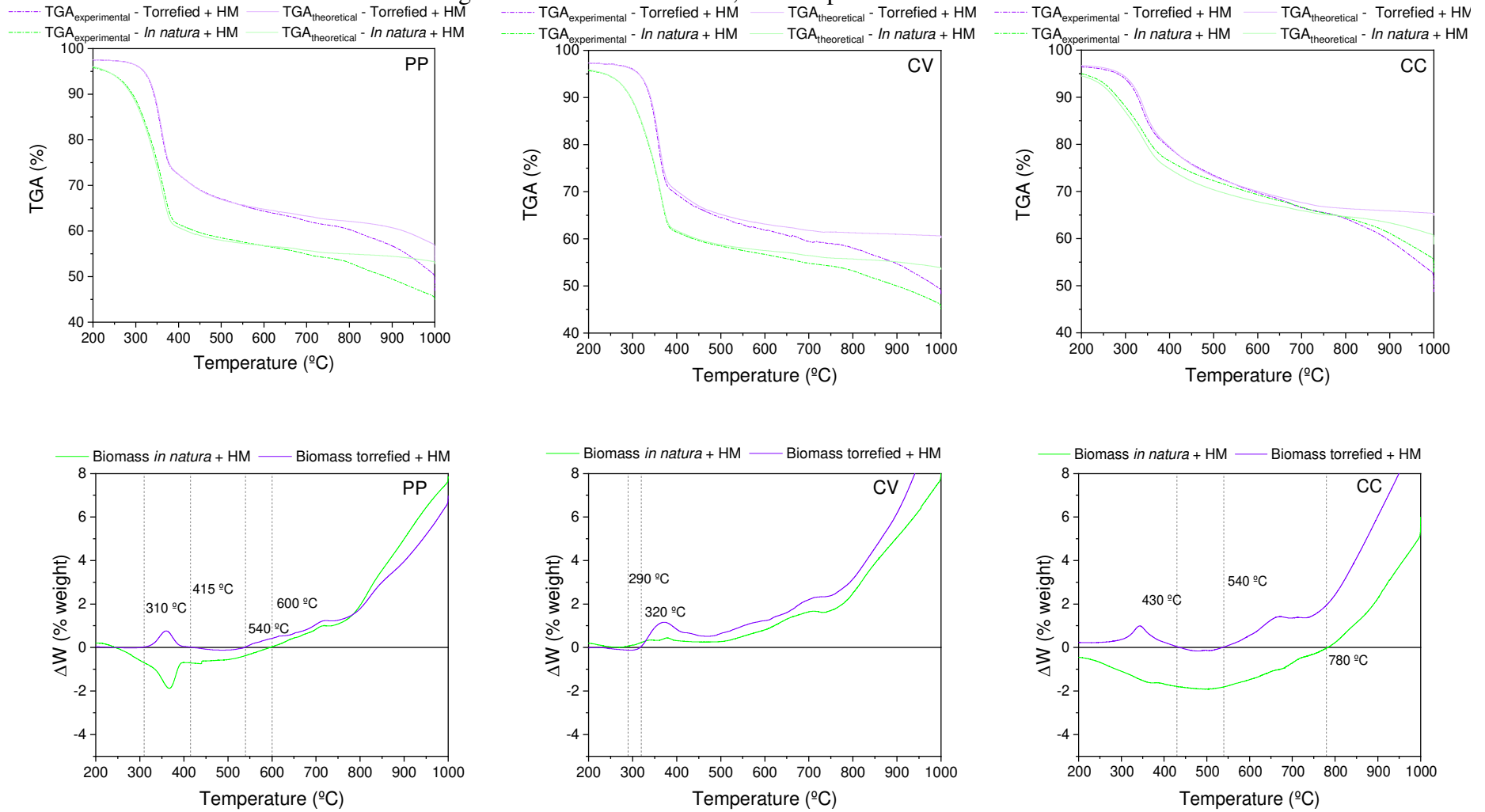
Source: The author, (2023).

Table 7.6 - Binding energies of iron oxides

Compound	Binding Energy
Fe metal	706.9±0.10
FeO	709.5±0.2
Fe <sup>3</sup> O <sub>4</sub> (Fe <sup>2+</sup> and Fe <sup>3+</sup> )	708.3±0.15
αFe <sub>2</sub> O <sub>3</sub>	711.0±0.15
γFe <sub>2</sub> O <sub>3</sub>	711.0±0.15

Source: Adapted from McIntyre & Zetaruk [29] and Wirecka *et al.* [30].

Figure 7.5 – TGA theoretical, TGA experimental and  $\Delta W$



Source: The author, (2023).

Regarding the biomass PP, this occurs from the temperatures of 540 °C for the mixture with torrefied biomass and 600 °C with the biomass as-received. For CV, this separation of the curves appears at 450 °C and 520 °C, respectively.

Regarding the mixture with the biomass of CC, the curve containing the biomass as-received did not follow an overlapping behavior in any of the temperatures, however, presented a similar behavior between the theoretical and experimental curves. On the other hand, the curve of the mixture with torrefied CC showed an overlapping behavior until 650 °C and then the curves separate. When the separation of the theoretical and experimental curves occurs, it means that the reduction process is happening.

Moreover, the space between the theoretical and experimental curves provides a measurement of the extent of hematite reduction. With this, the higher the reaction temperature the greater the degree of reduction due to the intensified gap [3]. Among the three mixtures with torrefied and as-received biomasses, it is noted that the largest gap occurs with the CV biomass, followed by CC and PP. Also, the beginning of the gap using the mixture with biomass CV presents lower temperature when compared to the other biomasses.

Also in relation to the theoretical and experimental TGA curves, it is noted that the mixtures containing torrefied biomasses PP and CV showed a lower temperature of onset of reduction (separation of the curves) when compared to the biomasses as-received. The other curves presented in Figure 7.5 are related to the values of  $\Delta W$  throughout all the temperatures of the study. The values of  $\Delta W$  show the degree of reduction during the test, with values of  $\Delta W$  greater than zero indicating the incidence of reduction, while values of  $\Delta W$  equal to zero indicate no occurrence of reduction.

Initially, analyzing the PP biomass it is observed that the indicator of reduction occurs in two different temperature ranges for the mixture that used torrefied biomass, being from 310-415 °C and from 540 °C. This also occurs in the mixture containing the torrefied biomass of CC, being the temperature ranges between 200-430 °C and from 540 °C as well as the torrefied PP biomass.

As for the other fresh biomass mixtures of PP, CV and CC and torrefied CV biomass, the degree of reduction occurs from only a certain temperature. They are, respectively, 600, 290, 780 and 320 °C. With this indication of the occurrence of reduction at low temperatures, it suggests that during the devolatilization of biomass it is possible that the process of reduction of iron oxide already begins to occur. And, as studied in the thermodynamic analysis of possible reduction reactions, it is noted that this is possible due to the temperature ranges shown in Table 7.4, both for direct and indirect reactions.

Also, comparing the results obtained through the DTG curves (Table 7.3), that is, the temperature range that possibly occurs the change of oxides with the results obtained by the values of  $\Delta W$ , it is noted that the results are congruent. In both it is possible to see the first peak (DTG) related to devolatilization and also to the possible reduction process as shown by  $\Delta W$ , besides visualizing in both results the reduction from 540 °C.

Finally, Equation (7.7) was used to obtain the reduction conversion for each temperature range shown in Figure 7.5, which presented  $\Delta W > 0$ , that is, where the reduction occurred. The results obtained are presented in Table 7.7.

Table 7.7 - Conversion related to iron ore reduction.

Mixture	Temperature range (°C)	Temperature range conversion (%)	Total conversion (%)
PP106 $\mu$ m+HM	600-1000	20.80	20.80
PPT106 $\mu$ m+HM	310-415	25.53	54.52
	540-1000	28.96	
CV106 $\mu$ m+HM	290-1000	51.62	51.62
CVT106 $\mu$ m+HM	320-1000	51.28	51.28
CC106 $\mu$ m+HM	780-1000	18.70	18.70
CCT106 $\mu$ m+HM	30-430	25.53	50.34
	540-1000	27.54	

Source: The author, (2023).

Initially, analyzing the conversion values, it is noted that, except for the mixture with CV biomass, the other mixtures that had torrefied biomass showed higher conversion when compared to the mixtures with biomass as-received. This shows the importance of torrefaction for the valorization of the chemical components present in the biomass, thus improving its efficiency in the application of iron ore reduction.

Comparing the conversion values obtained using mixtures with torrefied biomass, it is noted that all presented values above 50%, with PPT biomass being the one that presented the highest conversion. This converges with the results previously analyzed, in which it was suggested that the PP biomass had a greater potential for reducing hematite because it has a slightly darker color compared to the other biomasses, because it has more characteristic peaks in the DTG curves and because it has a signal more visible Fe on the XPS curve (Figure 7.4).

This can also be verified for the CC biomass, that is, that the previous results already indicated a lower reduction capacity compared to the other biomasses due to the lighter color compared to the other biomasses and by the DTG peaks and the Fe signal in the curve XPS that were less visible. It was found that there was a reduction, but with a lower potential compared to other biomasses. This is probably due to the higher lignin content in its composition.

For CV biomass, it can be noted that the reduction conversions of the mixtures containing as-received biomass and torrefied biomass were similar, around 51%. As expected, this value was closer to the mixture that used PPT in its composition, since the chemical compositions of CV and PP are very similar. Finally, taking into account all the biomasses used (before and after torrefaction) in the mixture and the conversion obtained by each one of them (Table 6), the biomasses that presented the greatest potential for reducing iron ore in descending order: PPT> CV>CVT>CCT>PP>CC.

#### 7.4 CONCLUSIONS

From the accomplishment of this study, it can be verified that the use of biomass for iron ore reduction is promising. The hematite iron oxide reduction tests using biomasses indicate that reduction occurred when observing the coloration of the samples before and after the thermogravimetric tests. Because it presents a very characteristic coloring, intense red, even after mixing with the biomasses the coloring of the hematite predominates. After the reduction tests the coloration of the final samples became darker, like black and dark grey, thus indicating the occurrence of reduction.

With the TGA and DTG curves it was possible to observe the mass loss of each sample as well as the peaks and the temperature ranges that each reduction occurred. Comparing the results obtained in this study with the literature, it is believed that from 500 °C occurred the gradual reduction of  $\text{Fe}_2\text{O}_3 \rightarrow \text{Fe}_3\text{O}_4 \rightarrow \text{FeO} \rightarrow \text{Fe}$ , in the following temperature ranges, respectively, 650 - 750 °C, 750 - 860 °C, 860-1000 °C. Still in the DTG curves, a peak was visualized in lower temperature, around 350 °C. Although this peak is related to the biomass devolatilization, it was possible to verify by the values of  $\Delta W$  and by thermodynamic analysis that the occurrence of reduction is also possible at this temperature.

The XPS results showed the presence of Fe and all other iron oxides ( $\text{Fe}_2\text{O}_3$ ,  $\text{Fe}_3\text{O}_4$ , FeO) in the samples that underwent the reduction process using torrefied biomass. Through this analysis, it can be seen that there was a partial reduction in iron ore. The results of the theoretical and experimental TGA curves also confirmed the occurrence of reduction by presenting gaps

from 500 °C. Finally, the conversion values the mixtures that contained torrefied biomass showed greater advances when mixtures with as received biomasses, thus showing the importance of the torrefaction process in this application. The highest conversion was mixture with PPT followed by CVT and CCT with values of 54.52, 51.28 and 50.34%.

## 7.5 REFERENCES

- [1] Khanna, R., Li, K., Wang, Z. Sun, M., Zhang, J., Mukherjee, P. S. 11 - Torrefied biomasses in iron and steel industries. M. Jeguirim, L. Limousy (Eds.), *Char and Carbon Materials Derived from Biomass*, Elsevier (2019), pp. 429-446 <https://doi.org/10.1016/B978-0-12-814893-8.00011-0>
- [2] H. Wang, C. Zhang, J. Qie, J. Zhou, Y. Liu, X. Li, F. Shangguan, Development trends of environmental protection technologies for Chinese steel industry, *Journal of Iron and Steel Research, International*, 2017, 24, pp. 235-242. [https://doi.org/10.1016/S1006-706X\(17\)30035-3](https://doi.org/10.1016/S1006-706X(17)30035-3)
- [3] A. T. Ubando, W. Chen, H. C. Ong, Iron oxide reduction by graphite and torrefied biomass analyzed by TG-FTIR for mitigating CO<sub>2</sub> emissions, *Energy*, 2019, 180, pp. 968-977. <https://doi.org/10.1016/j.energy.2019.05.149>
- [4] K. Zheng, H. Han, S. Hu, Q. Ren, S. Su, Y. Wan, L. Jiang, J. Xu, H. Li, Y. Tong, J. Xiang, Upgrading biomass waste to bio-coking coal by pressurized torrefaction: Synergistic effect between corncob and lignin, *Energy*, 2023, 267, pp. 126536. <https://doi.org/10.1016/j.energy.2022.126536>
- [5] O. Sheshukov, M. Mikheenkov, L. Vedmid, I. Nekrasov, D. Egiazaryan, Mechanism of Ion-Diffusion Solid-Phase Reduction of Iron Oxides of Technogenic Origin in the Presence of the Liquid Phase and without it, *Metals*, 2020, 10(12), pp. 1564. <https://doi.org/10.3390/met10121564>
- [6] Q. Hu, D. Yao, Y. Xie, Y. Zhu, H. Yang, Y. Chem H. Chen, Study on intrinsic reaction behavior and kinetics during reduction of iron ore pellets by utilization of biochar, *Energy Conversion and Management*, 2018, 158, pp. 1-8. <https://doi.org/10.1016/j.enconman.2017.12.037>
- [7] X. Liu, R. Rong, M. Dai, H. Bian, C. Peng, Preparation of red mud-based zero-valent iron materials by biomass pyrolysis reduction: Reduction mechanism and application study, *Science of The Total Environment*, 2023, 864, pp. 160907. <https://doi.org/10.1016/j.scitotenv.2022.160907>
- [8] L. Ye, Z. Peng, L. Wang, A. A. Anzulevich, I. Bychkov, H. Tang, M. Rao, Y. Zhang, G. Li, T. Jiang, Preparation of core-shell iron ore-biochar composite pellets for microwave reduction, *Powder Technology*, 2018, 338, pp. 365-375. <https://doi.org/10.1016/j.powtec.2018.07.037>

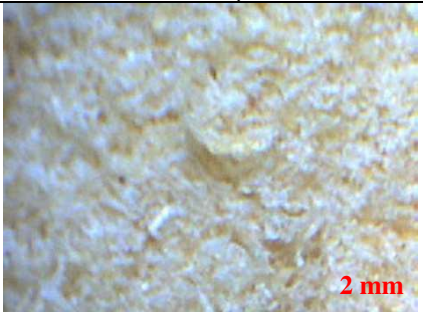
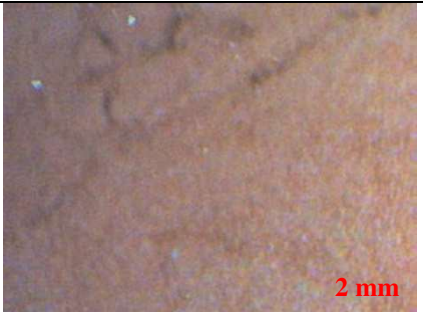
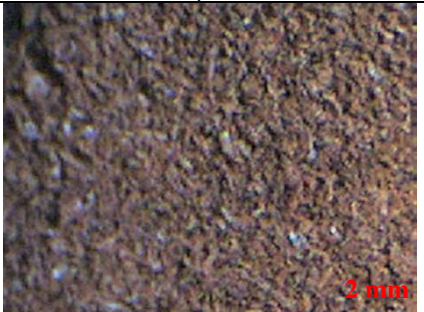
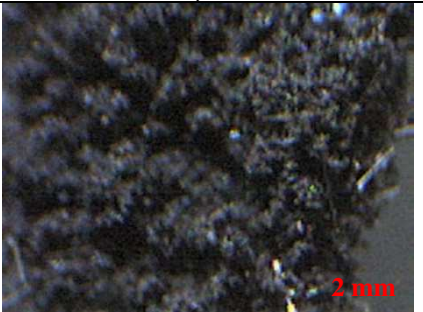
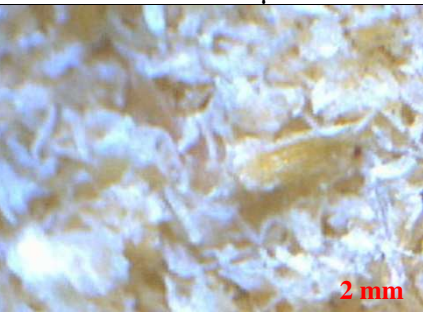
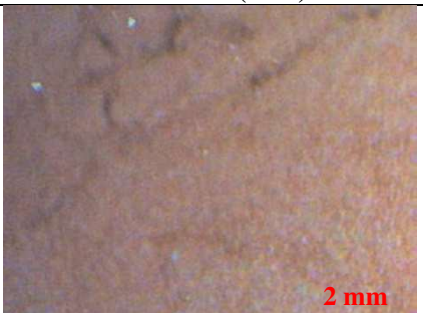

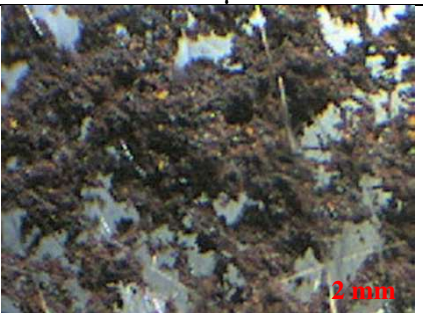
- [9] Mousa, E., Wang, C., Riesbeck, J., Larsson, M. Biomass applications in iron and steel industry: An overview of challenges and opportunities. *Renewable and Sustainable Energy Reviews*, [s.l.], v. 65, p. 1247-1266, 2016. <https://doi.org/10.1016/j.rser.2016.07.061>
- [10] Lu, L., Adam, M., Kilburn, M. Hapugoda, S., Somerville, M., Jahanshabi, S., Mathieson, J. G. Substitution of Charcoal for Coke Breeze in Iron Ore Sintering. *ISIJ Int.*, [s.l.], v. 53, p. 1607-1616, 2013. <https://doi.org/10.2355/isijinternational.53.1607>
- [11] Surup, G. R., Trubetskaya A., Tangstad, M. Charcoal as an Alternative Reductant in Ferroalloy Production: A Review. *Processes*, [s.l.], v. 8, p. 1-41, 2020. <https://doi.org/10.3390/pr8111432>
- [12] Jha, G., Shatrughan, S., Mehta, K. D. Partial substitution of coke breeze with biomass and charcoal in metallurgical sintering. *Fuel*, [s.l.], v. 278, p. 118-350, 2020. <https://doi.org/10.1016/j.fuel.2020.118350>
- [13] J. O. Brotto, T. A. Cruz, I. O. Pereira, J. L. Ienczak, R. A. Peralta, J. M. Lázaro-Martínez, H. J. José, E. Rodríguez-Castellón, R. F. P. M. Moreira, Mechanistic insights and kinetics of torrefaction of pine wood biomasses using solid-state NMR. *Journal of Analytical and Applied Pyrolysis*, 2023, XX, pp. XX. <https://doi.org/10.1016/j.jaap.2023.106019>
- [14] E. Kasai, K. Mae, F. Saito, Effect of mixed-grinding on reduction process of carbonaceous material and iron oxide composite, *ISIJ International*, 1995, 35, pp. 1444–1451. <https://doi.org/10.2355/isijinternational.35.1444>
- [15] G. Wang, J. Zhang, G. Zhang, H. Wang, D. Zhao, Experiments and Kinetic Modeling for Reduction of Ferric Oxide biochar Composite Pellets, *ISIJ International*, 2017, 57, pp. 1374–1383. <https://doi.org/10.2355/isijinternational.ISIJINT-2016-630>
- [16] J. Cai, Y. He, X. Yu, S. W. Banks, Y. Yang, X. Zhang, Y. Yu, R. Liu, A. V. Bridgwater. Review of physicochemical properties and analytical characterization of lignocellulosic biomass. *Renewable and Sustainable Energy Reviews*, 2017, 76, pp. 309-322. <https://doi.org/10.1016/j.rser.2017.03.072>
- [17] A.A. El-Tawil, H. M. Ahmed, A.A. El-Geassy, B. Bjorkman, Effect of volatile matter on reduction of iron oxide- containing carbon composite. The 54th annual conference of metallurgists (COM 2015) was held at the Fairmont Royal York in Toronto, Ontario, Canada, on August 23-26th, 2015 (2015), pp. 1-14.
- [18] L. Wang, Y. Yang, Q. Xhing, Q. Li, T. Jiang, Gasification of pine sawdust via synergetic conversion using iron ore as a catalyst. *Bioresource Technology*, 2022, 355, pp. 127240. <https://doi.org/10.1016/j.biortech.2022.127240>
- [19] Z. Cao, Q. Xu, H. Kang, J. Shi, X. Lu, B. Chen, L. Guo, Insights into direct reduction iron using bamboo biomass as a green and renewable reducer: Reduction behavior study and kinetics analysis. *Science of The Total Environment*, 2023, 880, pp. 163393. <https://doi.org/10.1016/j.scitotenv.2023.163393>



- [20] A. T. Ubando, W. Chen, V. Ashokkumar, J. Chang, Iron oxide reduction by torrefied microalgae for CO<sub>2</sub> capture and abatement in chemical-looping combustion. *Energy*, 2019, 186, pp. 115903. <https://doi.org/10.1016/j.energy.2019.115903>
- [21] F. Collard, J. Blin, A review on pyrolysis of biomass constituents: Mechanisms and composition of the products obtained from the conversion of cellulose, hemicelluloses and lignin. *Renewable and Sustainable Energy Reviews*, 2014, 38, pp. 594-608. <https://doi.org/10.1016/j.rser.2014.06.013>
- [22] H. Kim, S. Yu, M. Kim, C. Ryu, Progressive deconvolution of biomass thermogram to derive lignocellulosic composition and pyrolysis kinetics for parallel reaction model, *Energy*, 2022, 254, pp. 124446. <https://doi.org/10.1016/j.energy.2022.124446>
- [23] P. Zong, Y. Jiang, Y. Tian, J. Li, M. Yuan, Y. Ji, M. Chen, D. Li, Y. Qiao, Pyrolysis behavior and product distributions of biomass six group components: Starch, cellulose, hemicellulose, lignin, protein and oil, *Energy Conversion and Management*, 2020, 216, pp. 112777. <https://doi.org/10.1016/j.enconman.2020.112777>
- [24] A. Robles, Bio-coal pre-treatment for maximized addition in briquettes and coke, Master thesis, 2017.
- [25] D. Özçimen, A. Ersoy-Meriçboyu, Characterization of biochar and bio-oil samples obtained from carbonization of various biomass materials. *Renewable Energy*, 2010, 35, pp. 1319-1324. <https://doi.org/10.1016/j.renene.2009.11.042>
- [26] Z. Qi, T. Murakami, E. Kasai, Gasification and reduction behavior of iron ore-carbon composite under high pressure. *ISIJ International*, 2012, 10, pp. 1778. <http://doi.org/10.2355/isijinternational.52.1778>
- [27] Z. Chen, J. Dang, X. Hu, H. Yan, Reduction Kinetics of Hematite Powder in Hydrogen Atmosphere at Moderate Temperatures, *Metals*, 2018, 8, pp. 751. <https://doi.org/10.3390/met8100751>
- [28] Biesenger, M. C., Payne, B. P., Grosvenor, A., P., Lau, L. W. M., Gerson, A. R., Smart, R. St. C. Resolving surface chemical states in XPS analysis of first row transition metals, oxides and hydroxides: Cr, Mn, Fe, Co and Ni. *Applied Surface Science*, 2011, 257 (7), pp. 2717-2730. <https://doi.org/10.1016/j.apsusc.2010.10.051>
- [29] McIntyre, N. S. and Zetaruk, D. G. X-ray Photoelectron Spectroscopic Studies of Iron Oxides. *Analytical Chemistry*, [s.l.], v. 49 (11), pp. 1521, 1977.
- [30] Wirecka, R., Lachowicz, D., Berent, K., Marzec, M. M., Bernasik, A. Ion distribution in iron oxide, zinc and manganese ferrite nanoparticles studied by XPS combined with argon gas cluster ion beam sputtering. *Surfaces and Interfaces*, 2022, 30, pp.101865. <https://doi.org/10.1016/j.surfin.2022.101865>

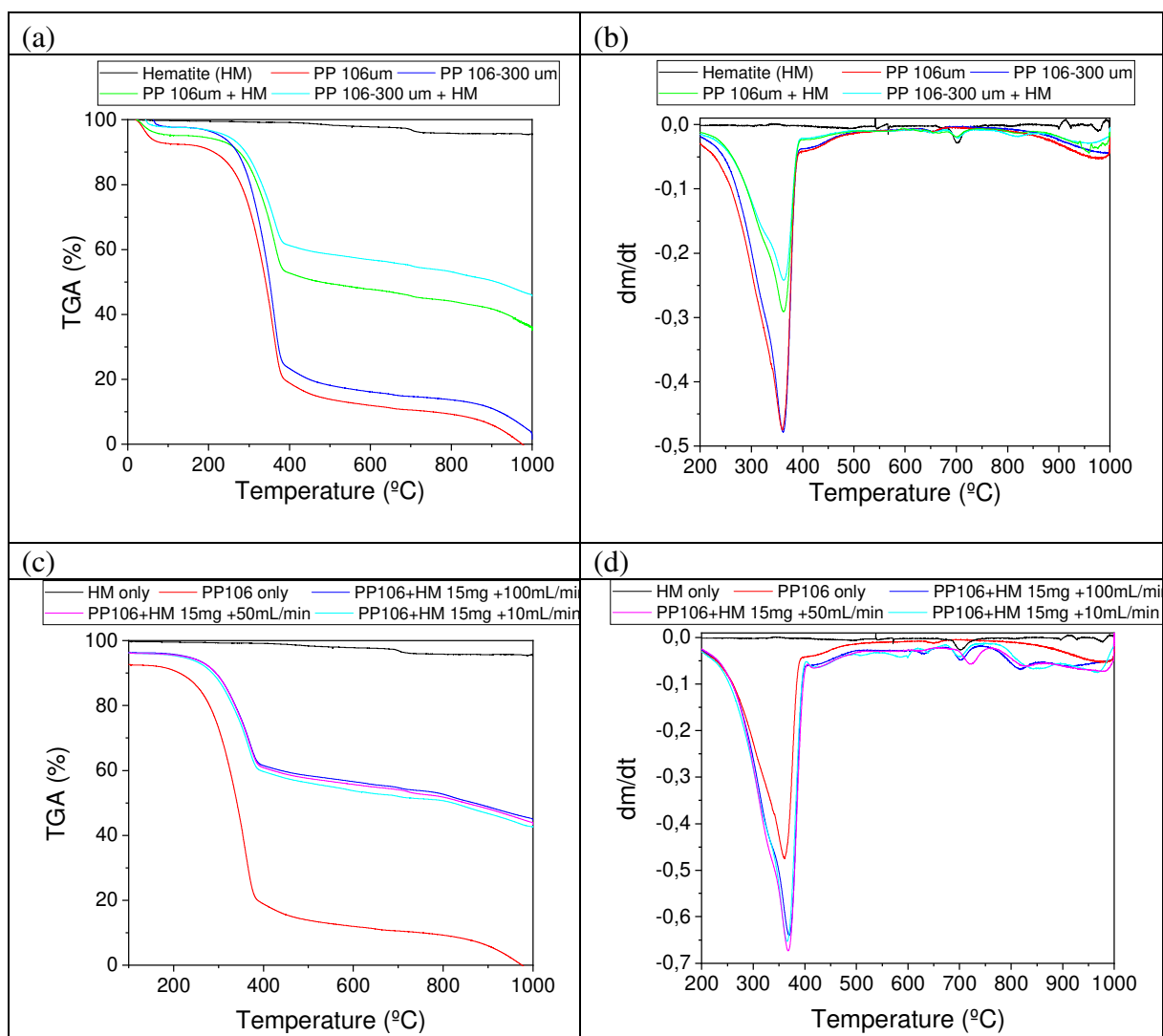
7.6 SUPPLEMENTARY MATERIAL

Figure S7.1 – Images of biomasses, hematite and mixture before and after reduction.

Samples		Mixed Samples	
		Before Reduction	After Reduction
PP 106 $\mu$ m	Hematite (HM)	PP 106 $\mu$ m +HM	PP 106 $\mu$ m +HM
			
PP106-300 $\mu$ m	Hematite (HM)	PP 106-300 $\mu$ m +HM	PP 106-300 $\mu$ m +HM
			

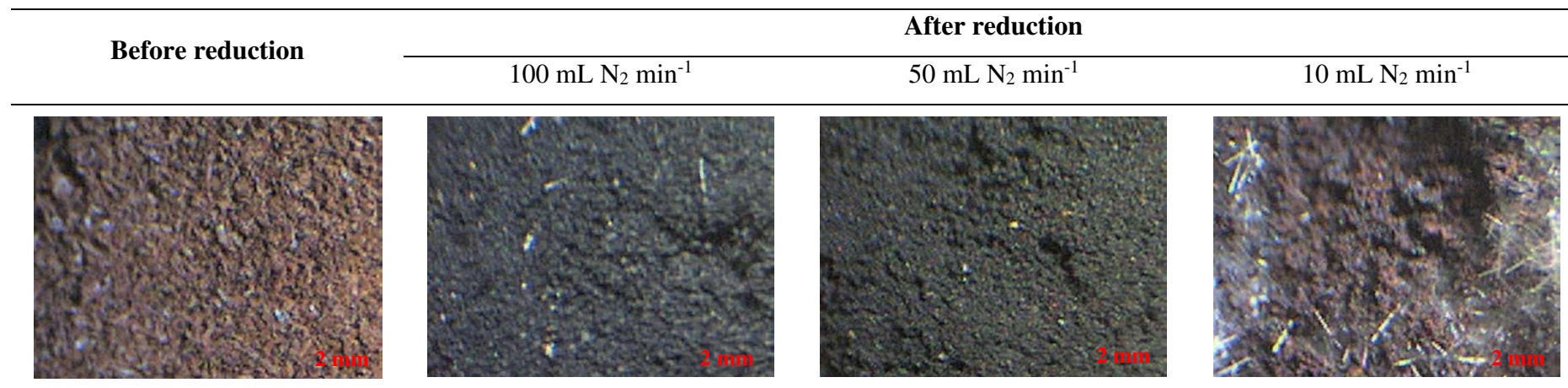
Source: The author, 2023.

Figure S7.2 – Preliminary tests a) and b) TGA and DTG of the as received biomass, hematite and mixtures of biomass and hematite using different particle sizes and 5 mg of sample c) e d) TGA and DTG of the as received biomass, hematite and mixtures of biomass and hematite varying nitrogen flow (10, 50 e 100 mL min<sup>-1</sup>).



Source: The author, 2023.

Figure S7.3 – Images of mixture after reduction using 3 different flow rates.

PP as received 106 $\mu$ m + HM

Source: The author, 2023.

Table S7.1 - Gibbs free energy values generated by Factsage software

Reaction	$\Delta G_0T$ , kJ/mol, temperature, °C									
	100	200	300	400	500	600	700	800	900	1000
$2Fe_2O_3 + 6C \rightleftharpoons 4Fe + 6CO \uparrow^a$	583,73	475,78	368,82	262,99	158,27	54,66	<b>-47,83</b>	<b>-149,78</b>	<b>-251,51</b>	<b>-352,86</b>
$3Fe_2O_3 + C \rightleftharpoons 2Fe_3O_4 + CO \uparrow^a$	49,58	27,41	5,19	<b>-17,21</b>	<b>-40,06</b>	<b>-63,62</b>	<b>-86,54</b>	<b>-108,67</b>	<b>-130,62</b>	<b>-152,52</b>
$6Fe_2O_3 + C \rightleftharpoons 4Fe_3O_4 + CO_2 \uparrow^a$	<b>-7,71</b>	<b>-34,21</b>	<b>-60,76</b>	<b>-87,72</b>	<b>-115,64</b>	<b>-145,08</b>	<b>-173,34</b>	<b>-200,11</b>	<b>-226,62</b>	<b>-253,12</b>
$Fe_3O_4 + C \rightleftharpoons 3FeO + CO \uparrow^a$	125,60	102,85	80,25	58,11	36,68	16,23	<b>-3,74</b>	<b>-23,52</b>	<b>-43,15</b>	<b>-62,69</b>
$Fe_3O_4 + 4C \rightleftharpoons 3FeO + 4CO \uparrow^a$	413,01	343,13	274,02	205,85	138,73	72,80	7,40	<b>-58,00</b>	<b>-123,32</b>	<b>-188,38</b>
$2Fe_3O_4 + C \rightleftharpoons 6FeO + CO_2 \uparrow^a$	144,33	116,67	89,37	62,92	37,83	14,61	<b>-7,73</b>	<b>-29,80</b>	<b>-51,68</b>	<b>-73,45</b>
$FeO + C \rightleftharpoons Fe + CO \uparrow^a$	95,80	80,10	64,59	49,25	34,02	18,86	3,71	<b>-11,49</b>	<b>-26,72</b>	<b>-41,90</b>
$2FeO + C \rightleftharpoons 2Fe + CO_2 \uparrow^a$	84,74	71,17	58,04	45,20	32,52	19,87	7,16	<b>-5,76</b>	<b>-18,82</b>	<b>-31,87</b>
	-	-	-	-	-	-	-	-	-	-
$6FeO + 5C \rightleftharpoons 2Fe_3C + 3CO_2 \uparrow^a$	<b>3009,7</b>	<b>2976,8</b>	<b>2942,7</b>	<b>2907,6</b>	<b>2872,0</b>	<b>2835,7</b>	<b>2799,0</b>	<b>2761,9</b>	<b>2724,3</b>	<b>2686,3</b>
	<b>8</b>	<b>6</b>	<b>1</b>	<b>9</b>	<b>1</b>	<b>8</b>	<b>8</b>	<b>3</b>	<b>4</b>	<b>0</b>
$C + CO_2 \uparrow \rightleftharpoons 2CO \uparrow^b$	106,87	89,02	71,14	53,29	35,52	17,84	0,26	<b>-17,23</b>	<b>-34,62</b>	<b>-51,92</b>
$Fe_3C + CO_2 \uparrow \rightleftharpoons 3Fe + 2CO \uparrow^c$	89,58	73,90	58,61	43,56	28,59	13,54	<b>-1,75</b>	<b>-17,49</b>	<b>-33,60</b>	<b>-49,87</b>
$Fe_2O_3 + 3CO \uparrow \rightleftharpoons 2Fe + 3CO_2 \uparrow^c$	<b>-28,73</b>	<b>-29,17</b>	<b>-29,00</b>	<b>-28,38</b>	<b>-27,43</b>	<b>-26,20</b>	<b>-24,70</b>	<b>-23,21</b>	<b>-21,89</b>	<b>-20,66</b>
$3Fe_2O_3 + CO \uparrow \rightleftharpoons 2Fe_3O_4 + CO_2 \uparrow^c$	<b>-57,29</b>	<b>-61,62</b>	<b>-65,95</b>	<b>-70,51</b>	<b>-75,58</b>	<b>-81,46</b>	<b>-86,80</b>	<b>-91,44</b>	<b>-96,00</b>	<b>-100,60</b>
$Fe_3O_4 + 4CO \uparrow \rightleftharpoons 3Fe + 4CO_2 \uparrow^c$	<b>-14,45</b>	<b>-12,95</b>	<b>-10,53</b>	<b>-7,32</b>	<b>-3,36</b>	1,43	6,36	10,91	15,16	19,32
$Fe_3O_4 + CO \uparrow \rightleftharpoons 3FeO + CO_2 \uparrow^c$	18,73	13,82	9,11	4,81	1,15	<b>-1,62</b>	<b>-4,00</b>	<b>-6,29</b>	<b>-8,53</b>	<b>-10,76</b>
$FeO + CO \uparrow \rightleftharpoons Fe + CO_2 \uparrow^c$	<b>-11,06</b>	<b>-8,93</b>	<b>-6,55</b>	<b>-4,05</b>	<b>-1,50</b>	1,02	3,45	5,73	7,90	10,03

<sup>a</sup> Direct reduction reactions, <sup>b</sup> Boudouard reaction and <sup>c</sup> Indirect reduction reactions.

## 8 FINAL REMARKS

With the realization of this thesis it was possible to study the valorization and application of three wood biomasses of the genus *Pine* in ore reduction processes. The main conclusions at this thesis were:

- Knowledge of the physical, chemical and thermal characteristics of the material is essential in order to properly assess its efficiency in the proposed application. In addition, carrying out a study of the optimal torrefaction experimental conditions was also of paramount importance for the development of the work;
- The chemical composition of volatile material content, ash, moisture and fixed carbon showed the positive potential of using the three biomasses as fuels. The results of the lignocellulosic characterization indicated the biomasses PP and CV presented very similar chemical compositions while the biomass CC was the one that presented the highest amount of lignin in its composition;
- The thermogravimetric tests of the biomass were essential for the initial choice of the operational parameters for torrefaction. The chosen parameters were 250 °C and 290 °C for temperature and 30 and 60 minutes for residence time in an inert atmosphere;
- The results of the evaluation of the reactivity of biomasses torrefied with CO<sub>2</sub> showed that CC had lower reactivity compared to PP and CV, possibly due to the higher lignin content. The optimal torrefaction parameters chosen from this analysis were 250 °C and 60 minutes for CC and 290 °C and 30 minutes for PP and CV;
- The chemical characterization of the torrefied biomasses showed a decrease in the volatile material content and an increase in the fixed carbon content, thus showing an improvement in the chemical characteristics for application in metallurgical processes;
- The proposed new methodology to obtain kinetic parameters from the *ss*-NMR results showed low torrefaction activation energy values, around 11.71-25.37 kJ mol<sup>-1</sup>;

- The liquid fraction, composed of condensable gases generated during torrefaction, showed a high concentration of aliphatic ketones in the composition with the highest presence of lignin;
- During torrefaction there was a low amount of gas generated, even at the longest residence time. The presence of lignin in high concentration (CC biomass) produced non-condensable gases rich in hydrogen;
- The results of the XPS characterization performed on mixtures of hematite with torrefied biomass after going through the reduction process showed the presence of Fe and the oxides  $\text{Fe}_2\text{O}_3$ ,  $\text{Fe}_3\text{O}_4$  and  $\text{FeO}$ ;
- The results of reduction conversion with hematite showed that torrefied biomasses have a greater reduction potential when compared to as received biomasses. They also pointed out that PP biomass has the greatest potential for reduction, followed by CV and CC. The values were 54.52, 51.28 and 50.34%, respectively;
- Finally, the use of torrefied biomass showed satisfactory results in the application for the reduction of hematite iron ore.

## 9 SUGGESTION FOR FUTURE WORK

For future work, some suggestions are proposed:

- Perform ore reduction tests using torrefied biomass and hematite in the presence of other gases such as CO and CO<sub>2</sub>;
- Varying the proportion of hematite mixture with torrefied biomass;
- Optimize the process of mixing torrefied biomass with hematite;
- Carry out ore reduction tests with mixtures containing torrefied biomass, mineral coal and hematite aiming at partial replacement of coal;
- Carry out a study to obtain kinetic parameters for the reduction of iron ore;
- Pelleting mixtures of torrefied biomass and hematite and verifying their influence on the iron ore reduction process;
- Carry out reduction tests using torrefied biomass in a fixed bed reactor and/or pilot plant.